

Copyright

by

Jeffrey Albin Kuhn

2010

The Dissertation Committee for Jeffrey Albin Kuhn certifies that
this is the approved version of the following dissertation:

**Characterization of the Swelling Potential of Expansive
Clays using Centrifuge Technology**

Committee:

Jorge G. Zornberg, Supervisor

Robert B. Gilbert

Bridget R. Scanlon

Kevin J. Folliard

David DiCarlo

**Characterization of the Swelling Potential of Expansive
Clays using Centrifuge Technology**

by

Jeffrey Albin Kuhn, B.S.C.E., M.S.

Dissertation

Presented to the Faculty of the Graduate School of

The University of Texas at Austin

in Partial Fulfillment

of the Requirements

for the Degree of

DOCTOR OF PHILOSOPHY

The University of Texas at Austin

May 2010

To Lou

Acknowledgments

The author would like to thank his advisor Dr. Jorge G. Zornberg for his advice and support throughout his masters and doctoral work. The author would also like to thank Dr. Robert B. Gilbert, Dr. Bridget R. Scanlon, Dr. Kevin J. Folliard, and Dr. David DiCarlo for their assistance with this research and the review of this manuscript. Special thanks are given to friends throughout The University of Texas who aided in this research. In particular, the author would like to thank his colleagues Michael Plaisted, Carlos Guzman, and Alejandro Martinez for thier assistance with various aspects of this research as noted in the text. The author also wishes to thank his parents, Albin and Susan, his older sister Laura, his youger sister Julie, and his wife Lou for their love and support throughout his doctoral studies. Finally, the author wishes to thank his new baby Ella for coming into his life during the last semester of his doctoral studies; you've made mom and I feel so blessed.

JEFFREY ALBIN KUHN

The University of Texas at Austin

May 2010

Characterization of the Swelling Potential of Expansive Clays using Centrifuge Technology

Publication No. _____

Jeffrey Albin Kuhn, Ph.D.

The University of Texas at Austin, 2010

Supervisor: Jorge G. Zornberg

The characterization of the swell potential of expansive clay is complicated by the fact that traditional swell testing methods require an excessive amount of time for specimens to swell to their maximum heights. As a result, the practicing engineer has typically referred to correlations between swell potential and index properties rather than directly measuring swelling in a laboratory experiment. The purpose of this study is to evaluate an alternate testing method using a geotechnical centrifuge in an attempt to decrease the time required to evaluate the swell potential of expansive clays so that experimentally obtained swelling properties may be obtained within a reasonable time period. This study includes an experimental program involving a series of tests in which compacted clay specimens are flown in a centrifuge and their heights are monitored as water infiltrates into them.

Contents

Acknowledgments	v
Abstract	vi
List of Tables	xii
List of Figures	xiii
Chapter 1 Overview of Research Study	1
1.1 Introduction	1
1.2 Motivation	3
1.3 Scope of Research	4
1.4 Organization	5
Chapter 2 Background on Swell Testing of Expansive Clays	6
2.1 Test Methods for Evaluating the Swelling Potential of Expansive Clays	7
2.1.1 Traditional Methods for Evaluating the Swelling Potential of Expansive Clays	7
2.1.2 The Potential Vertical Rise (PVR) Method	11
2.1.3 The Revised Potential Vertical Rise Method Revisited (TxDOT 0-4518)	17
2.1.4 Cyclical Wetting and Drying	20
2.1.5 Centrifuge Testing of Expansive Clay	23

2.2	Predictive Models for the Swelling Potential of Expansive Clays	26
2.2.1	One Dimensional versus Three Dimensional Swelling	26
2.2.2	Correlations for Swell Potential	27
2.2.3	Theories for the Swelling of Expansive Clays over Time and Space . .	30
2.3	Field Studies of the Swelling of Compacted Clays Subjected to Flooding Con- ditions	31
2.3.1	Gizienski and Lee 1965	32
2.3.2	Blight and DeWet 1965	35
Chapter 3 Materials and Methods		36
3.1	Index Properties of Eagle Ford Clay	36
3.1.1	Grain Size Distribution	37
3.1.2	Atterberg Limits	38
3.1.3	Moisture Density Relationship	41
3.1.4	Specific Gravity	42
3.1.5	Mineralogical Analysis	43
3.1.6	Saturated Hydraulic Conductivity	45
3.2	Centrifuge Equipment	48
3.2.1	General Overview	48
3.2.2	Data Acquisition System Details	55
3.2.3	Permeameter Details	56
3.2.4	Major Centrifuge Testing Parameters	59
3.2.5	Testing Procedure Overview	60
3.2.6	Fluid Potential in The Centrifuge Permeameter	62
3.2.7	G-level	64
3.2.8	Permeameter Cup	65
3.2.9	Permeameter Outflow Chamber	67
3.2.10	Permeameter Cap and Linear Position Sensor	68

3.2.11	Low-flow Hydraulic Rotary Union	70
3.2.12	Surcharge Pressure	71
3.2.13	Measurement of Soil Swelling	72
3.3	Centrifuge Testing Procedure	75
3.3.1	Soil Preparation	75
3.3.2	Permeameter cup preparation	78
3.3.3	Soil specimen preparation	79
3.3.4	Pre-flight preparation	80
3.3.5	Initiation of the test	81
3.3.6	Monitoring the test	82
3.3.7	Finishing the test	84
Chapter 4 Results from 1-G Testing Program		87
4.1	Free Swell Tests	87
4.1.1	Differentiation Between Primary and Secondary Swelling	89
4.1.2	Measured Swelling during Free-Swell Testing	92
4.1.3	Effects of the Specimen Aspect Ratio	95
4.2	1-G Infiltration of Centrifuge Testing	97
Chapter 5 Scope of the Experimental Testing Program		101
5.1	Pilot Tests in the Small Centrifuge	102
5.2	Preliminary Tests in the Large Centrifuge	104
5.3	Series (i): Centrifuge Tests with Constant Water Height and Surcharge Mass	109
5.4	Series (ii): Centrifuge Tests with Constant Total Stress	111
Chapter 6 Experimental Testing Results		113
6.1	Series (i): Centrifuge Tests with Constant Surcharge Mass and Water Height	113
6.2	Series (ii): Centrifuge Tests with Constant Water Pressure and Total Stress .	117
6.3	Long-Term Swell Tests in the Centrifuge	122

Chapter 7 Analysis of Test Results	126
7.1 Primary and Secondary Swelling	126
7.1.1 Free-Swell Tests	127
7.1.2 Centrifuge Tests	131
7.1.3 1-G Infiltration	137
7.1.4 14 Day Centrifuge Tests	140
7.1.5 Comparison of Primary and Secondary Swelling Observed from Free-Swell, Centrifuge, and 1-G Infiltration Tests	143
7.1.6 Square-Root of Time Analysis	150
7.2 Secondary Swelling - Displacement Rates for Long-Term, 14 Day, Tests	155
7.3 Wetting Front Advancement During Centrifugation	158
7.4 Outflow Rates and Hydraulic Conductivity from Centrifuge Testing	163
7.5 Total Stress Comparison of Free Swell and 1-G Infiltration Results with Centrifuge Testing	165
7.6 Effective Stress Comparison of Free Swell and 1-G Infiltration Results with Centrifuge Testing	167
7.6.1 Incremental Swell Profiles in Centrifuge Specimens	167
7.6.2 The Interpretation of Incremental Swell Profiles in Centrifuge Specimens	170
7.6.3 The Effective Stress at Mid-Depth in a Centrifuge Specimen Given a Linear Loss in Pore Water Pressure	174
7.7 Comparison of Laboratory Testing Results with Predictions from Empirical Correlations	178
7.8 Modeling Wetting Front Advancement in the Centrifuge	181
7.8.1 Finite Difference Model	182
7.8.2 Hydraulic Parameters	185
7.8.3 Modeled Wetting Front Advancement	187
Chapter 8 Conclusions and Recommendations	190

8.1	Conclusions	190
8.2	Recommendations for Future Investigations	194
	Appendix A Swell Testing with Basic Centrifuge Equipment	197
	Bibliography	201
	Vita	210

List of Tables

2.1	Correlations from the Literature for Determining Swelling Potential, S (percent swell)	28
3.1	Index Properties of Eagle Ford Clay	39
3.2	Descriptions of Eagle Ford Clay Strata (Farrow 1997)	40
3.3	Summary of Laboratory Tests on Eagle Ford Clay Strata (Farrow 1997)	41
3.4	Summary of Large Centrifuge Specifications	54
4.1	Swell after 72 hours / Swell after 14 Days for free swell tests	95
5.1	Testing Plan for Series (i) on 10-mm and 20-mm thick Specimens	109
6.1	Total Stress at which 10-mm thick Specimens were Tested at 25, 50, and 100 G with a Water Pressure Applied Over the Specimens of 400 psf (20 KPa)	118
6.2	Swell after 72 hours / Swell after 14 Days	124
7.1	Hydraulic Gradient for 14 Day Centrifuge Tests	165
7.2	Index Property Testing Used in Evaluating the Correlations in the order in which they are used in the Correlations	179
7.3	Correlations from the Literature for Determining Swelling Potential, S (percent swell)	179

List of Figures

1.1	Centrifuge Testing Setup for the Characterization of Swelling Clays	3
2.1	Fixed-Ring Consolidation Cell (Olson 2007)	8
2.2	Differentiation between Primary and Secondary Swelling (ASTM D4546)	10
2.3	Secondary Swelling (Haynes and Mason 1965)	10
2.4	Swell as a Function of Dry Density and Compaction Water Content for a Expansive Clay from San Diego, California (Gizienski and Lee 1965)	11
2.5	Percent Volumetric Change Versus Plasticity Index (McDowell 1956)	14
2.6	Potential Vertical Rise Versus Load as a Function of the Percent Volumetric Swell (McDowell 1956)	14
2.7	Testing Setup for Capillary Swell Test (McDowell 1954)	15
2.8	Linear Swell Versus Volumetric Swell (McDowell 1956)	15
2.9	Observed Field Movements Versus Movements Predicted Using the Potential Vertical Rise Method (Allen and Gilbert 2006)	16
2.10	Schematic of Laboratory Setup for Diffusion Experiment (pg. 43 of V.2)	18
2.11	Suction Log-time Plot for Determination of the Diffusion Coefficient α (pg. 60 of V.2)	18
2.12	Fatigue of Swelling (Chen 1965)	20
2.13	Height of an Expansive Clay Specimen (Tripathy et al. 2002)	22

2.14 Height of an Expansive Clay Specimen During Cyclical Wetting and Drying Using Forced Air (Allen and Gilbert 2006)	22
2.15 Garde and Chanraskaran (1994) Centrifuge Testing Setup	23
2.16 Swelling Versus Time in a Centrifuge, Garde and Charaskaran (1994)	24
2.17 Percent Swell by Layer for a Expansive Clay Tested in the Centrifuge Under Ponding Conditions (Frydman 1990)	25
2.18 Wetting Front Depth Versus Time for Centrifuge Tests on Expansive Clay Under Ponding Conditions (Frydman 1990)	25
2.19 Comparison of Vertical Swell in Odeometric and Trial Tests (Al-Mhaidib 1989) (a) Measured Swell Versus Overburden Pressure for Triaxial and Odeo- metric Swell Tests (b) Ratio of Swell Measured from Triaxial Tests to Swell Measured From Odeometric Tests Versus Overburden Pressure.	27
2.20 Void Ratio Constitutive Surface for An Unsaturated Soil (Modified from Fred- lund and Rahardjo 1993 Figure 12.24)	31
2.21 Swelling Versus Time for 1.1 ft Thick Test Slab A and 3.0 ft Thick Test Slab B (Gizienski and Lee 1965)	33
2.22 Free Swell Curves from Gizienski and Lee (1965)	34
2.23 Swell Prediction Based off of Free Swell Test Results (Gizienski and Lee 1965)	34
2.24 Field measurements and laboratory measurement of the coefficient of swell as a function of the percentage of maximum heave (Blight and DeWet 1965)	35
2.25 Predicted and maximum observed surface heave versus duration of flooding (Blight and DeWet 1965)	35
3.1 Location of Eagle Ford Formation (Robison 1997)	37
3.2 Grain Size Distribution for Eagle Ford Clay	38
3.3 (a) Frequency of Observed Plasticity Index for Eagle Ford Shale and (b) Casagrande Plot for Eagle Ford Shale Samples (Hsu and Nelson 2002)	39
3.4 Standard and Modified Proctor Compaction Curve for Eagle Ford Shale	42

3.5	Field Sampled Water Content for Eagle Ford Shale (Hsu and Nelson 2002)	42
3.6	X-ray Diffraction (a) Sample Preparation and (b) Prepared and Loaded Sample	44
3.7	X-ray Diffraction Pattern for Eagle Ford Clay	44
3.8	Screen-shot of “X’pert Highscore” X-ray Diffraction Database Software	45
3.9	B-Value during Saturation of Saturated Hydraulic Conductivity Specimens	46
3.10	Cell Inflow during Consolidation of Saturated Hydraulic Conductivity Specimens	47
3.11	Ratio of Inflow to Outflow during Saturated Hydraulic Conductivity Testing	47
3.12	Hydraulic Conductivity versus Effective Stress for Eagle Ford clay Compacted at Optimum Water Content with 100% of Standard Proctor Compaction Effort	48
3.13	The Centrifuge Permeameter	50
3.14	General Centrifuge Schematics (Broadbent 2006, Figures 1.1 and 2.3)	51
3.15	Small Permeameter Table Schematic (Broadbent 2006, Figure 1.10)	52
3.16	Schematic Cross-Section of the Centrifuge Permeameter (Broadbent 2006, Figure 1.3)	53
3.17	On-Board Data Acquisition System	55
3.18	Wireless Network Bridge	56
3.19	Schematic View of Centrifuge Permeameter Cup	57
3.20	The Centrifuge Permeameter Cup	58
3.21	Overview of Centrifuge Testing Process (DGS - Height Measured with Dial Indicator Stand, LPS - Height Measured with Linear Position Sensor, *LPS - Final Expansion can be Measured During Deceleration but not Between Specimen Removal and Measurement of Height with the Dial Indicator Stand)	61
3.22	Variation of G-level with Rotational Velocity Within a Centrifuge Specimen	65
3.23	Percent of Target G-level as a Function of the Height above the Base of the Permeameter	65
3.24	Acrylic Permeameter Cups with Compacted Specimens (Inner diameter of 70 mm with a maximum specimen height of 115 mm)	66

3.25 Acrylic Permeameter Cups with Compacted Specimens	67
3.26 Outflow Chamber Schematic (Inches)	68
3.27 Outflow chamber	68
3.28 Components of the permeameter system: (a) Permeameter Top Cap; (b) Linear Position Sensor	69
3.29 Linear Position Sensor	69
3.30 Detail of Hydraulic Rotary Union (Broadbent 2006, Figure 1.11)	71
3.31 Surcharge Pressure as a Function of G-level and Surcharge Mass	72
3.32 Machine Deflections	73
3.33 Height Changes in Soil Specimen during Centrifuge Test	74
3.34 Height Changes in Soil Specimen During Centrifuge Test Plotted with a Break Axis	74
3.35 Centrifuge Permeameter Data Sheet	77
3.36 Correlation Between Methodology to Verify Compaction Height and Ability to Compact to the Target Height	80
3.37 (a) Strobe Light (b) Image of Specimen During Test	82
3.38 Screen Shot of Windows Based Data Acquisition Program Acqlipse	83
3.39 Trimming Centrifuge Test Specimen to Obtain the Water Content Profile	85
3.40 Measurement of Slice Thickness Using the Vertical Dial Indicator	86
4.1 Free Swell Setup	88
4.2 Multiple Free Swell Setups	89
4.3 Swelling for a Free-Swell Test Conducted under a Total Stress of 250 psf	90
4.4 The Differentiation Between Primary and Secondary Swelling for a Free-Swell Test Conducted under and Total Stress of 250 psf	91
4.5 Primary and Secondary Swelling on an Arithmetic Scale	91
4.6 Free-swell Test on Eagle Ford Clay	93
4.7 Semi-log Plot of Free Swell Tests	93

4.8	Swelling of Swell Testing on Compacted Eagle Ford Clay Specimens Subjected to Range in Seating Loads	94
4.9	Final Void Ratio of Free Swell Specimens of Compacted Eagle Ford Clay Specimens Subjected to a Range in Seating Loads	94
4.10	Final Void Ratio of Free Swell Specimens of Compacted Eagle Ford Clay Specimens with the Same Height as Specimens Used in the Centrifuge (10-mm thick) and Specimens with the Same Aspect Ratio as Specimens Used in the Centrifuge	96
4.11	Swell Versus Time for Free Swell Specimens of Compacted Eagle Ford Clay Specimens with the Same Height as Specimens Used in the Centrifuge (10-mm thick) and Specimens with the Same Aspect Ratio as Specimens Used in the Centrifuge	97
4.12	1-G Infiltration Specimen Setup	98
4.13	1-G Infiltration Apparatus	98
4.14	1-G Infiltration Testing	99
4.15	(a) Final Void Ratio and (b) Swell Versus Total Stress for 1-G Infiltration Tests	100
5.1	Small Centrifuge Test Series on 30-mm thick Specimens with 20 mm of Pondered Water (modified from Plaisted 2009)	103
5.2	Small Centrifuge Test with Variable Specimen Heights at 200 G with 20 mm of Pondered Water (modified from Plaisted 2009)	104
5.3	Small Centrifuge Test Series with Variable Water Height (WH) on a 20-mm thick Test Specimen at 300g (modified from Plaisted 2009)	104
5.4	Series (o): Manual Swell Measurement for 30-mm thick Specimens with 20 mm of Pondered Water at 200 G	106
5.5	Series (o): Discrete Outflow Measurements for 30-mm thick Specimens with 20 mm of Pondered Water at 200 G	106

5.6	Series (o): (a) Displacement and (b) Swell for Centrifuge Tests Performed at 50 G on 20-mm and 10-mm thick Test Specimens with 30 mm of Ponded Water	108
5.7	Variability of Surcharge Pressure, Water Pressure, and Total Stress Applied Over the Profile with G-level in Series (i)	110
5.8	Trials for Constant Surcharge Pressure, Water Pressure, and Total Stress Applied Over the Profile with G-level in Ongoing Series (ii) in Comparison to Those in Series (i)	112
6.1	Measured Displacements for the 72 Hour Tests	115
6.2	Ratio of the Displacement of 20-mm thick to 10-mm thick Specimens after 72 Hours of Testing	115
6.3	Swell Versus Time for the 72 Hour Tests	116
6.4	Final Vertical Swell Versus G-level for 72 Hour Tests on 10-mm thick Specimens	116
6.5	Final Void Ratio Versus G-level for 72 Hour Tests on 10-mm thick Specimens	117
6.6	Swelling Versus Time for Specimens Tested for 72 Hours at 25, 50, and 100 G with a Water Pressure of 400 psf (20 KPa) Applied Over the Specimens	119
6.7	Void ratio Versus Total Stress for 10-mm thick Specimens with a Water Pressure of 400 psf (19 KPa) Applied Over the Specimens	120
6.8	Swelling Versus Total Stress for 10-mm thick Specimens with a Water Pressure of 400 psf (19 KPa) Applied Over the Specimens	121
6.9	Swelling Versus the Water Pressure Applied Over the Specimen with a Constant Surcharge Mass	122
6.10	Swelling Versus Time for Specimens Tested for 14 Days at 50 and 100 G with a Surcharge Pressure of 400 psf (20 KPa) and a Water Pressure of 400 psf (20 KPa) Applied Over the Specimens	124
6.11	Proportion of 72 Hour Swelling Versus Time for Specimens Tested for 14 Days at 50 and 100 G with a Surcharge Pressure of 400 psf (20 KPa) and a Water Pressure of 400 psf (20 KPa) Applied Over the Specimens	124

6.12 Swelling Versus Time Divided by the Square of the Height of Drainage for Specimens Tested for 14 Days at 50 and 100 G with a Surcharge Pressure of 400 psf (20 KPa) and a Water Pressure of 400 psf (20 KPa) Applied Over the Specimens	125
6.13 Proportion of 72 Hour Swelling Versus Time Divided by the Square of the Height of Drainage for Specimens Tested for 14 Days at 50 and 100 G with a Surcharge Pressure of 400 psf (20 KPa) and a Water Pressure of 400 psf (20 KPa) Applied Over the Specimens	125
7.1 Primary and Secondary Swelling in Free Swell Tests: (a) 250 psf; (b) 500 psf; (c) 1,000 psf; (d) 2,000 psf; and (e) 4,000 psf	129
7.2 Primary and Secondary Swelling for Free-Swell Tests: (a) Slope of Primary Swelling; (b) Slope of Secondary Swelling; (c) Proportion of Secondary Swell; and (d) Time of the Onset of Secondary Swelling	130
7.3 Comparison of the Slope of Secondary Swelling from Free Swell Tests to the Values of Saturated Hydraulic Conductivity Measured in Flexible-Wall Permeameter Tests	131
7.4 Primary and Secondary Swelling in 25 G Centrifuge Tests: (a) 500 psf; (b) 600 psf; (c) 800 psf; (d) 1,200 psf; and (e) 1,600 psf	133
7.5 Primary and Secondary Swelling in 50 G Centrifuge Tests: (a) 600 psf; (b) 800 psf; (c) 1,200 psf; and (d) 1,600 psf	134
7.6 Primary and Secondary Swelling in 100 G Centrifuge Tests: (a) 1,200 psf and (b) 1,600 psf	135
7.7 Primary and Secondary Swelling for Centrifuge Tests: (a) Slope of Primary Swelling; (b) Slope of Secondary Swelling; (c) Proportion of Secondary Swell; and (d) Time of the Onset of Secondary Swelling	136
7.8 Primary and Secondary Swelling in 1-G Infiltration Tests: (a) 600 psf; (b) 800 psf; and 1,200 psf	138

7.9 Primary and Secondary Swelling for 1-G Infiltration Tests: (a) Slope of Primary Swelling; (b) Slope of Secondary Swelling; (c) Proportion of Secondary Swell; and (d) Time of the Onset of Secondary Swelling	139
7.10 Primary and Secondary Swelling for 14 Day Centrifuge Tests on 10-mm thick Soil Samples	141
7.11 Primary and Secondary Swelling for 14 Day Centrifuge Tests on 20-mm thick Soil Samples	141
7.12 Primary and Secondary Swelling for 14 Day Centrifuge Tests: (a) Slope of Primary Swelling; (b) Slope of Secondary Swelling; (c) Proportion of Secondary Swell; and (d) Time of the Onset of Secondary Swelling	142
7.13 Primary and Secondary Swelling for All Tests: (a) Slope of Primary Swelling; (b) Slope of Secondary Swelling; (c) Proportion of Secondary Swell; and Time of Secondary Swell	145
7.14 Slope of Secondary Swelling Versus the Slope of Primary Swelling for All Tests	146
7.15 Primary and Secondary Swelling for All Tests: (a) Slope of Primary Swelling; (b) Slope of Secondary Swelling; (c) Proportion of Secondary Swell; and (d) Time of the Onset of Secondary Swelling	149
7.16 Time of Secondary Swelling Scaled by the Square of the Height of Drainage .	150
7.17 Swell versus the Square-root of Time for Free-Swell Tests	151
7.18 Swell versus the Square-root of Time for Centrifuge Tests: (a) 25 G; (b) 50 G; and (c) 100 G	152
7.19 Swell versus the Square-root of Time for 1-G Infiltration Tests	153
7.20 Swell versus the Square-root of Time for 14 Day Centrifuge Tests	153
7.21 The Slope of Primary Swelling in Root-Time Space in Terms of: (a) Total Stress and (b) Swell	154
7.22 The Slope of Secondary Swelling in Root-Time Space in Terms of: (a) Total Stress and (b) Swell	155

7.23 Swell Versus Time for Specimens Tested for 14 Days in Centrifuge and Free Swell Tests	156
7.24 Semi-log Plot of Swell Versus Time for Specimens Tested for 14 Days in Centrifuge and Free Swell Tests	157
7.25 Displacement Rate Versus Time for Specimens Tested for 14 Days in Centrifuge and Free Swell Tests	157
7.26 Water Content Profiles by G-level	160
7.27 Water Content Profiles by Time	161
7.28 Water Content Profiles by Time with Respect to Depth	162
7.29 Water Content Profiles for Long-term Tests	163
7.30 Cumulative Outflow Versus Time for 10-mm and 20-mm thick Specimens Tested for 14 Days in Centrifuge	164
7.31 Hydraulic Conductivity Versus Time for 10-mm and 20-mm thick Specimens Tested for 14 Days in Centrifuge	165
7.32 Final Void Ratio Versus Total Stress for Centrifuge Tests, Free Swell Tests and 1-G Infiltration Tests on 10-mm thick soil specimens with a Water pressure of 400 psf (19 KPa)	166
7.33 Swell Versus Total Stress for Centrifuge Tests, Free Swell Tests and 1-G Infiltration Tests on 10-mm thick soil specimens with a Water pressure of 400 psf (19 KPa)	167
7.34 Incremental Swell Profiles for Specimens Tested at 25, 50, and 100 G with a Water Pressure of 400 psf (20 KPa) Applied Over the Specimens	168
7.35 Incremental Swell Profiles for Specimens Tested at 400, 800, and 1,200 psf with a Water Pressure of 400 psf (20 KPa) applied over the Specimens	169
7.36 Incremental Swell Analysis Steps for specimens flown for 72 hours at 50 G with a water pressure of 400 psf and surcharge pressure of 800 psf	171

7.37	The Relationship between Swell and Effective Stress as Measured in the Centrifuge Permeameter (10-mm thick Specimens Tested at 25, 50, and 100 G with a Water Pressure of 400 psf (20 KPa) Applied Over the Specimens) . . .	172
7.38	Various Pore Water Pressure Assumptions	173
7.39	The Relationship Between Swell and Effective Stress as Measured in the Centrifuge Given Various Assumptions as to the Pore Water Pressure Distribution in the Soil Specimen	174
7.40	(a) Total Stress and (b) Effective Stress at Mid-depth for a 10-mm thick Soil Sample Given a Linear Loss in Pore Water Pressure with Depth	176
7.41	(a) Total Stress and (b) Effective Stress at Mid-depth for a 20-mm thick Soil Sample Given a Linear Loss in Pore Water Pressure with Depth	177
7.42	The Relationship Between Swell and Effective Stress as Measured in the Centrifuge Given Various Assumptions as to the Pore Water Pressure Distribution in the Soil Specimen	181
7.43	Generic Saturation and Hydraulic Conductivity Functions for an Expansive Clay	186
7.44	Moisture Front Progression during Free Swell	188
7.45	Moisture Front Progression During Infiltration	188
7.46	Moisture Front Progression During Infiltration in an Accelerated Gravity Field: (a) 25 G; (b) 50 G; and (c) 100 G	189
A.1	(a) Final Void Ratio and (b) Swell for Measurements Taken with a Vertical Dial Gauge (VDG) and in-flight Linear Position Sensor (LPS)	199
A.2	Ratio of Final Void Ratio Determined from Vertical Dial Gauge (VDG) Measurements to the Final Void Ratio Determined from in-flight Linear Position Sensor (LPS) Measurements	200

A.3 Ratio of Swell Determined from Vertical Dial Gauge (VDG) Measurements to the Final Void Ratio Determined from in-flight Linear Position Sensor (LPS) Measurements 200

Chapter 1

Overview of Research Study

1.1 Introduction

The volumetric changes undergone by expansive clays due to changes in moisture content can cause significant damages to structures built on them. Because of the prevalence of expansive clays in certain regions, building upon them may be unavoidable and thus the design engineer is in need of an expeditious manner to evaluate the swell potential of expansive clays for design purposes. Expansive clays are very common in Central and Eastern Texas where design and construction of roadways often take place on such soils. Roadways constructed on expansive clay subgrades are often damaged as the result of significant volumetric changes that occur when such soils undergo cycles of wetting and drying. These volumetric changes induce vertical movement of the roadway surface, accelerate the degradation of pavement materials, and ultimately shorten the service life of the roadway.

Proper characterization of expansive clays is required for the design and remediation of roadways constructed on poor subgrade materials. Current methods for characterization of expansive clays, however, do not properly replicate field conditions, require excessive time for testing, and often rely on the measurement of index properties rather than on the direct measurement of soil swelling. An alternative method of characterization is proposed in this

dissertation involving the use of a centrifuge. In this method, water is infiltrated into a expansive clay under an increased gravity field in a centrifuge.

In the summer of 2006, The University of Texas at Austin acquired a state-of-the-art centrifuge permeameter. This centrifuge permeameter was designed to provide an alternative method of characterizing the hydraulic properties of soils. This centrifuge permeameter is unique amongst geotechnical centrifuges since, while it operates at high rotational velocities (i.e. 900 RPM or 500 G at the base of a sample), it has a fully operation data acquisition system for in-flight monitoring as well as precise control of influx, which makes it ideal for the hydraulic characterization of soils.

The solid-state data acquisition system was used as part of this dissertation to measure the specimen height of and outflow rates from compacted clays during infiltration and subsequent swelling. A low-flow hydraulic rotary union was used to control the flow rate of water into the permeameter and provided in-flight control of the water level above the soil specimen during testing (Section 3.2).

For this research study, the objectives are as follows: (i) To develop a laboratory testing procedure in which a centrifuge permeameter is used to evaluate the swell potential of expansive clays; (ii) To compare the results of centrifuge tests with those of traditional swell testing; and (iii) To provide insight into the long-term mechanisms of swelling under conditions of infiltration and submersion. A schematic of the testing setup used for characterizing the swell potential of expansive clay is shown in Figure 1.1. In this setup, water is ponded above a soil specimen spinning around a central axis, inducing a high G-level environment that accelerates the flow of water through the expansive clay.

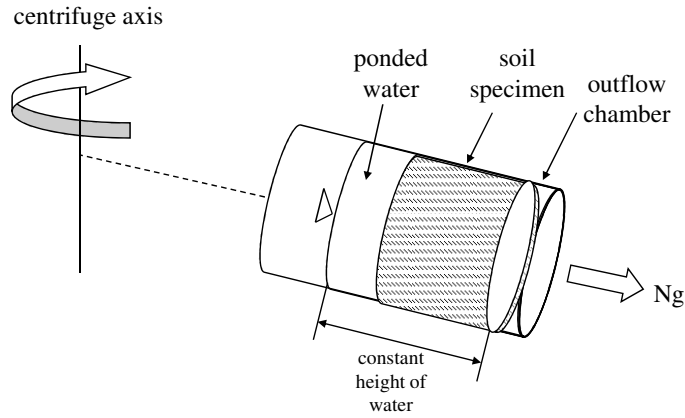


Figure 1.1: Centrifuge Testing Setup for the Characterization of Swelling Clays

1.2 Motivation

The motivation for using the centrifuge permeameter to study the swelling of expansive clay is to provide a testing method that accelerates the experimental measurement of swelling. In traditional free-swell tests on expansive clays, the rate of swelling may still be significant at the time at which the test is stopped. Accordingly, the amount of swelling measured in a free-swell test may be less than the amount of swelling the soil may undergo given an adequate amount of time or when placed under different boundary conditions. Since, specimens are submerged in free-swell test, capillarity largely drives the flow of moisture into the specimen. In the centrifuge, an infiltration process is performed where capillarity is accompanied by a greatly accelerated gravitational field in driving the flow of moisture into the specimen. It is thought that the process of infiltrating water into an expansive clay in an accelerated gravitational field will thus accelerate the swelling of expansive clays and lead to a quicker method of testing. Since the process of measuring the swelling of expansive clays may be accelerated through the use of a centrifuge, this expedited method may encourage the use of experimentally measured swelling data over the use of empirical correlations for swelling based on index properties.

1.3 Scope of Research

The objectives of this study are listed with the corresponding tasks for achieving them.

A) To develop a laboratory testing procedure in which a centrifuge permeameter is used to evaluate the swell potential of expansive clay. This objective was achieved by:

A.1 Reviewing traditional methods of evaluating the swell potential of expansive clays.

A.2 Reviewing the use of centrifuge testing in geotechnical engineering for the measurement of the swelling of expansive clay.

A.3 Determining the time required for soil specimens of varying heights to reach a state of equilibrium at varying G-levels.

A.4 Evaluating the progression of a wetting front over time in a soil specimen during the swelling process at varying G-levels.

A.5 Evaluating the effect of water pressure and surcharge pressure on the swell of a soil specimen at varying G-levels.

A.6 Establishing a set of specimen heights, G-levels, water heights, and surcharge pressures over which swelling tests should be conducted in the centrifuge.

B) To relate the results of centrifuge tests with traditional swell tests. This objective was achieved by:

B.1 Determining the relationship between swell and effective stress using the traditional testing techniques.

B.2 Evaluating incremental swelling in the soil specimen profile at the end of testing through specimen dissection.

B.3 Evaluating the pore water pressure profile in a centrifuge specimen given the relationship between swell and effective stress established using traditional testing and the incremental swelling measured at the end of centrifuge testing.

B.4 Determining the relative advantages and disadvantages of using a centrifuge permeameter to evaluate the swell potential of expansive clay.

C) To provide insight into the long-term mechanisms of swelling under conditions of infiltration and submersion. This objective was achieved by:

C.1 Evaluating primary and secondary swelling rates in traditional free-swell testing, 1-g infiltration testing, and centrifuge infiltration testing.

C.2 Evaluating long-term swelling rates in traditional free-swell testing and centrifuge infiltration testing.

1.4 Organization

A background on centrifuge testing of expansive clay is presented in Chapter 2 of this dissertation. The materials and methods used in the experimental testing program are covered in Chapter 3. Results from tests that compliment the testing done in the centrifuge are presented in Chapter 4. Results from the centrifuge testing program conducted in the centrifuge permeameter are presented in Chapter 5. An analysis of the results of centrifuge and complimentary testing is then presented in Chapter 7. Finally, conclusions drawn from the study are presented in Chapter 8.

Chapter 2

Background on Swell Testing of Expansive Clays

Compacted expansive clays are commonly used in engineering applications such as hydraulic barriers. They are also increasingly being used as an alternative backfill material for earthen structures. This is the case in many regions of the United States, such as Texas, where conventional backfill materials (e.g. granular soils and non-expansive clays) are not readily available or are too expensive to transport to a construction site. While there is an abundance of literature concerning the swelling of expansive clay, very little research can be found concerning the measurement of the swelling of expansive clays during infiltration. In traditional testing techniques, clay specimens have been tested in a consolidation frame where the soil specimens are submerged in water. Infiltration tests have, however, typically not been performed to measure the swell potential of expansive clay because of the excessive time requirements. It could, however, be argued that infiltration testing is more representative of field conditions. The centrifuge presents a testing setup in which infiltration tests can be conducted on clay specimens within a reasonable amount of time.

In this assessment of existing information the following subjects are covered: (1) Test

methods for evaluating the swell potential of expansive clay; (2) Predictive swell models for the swell potential of expansive clays; and (3) Field studies for swelling of compacted clays in the field under flooding conditions.

2.1 Test Methods for Evaluating the Swelling Potential of Expansive Clays

Several test methods exist for evaluating the swell potential of expansive clays, five of which are discussed here. The first method discussed is the American Society of Testing and Materials (ASTM) standard for the evaluation of the swelling of cohesive soils using traditional one dimensional oedometer equipment. The second method is the conventional version of the Potential Vertical Rise (PVR) method, which is a popular method in Texas that uses index properties of the soil and the overburden pressure to predict swell. The third method is a recently proposed revision to the PVR method which includes a model for predicting swelling as a function of time. The fourth method presented here involves the cyclical wetting and drying of expansive clays to determine their potential for volumetric change. The fifth and final method to be discussed is the use of a centrifuge to study the swell potential of expansive clays.

2.1.1 Traditional Methods for Evaluating the Swelling Potential of Expansive Clays

The traditional test method for evaluating the swell potential of expansive clay involves use of the same one-dimensional oedometer conventionally used in incremental vertical-flow consolidation (Figure 2.1). There are several variations of the testing procedure which are detailed in ASTM D4546, “Standard Test Methods for One-Dimensional Swell or Collapse of Cohesive Soils.” The general setup for these tests is similar to traditional incremental consolidation testing in that a specimen is placed into a ring and sandwiched between two

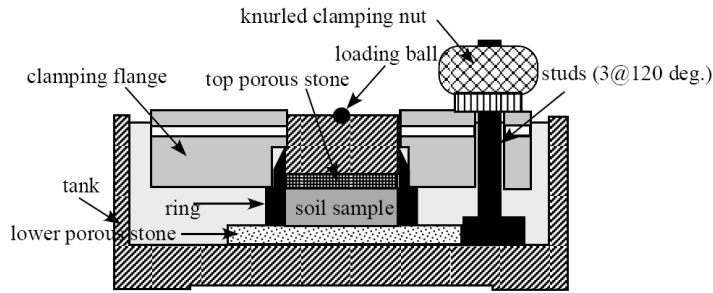


Figure 2.1: Fixed-Ring Consolidation Cell (Olson 2007)

porous stones that are protected from clogging by filter paper. The ring is then fixed into a water tank by a clamping flange and a series of knurled clamping nuts. A load is placed on the top porous stone to confine the soil specimen and the test is then started by filling the consolidation cell with water.

The three methods reported in ASTM D4546 differ on the number of tests performed for each method and the number of loading sequences in each method. In the first method, Method A, four or more tests are run at different vertical stresses on “identical” specimens. Method A is referred to as “wetting-after-loading tests on multiple specimens.” In Method B, only one specimen is tested, but the vertical stress used in testing is representative of the anticipated effective stress in the field or alternatively to a vertical stress of 1 kPa (20 psf). Method B is referred to as “single point wetting-after-loading test on a single specimen.” Method C is an extension of test Methods A and B in which the swelled or collapsed specimen is then loaded to study its consolidation response. Method C is referred to as a “loading-after-wetting test.” For a swelling soil, Methods A and B have been broadly referred to as “free-swell” tests as the soil is given the opportunity to swell with ready access to water. The results of the test methods detailed in ASTM D4546 can be used to predict the wetting-induced heave or settlement of a soil. The results can also be used to determine the load necessary to prevent such heave from occurring.

Some aspects of the testing method that are discussed in this standard include the measured swell/collapse, the ultimate degree of saturation, the time for swelling to occur,

and “secondary swelling.” The measured swell/collapse are reported to be at the upper bound of the swell/collapse observed in the field. The ultimate degree of saturation in swell/collapse tests is reported to be between 90 and 95%, which is noted to be higher than expected in the field where soil is typically not inundated with water. The time for swell/collapse to occur in the laboratory may be different than that in the field due to non-representative soil samples, nonuniform wetting, and soil variability.

In the standard, it is suggested that the slope of swelling versus the log of time can be used to predict “secondary swelling.” A figure is presented in the standard showing the differentiation of primary and secondary swelling (Figure 2.2). The tangential constructions used to differentiate primary and “secondary swelling” appear similar to Casagrande’s tangential constructions used to differentiate primary and secondary consolidation. There is, however, no guidance given by the standard as to what secondary swelling is and as to why the ultimate degree of swelling should be based on this log-linear trend.

The concept of secondary swell has been reported in the literature (Chen 1965, Haynes and Mason 1965, Allen and Gilbert 2006). Laboratory swell data from Haynes and Mason (1965) in which secondary swelling is clearly identified by the author is shown in Figure 2.3. Haynes and Mason state that their soil samples had not reached an equilibrium condition within the testing time of seven days. Haynes and Mason reported a factor P_s , which is the percent of total swelling corresponding to secondary swelling and noted that “Secondary Swell” is the name given to swelling that occurs after primary swelling.

An extensive number of swell tests were conducted by Woodward-Clyde-Sherard and Associates on an expansive clay from San Diego, California (Gizienski and Lee 1965). The results of these tests on expansive clays from San Diego are shown in Figure 2.4. For this particular soil, the optimum water content for standard proctor compaction was 10.5 percent. The measured swell is plotted as a function of the dry density and trend lines were drawn to approximate constant compaction water contents. The swell tests conducted as part of this series were conducted under a surcharge load of 160 psf. The significance of these tests is that they demonstrate the general effects of dry density and compaction water

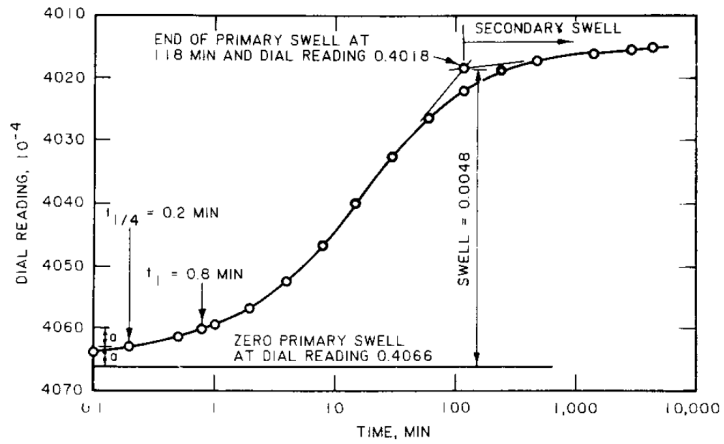


Figure 2.2: Differentiation between Primary and Secondary Swelling (ASTM D4546)

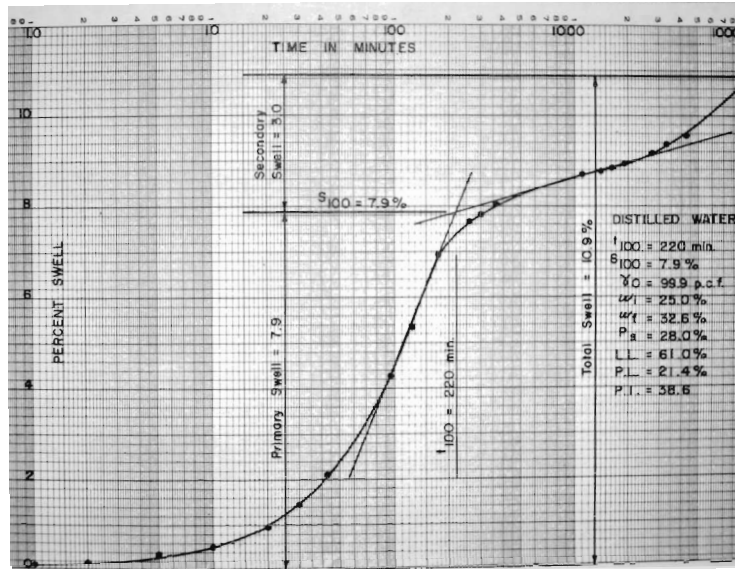


Figure 2.3: Secondary Swelling (Haynes and Mason 1965)

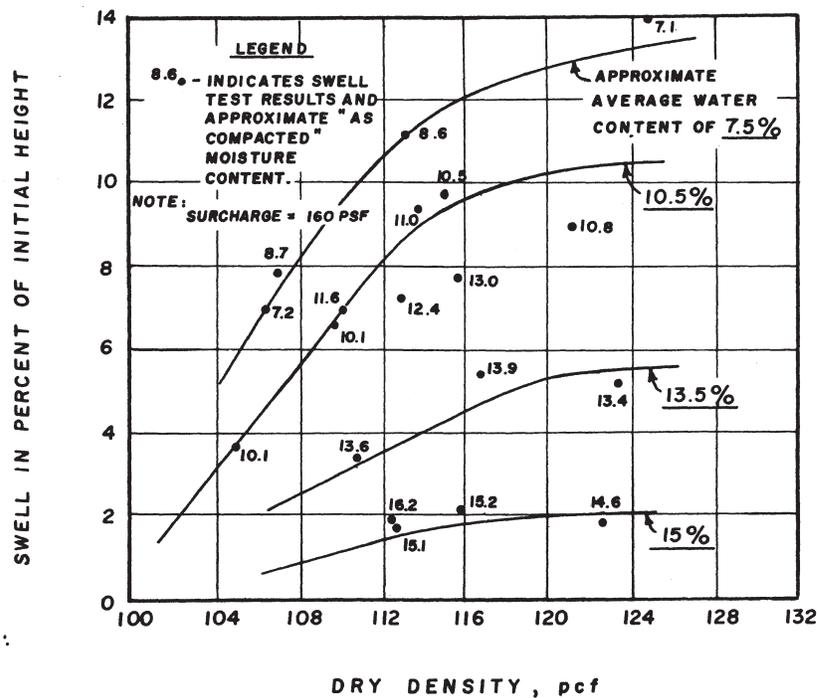


Figure 2.4: Swell as a Function of Dry Density and Compaction Water Content for a Expansive Clay from San Diego, California (Gizienski and Lee 1965)

content on the swell potential of a expansive clay. Furthermore, these test were conducted as a part of an evaluation of the potential swelling of small scale field tests, which is discussed in Section 2.3. At the optimum water content, a dry density of 115 pcf could be achieved. The tests series from Woodward-Clyde-Sherard and Associates shows an increase in swell potential with increasing compaction dry density and decreasing compaction water content. These tests show that within the range of compacting dry densities, the effect of compaction water content on swelling is more relevant than the effect of dry density on swelling.

2.1.2 The Potential Vertical Rise (PVR) Method

The potential vertical rise (PVR) method is a predictive design procedure that was originally proposed by Chester McDowell in 1956. In this procedure, the plasticity index of the soil and the field loading are used to the predicted vertical rise. The method correlates the

plasticity index of a soil with the predicted volumetric change (Figure 2.5). This correlation is based on laboratory swell testing of three test soils under capillary adsorption (McDowell 1954). The soils were remolded prior to testing and were sampled in Guadalupe County, Texas. The testing setup for the capillary adsorption is shown in Figure 2.7. In accordance with the capillary adsorption method described by McDowell (1954) a specimen was placed atop a water reservoir allowed to swell while drawing water by capillary rise for a minimum period of 10 days. For specimens with plasticity indexes exceeding 15, a period of time equivalent, in days, to the plasticity index was proposed. The percent volumetric change was then corrected for the overburden pressure to yield a predicted vertical rise (Figure 2.6). Finally, the percent volumetric changes was converted to a linear swell using the relationship shown in Figure 2.8.

The procedure for determining the Potential Vertical Rise is covered in Tex-124-E. The procedure does, however, present modifications of the original figures presented by McDowell without additional data. In the version of Figure 2.5 presented in Tex-124-E, the chart is expanded to a plasticity index of 140 and a percent volumetric change. The trend lines presented by McDowell (1956) are then extrapolated across this range. No additional data points are presented for the extrapolated range presented in Tex-124-E, which is outside of the range originally intended by McDowell. Accordingly, in presenting the steps involved in calculating the PVR of a soil, the original figures as presented by McDowell (1956) are used instead of those presented in Tex-124-E.

The steps involved in calculating the PVR are as follows:

1. Divide the substrate of interest into 0.6 m [2 ft] layers
2. Determine the average total stress (termed “average load” in Tex-124-E) in each layer assuming a bulk density of 19.7 KN/m^3 [125 lb/ft^3]
3. Calculate the “dry condition” for each layer as two-tenths the liquid limit of that layer plus nine
4. Calculate the “wet condition” (termed “optimum condition” in Figure 2.5) for each

layer as 0.47 times the liquid limit of that layer plus two

5. Given the plasticity index for each layer, calculate the percent volumetric change (PVC) from Figure 2.5 by interpolating between “dry conditions” and “optimum conditions” based on the measured water content for the layer. This is the percent volumetric change for a surcharge of 6.9 kPa (1psi).
6. Calculate the percent free swell (PFS), as: $PFS = (PVC) \cdot 1.07 + 2.6$.
7. Calculate the percent volumetric change at the top and bottom of each layer from Figure 2.6. The load should be the total stress at the top and bottom of each layer. The family member curves correspond to the percent free swell calculated in the previous step.
8. Calculate the difference between the percent volumetric change at the top and bottom of each layer. This is the PVR for that layer.
9. If the bulk density of the soil was measured, the PVR for the layer is multiplied by the ratio of the measured bulk density to the assumed bulk density.
10. If, for the layer, the percent passing the #40 sieve exceeds 25%, the PVR for the layer is multiplied by the percent passing the #40 sieve.
11. Calculate the PVR for subsequent layers until the PVR for a layer becomes negligible.
12. Sum the calculated PVR values for each layer to determine the total PVR (termed the “PVR for the site” in Tex-124-E).

In a report published nine years later than McDowell 1956, McDowell revisited the PVR method and recounted the principal factors affecting the PVR and set forth a list of recommended procedures for mitigating the damage (McDowell 1965). Additionally, McDowell presented two case histories in which structures designed using the PVR methodology were found to have “high satisfactory performance,” presented a case history in which ponding

was used to increase the moisture content of a clay subgrade prior to construction, and suggests that the use of ponding may become more prevalent in the future.

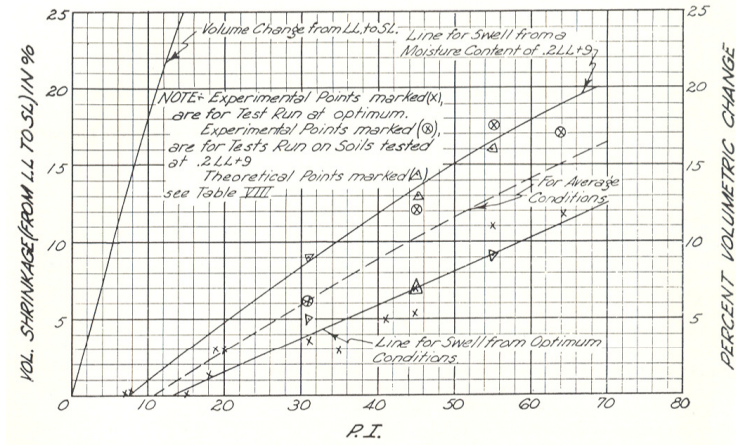


Figure 2.5: Percent Volumetric Change Versus Plasticity Index (McDowell 1956)

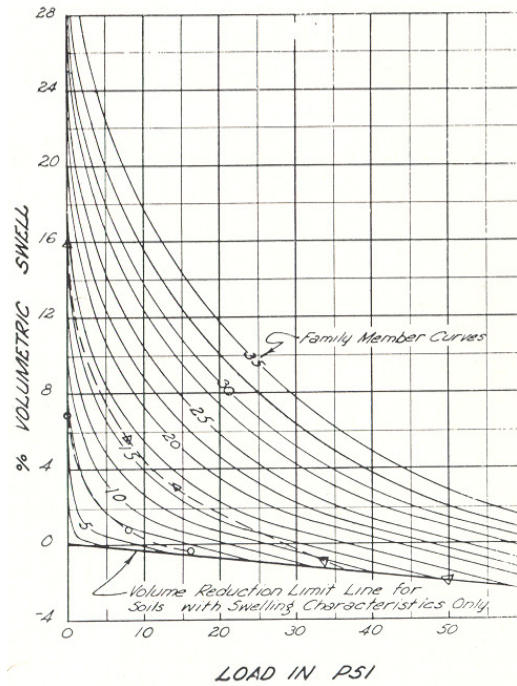


Figure 2.6: Potential Vertical Rise Versus Load as a Function of the Percent Volumetric Swell (McDowell 1956)

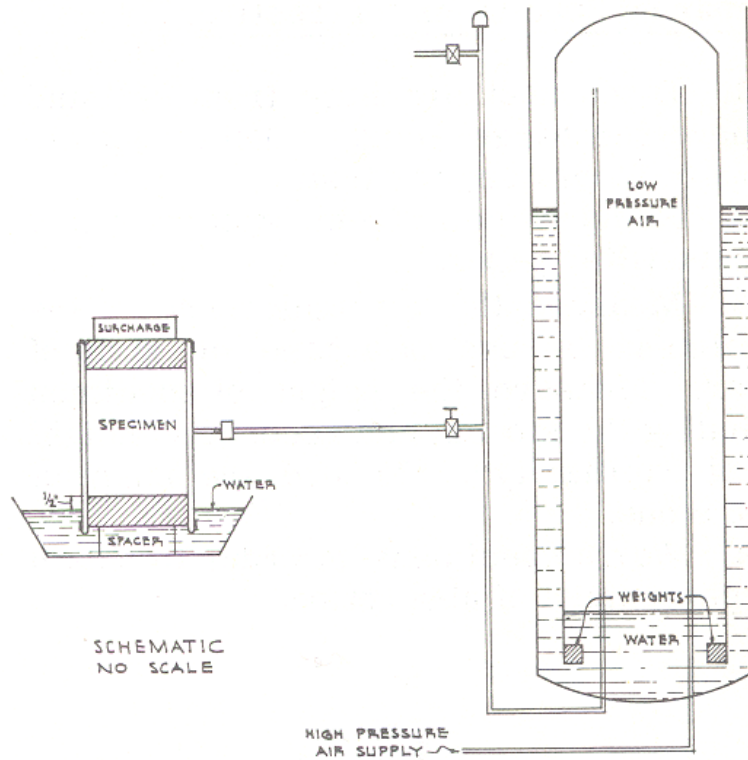


Figure 2.7: Testing Setup for Capillary Swell Test (McDowell 1954)

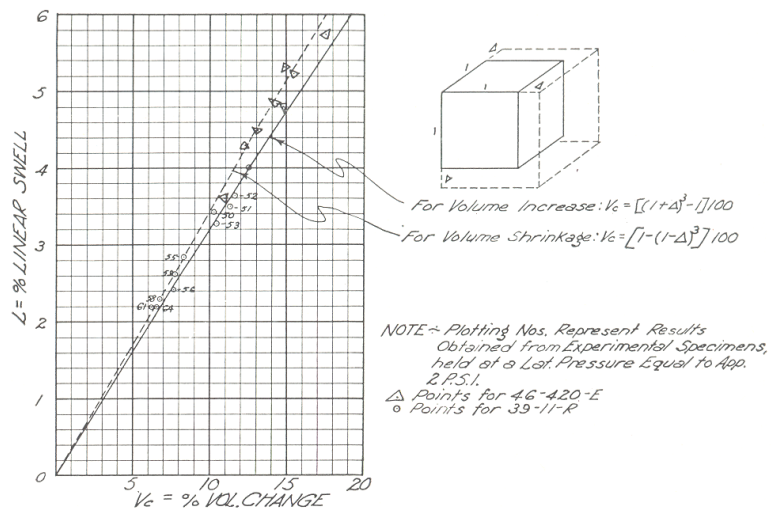


Figure 2.8: Linear Swell Versus Volumetric Swell (McDowell 1956)

Several case studies exist in the literature in which sufficient information was available to conduct a PVR analysis (Allen 2007). Comparison of PVR prediction with observed field results showed that in many of the cases the PVR method over predicted the vertical rise that would occur in the field (Figure 2.9).

There are several questionable aspects of McDowell's PVR method. Firstly, the method is based on a small number of tests in which all of the samples were remolded. Additionally, the minimum water content used for testing was two tenths of the liquid limit plus 9. Accordingly, no tests were conducted on soils at initially low water content. Finally, the method has been extrapolated (Tex-124-E) to plasticity indexes of 140, which is outside the range of testing. Despite these limitations, the method has been used by TxDOT for approximately fifty years throughout the state of Texas before being reconsidered by project TxDOT 0-4518 which concluded in 2005.

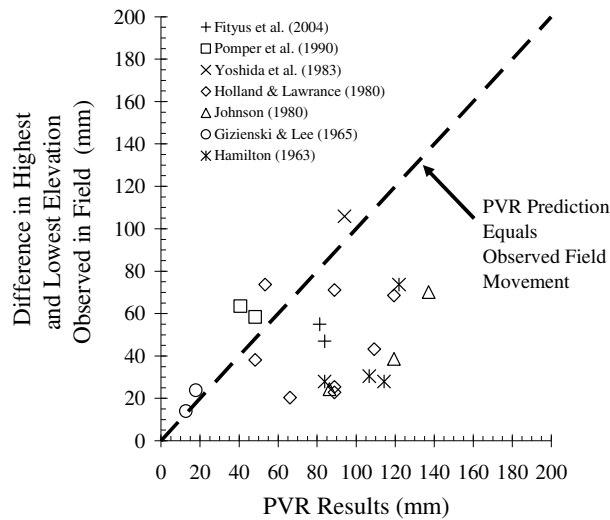


Figure 2.9: Observed Field Movements Versus Movements Predicted Using the Potential Vertical Rise Method (Allen and Gilbert 2006)

2.1.3 The Revised Potential Vertical Rise Method Revisited (Tx-DOT 0-4518)

The potential vertical rise (PVR) method as proposed by Chester McDowell in 1956 was revisited in 2005 as part of TxDOT project 0-4518. The intention of this project was to resolve issues of over-prediction associated with the use of the original PVR method. In project 0-4518, Lytton et al. (2005) proposed a model for moisture movement based on a diffusion analysis and a model for volumetric change based on changes in suction. The project reviewed the basic assumptions of the existing PVR methodology and suggested an alternative procedure for evaluating PVR.

In this revised PVR methodology, an evaporation experiment is conducted in order to determine the diffusion coefficient of a soil. The diffusion analysis is then used to predict changes in suction with time. Based on modeled spatial changes in suction, volumetric changes in the soil are predicted for one-dimensional profiles of soil and the potential vertical rise is estimated. The swelling of a soil is calculated by using the correlation established by Covar and Lytton (2001) presented in Section 2.2.2. This correlation is based on the liquid limit, plastic limit, cation exchange capacity, coefficient of linear extensibility, percent passing 2 μm , and percent passing the number 200 sieve.

In order to establish the variation of swelling with space and time, a new laboratory procedure was proposed as part of this project in order to estimate the diffusion coefficient. The setup of the diffusion experiment used to determine the diffusion coefficient, α , is shown in Figure 2.10. A specimen of expansive clay is first extracted from a Shelby tube. Holes are then drilled along its length for the placement of thermocouple psychrometers. The specimen is then wrapped in aluminum foil and placed inside of Styrofoam in a vertical tube that has one end sealed. Finally, the specimen is placed in a temperature controlled environment with the sealed end facing down and suction is monitored along the soil specimen's length as evaporation occurs from the open end of the specimen. The experiment is analyzed by first plotting the soil suctions measured during the experiment versus the log of time as shown in Figure 2.11. Then, the measured suctions values at the boundaries and the geometry of the

soil specimen are input into a MATLAB program written by the researchers (alphadrytest and drytest) and an α coefficient is determined by fitting the diffusion relationship to the measured values of suction. The authors ask that this soil diffusion coefficient be reported to the nearest seven decimal places. The authors do not justify why so many significant digits are necessary for their procedure.

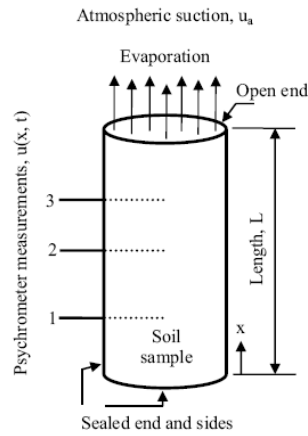


Figure 2.10: Schematic of Laboratory Setup for Diffusion Experiment (pg. 43 of V.2)

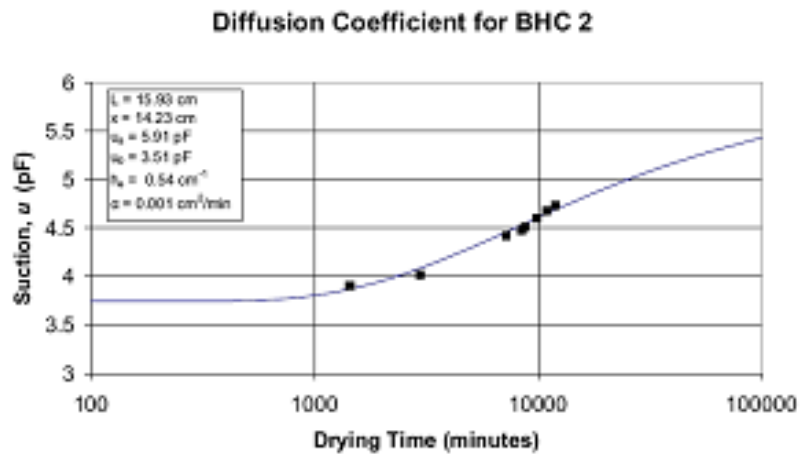


Figure 2.11: Suction Log-time Plot for Determination of the Diffusion Coefficient α (pg. 60 of V.2)

As shown in the suction versus time data plotted in Figure 2.4, data are only plotted for times between 1,000 and 10,000 minutes. It is unclear as to why data is not plotted for earlier or later time periods. The results also show that the model does not appear to fit the observed data very well. For times greater than 10,000 minutes the predictive relationship indicates that suction should continue to increase. In order to verify this curve fitting methodology and the resulting predictive relationship, suction records at larger times would be needed.

As with any testing method, there are issues that arise with respect to the methods ability to measure the variables of interest and the methods repeatability. In the revisited version of the PVR method, an evaporation test is conducted in order to evaluate moisture movement. It should be noted that swelling occurs during a wetting process in the soil and that moisture movement during wetting and drying may differ substantially based on the hysteretic nature of the permeability of the soil. Furthermore, the method makes use of a diffusion coefficient. The use of a single diffusion coefficient value to express the rate of moisture movement may be a simplistic representation of the process of moisture movement. The representation of moisture flow may be a simplified one since the diffusion coefficient is based on a simplification of Richard's equation, the equation that expresses the relationship between head gradients and flow through an unsaturated soil.

The revisited PVR method also makes use of the slope of the soil water retention curve for determination of the α coefficient. As per the procedure the soil water retention curve is not necessarily measured and is instead determined from an empirical relationship. This analysis procedure is further complicated by the fact that the diffusion coefficient is based on the volumetric change coefficient which is not determined experimentally but rather based on a set of correlations. The correlations for the volumetric change were established by Covar and Lytton (2001), which is presented in Section 2.2.2. Again, this correlation is based on the liquid limit, plastic limit, cation exchange capacity, coefficient of linear extensibility, percent passing 2 micron, and percent passing the number 200 sieve. Unfortunately, this method does not use direct measurements of volumetric change in order

to predict the swelling of the soil.

2.1.4 Cyclical Wetting and Drying

In a traditional swell test, as described in Section 2.1.1, a normal pressure is applied to a compacted soil specimen which is then inundated with water. The change in height of the soil is then measured with time to determine the swell potential of the soil. In the field, however, an expansive clay may undergo cycles of wetting and drying that cause the soil to alternately swell and shrink. Chen (1965) reported that clays undergo less swelling with each subsequent cycle of wetting and drying. The swell of a soil sample tested is plotted versus the number of cycles of wetting and drying in Figure 2.12. From the first cycle to the sixth cycle, the percent swell decreases from approximately 4.4% to 2.5%. Chen states that the samples were subjected to full swelling in the consolidometer prior to being dried back to its initial moisture content. No information is presented as to how long the samples took to reach this state of full swell nor the criteria used to determine when the specimen is fully swollen. This point is investigated in this dissertation and is reported in Section 7.2.

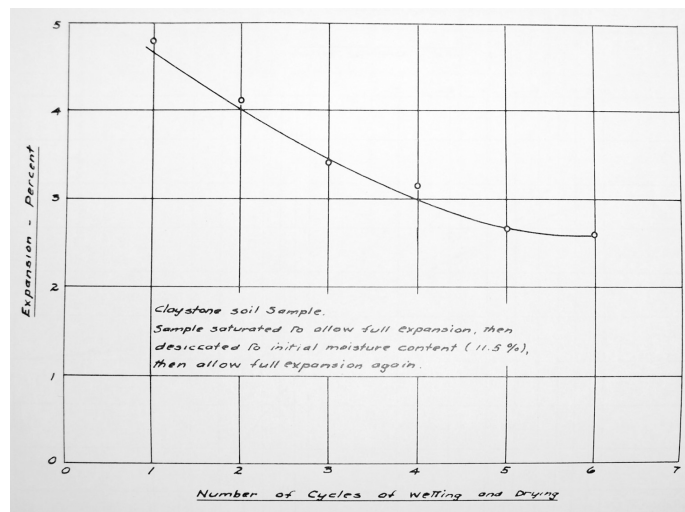


Figure 2.12: Fatigue of Swelling (Chen 1965)

The greatest limiting factor to studying the cyclical wetting and drying of a clay is

the amount of testing time required. As is evidenced in Section 4.1, a period of two weeks to a month can be required for a soil specimen to approach its ultimate height at varying values of total stress for an expansive clay. Disregarding this limitation on the time required for swelling to occur, both heating and forced air have been used to accelerate the drying cycle in studies aimed at better understanding cyclical wetting and drying. Tripathy et al. (2002) used an insulated oedometer that was raised to approximately $40^{\circ}C$ [$104^{\circ}F$]. The equilibrium relationship between void ratio and water content produced by Tripathy et al. for a series of surcharge pressures is presented in Figure 2.13.

Like Tripathy et al (2002), Allen and Gilbert (2006) designed a testing procedure in which the drying phase is accelerated. Unlike Tripathy et al., the specimens were dried out with forced air at the end of swelling. Unlike in Chen (1965) the drying phase was not stopped when the soil reached its initial moisture content but was continued until the end of primary shrinkage. At this point, the soil specimen is again submerged in water and swelled. This process was repeated until the height changes of the soil specimen were found to remain consistent over subsequent cycles. During this testing procedure, the water content of the soil specimen was determined by the removal of the soil specimen from the oedometer apparatus to determine its mass. Accordingly, the water content at the beginning and ending of each wetting and drying cycle was determined and can be plotted versus the height of the soil specimen as shown in Figure 2.14. Given this testing procedure, the engineer need only determine the changes in water content that incremental layers in a clay substrate will typically undergo in order to determine the changes in height that the soil profile will undergo. The changes in water content that these incremental layers in a clay substrate will typically undergo can be determined if representative historical boring logs are available.

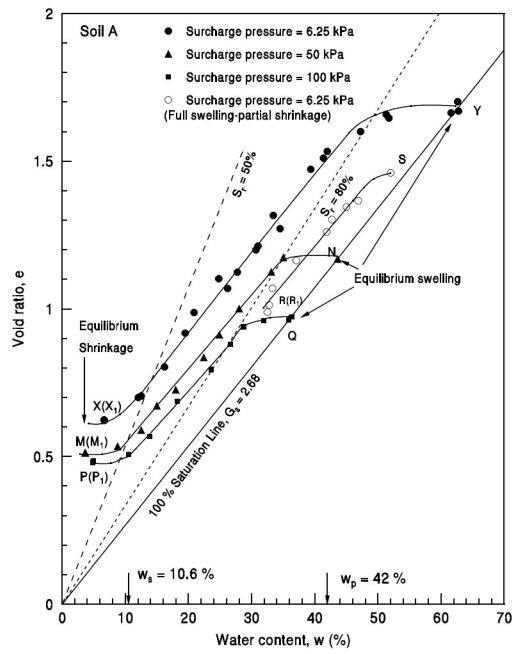


Figure 2.13: Height of an Expansive Clay Specimen (Tripathy et al. 2002)

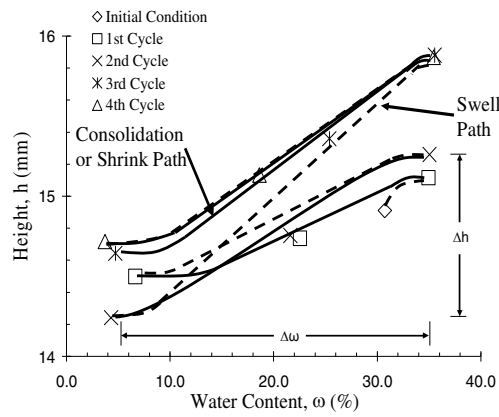


Figure 2.14: Height of an Expansive Clay Specimen During Cyclical Wetting and Drying Using Forced Air (Allen and Gilbert 2006)

2.1.5 Centrifuge Testing of Expansive Clay

The use of centrifuge technology for characterization of volumetric changes in expansive clay has been rarely documented in the literature. There are, however, a few studies that did address the swelling of compacted clay during infiltration in the centrifuge. To this respect, a study performed by Garde and Chanraskaran (1994) use the experimental setup shown in Figure 2.15. The principal difference between the testing setup of Garde and Chanraskaran and the testing setup used in this dissertation is the way in which the specimen is wetted. In Garde and Chanraskaran’s testing setup the base of the base of the soil specimen is subjected to a positive pore water pressure. Accordingly, swelling of the soil specimen began at the base of the specimen and propagated up through the specimen over time.

Garde and Chanraskaran performed their centrifuge test on a 12.5-mm thick specimen of “fat clay” at 150 G. The change in height of the soil specimen during testing is shown in Figure 2.16. Similar to the laboratory setup used in this dissertation, a displacement transducer in conjunction with an electrical slip ring stack was used to monitor the height of the specimen over the course of the experiment. It is notable in this experimental study that the test was performed within a time period of 30 minutes and that the soil sample reached an ultimate swell of approximately 35% within that time period.

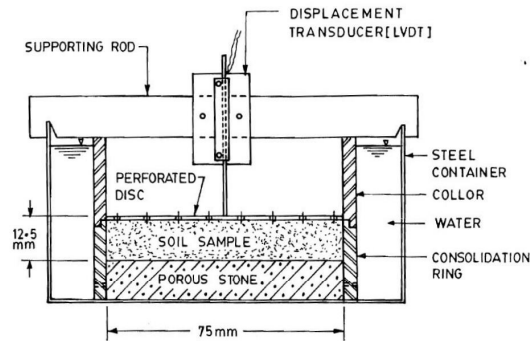


Figure 2.15: Garde and Chanraskaran (1994) Centrifuge Testing Setup

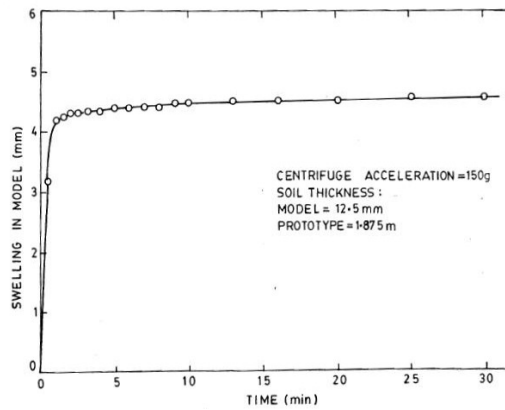


Figure 2.16: Swelling Versus Time in a Centrifuge, Garde and Charaskaran (1994)

A series of centrifuge tests on expansive clays was conducted by Frydman (1990). The boundary conditions in these tests were similar to those used in this research study. In Frydman's experimental setup, water was ponded atop a expansive clay from Israel, locally known as Mizra Clay. Frydman used a total of seven compaction layers and placed lead markers between each layer. At the end of testing the location of these markers was measured using a radioactive source and receiver. The percent swell for each layer is shown in Figure 2.17. Frydman conducted a large number of tests under G-levels ranging from 1 to 30. Frydman also varied the water pressure atop the specimen. Frydman does not, however, present the swelling profiles of these tests but rather shows the advancement of a wetting front with time through the testing profiles (Figure 2.18). From the results, it is evident that the general effect of increasing G-level was to increase the rate of advancement of the wetting front. It should also be noted that a higher water pressure atop the specimen lead to a faster advancement of the wetting front.

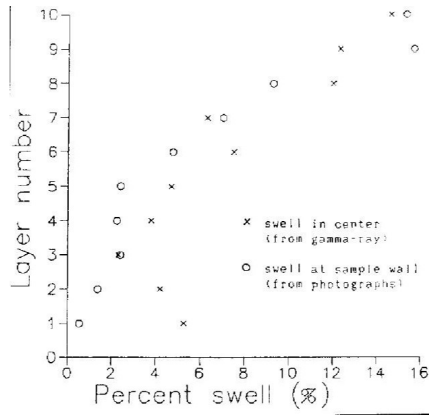


Figure 2.17: Percent Swell by Layer for an Expansive Clay Tested in the Centrifuge Under Ponding Conditions (Frydman 1990)

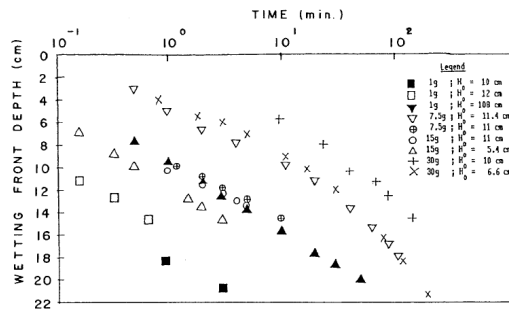


Figure 2.18: Wetting Front Depth Versus Time for Centrifuge Tests on Expansive Clay Under Ponding Conditions (Frydman 1990)

Other studies including Robinson et al. (2003) and Lee and Fox (2005) report on seepage consolidation in the centrifuge, but do not report swelling measurements in the centrifuge. Another study by Mitchell (1995) details the use of centrifuge testing for clay liner samples but again does not address swelling measurements in the centrifuge.

2.2 Predictive Models for the Swelling Potential of Expansive Clays

2.2.1 One Dimensional versus Three Dimensional Swelling

The amount of swelling measured in the laboratory depends on the boundary conditions under which the soil is tested. When swelling of a soil specimen is tested in a oedometer cell, it is constrained to move in only one dimension. When, however, a swell test is conducted in a triaxial cell, it is allowed to move in a three dimensional manner. A study comparing the measured vertical swell under oedometric loading conditions and triaxial loading conditions was performed by Al-Mhaidib (1999). The resulting vertical swell as a function of the applied pressure for oedometric testing and triaxial testing is shown in Figure 2.19(a). The ratio of triaxial swell to oedometric swell is shown in Figure 2.19(b) with respect to the applied overburden pressure. Based on the findings of this testing program, a ratio of 1/3 was found between the vertical swelling measured under triaxial and oedometric conditions. In the field, the conditions under which the soil specimen is constrained may allow for three dimensional expansions that will dictate the relationship between laboratory tests and the swelling observed in the field. Further investigation of this phenomenon by Al-Sharmrani (2004) revealed that this ratio between triaxial and oedometric swell decreases with increasing compaction water content and increasing applied pressure. Al-Sharmrani found that the ratio ranged between 0.30 to 0.66. Al-Sharmrani (2004) also found that the ratio between volumetric swell and vertical swell ranged between 0.40 and 0.78 with an average value of 0.57 for all of the tests conducted in their study. In a similar finding, Xiquan and Zhongwei (1984) conducted 40 bearing plate tests and found that this ratio to be 0.47 but recommended using a ratio of 0.6 (Olson 2007).

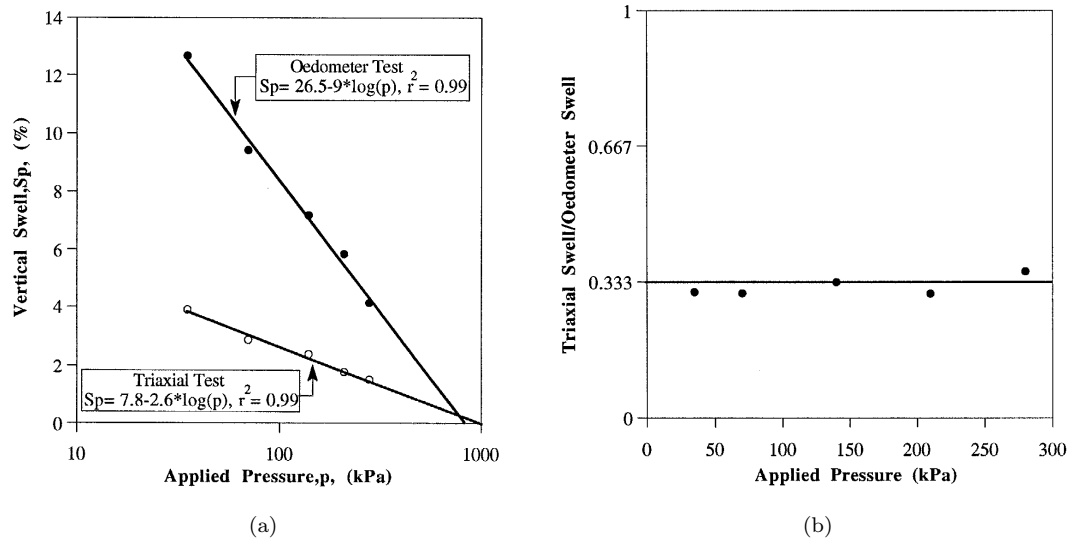


Figure 2.19: Comparison of Vertical Swell in Oedeometric and Triaxial Tests (Al-Mhaidib 1989)
 (a) Measured Swell Versus Overburden Pressure for Triaxial and Oedeometric Swell Tests
 (b) Ratio of Swell Measured from Triaxial Tests to Swell Measured From Oedeometric Tests Versus Overburden Pressure.

2.2.2 Correlations for Swell Potential

A series of correlations between soil properties and swell potential have been reported in the literature. A summary of these relationships is presented in Table 2.1, which is expanded from Arnold (1984). S is the predicted swell expressed in percent swell. The predictive relationships reported in Table 2.1 are compared with the results of free-swell and centrifuge testing in Section 7.7.

Table 2.1: Correlations from the Literature for Determining Swelling Potential, S (percent swell)

Properties	Correlation
McDowell (1956)	
Percent Finer than #40, In-Situ Water Content, Liquid Limit, Shrinkage Limit, Bulk Density, Sublayer Thickness, and Stress at the Top and Bottom of the Profile.	Chart Solution
Seed, Woodward, and Lundgren (1962)	
Plasticity index, PI	$S = 2.16 \cdot 10^{-3} \cdot PI^{2.44}$
Ranganathan and Satyanarayan (1965)	
Liquid limit, LL Shrinkage limit, SL	$S = 4.13 \cdot 10^{-4} \cdot (LL - SL)^{2.67}$
Nayak and Christensen (1971)	
Plasticity index, PI Clay content, C Initial water content, ω_0	$S = 2.29 \cdot 10^{-2} * PI^{1.45} \cdot \left(\frac{c}{\omega_0}\right) + 6.38$
Vijayvergiya and Ghazzalay (1973)	
Liquid limit, LL Dry unit weight, γ_d (pcf)	$\log(S) = \frac{1}{19.5} (\gamma_d + 0.65 \cdot LL - 130.5)$
Chen (1975)	
Void ratio, e Plasticity index, PI	$S = 0.2558 \cdot e^{0.08381 \cdot PI}$
Weston (1980)	
Liquid limit, LL Initial water content, ω_0 Effective stress, σ' (KPa)	$S = 1.95 \cdot 10^{-4} \cdot LL^{4.17} \cdot \omega_0^{-2.33}$ $S = 4.11 \cdot 10^{-4} \cdot LL^{4.17} \cdot \sigma'^{-0.386} \cdot \omega^{-2.33}$
Covar and Lytton (2001)	
Matric suction compression index, γ_h^* Initial and final water potentials, h_i and h_f Mean principal compression index, γ_σ^* Initial and final normal stress, σ_i and σ_f * See Covar and Lytton (2001)	$S = -\gamma_h \cdot \log_{10} \left(\frac{h_f}{h_i}\right) - \gamma_\sigma \cdot \log_{10} \left(\frac{\sigma_f}{\sigma_i}\right)$
Rao et al. (2004)	
Dry unit weight, γ_d (pcf) Initial water content, ω_0 Overburden pressure, q (kPa) Free swell index, FSI	$S = 4.24 \cdot \gamma_d - 0.47 \cdot \omega_0 - 0.14 \cdot q + 0.06 \cdot FSI - 55$

According to McDowell (1956) the principal factors that affect the PVR are as follows:

- Soil Type
- Moisture Content Fluctuations
- Density
- Sublayer Thickness
- Surcharge Load

McDowell accounted for the soil type in requiring the percent finer than #40, liquid limit, and shrinkage limit for the PVR procedure. Moisture content fluctuations in the soil are accounted for in the method by comparing the in-situ water content to the swell limit, calculated from the liquid limit, and the shrinkage limit, either measured or estimated from the liquid limit. The density of the soil was accounted for by a field measurement of bulk density and the sublayer thickness was based on field data. Finally, the stress at the top and bottom of the profile are estimated from the surcharge load and the bulk density of the soil. Accordingly, while many factors affecting the swell potential of a clay are considered in the PVR method, the pore water pressure and thus the effective stress in the soil is not considered. This was possibly because the relationship between pore water pressure and effective stress is extremely complicated for unsaturated soils and McDowell was presenting a generalized procedure.

More generalized relationships based on plasticity indices were presented by Seed, Woodward, and Lundgren (1962) and Ranganathan and Satyanarayan (1965). A relationship presented by Nayak and Christensen (1971) also considered plasticity indices but took the clay content and the initial water content of the soil into account. The plasticity indices were used again in a correlation by Vijayvergiya and Ghazzalay (1973) and the density of the soil was considered in terms of the dry unit weight of the soil. Additional relationships considering the plasticity indices were presented by Chen (1975), in which the initial void

ratio of the soil is considered, and Weston (1980), in which the initial water content of the soil was considered, were also presented in the literature.

More recent correlations presented by Cover and Lytton (2001) and Rao et al. (2004) are the first relationships presented since McDowell (1965) to consider the overburden pressure on the soil. In Cover and Lytton (2001), matric suction, normal stress, and the relationship between suction and compression were also considered. In Rao et al. (2004), an additional index property termed the free swell index (FSI) of the soil was also measured. The correlation between FSI and Swelling presented in Rao et al. (2004) is relatively poor and the procedure for measuring the FSI is not a standard index test.

2.2.3 Theories for the Swelling of Expansive Clays over Time and Space

A theory for the swelling of clay with time in which suction and effective stress were related with Bishop and Aitchison's "Chi factor," χ (Bishop and Aitchison 1961) was presented in Blight (1965). Blight presented an equation of the following form to relate swelling and change in pore water pressure:

$$\epsilon = C [\Delta\sigma_v - \Delta(\chi \cdot \mu_w)] \quad (2.1)$$

where ϵ is swell, C is the compressibility of the soil, σ_v is the total vertical stress, and u_w is the pore water pressure. Relationships were also presented for the relationships between gravimetric water content and suction, the coefficient of swelling and suction, and the effective stress parameter Chi and suction. Given these relationships, a finite difference flow and swell analysis was conducted. The results of using this technique will subsequently be discussed in Section 2.3.2 and can be seen in Figure 2.25.

Another theory for the swelling of clay with time is presented by Cover and Lytton (2001). In this technique, moisture movement and swell are separately quantified and then used in conjunction to calculate swelling with time and space. The testing techniques

for determining the diffusion coefficient is discussed in Section 2.1.3. The relationship for determining swell is presented in Section 2.2.2.

In another approach, measurements of the relationship between void ratio, net stress, and matric suction is conducted. Net stress is the difference between the total stress, σ and the pore air pressure, u_a . Matric suction is the difference between pore air pressure and pore water pressure, u_w . This relationship theoretically produces a constitutive surface as pictured in Figure 2.20. The problem with establishing a constitutive surface for a soil is the difficulty to characterize the surface. Accordingly, different approaches have been proposed in which relationships are measured separately and then combined to generate the constitutive surface. Furthermore, measuring the surface for an expansive soil is particularly difficult since the time required to establish the constitutive surface is time prohibitive.

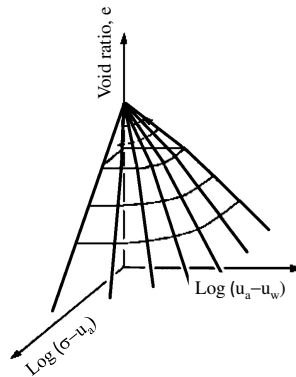


Figure 2.20: Void Ratio Constitutive Surface for An Unsaturated Soil (Modified from Fredlund and Rahardjo 1993 Figure 12.24)

2.3 Field Studies of the Swelling of Compacted Clays Subjected to Flooding Conditions

Field studies of the effects of flooding on the swelling of compacted clay are limited. Two large-scale studies are presented in this section. The study by Gizienski and Lee (1965) involves the measurement of the swelling of a 3.0 thick foot thick clay slab during swelling.

The study includes laboratory measurements of soil swelling and uses the results of laboratory testing to evaluate soil swelling in the field. The study by Blight and DeWet (1965) also includes the measurement of the swelling of a clay slab. In this study, however, a model is used to predict swelling over time.

2.3.1 Gizienski and Lee 1965

Field studies for swelling of compacted clays are rare because of the length of time required to conduct the studies. A relevant field study to this research program was conducted by Gizienski and Lee (1965). In this study, two 4 ft by 4 ft test slabs of compacted clay were constructed in Southern California. The clay was of medium plasticity with a plasticity index of 20 and a liquid limit of 40. The test sections were allowed to stabilize for one month after compaction at which point the site was flooded for a period of three months. The heave of each test section was measured throughout testing and is shown in Figure 2.21. The thickness of test slab “A” is 1.1 feet and the thickness of test section “B” is 3.0 feet. The swelling at the end of the flooding stage translated to 0.4 inches for the 1.1 foot thick slab and 0.9 inches for the 3.0 foot thick slab, or approximately three times as much swell for the section approximately three times thicker.

In an effort to calculate the amount of swelling expected in the field a series of laboratory tests were conducted to determine the effects of dry density and compaction water content on swelling. These results are discussed in Section 2.1 and shown in Figure 2.4. The tests from this test series that best approximate the field compaction conditions for the two sections are a compaction water content of 10.6% and a dry density of 113 pcf. The relationship between swell and surcharge load for this test series is presented in Figure 2.22. The results of the free swell testing were then used to predict the swelling expected in the field by integrating the results of the free swell tests over the stress profile for the site as shown in Figure 2.23. Given the relationship between swell and overburden determined in the laboratory and assuming a total unit weight for the soil of 130 pcf, Gizienski and Lee estimated a total swell of 1.3 inches for the 1.1 foot thick slab and 3.0 inches for the 3.0

foot thick slab. Accordingly, the predicted swell was approximately three times that of the observed swell for each test section.

The authors attributed this discrepancy to variable compaction and environmental conditions but did not consider their assumed pore water pressure profile or the difference between one dimensional and three dimensional swelling as discussed in Section 2.2.1. As demonstrated by Al-Mhaidib (1999) in laboratory tests, the difference in measured swell between oedometric stress conditions and triaxial tests in the lab is a factor of three. Since the compacted clay sections in this study were surrounded by fine sands they were likely given the ability to swell three dimensionally. Accordingly, the swell predicted by laboratory testing, given the boundary conditions in the field, may have been accurate despite the authors assertions as to the contrary. The authors also did not consider their assumed pore water pressure profile of atmospheric pressure throughout their profile, which essentially assumes a total stress analysis, in this discrepancy.

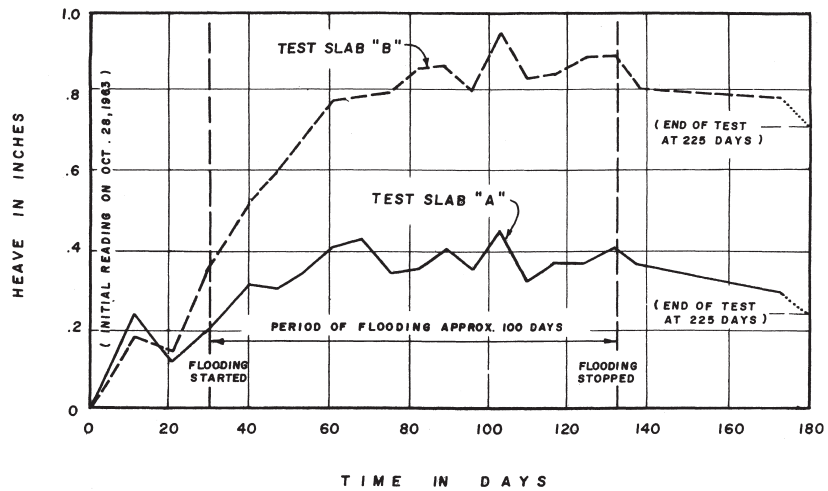


Figure 2.21: Swelling Versus Time for 1.1 ft Thick Test Slab A and 3.0 ft Thick Test Slab B (Gizienski and Lee 1965)

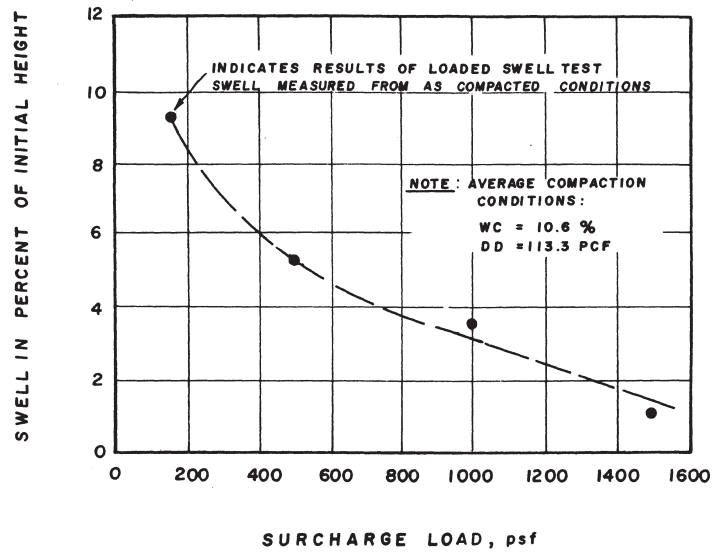


Figure 2.22: Free Swell Curves from Gizienski and Lee (1965)

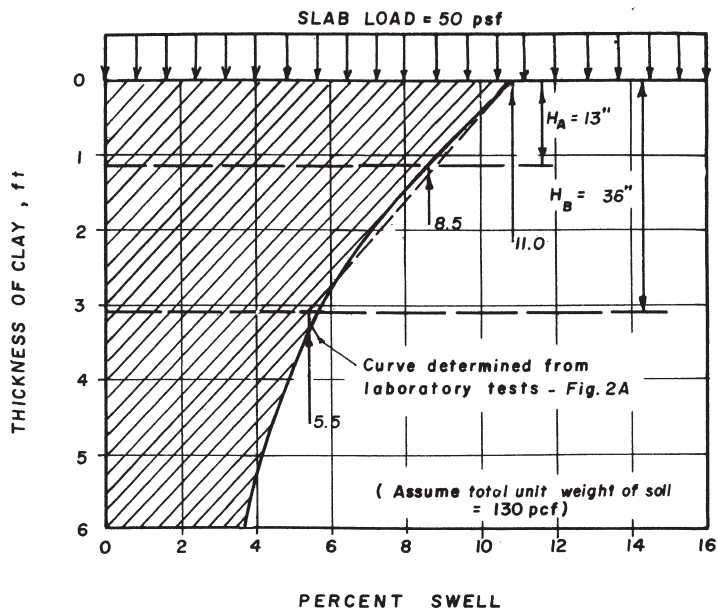


Figure 2.23: Swell Prediction Based off of Free Swell Test Results (Gizienski and Lee 1965)

2.3.2 Blight and DeWet 1965

In a study conducted by Blight and DeWet (1965) flooding of expansive clays is presented as a means of accelerating the swell for the construction of light structures. The theory for the time-rate of swell used in this study for predicting the swelling height of the soil with time is presented in Blight (1965). A “coefficient of swelling” was defined in Blight (1965) and good agreement was found between field and laboratory measured values (Figure 2.24). Using the theory presented in Blight (1965), the results of laboratory testing were used to predict swelling over time after flooding in the field. Good agreement was found between the predicted and measured values of soil swelling over time after flooding (Figure 2.25).

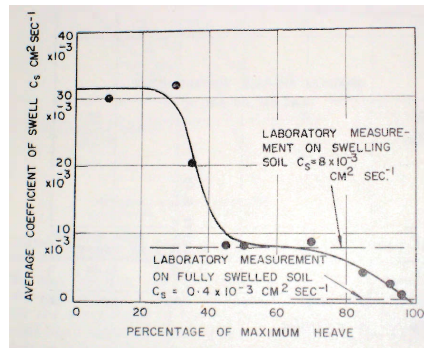


Figure 2.24: Field measurements and laboratory measurement of the coefficient of swell as a function of the percentage of maximum heave (Blight and DeWet 1965)

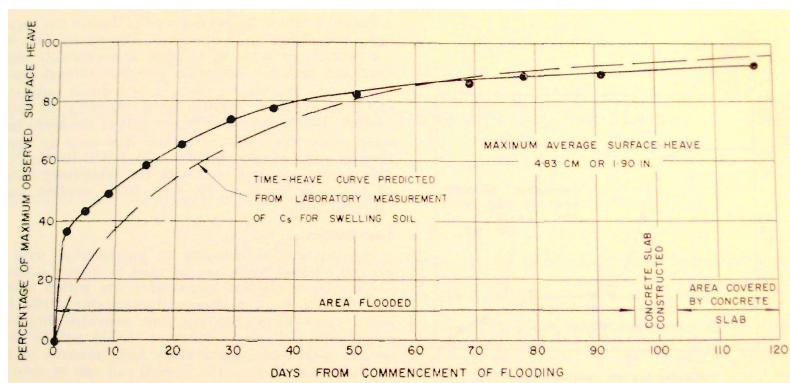


Figure 2.25: Predicted and maximum observed surface heave versus duration of flooding (Blight and DeWet 1965)

Chapter 3

Materials and Methods

3.1 Index Properties of Eagle Ford Clay

The expansive clay selected for this study was excavated from the Eagle Ford formation in Round Rock, Texas, a city located approximately 15 miles north of Austin, Texas. A map detailing the outcropping of Eagle Ford Shale in the state of Texas is shown in Figure 3.1. Clay from the Eagle Ford formation was selected for this study because it is known to generally have a high swell potential. The Eagle Ford clay used in this research study was excavated at the site from a depth of 3 meters [10 feet] with a backhoe. The excavation took place on the Southeast embankment of the intersection of Hester's Crossing and Interstate 35. The excavated soil was mostly gray with streaks of yellow. The soil was transported in a series of six 190 liter [50 gallon] plastic barrels. Since the excavated soil was in large blocks and needed to be broken down for testing, these large blocks were broken down by hand with a sledge hammer and then placed in a temperature controlled room at a temperature of approximately 50°C [120°F] for a minimum of 48 hours so that the soil was dry enough for subsequent processing. A temperature of 50°C [120°F] was chosen as to stay well below a temperature 60°C (140°F) above which change in the properties of the soil, denaturing, may occur (ASTM D 698-00A). Accordingly, any soil which was used for measuring the

water content during testing was discarded as it was placed in a standard laboratory oven at 100° C [210°F] which likely denatured the clay.

At this stage in processing, the soil consisted of fist sized chunks of dried clay. These chunks were then broken down with a hammer and passed through a soil crushing machine (Chipmunk Jaw Crusher model VD 67, Bisco Inc., Burbank, CA). This soil was then passed through a #10 sieve. Soil particles not passing the #10 sieve were reprocessed using the soil crushing machine until they passed the #10 sieve. Prior to testing, processed soil was moisture conditioned and placed in a container for a minimum of 48 hours in order to allow water to evenly distribute throughout the prepared soil.

Standard geotechnical index properties were obtained for the soil including: grain size distribution; Atterberg limits; moisture density relationships; and specific gravity. All index properties were determined in general accordance with American Society of Testing and Materials (ASTM) Standards.

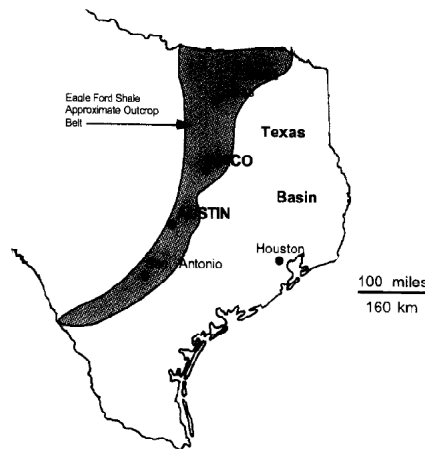


Figure 3.1: Location of Eagle Ford Formation (Robison 1997)

3.1.1 Grain Size Distribution

A hydrometer test was conducted according to ASTM D 422-63 on the soil passing the number 10 sieve. The hydrometer test revealed nearly 89.5% of the Eagle Ford Shale was

finer than the number 200 sieve. The results of the hydrometer test are shown in Figure 3.2. According to the results of grain size distribution testing, the clay fraction for the processed soil is 64%.

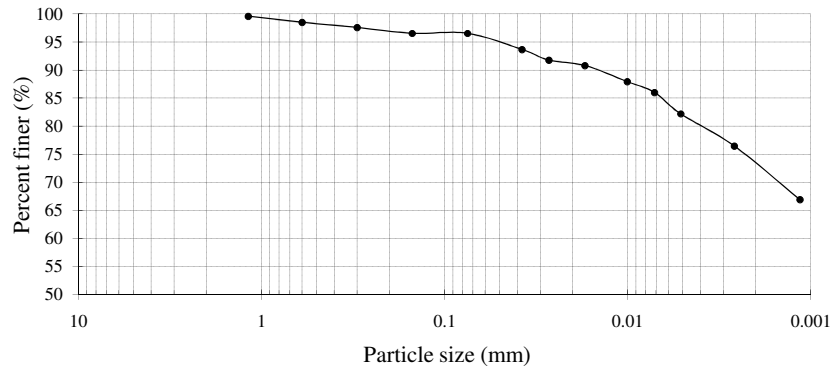


Figure 3.2: Grain Size Distribution for Eagle Ford Clay

3.1.2 Atterberg Limits

Atterberg limits were performed on the processed Eagle Ford Shale according to the procedures outlined in ASTM D 4318. The Eagle Ford clay used in this study is an expansive clay with a liquid limit of 88, a plastic limit of 39, and a plasticity index of 49. The processed soil classifies as a clay of high plasticity in accordance with the Unified Soil Classification system. Given the clay fraction of 64 and the Atterberg limits, the activity of the soil is 0.77. The Atterberg limits for Eagle Ford Shale are also presented in Table 3.1. The shrinkage limit of the soil was determined following ASTM D 4943, and was measured as 18.

A large series of classification and strength testing on Eagle Ford Shale was performed in anticipation of the construction of the Superconducting Super Collider in Texas. The results of these tests were reported by Hsu and Nelson (2002). A plot of the frequency of observed plasticity index for Eagle Ford Shale from Hsu and Nelson is presented in Figure 3.3 (a). The observed plasticity index of 49 is also marked on this plot. The observed value of 49 is less than the average value of 58 reported by Hsu and Nelson. Hsu and Nelson also presented a Casagrande Plot for all of the samples for which the plasticity index and

liquid limit were measured in their study. The observed values of 88 for the liquid limit of 88 and the plasticity index of 39 are also plotted in this figure. The observed value of 49 for the plasticity index was on the lower end of values of plasticity index reported by Hsu and Nelson for a liquid limit of approximately 88 (Figure 3.3 b).

Table 3.1: Index Properties of Eagle Ford Clay

Index Property	Value
Liquid Limit (LL)	88
Plastic Limit (PL)	39
Shrinkage Limit (SL)	18
Plasticity Index (PI)	49
Clay Fraction (CF)	64
Activity	0.77

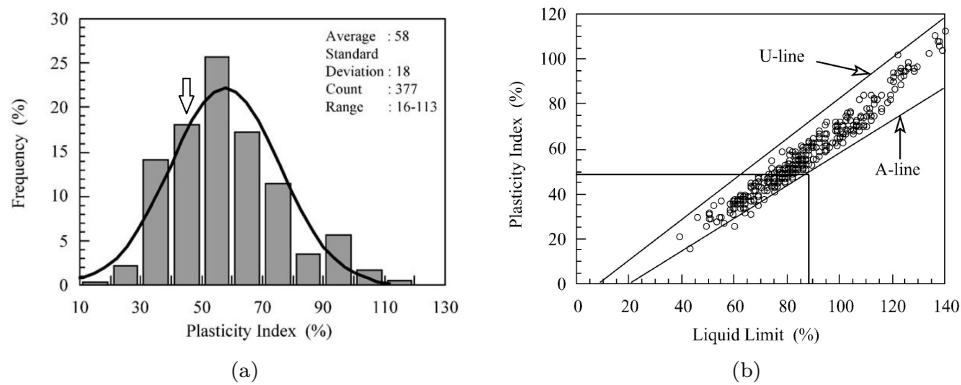


Figure 3.3: (a) Frequency of Observed Plasticity Index for Eagle Ford Shale and (b) Casagrande Plot for Eagle Ford Shale Samples (Hsu and Nelson 2002)

Index properties of Eagle Ford Clay were also reported by Farrow (1997), a geotechnical engineer working in Dallas, Texas. Farrow presented detailed descriptions of the different strata of Eagle Ford that he had encountered in practice (Table 3.2). In accordance with Farrow’s descriptions, the soil attained for this study most closely resembles “Yellowish Tan Clay.” Farrow also presented a table summarizing index properties that were measured for the various strata (Table 3.3). The liquid limit of 70 and plastic limit of 27 measured by Farrow for “Yellowish Tan Clay” are both less than the liquid limit of 88 and the plastic limit

of 39 that were measured for the soil used in this study. It is also interesting to note that when comparing the liquid limit for “Unweathered Shale” reported by Farrow to the liquid limit for the weathered clay stratum that the liquid limit for the “Unweathered Shale” is significantly less. Farrow also reported significantly large crushing strength and unconfined compressive strength for the “Unweathered Shale.”

Table 3.2: Descriptions of Eagle Ford Clay Strata (Farrow 1997)

Stratum	Description
SURFICIAL CLAY	Dark brown to brown surficial clay with varying amounts of calcareous nodules, highly slickensided and highly fissured
YELLOWISH TAN CLAY	Yellowish tan and light gray clay with varying amounts of silt seams, highly slickensided and highly fissured
HIGHLY FISSURED SHALY CLAY	Yellowish tan, olive brown and light gray shaly clay, with horizontal striations, highly slickensided, severely fractured, highly fissured with calcareous nodules and iron deposits (crumbly and friable)
SLIGHTLY FISSURED SHALY CLAY	Tan, yellowish tan, olive brown and gray shaly clay, blocky, slightly fissured with calcite deposits, silt seams, selenite crystals and iron stains (massive blocks of hard clay)
DARK GRAY SHALY CLAY	Dark gray shaly clay with tan bands and iron-stained fractures (massive blocks of hard clay)
UNWEATHERED SHALE ROCK	Dark gray unweathered shale with bentonite seams and selenite crystals

Table 3.3: Summary of Laboratory Tests on Eagle Ford Clay Strata (Farrow 1997)

ENGINEERING PROPERTIES	SURFICIAL CLAY	YELLOWISH TAN CLAY	HIGHLY FISSURED SHALY CLAY	SLIGHTLY FISSURED SHALY CLAY	DARK GRAY SHALY CLAY	UNWEATH. SHALE
MOISTURE CONTENT %	23 - 24	22 - 23	24 - 25	23 - 28	25 - 30	16
UNIT DRY WEIGHT (pcf)	105 - 106	104 - 105	102 - 105	95 - 105	88 - 101	112
LIQUID LIMIT (%)	71	70	70 - 71	75	74	59
PLASTIC LIMIT (%)	25	27	26 - 27	27	27	25
PLASTICITY INDEX (%)	46	43	44	48	47	34
POCKET PENETROMETER (tsf)	4.5+	4.5+	3.75 - 4.5+	3.25 - 4.5+	4.5+	4.5+++
UNCONFINED COMPRESSION* (ksf)	4.5 - 8.7	7.3 - 9.2	4.4 - 7.2	6.1 - 7.8	3.2 - 4.1	16 - 110
CRUSHING STRENGTH (ksf)	5.9	8.8	11.1	9.0	9.0	18 - 130
LINEAR SHRINKAGE (%)	14.74	15	15	14	13	11
ABSORPTION Swell (%)**	7.3	7.0	5.4 - 6.5	2.0 - 3.5	0.0 - 0.6	0

* Failure occurred along existing fracture planes where compressive strengths of less than 7.0 ksf are indicated.

** Volumetric swell potential measured under existing overburden surcharge.

3.1.3 Moisture Density Relationship

Standard and Modified Proctor compaction tests were performed in accordance with ASTM D 698-00a and ASTM D 1557-02, respectively, to determine the compaction moisture content - dry unit weight relationships for Eagle Ford Shale (Figure 3.2). The Standard Proctor optimum moisture content is approximately 24 % with a corresponding maximum dry unit weight of 97 pcf (15.2 kN/m^3). The Modified Proctor optimum moisture content is approximately 14% at a corresponding maximum dry unit weight of 113.5 pcf (17.8 kN/m^3).

Hsu and Nelson (2002) reported the water contents of Eagle Ford Shale samples that were taken as a part of their study. A histogram of the observed water contents is presented in Figure 3.5. The average water content measured for field samples was 16%. If this is compared to the water contents reported by Farrow (1997) and presented in Table 3.3, it is evident that the water contents most closely match those of Unweathered shale.

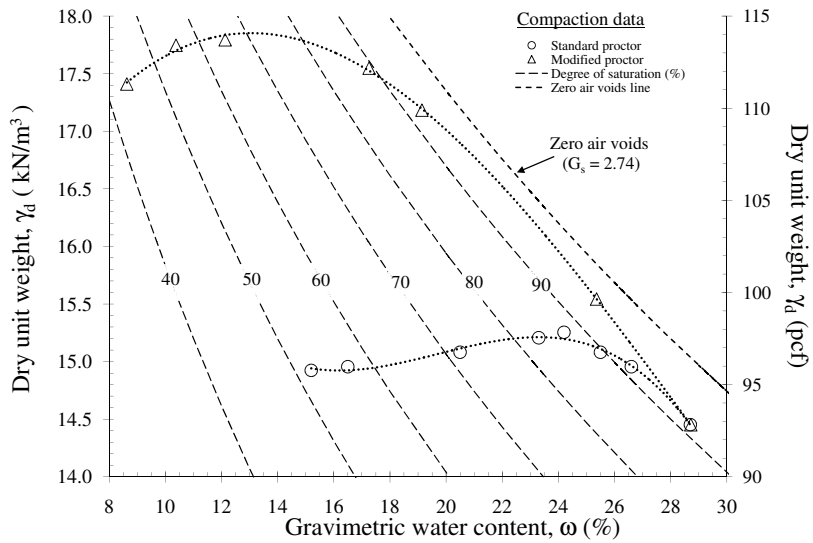


Figure 3.4: Standard and Modified Proctor Compaction Curve for Eagle Ford Shale

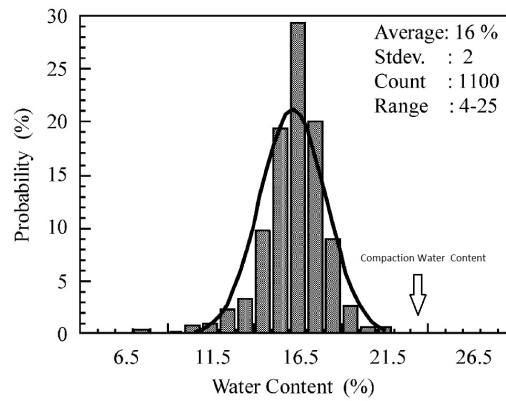


Figure 3.5: Field Sampled Water Content for Eagle Ford Shale (Hsu and Nelson 2002)

3.1.4 Specific Gravity

Two specific gravity measurements were performed on the fraction of soil passing the No. 4 sieve in accordance with ASTM D 854-02. The specific gravity values from the two measurements were 2.731 and 2.742, yielding an average value of 2.74.

3.1.5 Mineralogical Analysis

In order to determine the composition of the Eagle Ford clay used in this research study, X-ray diffraction was performed. The tests were performed under the supervision of Clifton Coward, a chemist with the Construction Division of the Texas Department of Transportation. For the tests, a Panalytical's X'pert Pro Materials Research Diffractometer was used. The unit was outfitted with a multi-array detector that allowed for scans that would typically require 25 hours to perform to be performed within 20 minutes.

The specimen was prepared for X-ray diffraction by a processes termed backpacking. In carrying out this process, soil passing the #325 Sieve (45 micrometers) was placed in a metal ring over top of a glass slide. The specimen was cut with a razor blade, compressed with a second slide, and scalped with a razor blade (Figure 3.6 a). A backing was then placed on the specimen and the specimen is flipped. The slide which was facing down during the cutting process is removed and the exposed surface is targeted in the X-ray diffraction machine (Figure 3.6 b). The measured count is plotted versus the position of the sensor in Figure 3.7. Through using a data base of mineralogical patterns the following compounds were very likely present in the sample:

Compound Name	Chemical Formula	Reference Code*
Quartz	SiO_2	01-078-1252
Kaolinite	$Al_2Si_2O_5(OH)_4$	00-006-0221
Jarosite	$KFe_3(SO_4)_2(OH)_6$	01-071-1777

*International Center for Diffraction Data Reference Code

A screen-shot of the proprietary Panalytical's "X'pert Highscore" software is shown in Figure 3.8. A number of other compounds that were potentially present are also listed in this screen-shot.

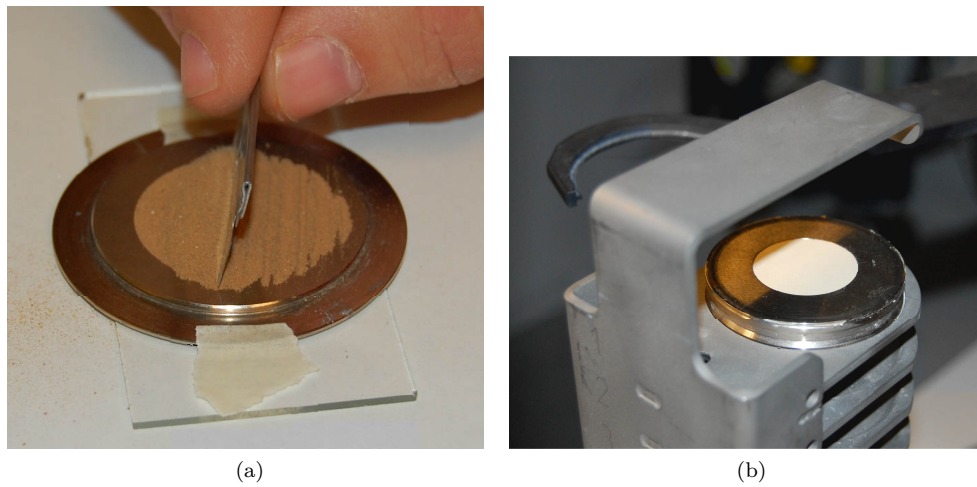


Figure 3.6: X-ray Diffraction (a) Sample Preparation and (b) Prepared and Loaded Sample

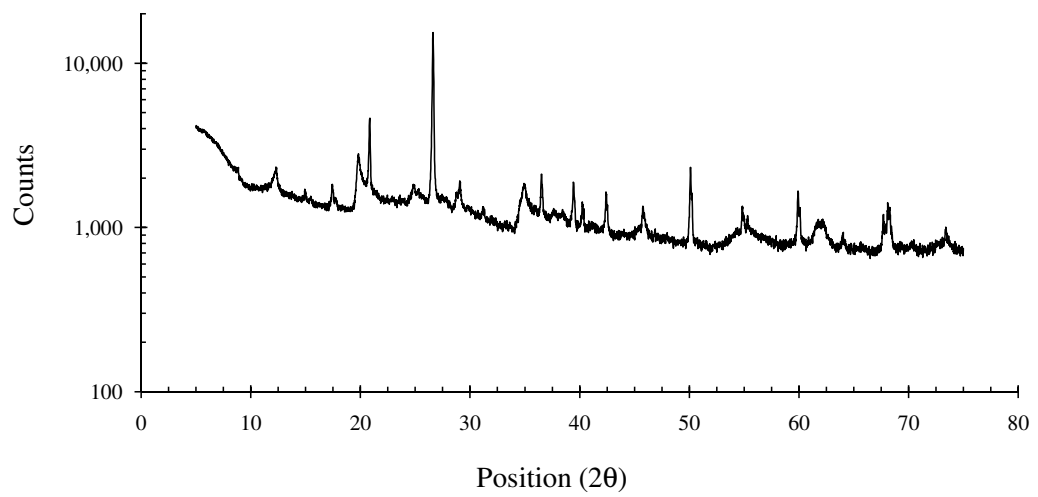


Figure 3.7: X-ray Diffraction Pattern for Eagle Ford Clay

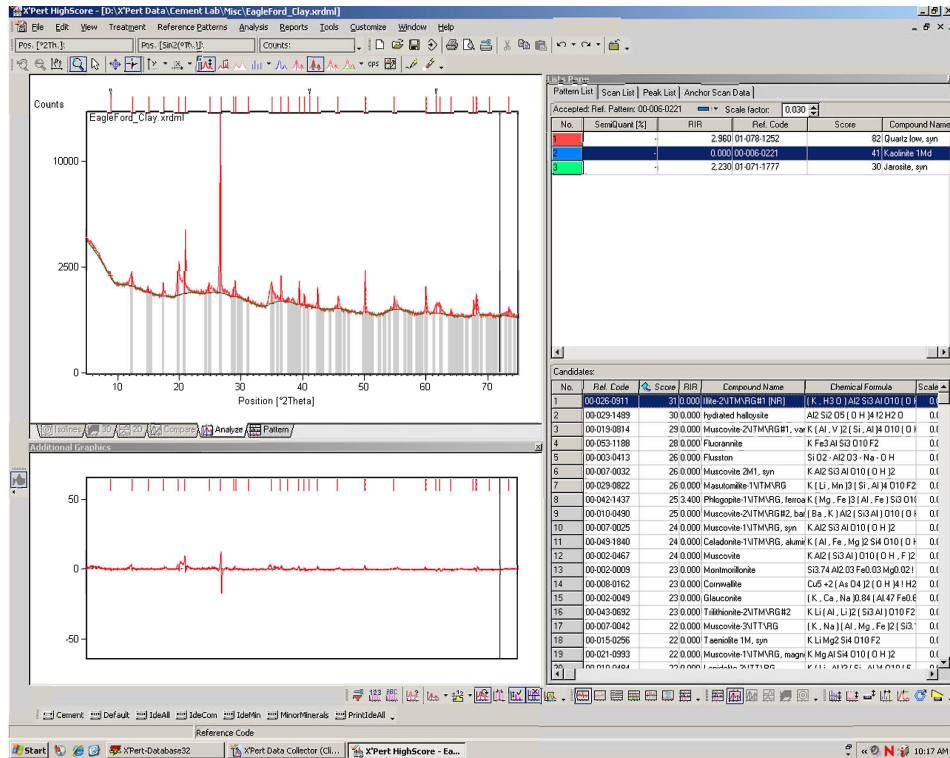


Figure 3.8: Screen-shot of “X’pert Highscore” X-ray Diffraction Database Software

3.1.6 Saturated Hydraulic Conductivity

The standard test method for evaluating the movement of water through a saturated expansive clays is to measure the hydraulic conductivity of a saturated specimen in a flexible wall permeameter cell. For this test, Eagle Ford clay was compacted at a moisture content of 23.6%, which is within 1% of optimum (24%), and a dry unit weight of 98.7 pcf ($\gamma_{d,max} = 97.5$ pcf). The height-to-diameter ratio of this specimen was approximately 0.5. The hydraulic conductivity was determined for effective stresses of 1,000 psf, 2,000 psf, and 4,000 psf. These tests were performed with the assistance of undergraduate research assistant Alejandro Martinez. In a previous study, a hydraulic conductivity of 4×10^{-11} m/s was measured at an effective stress of 250 psf (Kuhn 2005 and Aguetant 2006).

Since this clay is Expansive and has a low hydraulic conductivity, the back-pressure

saturation and consolidation of the specimen was time consuming. The B-value, which is an indicator of the saturation of the soil specimen, was determined during saturation and is plotted in Figure 3.9. In order to attain a B-value of 0.95 each of the three specimens, a time period of just less than two weeks was required.

After back-pressure saturation, the specimens were consolidated to the effective stress values of interest. The cell inflow is plotted versus time for each of the test specimens in Figure 3.10. A time period of approximately three days was required to reach 100% of primary consolidation for each of the test specimens. At this point, a hydraulic gradient of 30 was applied across each of the specimens. The flow rate into and out of the specimen was then measured until the ratio of the outflow to inflow was at least 0.99 (Figure 3.11). The measured values of hydraulic conductivity are plotted versus effective stress in Figure 3.12. As expected, the hydraulic conductivity was found to decrease with effective stress. The hydraulic conductivity reported by Kuhn (2005) and Aguetant (2006) for an effective stress of 250 psf is on the same order of magnitude as the hydraulic conductivity value of 1,000 psf. The value of hydraulic conductivity measured at an effective stress of 2,000 psf was found to be four times the value measured at 4,000 psf. The value of hydraulic conductivity measured at an effective stress of 1,000 psf was found to be eight and one-half times the value of measured at 8,000 psf.

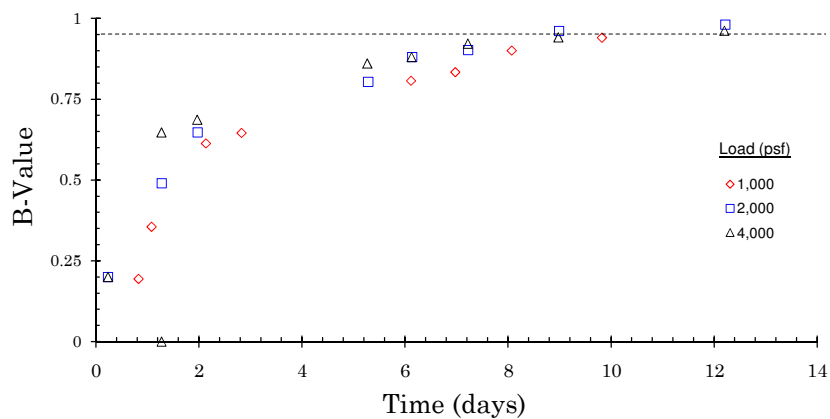


Figure 3.9: B-Value during Saturation of Saturated Hydraulic Conductivity Specimens

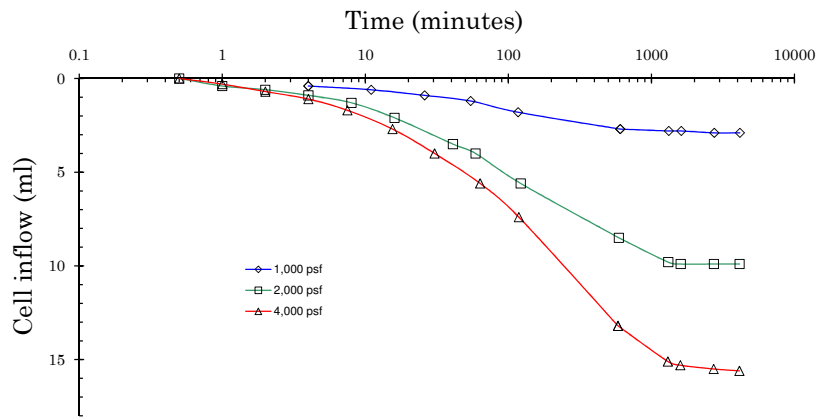


Figure 3.10: Cell Inflow during Consolidation of Saturated Hydraulic Conductivity Specimens

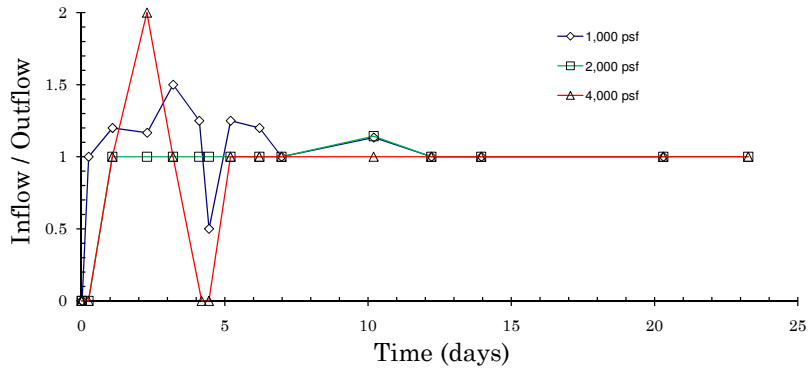


Figure 3.11: Ratio of Inflow to Outflow during Saturated Hydraulic Conductivity Testing

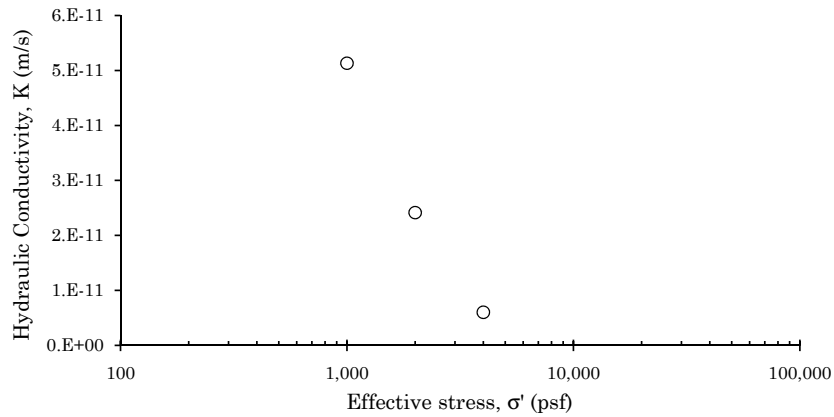


Figure 3.12: Hydraulic Conductivity versus Effective Stress for Eagle Ford clay Compacted at Optimum Water Content with 100% of Standard Proctor Compaction Effort

3.2 Centrifuge Equipment

A state-of-the-art centrifuge laboratory has been recently added to the geotechnical laboratories at the University of Texas at Austin. The centrifuge is a custom built piece of equipment specifically designed with geotechnical flow applications in mind. The centrifuge was designed at The University of Texas and manufactured by Broadbent, UK. It includes a low-flow fluid rotary union that allows fluid to be introduced into samples in flight. The centrifuge also includes a solid-state data acquisition system which digitizes sensor readings in flight and transmits them to the 1 g environment as to minimize noise. Since measurements are made in-flight in a continuous manner during testing, both transient and steady state flow processes may be monitored without stopping the centrifuge. Since the centrifugal acceleration increases the rate of fluid flow, tests that involve studying the flow of fluid through soils may be conducted in considerably shorter time periods.

3.2.1 General Overview

A picture of the centrifuge permeameter laboratory is shown in Figure 3.13. The upper portion, white, portion of the centrifuge permeameter houses the spinning environment

while the lower, orange, portion of the permeameter houses the driving mechanism and the electrical slip ring stack for powering the solid state data acquisition system. A series of schematics which break down this arrangement are presented in Figure 3.14. In Figure 3.14(a), the drum environment, the lid lock assembly, the vibration isolators, the 36 channel user slip ring stack, the 4 port user rotary union, and the user fiber optic rotary joint are pictured. The drum environment is not used in this testing program. Instead, a permeameter table is used (Figure 3.15). The lid lock assembly is used to ensure that the centrifuge lid remains closed during operation. The vibration isolators are used to prevent loads caused by the rotation of the centrifuge to be transmitted into the foundation upon which the centrifuge is mounted. The 36 channel user slip ring stack is used to power the data acquisition system and can be used to as a back-up for communicating with the data acquisition system in case of problems with the wireless Ethernet bridge currently in use. The fiber optic rotary joint serves the same purpose and may also be used as a means of communicating with the data acquisition system.

In Figure 3.14(b), the casing lid, gas struts, observation window, casing top, upper casing, casing drain main outlet, siphon actuator, drive motor, and drive pulley are pictured. The casing lid is held in place while the centrifuge is loaded by a pair of gas struts. The lid is then secured to the upper casing when testing is started. The upper casing houses the casing lid and the observation window. In conjunction with a strobe light, the observation window is used to visually monitor spinning tests. This includes monitoring of the test specimens along with routine inspection to ensure that all cables have remained restrained during testing. The casing main drain outlet is used to exhaust air and other fluids from the upper casing during testing. The siphon actuator operates a siphon which works in conjunction with the drum environment which is not used in this investigation. The drive motor rotates the drive pulley which is attached to the drive belt. Figure 3.14(c), provides an alternative view of previously discussed components.

The support base is removed for Figure 3.14 (c) to better show the components that are housed within its confines. Components which have not previously been discussed in-



Figure 3.13: The Centrifuge Permeameter

clude the drive motor support plate, the driven pulley, the speed sensors, the brake calipers, and the brake disc. The drive motor support plate is used to anchor the drive motor to the centrifuge. The driven pulley is rotated via the toothed drive belt which is connected to the driving pulley. The speed sensor is used to monitor the rotational velocity of the centrifuge so that the power provided to the drive motor can be adjusted to achieve a constant rotational velocity with various loads. Finally, the brake caliper and disc are used to stop the centrifuge and must be released prior to rotating the centrifuge by hand.

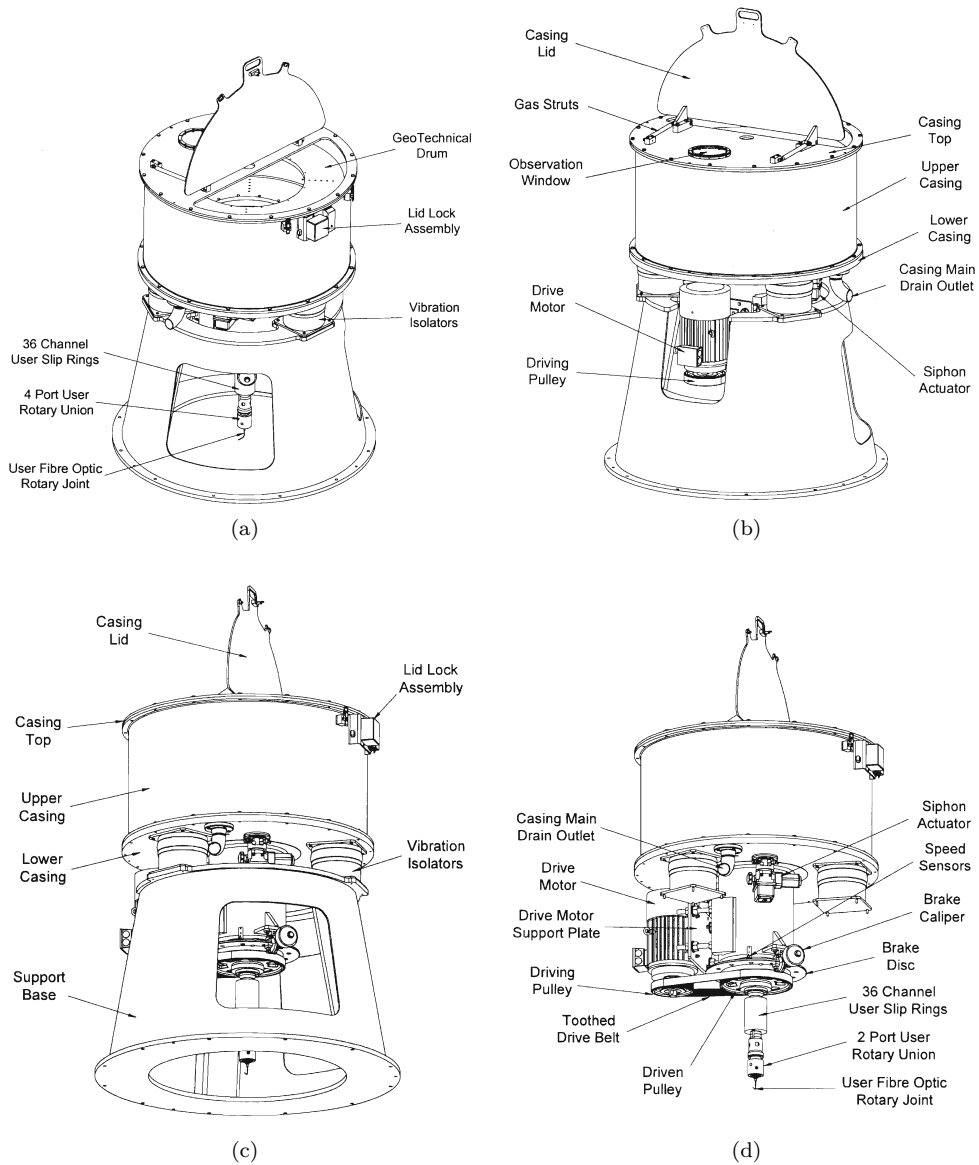


Figure 3.14: General Centrifuge Schematics (Broadbent 2006, Figures 1.1 and 2.3)

The schematic of the small permeameter table shows the low flow rotary union, the small permeameter, cut-outs for access to the DAS connectors, and the pivot pins. The low flow rotary union, as further explained in Section 3.2.11, allows for water to be added to the

spinning environment to the stationary environment during testing. The small permeameter is placed into the centrifuge in a vertical position and rotates to a near horizontal position on the pivot pins during testing. The cutouts in the small permeameter table allow access to gain adjustments on the data acquisition system board.

A schematic cross-section of the centrifuge permeameter is shown in Figure 3.16. Both a large and small permeameter can be used with the table environment. Unlike the small permeameter used in this study, the large permeameter is fixed in place and does not “swing-up” during testing. Additional components that are pictured in this schematic that were not previously discussed include: The DAS cover plates and connectors, the DAS electronic boards, the DAS hub, the flexible guard skirt, the spindle, the spacer tube, and the bearing cartridge. The DAS cover plate sites beneath the permeameter table and connectors atop it allow for instruments to be connected to the DAS board with military connectors. A seal between the DAS hub, and the DAS cover plate provides a water-tight environment for the DAS. The DAS electronic boards are mounted on the underside of the DAS cover plate. The flexible guard skirt blocks users from coming into contact with the vibration isolators during operation. The spindle provides a conduit within the slip ring stack for the fiber optic cables and tubing that leads to the rotary union. Finally, the spacer tube separates the rotary union from the slip ring stack.

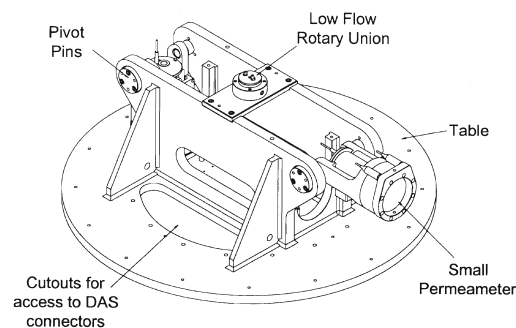


Figure 3.15: Small Permeameter Table Schematic (Broadbent 2006, Figure 1.10)

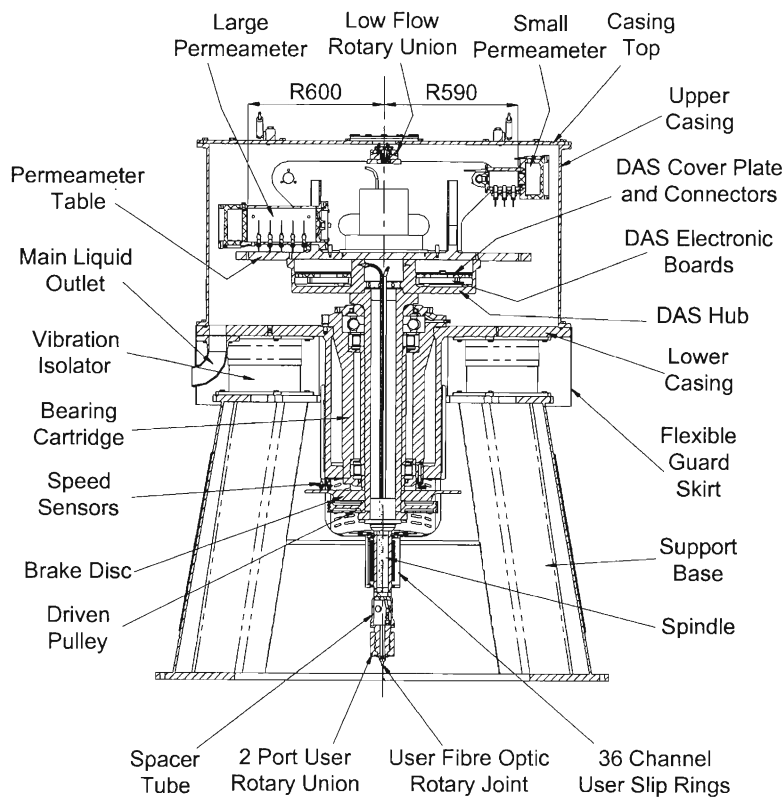


Figure 3.16: Schematic Cross-Section of the Centrifuge Permeameter (Broadbent 2006, Figure 1.3)

A summary of the specifications for the large centrifuge are presented in Table 3.4. The centrifuge permeameter is capable of being flown at a maximum rotational velocity of 900 RPM. The distance from the center of rotation to the base of the specimen cylinder is 613 mm. Given the maximum rotational velocity of the centrifuge, this corresponds to a maximum g-level at the base of the specimen of 500 G. The specimen cylinder itself measures 71 mm in diameter and is capable of housing a specimen with a maximum height of 127 mm.

The measurement and control capabilities of the centrifuge include the ability control the height of water on top of the specimen, control the flow rate into the specimen, measure the volume of outflow during testing, measure the specimen height, measure soil suction,

Table 3.4: Summary of Large Centrifuge Specifications

Capacity details	
Maximum rotational velocity	900 RPM
Centrifuge arm to base of the specimen cylinder	590 mm (23")
Maximum g-level at the base of the specimen cylinder	500

Specimen Cylinder	
Diameter	70 mm (2.76")
Maximum specimen height	115 mm (4.5")

Measurement and control capabilities	
Height of water on top of specimen	Addition of fluid through low-flow rotary joint
Flow rate into the specimen	Addition of fluid with an infusion pump through a rotary joint
Outflow volume	In-flight via pressure transducer
Specimen height	In-flight linear position sensor
Soil suction	In-flight via tensiometers
Volumetric water content	In-flight, bulk measurement via time domain reflectometry probe

and measure the volumetric water content of the specimen. The height of water on top of the specimen is controlled by adding water through the low-flow rotary union and through a series of overflow ports (Section 3.2.3). The flow rate into the specimen is controlled using either a peristaltic or syringe pump to add water through a low-flow fluid rotary union (Section 3.2.11). The outflow volume is measured using an in-flight pressure transducer (Section 3.2.9). The height of a soil specimen is measured with a linear position sensor (Section 3.2.10). While not used in this testing program, soil suction can be measured during testing using tensiometers and the volumetric water content can be measured using time domain reflectometry. For details concerning the capabilities of this centrifuge in utilizing tensiometers for suction measurement and time domain reflectometry probes for volumetric water content measurements please refer to McCartney 2007.

3.2.2 Data Acquisition System Details

The solid state data acquisition system is housed in a water-tight environment beneath the permeameter table. A picture of the solid state data acquisition system positioned up-side-down outside of the permeameter environment is shown in Figure 3.17. The data acquisition system was custom built for this testing setup by Broadbent Incorporated and consists of components which are capable of withstanding the high G-levels which the centrifuge was designed for. The data acquisition system communicates with a laboratory computer through a wireless bridge (Figure 3.18) which is housed atop the permeameter table. The data acquisition board (DAQOEM 2001) digitizes signals from a 16-channel multiplexer. Amplification and filtration of the equipment signals is achieved by two 16-channel amplifier/filters (“8 CH AMP”). Power is supplied by a power power converter which is capable of supply 24, 15, 12, and 10 volts (“DC PSUs”. Finally, power is supplied to the data acquisition system through connections which travel through the central access shaft and through the slip-ring stack.

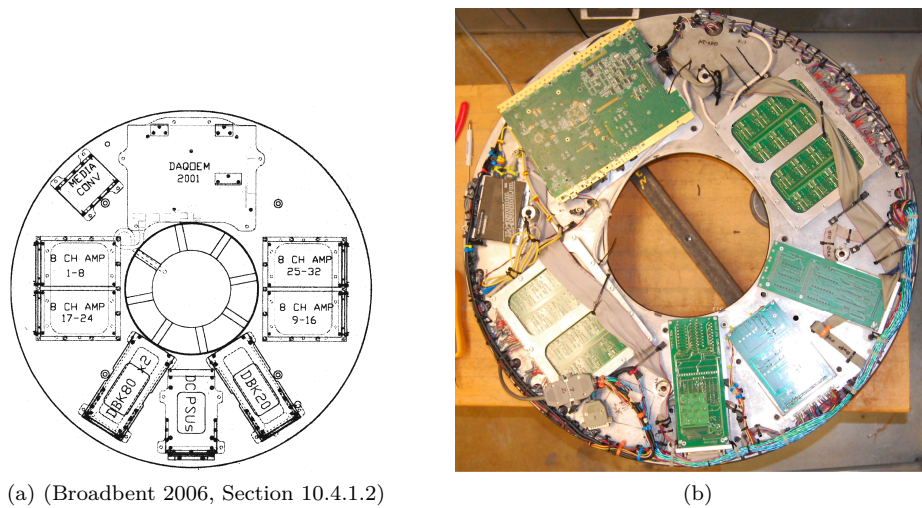


Figure 3.17: On-Board Data Acquisition System

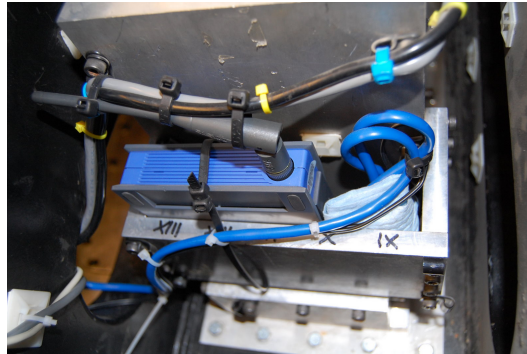


Figure 3.18: Wireless Network Bridge

3.2.3 Permeameter Details

The centrifuge permeameter consists of a top cap, a specimen cylinder, and an outflow chamber as shown in Figure 3.19. A picture of the centrifuge permeameter is shown in Figure 3.20. The top cap sits applied over the permeameter profile and holds the linear position sensor in place. The top cap also has a water supply port through which water is added to the permeameter cup during testing. The specimen cylinder rests below the top cap and houses the soil specimen. The soil specimen sits between a top plate and a bottom plate. A series of overflow ports are located along the wall to control the height of ponding. Overflow ports that are not currently in use are closed off with plugs. The linear position rod from the linear position sensor, which is housed in the top cap, rests atop the top plate and measured the height of the soil specimen during testing. Finally, the specimen cylinder is threaded onto the outflow chamber that houses the outflow reservoir and to which a pressure sensor is attached in order to measure the volume of outflow in the outflow chamber during testing. Each of these components are discussed in detail later in this section.

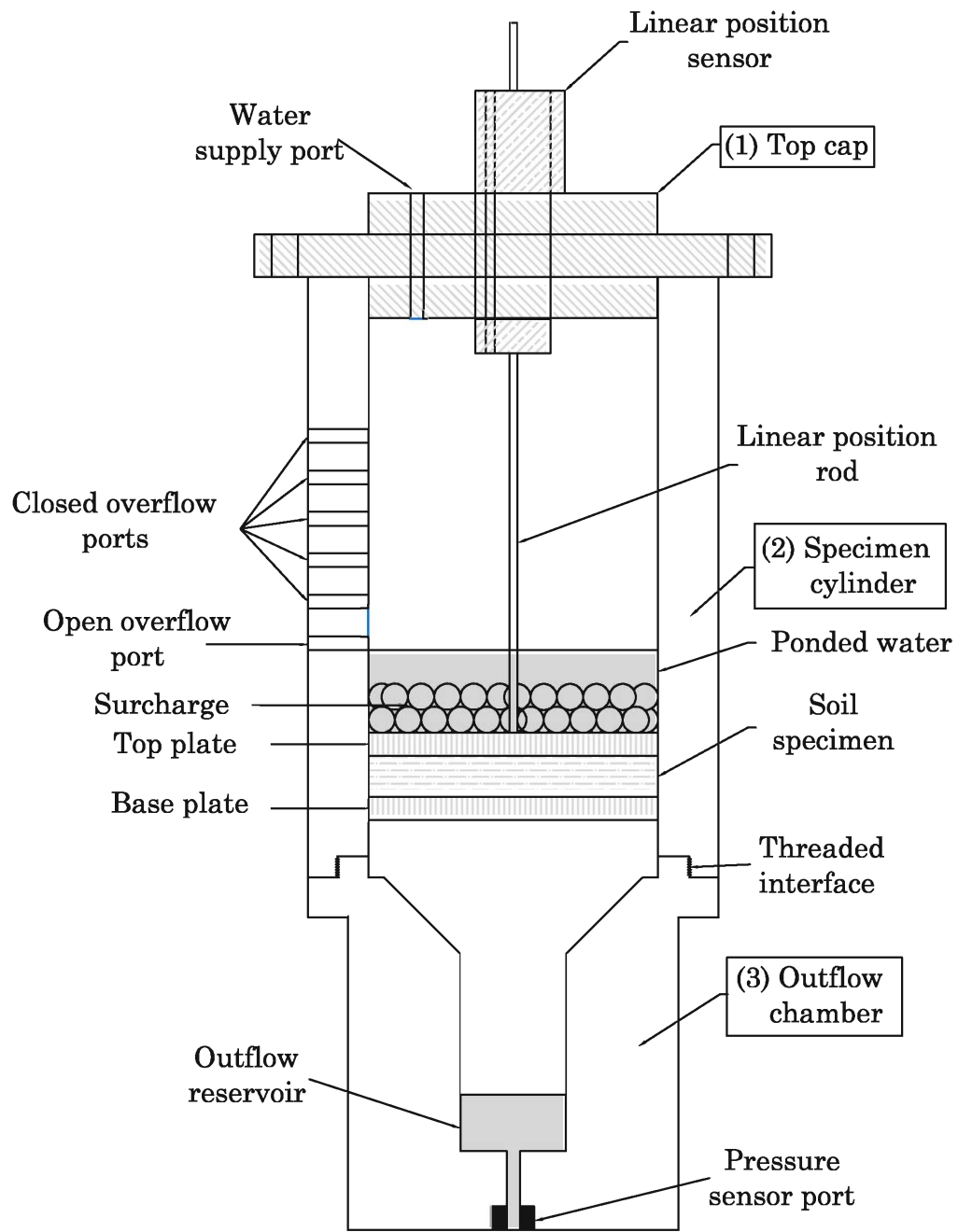


Figure 3.19: Schematic View of Centrifuge Permeameter Cup

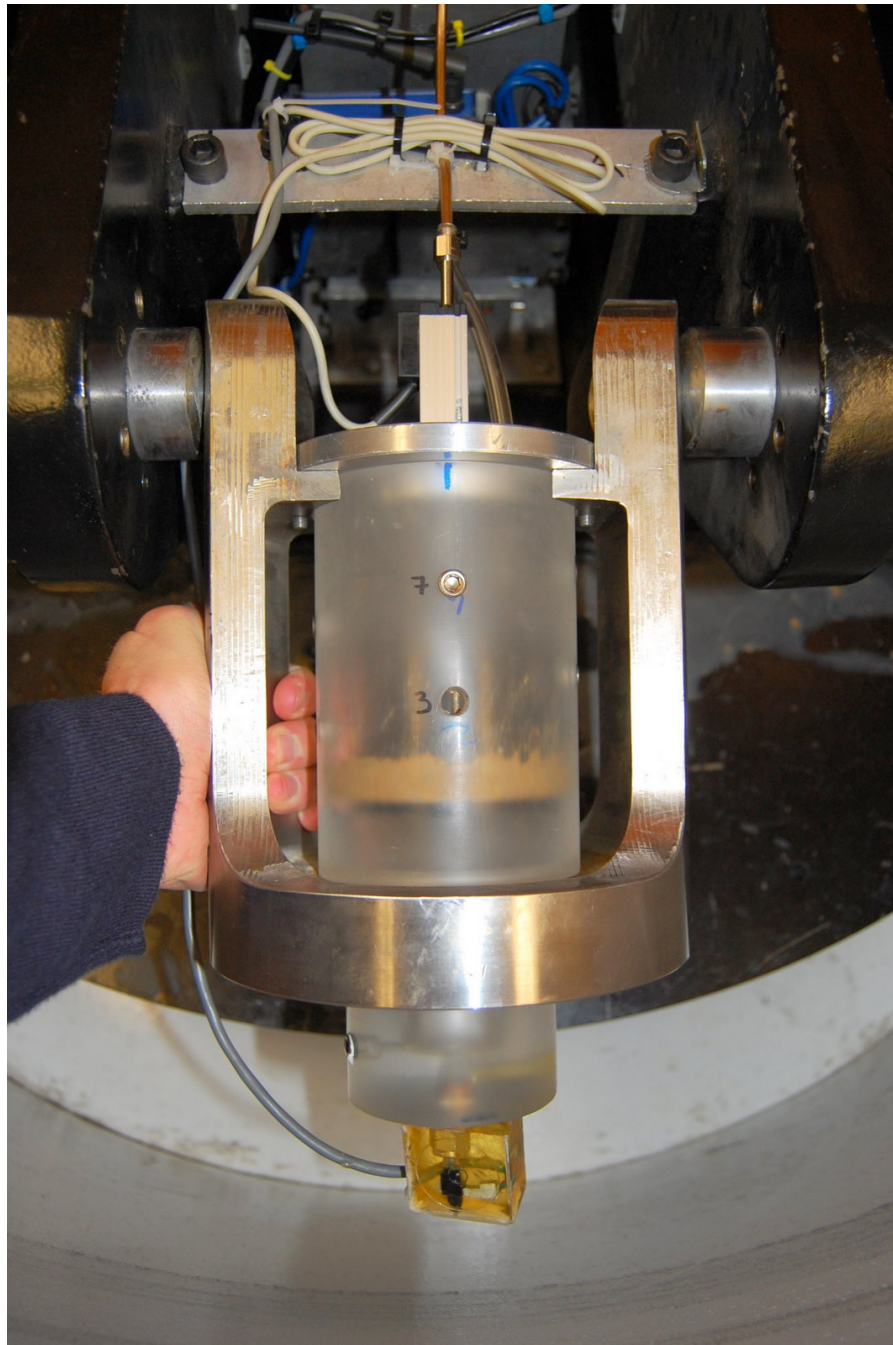


Figure 3.20: The Centrifuge Permeameter Cup

3.2.4 Major Centrifuge Testing Parameters

Given the basic setup of the centrifuge permeameter, it becomes evident that there are several major testing parameters for swell testing with this setup. These include:

- G-level
- Specimen height
- Compaction water content and density
- Surcharge pressure
- Water pressure applied over the specimen
- Bottom boundary condition
- Duration

The G-level within the soil specimen is controlled through controlling the rotational velocity of the centrifuge which can be set and maintained through the centrifuge control panel. The specimen has a fixed diameter of 71 mm diameter but the permeameter is capable of housing specimens of up to 115 mm in height . This height is however, limited in this testing program in that the upper portion of the specimen cylinder is used for ponding water atop the specimen and since the soil specimens can swell during testing adequate room has to be allotted above the specimen for this expansion. In this testing program, only one type of soil is used, however the effects of varying compaction after content and density are investigated. The surcharge pressure on the soil specimen is controlled with a series of stainless steel ball bearings which are placed atop the top plate as a surcharge. The water pressure applied over the specimen is controlled using a series of overflow ports. The bottom boundary condition can be controlled by subjecting the specimen to a controlled water pressure or by allowing for an open-flow boundary condition as in the majority of this testing program. Durations of up to 14 days were used in this testing program.

3.2.5 Testing Procedure Overview

The centrifuge testing procedure was established for as part of TxDOT Project No. 0-6048. The testing stages are illustrated in Figure 3.21 and is discussed here. A detailed description of the procedure by which these tests are run is detailed in Section 3.3. Furthermore, the method of analyzing the height changes that occur in the soil specimen during testing is discussed later in Section 3.2.13.

Prior to testing a soil specimen is compacted into a permeameter cup atop a base plate. A top plate is then placed on the soil specimen and as shown in Stage 1, the height of the compacted specimen is measured with the vertical dial stand and the soil specimen is placed into the centrifuge. In the second stage, the centrifuge is spun up to the desired rotational velocity. During the acceleration of the soil specimen the soil undergoes an initial settlement. Following this initial settlement, Stage 3 is started when water is added to the permeameters to create a ponded height of water. At the end of the desired testing duration, Stage 4, the soil specimen has undergone swelling and the test is stopped at Stage 5. Finally, as the centrifuge spins down to a stop the specimen undergoes some expansion. To end the test, Stage 6, water is removed from the permeameter and the final height of the soil specimen is measured with the vertical dial stand.

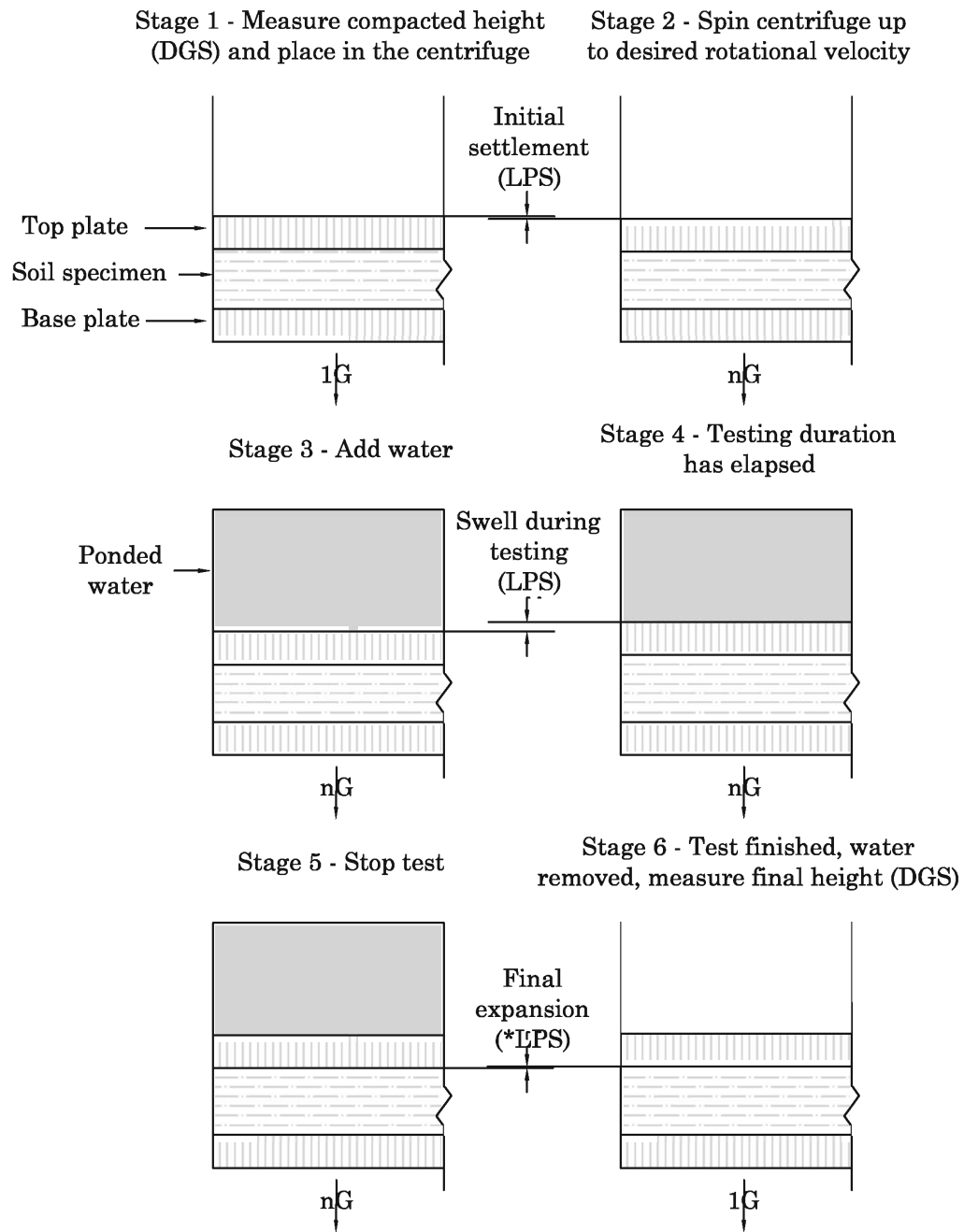


Figure 3.21: Overview of Centrifuge Testing Process (DGS - Height Measured with Dial Indicator Stand, LPS - Height Measured with Linear Position Sensor, *LPS - Final Expansion can be Measured During Deceleration but not Between Specimen Removal and Measurement of Height with the Dial Indicator Stand)

3.2.6 Fluid Potential in The Centrifuge Permeameter

In order to discuss the flow of water through a soil specimen in a centrifuge, a framework for expressing the fluid potential at various positions in the specimen must be established. For this research study, the framework developed by Dell'Avanzi et al. (2005) is used to express the fluid potential within a soil specimen. Furthermore, the framework is used to relate the seepage velocity within the centrifuge test specimen to the hydraulic conductivity of the soil specimen. Dell'Avanzi et al. (2005) evaluated scaling flows in the centrifuge by defining the fluid potential induced by the acceleration field under the assumption that Darcy's law is valid within a soil specimen in a centrifuge field.

The centripetal acceleration, a_c , can be related to the angular velocity, ω , and radial distance from the centrifuge axis to the control volume, r , as follows:

$$a_c = \omega^2 r = N_r g \quad (3.1)$$

where N_r is the ratio between the centripetal acceleration and gravity, g , and is commonly referred to as the "G-level."

In order to define fluid potentials in the centrifuge field, a datum must be defined. For this study, the datum is taken as the top of the outflow plate. The radial distance from the centripetal axis to the datum is termed r_o . For sake of discussing fluid potentials throughout the profile of a specimen within the centrifuge field, the coordinate z_m is termed the elevation within the centrifuge and is defined as follows:

$$z_m = r_o - r \quad (3.2)$$

Given Equations 3.1 and 3.2, the G-level at any elevation within the centrifuge can be defined as:

$$N_r = \frac{\omega^2}{g} (r_o - z_m) \quad (3.3)$$

In the centrifuge, fluid flow is driven by both the centrifugal acceleration and the fluid potential within the model. The fluid potential, ϕ_m , can generally be described by the following equation:

$$\phi_m = g \cdot z_m + \frac{1}{2} \left(\frac{\nu}{n} \right)^2 - \frac{\psi}{\rho_w} \quad (3.4)$$

where g is the acceleration due to gravity, z is the distance above the datum, ν is the discharge velocity, n is the soil porosity, ψ is the total suction, and ρ_w is the density of water.

Given that the ratio between the discharge velocity and the soil porosity (i.e. the seepage velocity) is small and by combining Equations 3.3 and 3.4, the component due to kinetic energy becomes negligible and the fluid potential becomes:

$$\phi_m = -\frac{1}{2} \omega^2 (r_o - z_m)^2 - \frac{\psi}{\rho_w} \quad (3.5)$$

Assuming the validity of Darcy's law, the discharge velocity from the centrifuge can be expressed as:

$$\nu_m = -\frac{k(\psi)}{g} \frac{\delta \phi}{\delta z_c} \quad (3.6)$$

where $k(\psi)$ is the hydraulic conductivity of the soil as function of total suction.

Given Equations 3.5 and 3.6, the following equation can be derived:

$$\nu_m = -\frac{k(\psi)}{\rho_w g} \left(\rho_w \omega^2 (r_o - z_m) - \frac{\delta \psi_m}{\delta z_m} \right) \quad (3.7)$$

The coordinate system established here is used throughout this dissertation. Additionally, a preliminary evaluation of the hydraulic conductivity of the soil specimen is conducted given the established relationship between the measured seepage velocity and the testing conditions.

3.2.7 G-level

The theoretical framework for fluid potential in the centrifuge as expressed in the previous section can be used to express the G-level as a function of the rotational velocity and the variation of the G-level along a specimen tested in the centrifuge. The variation of the G-level with rotational velocity is shown in Figure 3.22 for three points within the permeameter: at the specimen base, 10 mm above the base, and 20 mm above the base. Since the base of the soil specimen is at a greater radius from the centripetal axis, the G-level at the base of the specimen is greater than at points higher in the specimen's profile.

For centrifuge tests, the rotational velocity at which the centrifuge is spun is determined by the desired G-level. For purposes of testing, the radius at which the rotational velocity is calculated for the desired G-level is the distance from the centrifugal axis to the top of the outflow plate (i.e. base of the soil specimen). Since the G-level is a linear function of the radius, then the G-level at any height above the outflow plate can be expressed as a percent of the target G-level. This relationship is shown in Figure 3.23. In accordance with this relationship, for any given G-level, the G-level 20 mm above the outflow plate is 96.5% of the target G-level. The small variation of the G-level across the soil specimen results from the fact that the distance between the centrifuge axis and the outflow plate is greatest within the soil specimen.

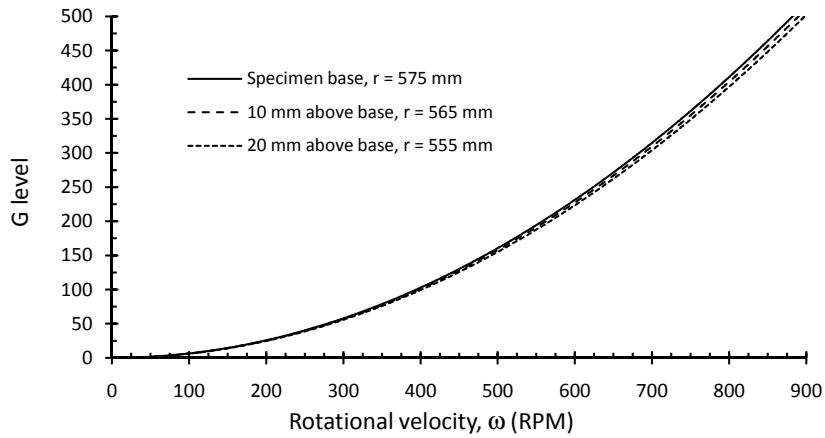


Figure 3.22: Variation of G-level with Rotational Velocity Within a Centrifuge Specimen

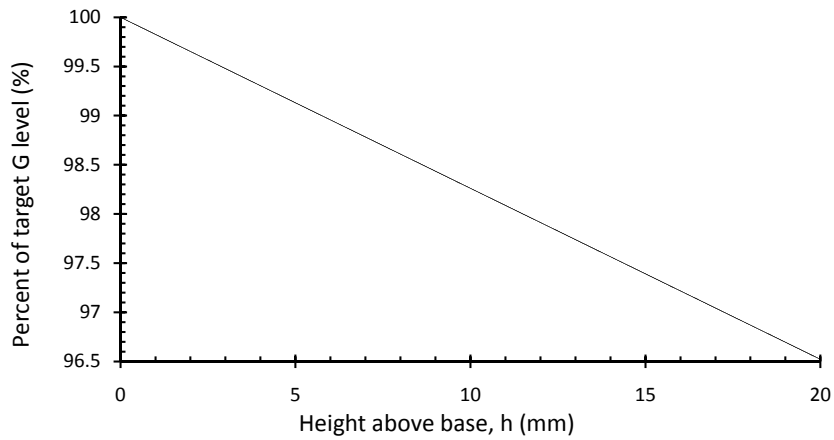


Figure 3.23: Percent of Target G-level as a Function of the Height above the Base of the Permeameter

3.2.8 Permeameter Cup

The specimen holders for the centrifuge have an inner diameter of 70 mm (2.76”) and a height of 147 mm (5.8”) (Figure 3.24). A newer design has been implemented in which the supports have been replaced by an acrylic cup and the outflow ports have been located at different positions around the perimeter of the cup to reduce cracking due to stress

concentrations at the overflow ports. A picture of the newer permeameter cups is shown in Figure 3.25. The diameter of the centrifuge permeameter cup is based on its suitability for use with specimens trimmed from Shelby tube samples. In this investigation, however, all specimens are compacted into the permeameter cup in the laboratory. The specimen holder sits atop an outflow plate that overlies the outflow chamber.

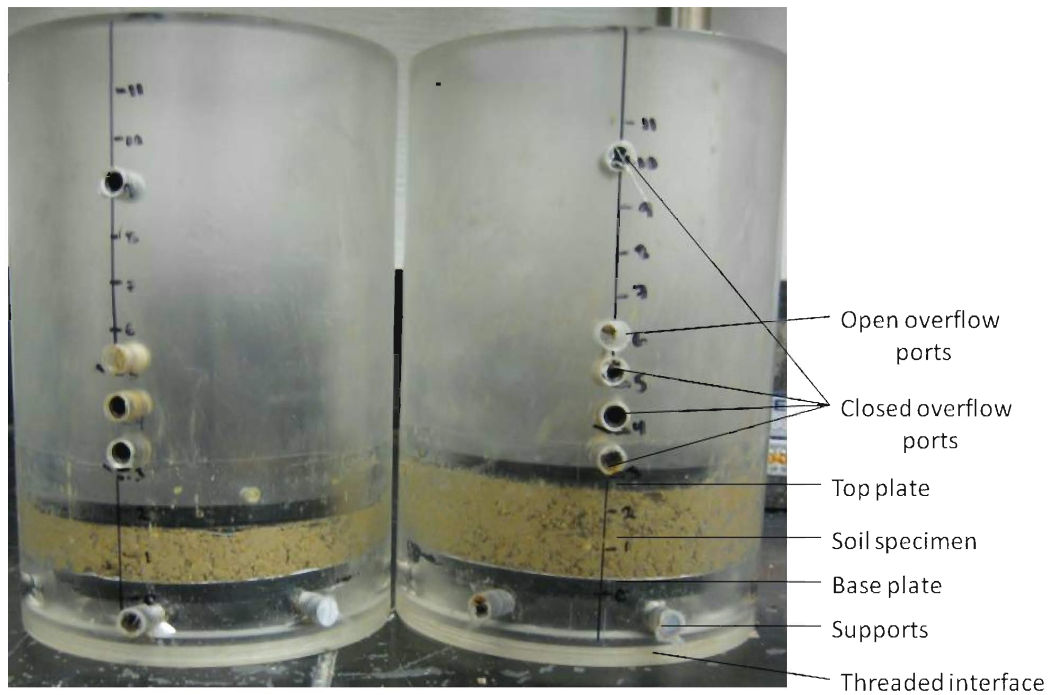


Figure 3.24: Acrylic Permeameter Cups with Compacted Specimens (Inner diameter of 70 mm with a maximum specimen height of 115 mm)

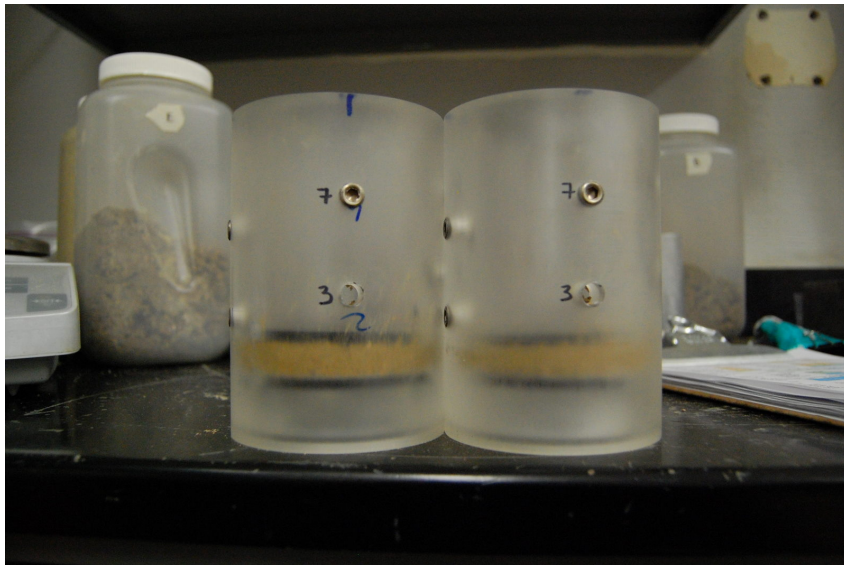


Figure 3.25: Acrylic Permeameter Cups with Compacted Specimens

3.2.9 Permeameter Outflow Chamber

The permeameter outflow chamber captures water that has permeated through the soil sample, filter paper, and base plate. A pressure sensor located at the base of the outflow chamber is used to monitor the volume of water in the outflow chamber and ultimately to determine the rate of water outflow from the specimen. A schematic view and a picture of the outflow chamber are shown in Figures [3.26](#) and [3.27](#).

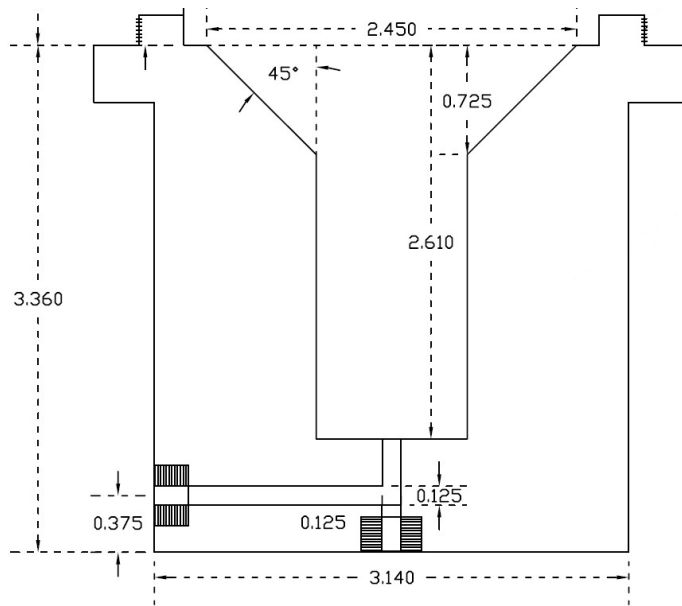


Figure 3.26: Outflow Chamber Schematic (Inches)

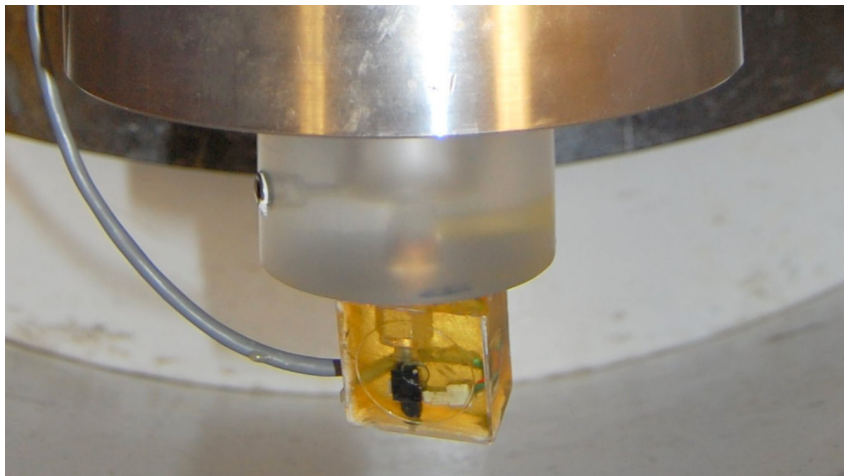


Figure 3.27: Outflow chamber

3.2.10 Permeameter Cap and Linear Position Sensor

The permeameter incorporates a top cap (Figure 3.28) used to hold a linear position sensor (Figure 3.29). The top cap incorporates a pair of set screws that are used to adjust the

height of the linear position sensor in order to accommodate specimens of varying height. The linear position sensor used in the permeameter is resistance-based and has a range of one inch. The linear position sensor, in combination with the solid state data acquisition system, allows continuous monitoring of vertical movements in the centrifuge permeameter. The linear position sensor has an accuracy of one-thousandth of an inch. For a 10-mm thick specimen, this translates to an accuracy of 0.25% swell.

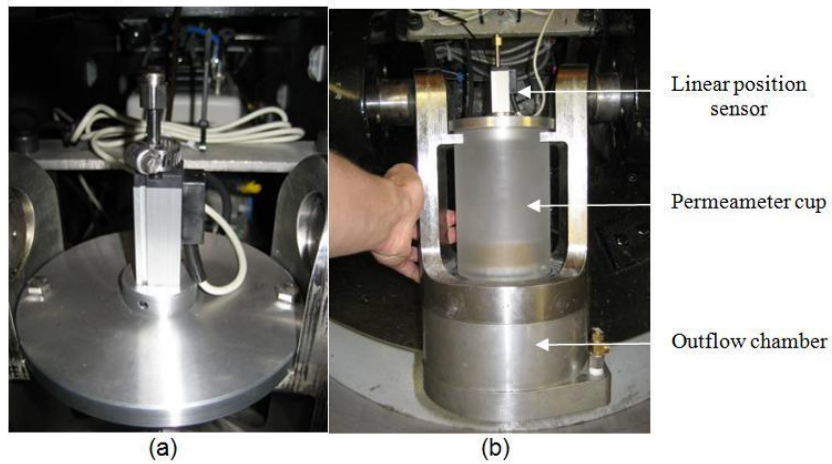


Figure 3.28: Components of the permeameter system: (a) Permeameter Top Cap; (b) Linear Position Sensor

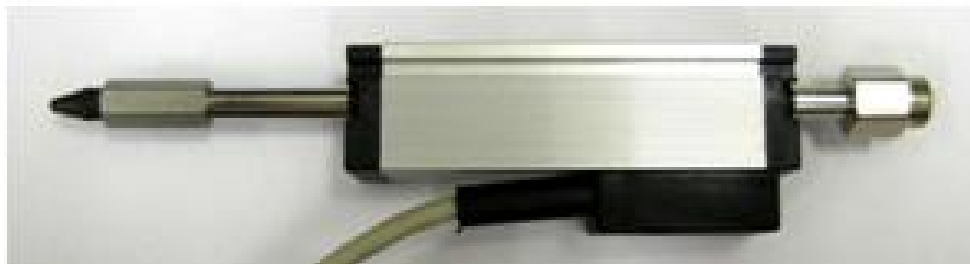


Figure 3.29: Linear Position Sensor

3.2.11 Low-flow Hydraulic Rotary Union

A constant height of water is maintained in the permeameter cup during testing. The water height is maintained by adding water using a set of flow pumps and a low-flow rotary hydraulic joint. The pumps and the hydraulic joint are used to deliver water to the top of the soil specimens while the centrifuge is spinning. During the test, constant height of water is set by the removal of a set screw from the wall of the permeameter cylinder. The inflow rate from the pumps is set to a greater rate than the outflow rate from the specimen, so excess water will spill out of this hole in the permeameter wall and a constant height of water is maintained.

Just as in free-swell testing (Section 4.1), the specimen is allowed to reach a steady height under the seating load prior to the addition of water. Once the specimen has reached a steady height, this height is taken as the initial height of the specimen. Once water is added, the height of the specimen is recorded with time and the vertical swell of the specimen is calculated considering the initial height of the specimen. This procedure is followed so that any swelling measured is due to changes in moisture rather than the addition of the seating load to the as-compacted specimen. In centrifuge testing the same procedure can be replicated. In the centrifuge the loading of the soil-specimen comes from the centrifugal force caused by the rotation of the permeameter. Accordingly, water must be added after the soil specimen is in flight.

The centrifuge is equipped with a low-flow hydraulic joint. Once the specimen is compacted it is flown up to speed and the height is monitored. Water is continuously added to the permeameter chamber and the constant height of water in the permeameter is maintained by an outflow port. In this manner, the centrifuge permeameter can be used to duplicate the procedure used in free-swell testing meant to isolate the effects of saturation on the swelling of a soil under a particular state of total stress.

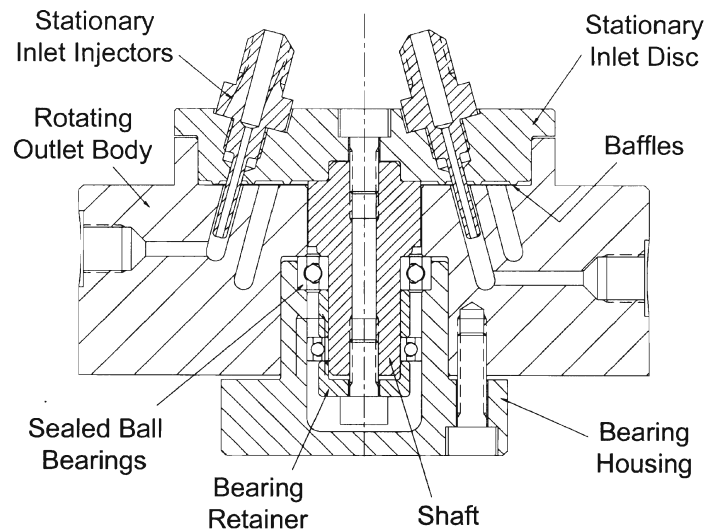


Figure 3.30: Detail of Hydraulic Rotary Union (Broadbent 2006, Figure 1.11)

3.2.12 Surcharge Pressure

The surcharge pressure atop a soil specimen is a function of the G-level and the mass of ball bearings placed atop the top platen. Since, at a minimum, the linear position sensor and the top platen must be placed atop the soil specimen, the mass of these two objects create a minimum surcharge pressure during testing. The variation of this minimum surcharge pressure is shown as a function of G-level in Figure 3.31. Also shown in the figure is the effect of additional mass, added in the form of stainless steel ball bearings, on surcharge pressure.

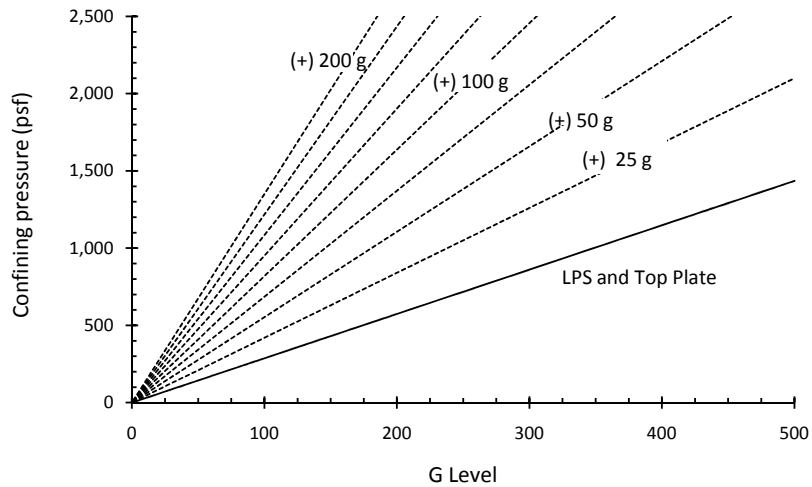


Figure 3.31: Surcharge Pressure as a Function of G-level and Surcharge Mass

3.2.13 Measurement of Soil Swelling

The change in height of soil specimens in the centrifuge is measured using a linear position sensor (Section 3.2.10). The changes in height registered by the linear position sensor are, however, not entirely due to changes in the height of the soil specimen. A portion of the changes in height registered by the linear position sensor are due to machine deflections. As the centrifuge is flown up to speed the metal top cap, the rod of the linear position sensor, and even the base of the permeameter may deflect. Accordingly, these deflections need to be accounted for so that they are not interpreted as changes in the height of the soil specimen. The machine deflections were measured for both permeameters by flying the centrifuge at a series of G-levels in the absence of a soil specimen with the top and bottom caps in direct contact (Figure 3.32). The machine deflections at 125 G, the highest G-level tested, were less than 0.2 mm. Given the relationship between the machine deflection and G-level, the height changes measured using the linear position sensor can be corrected.

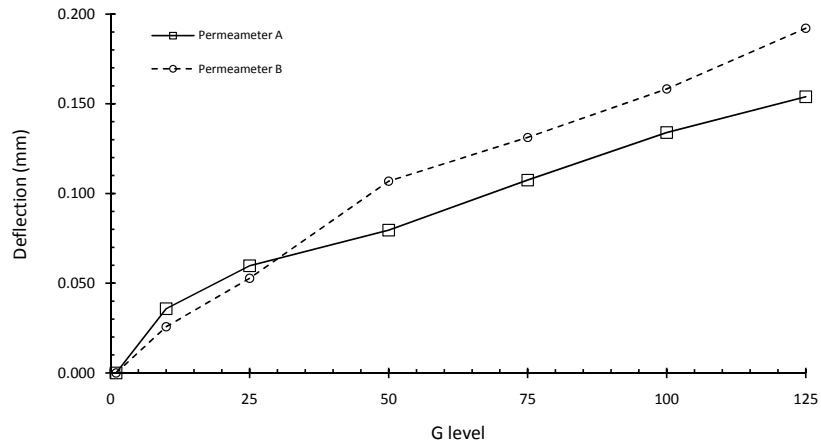


Figure 3.32: Machine Deflections

The changes in soil height registered by the linear position sensor are not only due to the swelling of the soil specimen. Instead, the changes in soil height include the initial compression of the soil specimen as the centrifuge is flown up to full speed, the swelling of the soil specimen with the addition of water, and the expansion of the soil specimen when the test is stopped. Accordingly, the height changes measured by the linear position sensor during the test must be broken down into a series of stages. In order to better explain this process, the height of soil specimen, H , is given a subscript denoting the testing stage. The various testing stage heights are shown in Figure 3.33. The same testing stage heights are also shown in Figure 3.34 with the a largest time scale in the beginning and end of the test in order to better illustrate the changes in height that occur during these time periods.

In the first stage of testing, the height of the compacted soil specimen, H_1 , is measured with the vertical dial stand. The specimen is then placed into the centrifuge and flown up to speed. During this process the soil specimen compresses to H_2 , at which point water is added above the soil specimen. Subsequently, the soil specimen is allowed to swell for a period of time, in this example 72 hours, at which point the specimen reaches H_3 . Once the test is stopped and the centrifuge is turned off bringing the centrifuge to a gradual stop, the soil expands to H_4 . Finally, the specimen is removed from the centrifuge and expands

to H_5 .

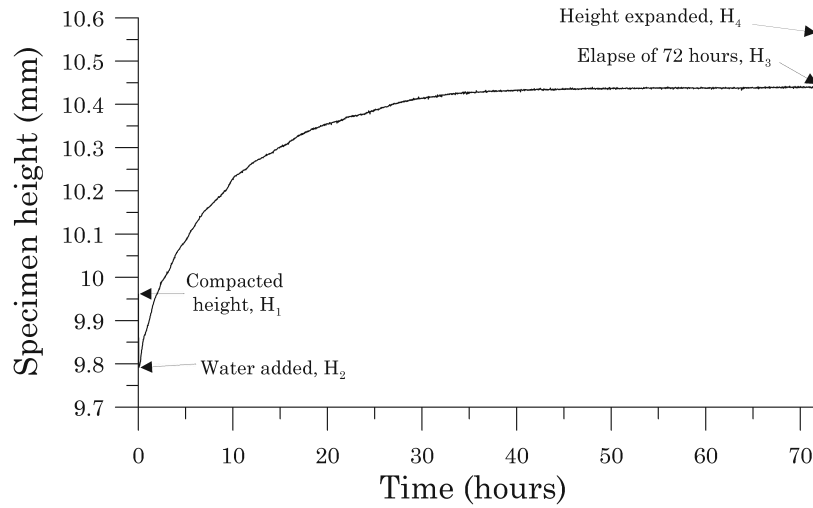


Figure 3.33: Height Changes in Soil Specimen during Centrifuge Test

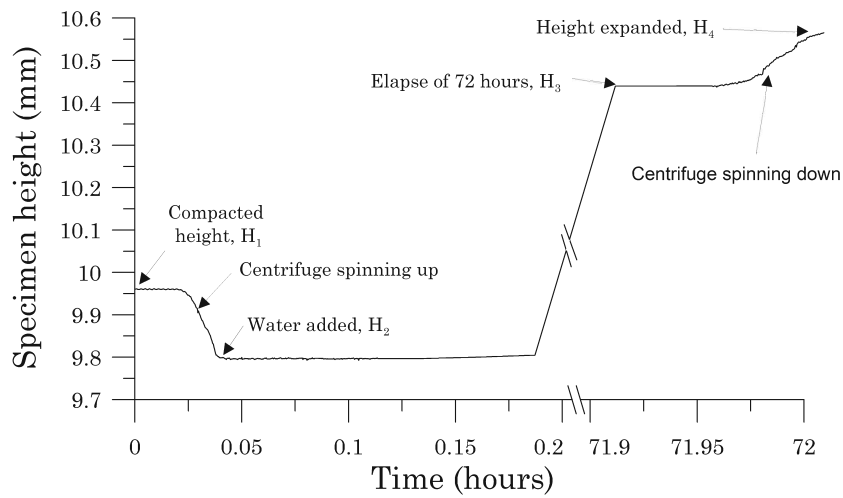


Figure 3.34: Height Changes in Soil Specimen During Centrifuge Test Plotted with a Break Axis

The compression, swell, and expansion of the soil specimen during testing can be calculated from the four heights (H_1 , H_2 , H_3 , and H_4) as follows:

$$\textit{Compression} = H_1 - H_2 - \textit{Machine} \quad (3.8)$$

$$\textit{Swell} = H_3 - H_2 \quad (3.9)$$

$$\textit{Expansion} = H_4 - H_3 + \textit{Machine} \quad (3.10)$$

where “Machine” is the machine deflection for the permeameter at the rotational velocity of the test.

3.3 Centrifuge Testing Procedure

The following steps outline the testing procedure for the centrifuge permeameter. A data sheet that has been developed for centrifuge testing is presented in Figure 3.35.

3.3.1 Soil Preparation

The soil specimen used for testing should be prepared in a manner similar to how it is prepared in the field for the application of interest. If construction is to take place on a natural soil, then testing should be carried out on samples that are trimmed into the testing device. Testing for this study has only been performed on remolded samples and thus only the testing of remolded soils is addressed in this procedure. Index testing and preparation of the soil for a test on remolded soil is to proceed as follows:

1. Soil processing: Process an adequate amount of soil for running several tests. This processed soil is the source for of soil for your centrifuge test. Prior to testing, the soil was air-dried, crushed, and processed. Air drying was conducted at a temperature of approximately 120°F, not exceeding 140°F according to ASTM D 698-00a so that changes in the soil properties would not occur.

2. Target moisture content: Once the target water content and density are determined, sufficient soil to form two specimens should be mixed to the target water content. First, the water content of the source soil should be determined and entered into the data sheet. Then, using the target water content and density, the mass of soil to be used from the source material and the mass of water that should be added should be determined.
3. Moisture equilibration: The mixed soil should be placed in an air-tight plastic bag for 48 hours. It is preferable that this plastic bag is kept in a humidity chamber for this 48 hour period.

Test #				Date (yyyy/mm/dd)	/	/	
Test description	(i.e. "50G-S1W2-Opt-48HR")			Start time		End time	
Technician	Jeffrey Kuhn			H _s (cm)		H _w (cm)	
Soil	Eagle Ford	Atterberg	88-39=49	ω _{target} (%)		Duration (hr)	
Specific gravity, G_s	2.73	Clay frac.	64%	G _{target}		ω, RPM	
Sample preparation							
Cross sectional area	38.5	(cm ²)		Sample A	Sample B		
Height		(cm)	Target specimen height				(in)
Volume		(cc)	Thickness of top				(in)
Target dry density		(pcf)	Thickness of base				(in)
(g/cc = pcf*0.157*0.102)		(g/cc)	Σ = Target thickness				(in)
Target water content		(%)	Actual thickness				(in)
Target wet density		(g/cc)	Final thickness				(in)
Mass of wet soil per lift		(g)					
Prepared water content	LBL	W _c (g)	W ₁ (g)	W ₂ (g)	ω (%)		
Tests							
Sample A							<input type="checkbox"/> Outflow
Permeameter**	Weight (g)						<input type="checkbox"/> Filter ppr.
Compacted							<input type="checkbox"/> Lubricate
With weights							<input type="checkbox"/> t _{top}
With water				W _{top} paper (g)			<input type="checkbox"/> t _{base}
Without water				W _{base} paper (g)			<input type="checkbox"/> W _{permeameter}
							<input type="checkbox"/> target h
Spacer thickness (mils)							<input type="checkbox"/> weigh soil
Water contents	LBL	W _{dish} (g)	t _{Dish} (mil)	Meas (mil)	W ₁ (g)	W ₂ (g)	<input type="checkbox"/> Compact
Top							<input type="checkbox"/> t _{actual}
Base							<input type="checkbox"/> W _{compacted}
							<input type="checkbox"/> Holes facing
							<input type="checkbox"/> Inflow tube
Sample B							<input type="checkbox"/> LPS voltage
Permeameter**	Weight (g)						<input type="checkbox"/> Spreadsheet
Compacted							<input type="checkbox"/> DAS T = 1s
With weights							<input type="checkbox"/> Spin 2 settle
With water				W _{top} paper (g)			<input type="checkbox"/> (+) water
Without water				W _{base} paper (g)			<input type="checkbox"/> DAS T = 100s
							<input type="checkbox"/> Observe
							<input type="checkbox"/> DAS T = 1s
Water contents	LBL	W _{dish} (g)	t _{Dish} (mil)	Meas (mil)	W ₁ (g)	W ₂ (g)	<input type="checkbox"/> Stop
Top							<input type="checkbox"/> W _{dish}
							<input type="checkbox"/> t _{dish}
							<input type="checkbox"/> W _{water}
							<input type="checkbox"/> W _{w/out} water
							<input type="checkbox"/> t _{final}
Base							<input type="checkbox"/> t _{spacer}
							<input type="checkbox"/> Meas (mil)
							<input type="checkbox"/> W ₁
							<input type="checkbox"/> W ₂
*H _{soil} = (D _{base}) - (D _{top}) - (t _{top})							
** Permeameter weight - Permeameter cylinder + base plate + top plate + filter papers +vacuum grease							

Figure 3.35: Centrifuge Permeameter Data Sheet

3.3.2 Permeameter cup preparation

Each test, the centrifuge cup must be properly cleaned, re-assembled, and weighed in preparation for compacting the specimen into the permeameter cup.

1. Cleaning: The permeameter cup should be clean prior to starting specimen preparation. If the cup was not cleaned after the previous test, it should be cleaned with soap and water. The permeameter cup should then be dried out with a towel.
2. Grease application: To minimize ring friction and sidewall leakage during testing, a thin layer of high vacuum grease should be spread around the inner wall of the permeameter cup. The easiest way to apply the grease is with the tip of one's finger. Down Corning High Vacuum Grease is used for this purpose.
3. Ponding height selection: The height to which water is to be ponded above the base plate should be selected and the set-screws in the wall of the permeameter should be re-arranged as appropriate.
4. Weight of the prepared permeameter: The permeameter cylinder, base plate, top plate, filter papers, and vacuum grease should be weighed together on a laboratory scale.
5. Base plate and base filter paper: After the permeameter is weighed, the base plate is then placed inside of the permeameter cylinder and a piece of filter paper is placed atop the porous plate. The filter paper that are used for the centrifuge permeameter are pre-cut and are a product of Humboldt Manufacturing Company out of Schiller Park, Illinois. The filter paper is 2.8 inches (70 mm) in diameter and is model HM-4189.28.
6. Height determination: In order that the initial and final heights of the soil specimen can be determined, the height of the base plate and the thickness of the top plate are measured with the vertical dial indicator.

3.3.3 Soil specimen preparation

The soil specimen is compacted in 10 mm lifts up to the desired specimen height using using a Marsh-Bellofram actuator air piston (product number 980-077-000). The air piston was outfitted with a 5-inch long, 0.5-inch diameter rod screwed onto the actuator air piston to serve as a compaction ram and used to impart energy into the soil.

1. Soil placement: In order to begin the compaction process, soil is placed in the cup and kneaded into place with one's finger. If this kneading is not carried out, the compaction foot will penetrate the soil and strike the base plate without compacting the soil.
2. Piston compaction: Once the soil is kneaded into place, the air regulator on the Bellofram pump is set to 15 psi for standard Proctor compaction effort and the footing is brought down onto the surface of the soil in 1 second intervals, moving around the surface of the soil to provide a uniform compaction height. Once the soil has been kneaded at all points, the height of the top of the soil specimen is checked with a Vernier caliper. When the height of the soil specimen is within 0.1 mm of the target height, proceed to final compaction.
3. Additional lifts: If a specimen height of greater than 10 mm is desired then it is necessary to prepare multiple compaction lifts. In this case, the top of the previous lift is scarified prior to compaction. The digital vernier caliper is unlocked, retracted an additional 10 mm and then locked again. Finally, steps two and three are repeated.
4. Final compaction: At this point, the top filter paper and plate are placed onto the soil and pressed firmly into place. The vertical dial indicator is then used to measure the height of the top plate. The height of the top plate is compared to its target height and the technician proceeds with the final compaction. For final compaction, a metal cylinder with a diameter approximate of the specimen diameter is struck with a rubber hammer to force the soil specimen to its target height. The technician will

strike the metal cylinder several times, gaging the number of strikes based on the progression to the target height, measuring the height of the soil specimen between trials. Prior to using this procedure, the final height was reached with the Bellofram pump and by using a vernier caliper. When the vernier caliper was used for measuring the compaction height, the the target height could only be reached within +/- 0.5 mm of the desired height. After implementing the final compaction procedure, the target height can be reached within +/- 0.01 mm of the desired height (Figure 3.36).

5. Initial total weight: The permeameter containing the compacted soils specimen sandwiched between filter papers and outflow plates is weighed and the weight is noted as W_{total} in the data sheet.

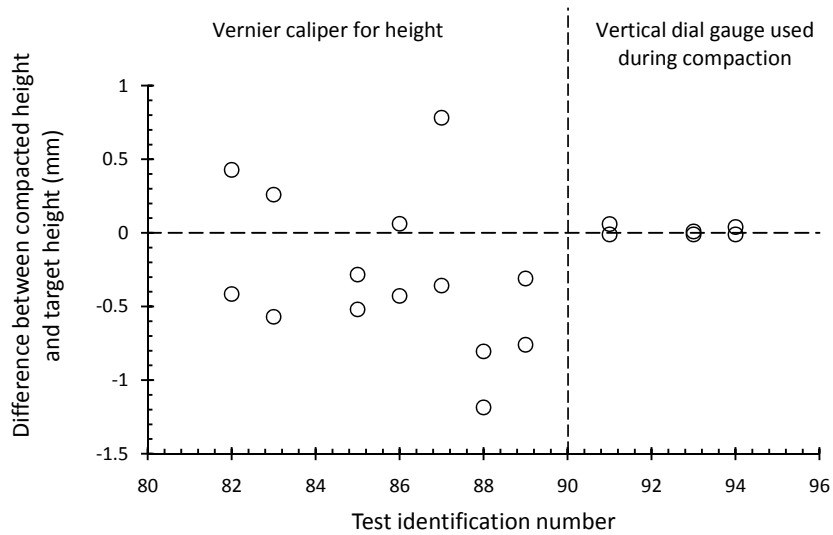


Figure 3.36: Correlation Between Methodology to Verify Compaction Height and Ability to Compact to the Target Height

3.3.4 Pre-flight preparation

After the specimen has been prepared, several steps are taken in placing the specimen in the centrifuge and preparing it for flight.

1. Outflow chamber: Fill the outflow chamber with 5 ml of fluid
2. Test cylinder insertion: Screw the test cylinder onto the top of the outflow chamber
3. Initial height measurement: A vernier caliper is used to measure the distance between the top of the permeameter cylinder and the top of the top plate. Four measurements of this distance are taken starting at the twelve o'clock position, proceeding to three o'clock, six o'clock, and nine o'clock. These height measurements are recorded in the data sheet as D_top and are separated by a pipe symbol, |.
4. Permeameter lid placement: Place the permeameter lid with the linear position sensor onto the chamber. Screw the lid down to the permeameter swing arm
5. Inflow tubing insertion: The inflow tubing is inserted into the permeameter lid.
6. LPS: The height of the linear position sensor (LPS) can be adjusted with the set screws in the lid

3.3.5 Initiation of the test

Once the centrifuge has been prepared for flight, it is now necessary to start the centrifuge.

1. Obstruction check: Check the inside of the centrifuge to make sure that it is free of any foreign objects and that everything is properly secured.
2. Centrifuge closure: Close and secure the centrifuge lid. Turn off the brake override
3. Start DAS: Turn on the data acquisition system (DAS) and start logging data at 30 second intervals
4. Start Centrifuge: Log into the centrifuge system, set the target rotational velocity, and start the centrifuge
5. Initial equilibrium: Monitor the height of the soil specimen until it comes to an initial equilibrium. Note the initial equilibrium time in terms of elapsed seconds since the start of data acquisition on the data sheet.

6. Initial ponding height: To establish the initial height of ponded water, pump 5 ml of water per mm of desired water height of above the initial soil height into the soil cylinder at a rate of 10 ml/min to reach the desired ponding height. The addition of water can be monitored through a portal located on the top of the centrifuge using a strobe light (Figure 3.37(a)) A picture of a specimen during a test captured using a digital camera and the strobe light is shown in Figure 3.37(b). Although not very evident in this image, the height of water above the specimen can be monitored to ensure that an adequate flow rate is maintained over the course of testing. During testing, a flow rate of 2 ml/hr has been found more than sufficient for maintaining the ponded height of water.

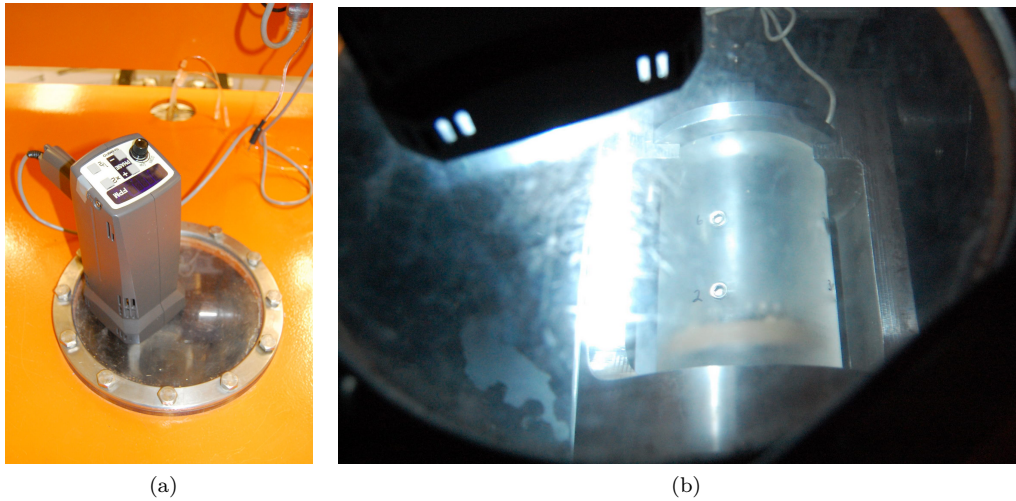


Figure 3.37: (a) Strobe Light (b) Image of Specimen During Test

3.3.6 Monitoring the test

Once the test is running, it is necessary to monitor the data acquisition system to determine if the proper height of water is being maintained and to monitor the outflow rate from the specimen.

1. Ponding height and Inflow Rate: The strobe light should be used to monitor the height

of ponded water in the chamber. As prior mentioned, an inflow rate of 2 ml/hr was adequate for maintaining the height of water. If the height is found to have decreased the system should be pulsed with 5 ml of water per each mm of desired water height above the initial soil height to guarantee the desired height of water is achieved.

2. Data logging: During testing, a computer in the laboratory is used to communicate with the solid state data acquisition system rotating in the centrifuge via a wireless Ethernet connection. The proprietary program Acqlipse that was developed by Broadbent Inc. is used to interact with the centrifuge. A screen shot Acqlipse during a centrifuge test is shown in Figure 3.38. During testing, it is the responsibility of the technician to ensure that that operation of the laboratory computer is uninterrupted.

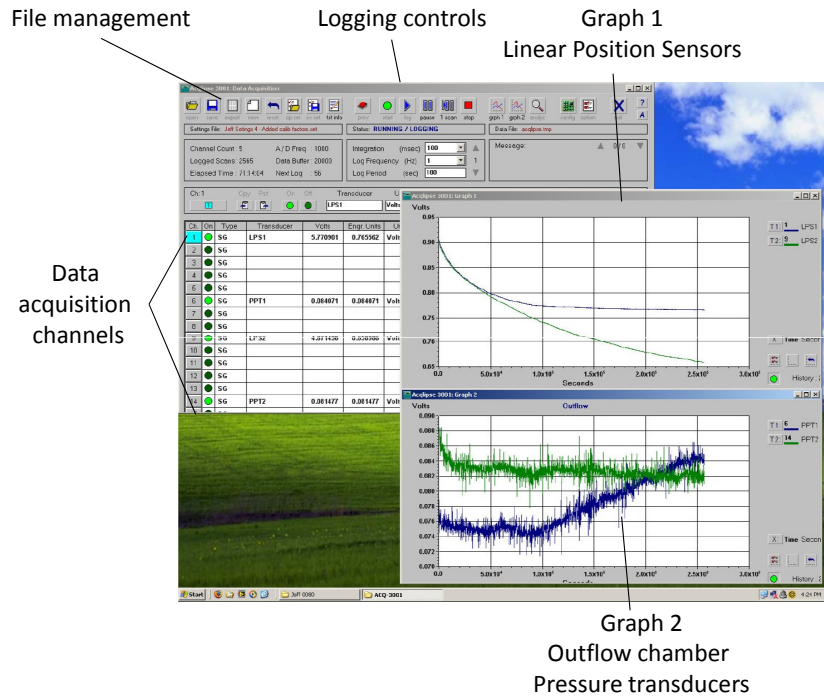


Figure 3.38: Screen Shot of Windows Based Data Acquisition Program Acqlipse

3.3.7 Finishing the test

1. Stopping the centrifuge: Once the test is finished, the centrifuge may be stopped by activating the stop button on the centrifuge control panel. The centrifuge will then take several minutes to slow down. Once the centrifuge has slowed down completely, the operator will hear the sound of the air-brakes locking into place. This is immediately followed by the sound of the lid safety latch releasing. These two sounds indicate that the centrifuge has stopped and that the user is able to open the centrifuge lid.
2. Brake override: The brake override switch should be activated. When the centrifuge is at rest, the air-brakes are locked preventing the centrifuge table from being rotated. The brake override switch can be activated to allow the table to be rotated giving the user the ability to access each permeameter.
3. Inflow tubing removal: The inflow tubing is removed from the permeameter lid.
4. Permeameter lid removal: The two bolts holding the permeameter lid are unscrewed and the lid is removed from the top of the permeameter.
5. Water removal: Water that remains ponded atop the specimen is poured or vacuumed off.
6. Final height measurement: A vernier caliper is used to measure the distance between the top of the permeameter cylinder and the top of the top plate. Four measurements of this distance are taken starting at the twelve o'clock position, proceeding to three o'clock, six o'clock, and nine o'clock. These height measurements are recorded in the data sheet as D_top and are separated by a pipe symbol, |.
7. Test cylinder removal: The test cylinder is screwed off of the outflow chamber.
8. Final total weight: The permeameter is turned on its side and excess ponded water is allowed to drain out. The permeameter is then placed atop of a laboratory scale to determine the final weight noted as W_total in the data sheet.

9. Water content determination: Six water content trays (i.e. three for each specimen) should be weighed and their labels and weights should be noted in the data sheet. The specimens are extruded from test cylinder and as they are cut off with a cheese cutter in 3.33-mm thick disks (Figure 3.39). The trimmed soil specimens are placed into soil trays, a flat plate is placed atop them and their height is measured using the vertical dial indicator.
10. Cleaning: The permeameter cup should be cleaned with soap and water and then dried with a towel in the case that the next test is to begin immediately or left to air-dry on an equipment rack in the case that the next test is planned for the following day.



Figure 3.39: Trimming Centrifuge Test Specimen to Obtain the Water Content Profile

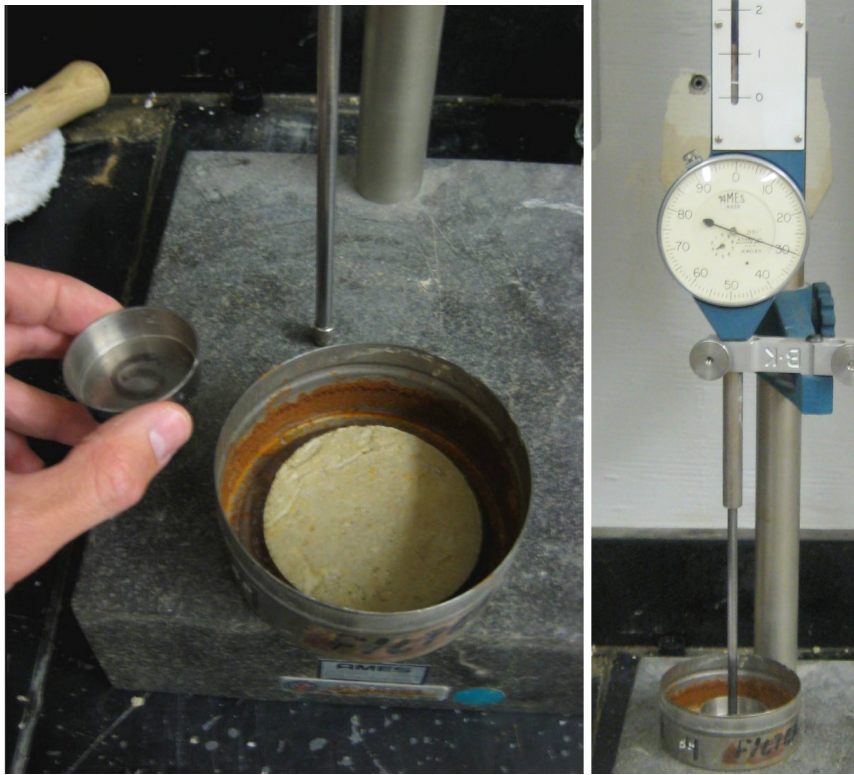


Figure 3.40: Measurement of Slice Thickness Using the Vertical Dial Indicator

Chapter 4

Results from 1-G Testing Program

A testing program that was complimentary to centrifuge testing was developed in order to better understand the results of centrifuge testing. The testing program consisted of free swell tests and 1-G infiltration tests. An overview of these testing methods and the results obtained from these testing methods are presented in this section. The free swell tests were conducted in accordance with current standards in order to provide a basis of comparison with tests that are performed in practice. The 1-G infiltration tests were conducted in order to better represent the infiltration conditions in the centrifuge and help provide a tie between free swell testing and centrifuge testing.

4.1 Free Swell Tests

A series of free-swell tests were conducted on a specimen of Eagle Ford clay compacted at optimum water content and to a density equivalent to 100% of standard proctor compaction (Section 3.1.3). The apparatus used for free swell testing is the oedometer pictured in Figure 4.1. In this test, the soil specimen is placed in a fixed-ring consolidation cell, as described

in Section 2.2, and a load is applied to the specimen. During testing, vertical movements of the specimen were monitored with a dial gauge and a linear variable differential transducer (LVDT). After the specimen is placed in the apparatus and then seating load is applied, the height of the specimen is monitored. Once the height of the specimen comes to equilibrium, data logging is started, and water is added to the reservoir in which the soil specimen is sitting in order to begin swell testing of the specimen.

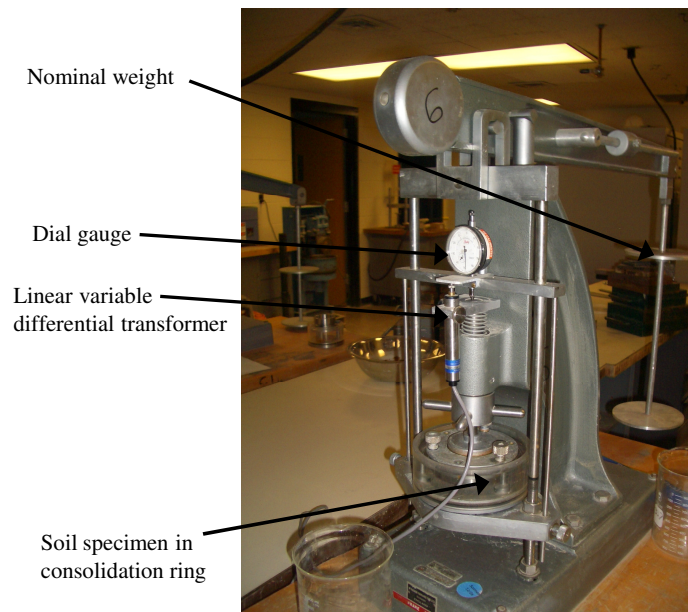


Figure 4.1: Free Swell Setup



Figure 4.2: Multiple Free Swell Setups

4.1.1 Differentiation Between Primary and Secondary Swelling

During centrifuge, free-swell, and 1-G infiltration testing, the rate of swelling was observed to reduce significantly within the first day of testing. As an example of this phenomena, the results of a free-swell test on a specimen confined at 250 psf are presented in Figure 4.3. During this test, it is evident that there is a significant reduction in the rate of swelling occurring between one and two days of testing. The concepts of and differentiation between primary and secondary swelling is presented in ASTM D4546 and was first introduced in Section 2.1.1. In ASTM D4546, the results of testing are plotted in a logarithmic time scale in order to differentiate between primary and secondary swelling.

The results for the free-swell test conducted at 250 psf are presented in a logarithmic time scale in Figure 4.4. In order to differentiate primary and secondary swelling, tangent lines are constructed about the point of inflection observed when the rate of swelling is seen to decrease significantly. These tangent lines can then be used to calculate the slope

of primary and secondary swelling. For this particular test, the slope of primary swelling was $3.6\%/log(min)$ whereas the slope of secondary swelling was $1.2\%/log(min)$. Accordingly, the rate of swelling was reduced by a factor of three. Also presented in Figure 4.4 is the time of secondary swelling and the magnitudes of total, primary, and secondary swelling. The time of secondary swelling was taken as the intersection of the tangent lines constructed about the point of inflection. For this test, the total swelling was 15.1%. Of this 15.1% swelling, 10.0% was found to be primary swelling whereas 5.1% was found to be secondary swelling. If the test would have been carried out for a period of time greater than 14 days, the magnitude of secondary swelling would be expected to increase. As the test was conducted, the magnitude of secondary swelling was approximately half of that of primary swelling. The duration of primary swelling was, however, only 12 hours whereas secondary swelling was allowed to occur for a period of 13.5 days. Given the determination of the time of secondary swelling, the results of the free-swell test are again presented in arithmetic time in Figure 4.5.

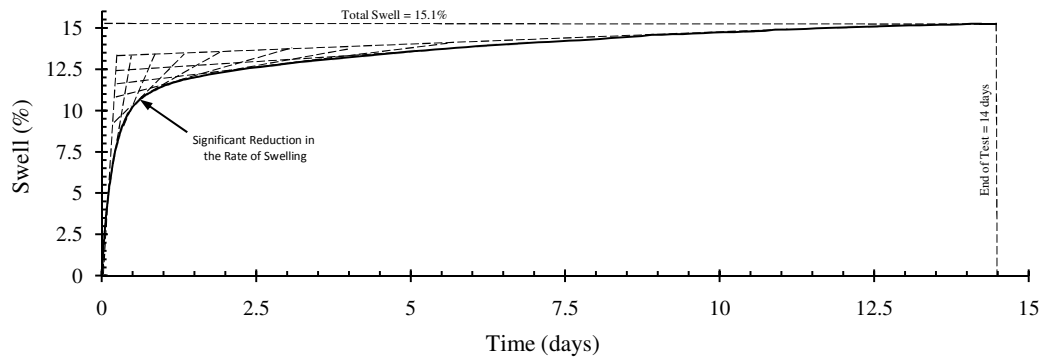


Figure 4.3: Swelling for a Free-Swell Test Conducted under a Total Stress of 250 psf

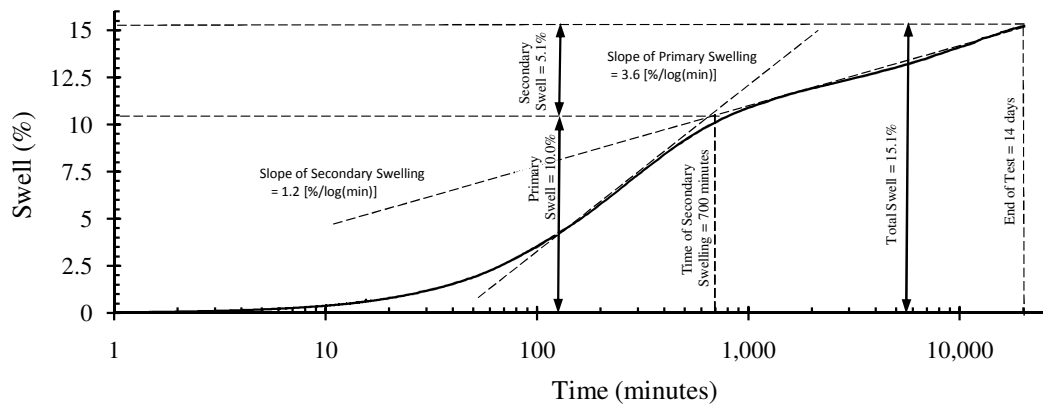


Figure 4.4: The Differentiation Between Primary and Secondary Swelling for a Free-Swell Test Conducted under and Total Stress of 250 psf

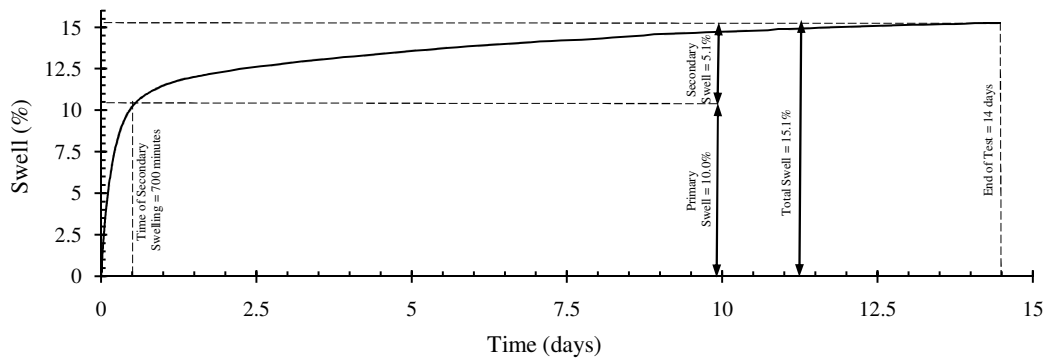


Figure 4.5: Primary and Secondary Swelling on an Arithmetic Scale

In free-swell testing, it is capillary forces (i.e. matric suction) within the soil that drive the flow of water into the soil specimen. It is likely that during primary swelling these forces dominate water flow into the specimen but that under long-term conditions matric suctions dissipate and there is a long-term hydration of the clay occurring that may be driven by osmotic suction. Due to the setup of the free-swell tests, air entrapped within the specimen has no easy means of escaping and thus it may be the diffusion of this air through the pore fluid of the soil that may lead to secondary swelling as soil particles that were previously bounded by air bubbles are now exposed to water. During an infiltration test, however, a gradient is maintained across the specimen and as water infiltrates into the soil,

entrapped air can diffuse into the water and flow out of the specimen. In the centrifuge, this gradient is significant as the weight of the pore fluid is effectively increased and thus the flow of water is driven more quickly through the soil.

4.1.2 Measured Swelling during Free-Swell Testing

The swelling of the soil specimens tested in the free-swell tests with total stress values ranging from 250 psf to 4,000 psf are shown in Figure 4.6. The height changes of the specimen over time demonstrate that as expected, specimens under higher total stresses swell less and require less time to reach a steady height. The specimen under lower total stresses, however, required a greater amount of time to reach a steady height and swelled more.

The swell behavior of the specimens at smaller times can be seen in the semi-log plot of swell versus time in Figure 4.7. Based on these free-swell tests, the rate of swelling is seen to decrease with increasing total stress. From this plot, it is also evident that the slope of swell versus time is still significant at a time of 14 days when the test is finished. The rates of primary and secondary, as discussed in the previous section, is presented in Section

At the end of free-swell testing, the specimen is assumed to have reached saturation. Accordingly, the pore water pressure in the specimen is essentially zero and the seating load, or total stress, is assumed to be the effective stress. Given this assumption, the relationship between swell and effective stress is presented in Figure 4.8. The relationship between swell and effective stress was found to be strongly linear in a semi-logarithmic scale. Furthermore, the pressure required to prevent the swelling of the soil, often known as the “swell pressure” would be expected to be 6,000 psf based on the relationship between swell and effective stress. This same relationship can also be expressed in terms of the final void ratio and the effective stress as shown in figure 4.9.

In order to determine the proportion of swelling which occurs over a short testing time period, the amount of swell observed after 3 days of testing was compared to the amount of swell observed after 14 days. This comparison was made by taking the proportion of swell

after 3 days to that after 14 days^{4.1}. For free-swell testing, this value was found to range from 0.84 for 250 psf to 0.96 for 2,000 psf. Accordingly, between 5 and 10% of the swell observed during free swell testing occurred between 3 and 14 days of testing.

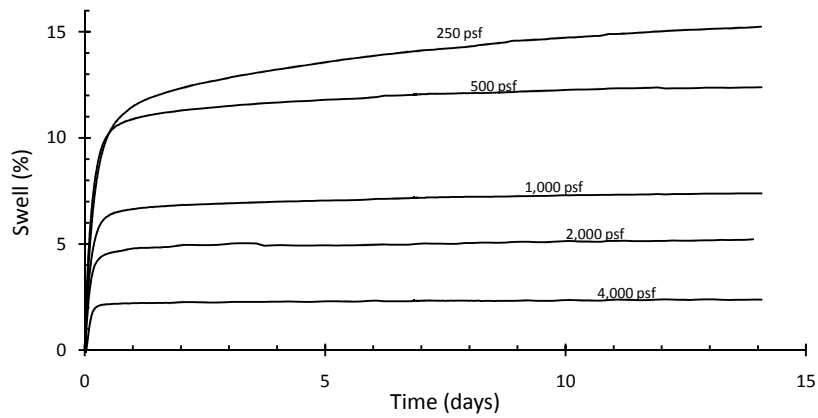


Figure 4.6: Free-swell Test on Eagle Ford Clay

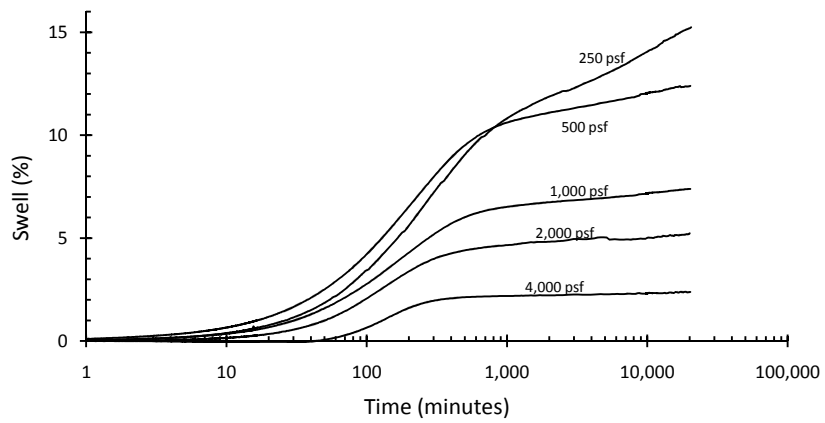


Figure 4.7: Semi-log Plot of Free Swell Tests

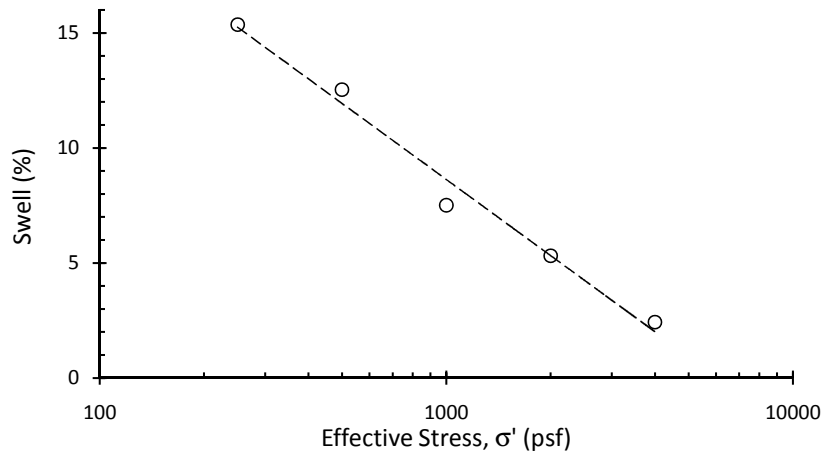


Figure 4.8: Swelling of Swell Testing on Compacted Eagle Ford Clay Specimens Subjected to Range in Seating Loads

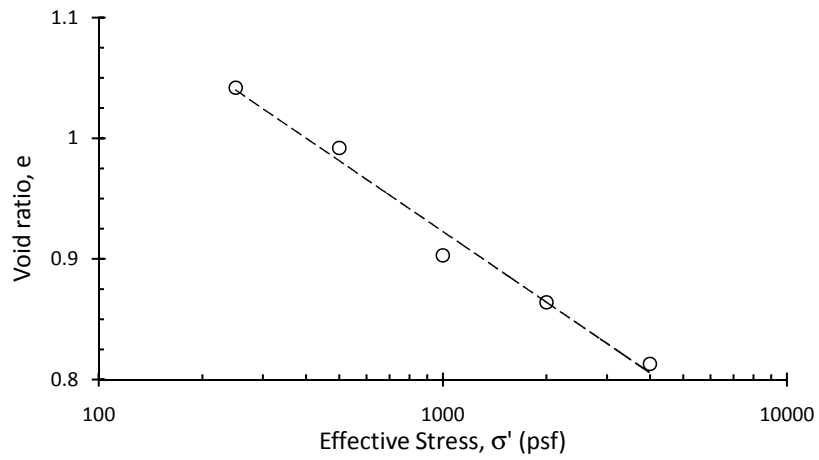


Figure 4.9: Final Void Ratio of Free Swell Specimens of Compacted Eagle Ford Clay Specimens Subjected to a Range in Seating Loads

Table 4.1: Swell after 72 hours / Swell after 14 Days for free swell tests

Total Stress (psf)	$\epsilon_{72 \text{ hour}}/\epsilon_{14 \text{ day}}$
250	0.84
500	0.93
1,000	0.94
2,000	0.96
4,000	0.95

4.1.3 Effects of the Specimen Aspect Ratio

When setting up free swell tests, the height of the soil specimens were chosen to match the soil specimen height of 10 mm used in centrifuge testing. However, since the diameter of the centrifuge and free swell specimens differed, the aspect ratios for the two testing setups were differed. With a diameter of 63.4 mm, the aspect ratio for free swell testing on a 10-mm thick specimen is 0.16. With a diameter of 70.0 mm, the aspect ratio (i.e. height to diameter ratio) for centrifuge testing on a 10-mm thick specimen is 0.14. Since these testing setups had different aspect ratios, it was necessary to check whether the relationship between void ratio and effective stress was independent of the aspect ratio of the testing setup. By using a specimen height of 9 mm for a series of free swell tests, the aspect ratio of the free swell testing setup was able to match that of the centrifuge testing setup. The resulting relationship between void ratio and effective stress is shown for the 10-mm and 9-mm thick free swell specimens in Figure 4.10. Strong agreement between the two different tests was found for effective stresses of 500 psf and greater. For an effective stress of 250 psf, the swell of the specimen with a aspect ratio equal to the of the centrifuge exceeded the swell of the specimen with the same height as the centrifuge sample. Specifically, the 10-mm thick sample swelled by 15.4% whereas the 9-mm thick specimen strained 16.8%. Although the sides of the oedometer rings were greased prior to testing, the 10% decrease in the soil specimen height could have resulted in reduced side shear and thus allowed for greater swelling. Accordingly, swelling measured in the centrifuge for 10-mm thick specimens at smaller values of effective stress may better agree with the 9-mm thick soil samples.

The free swell tests with different heights can also be compared in terms of the measured swell versus time. A plot of the swell versus time for the 10-mm and 9-mm thick samples is shown in Figure 4.11. As expected, the swell versus time curves for the 9-mm thick specimens decrease in slope at a more significant rate than for the 10-mm thick specimens as the initial distance to the wetting boundary has been decreased by 10%.

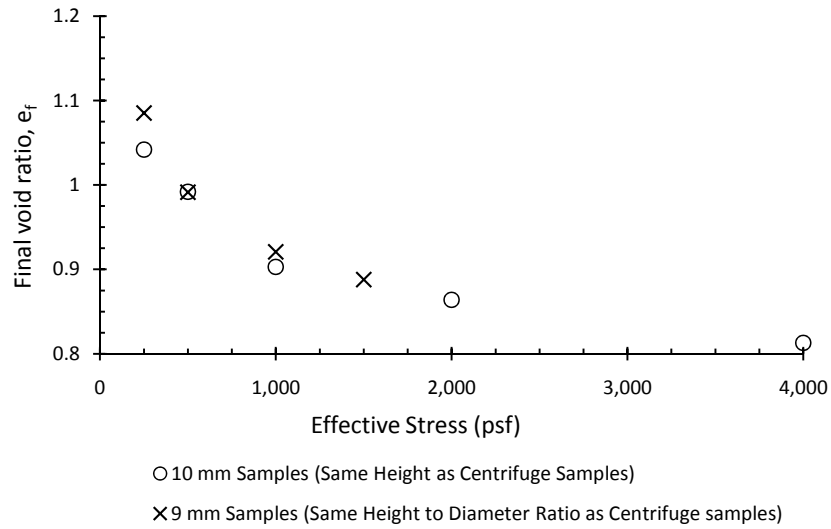


Figure 4.10: Final Void Ratio of Free Swell Specimens of Compacted Eagle Ford Clay Specimens with the Same Height as Specimens Used in the Centrifuge (10-mm thick) and Specimens with the Same Aspect Ratio as Specimens Used in the Centrifuge

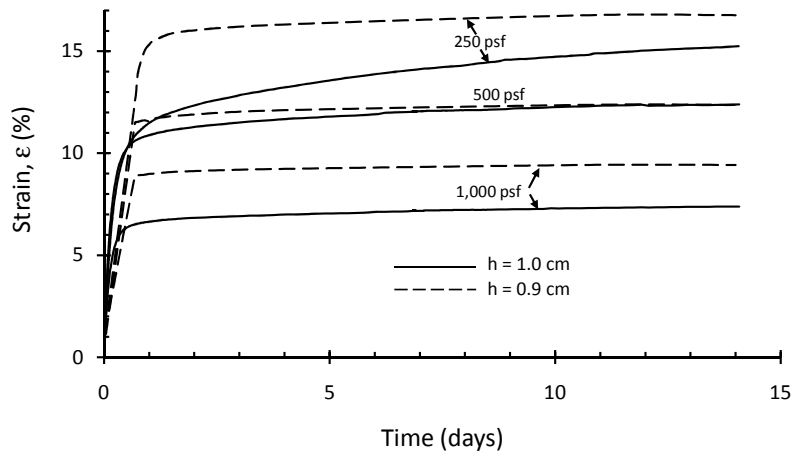


Figure 4.11: Swell Versus Time for Free Swell Specimens of Compacted Eagle Ford Clay Specimens with the Same Height as Specimens Used in the Centrifuge (10-mm thick) and Specimens with the Same Aspect Ratio as Specimens Used in the Centrifuge

4.2 1-G Infiltration of Centrifuge Testing

In order to better understand the behavior of a soil specimen which is infiltrated from the top under constant water and surcharge pressures a series of tests are conducted using a modified triaxial cell. A picture of the specimen setup for this test is presented in Figure 4.12. In this setup, the specimen is placed within an acrylic tube. The acrylic tube sits on the triaxial base plate and a membrane is used to seal the acrylic tube to the base plate. Spacers, which consequently act as seating loads, are placed on top of the soil specimen so that the triaxial piston can act on the top of the specimen. An outflow tube from the base of the specimen is fed into a graduated cylinder and is intended to catch any outflow that may occur. The assembled apparatus is pictured in Figure 4.13. In this setup, a dial gauge is used to measure the movement of the triaxial piston. Weights are placed atop a plate which is fixed to the triaxial piston to provide the surcharge pressure on the sample. The chamber is filled with pressurized water which infiltrates into the top of the soil specimen. These tests were performed as part of a joint effort with Master's student Carlos J. Guzman.

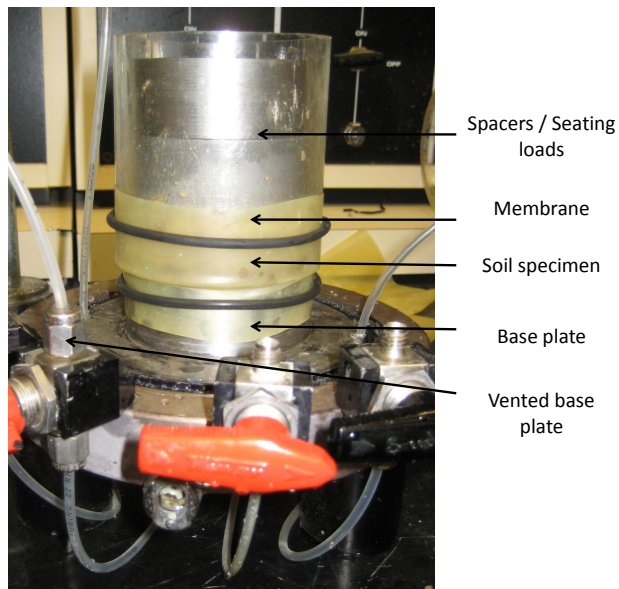


Figure 4.12: 1-G Infiltration Specimen Setup

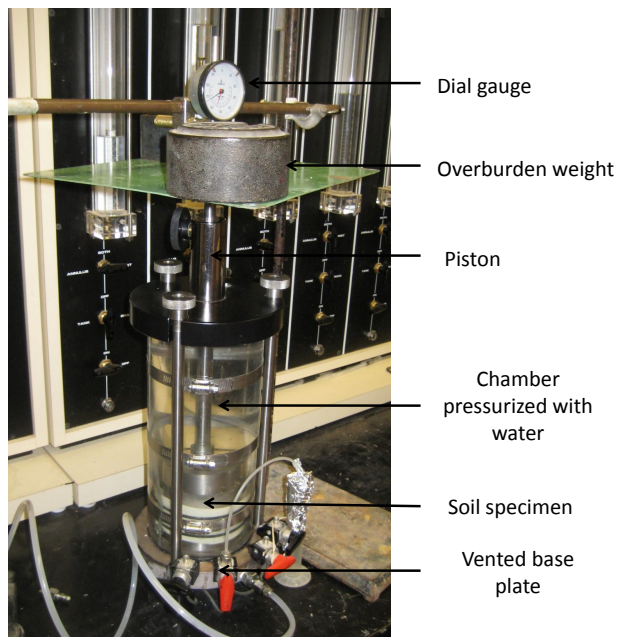


Figure 4.13: 1-G Infiltration Apparatus

The measurements of swell versus time for the 1-G infiltration tests are shown in Figure 4.14. As expected, and as found for free-swell testing, the measured swell was found to decrease with greater values of total stress. For free-swell tests, the rate of swell was shown to clearly decrease with total stress. For 1-G infiltration tests, the rate of swelling generally decreased with total stress. For the 1-G infiltration tests performed at 600 and 800 psf, the rate of swelling was found to be similar for the first 10 hours of testing. At times greater than 10 hours of testing the rate of swelling was found to decrease more rapidly for the tests performed at 800 psf than for 600 psf. The rate of swelling for 1-G tests is calculated in Section 7.1 and compared to the rate of swelling observed in free-swell and centrifuge testing.

The final void ratio of the soil specimen and the swell are plotted versus total stress in Figure 4.15. These relationship were found to be highly linear on a semi-log plot. The measured values of the void ratio and swell are compared to values measured during centrifuge and free swell testing in the next section.

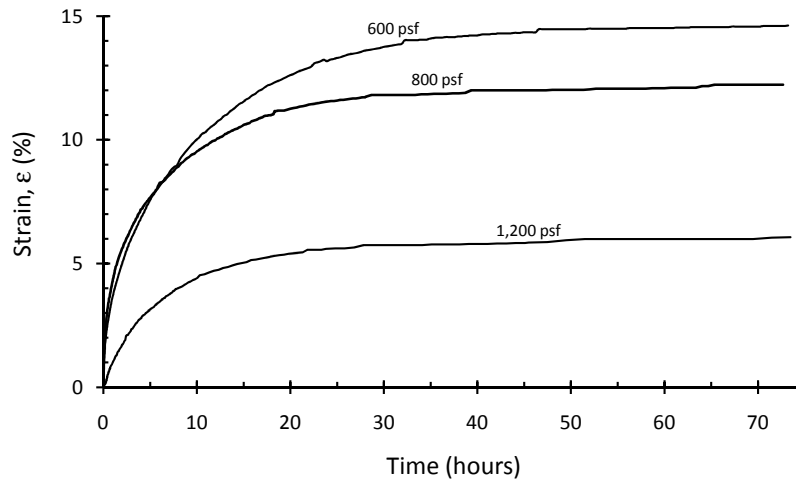


Figure 4.14: 1-G Infiltration Testing

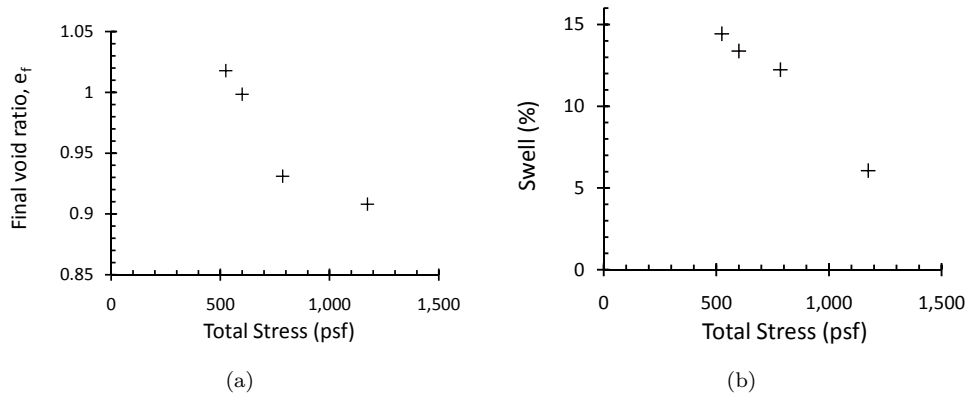


Figure 4.15: (a) Final Void Ratio and (b) Swell Versus Total Stress for 1-G Infiltration Tests

Chapter 5

Scope of the Experimental Testing Program

The bulk of experimental testing for this research study was conducted in the centrifuge permeameter described in Section 3.2 in accordance with the testing procedure described in Section 3.3. Pilot centrifuge testing was, however, conducted in a small centrifuge. Details concerning the equipment and testing procedures for this pilot centrifuge testing are presented in Plaisted (2009). Given the results of the pilot tests that were conducted in the small centrifuge, a series of preliminary tests were performed in the main centrifuge. Based on the results of preliminary testing in the main centrifuge, two testing series were subsequently planned and performed. In the first series, Series (i), centrifuge tests were performed with constant height of water and surcharge mass. In the second series, Series (ii), centrifuge tests were performed with constant water pressure and surcharge pressure.

In this chapter, each of the experimental testing programs are detailed. In subsequent chapters the results of these testing programs and an analysis of these results will also be presented.

5.1 Pilot Tests in the Small Centrifuge

Pilot testing to investigate the feasibility of centrifuge technology for evaluating the swell potential of expansive clay was performed in a centrifuge smaller than that described in Section 3.2. This smaller centrifuge can accommodate specimens with a diameter of 57 mm as supposed to the 71 mm diameter specimens tested in the centrifuge permeameter. The main difference between the small centrifuge and the centrifuge permeameter is the lack of a data acquisition system in the smaller centrifuge. In order to determine the swell of the soil specimen over time in the small centrifuge it is necessary to stop the small centrifuge, remove the specimen, and measure the height with a vertical dial stand. Additionally, water can not be added to a specimen while in flight in the small centrifuge and thus water must be added at the start of testing.

Three parametric evaluations were conducted using the small centrifuge as part of TxDOT Project No. 0-6048: Soil Testing Using Centrifuge Technology (Zornberg et al. 2009; Plaisted 2009). These three investigations evaluated the effects of G-level, specimen height, and ponding height. In the first, the effects of G-level on swelling were evaluated. In this test series, a 30-mm thick soil specimen was covered with 20 mm of water and flown at 25, 100, 200, and 400 G are shown in Figure 5.1. From these results, it was confirmed that the amount of swelling decreases with increasing G-level. It is, however, difficult to assess at which G-levels the specimens reached an equilibrium swell height as the degree of scatter in the results is considerable. Accordingly, it is also not possible to determine the time at which the specimens reached an equilibrium swell height.

In the second test series the effects of specimen height at a constant G-level were evaluated. In this test series, specimens of varying heights were flown at 200 G with 20 mm of ponded water (Figure 5.2). Despite the scatter in the results, it is evident that the 20-mm thick specimen reached a steady height of swell prior to the 30- and 40-mm thick specimens.

In the third and final test series the effects of varying the height of ponded water was evaluated. In this test series, specimens were flown at 300 G while the height of water

was varied (Figure 5.3). For the 20 and 30 mm ponding heights it does not appear that the height of ponded water has any significant effect on the degree or rate of swelling.

The preliminary tests performed in the small centrifuge show a decrease in swelling with increasing G-level. The test results do not, however, clearly show an equilibrium in swell height due to a large amount of scatter in the height measurements. The tests do, however, reveal that the the magnitude of swelling may be independent of the height of ponded water for the range of water heights used in this study.

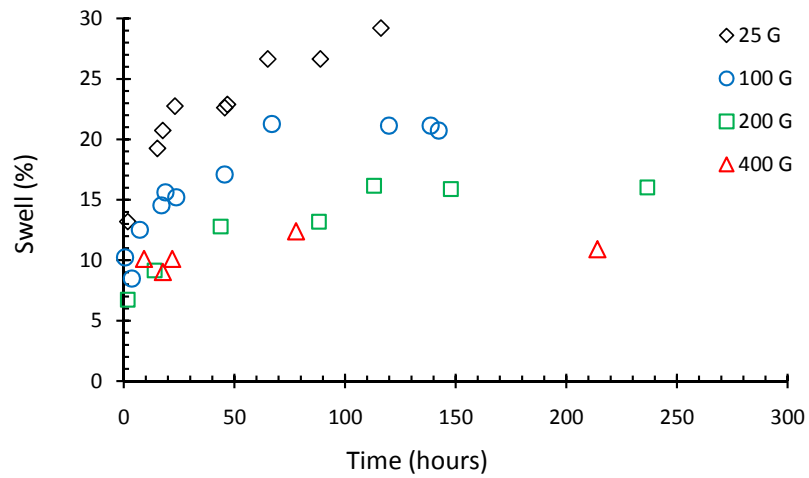


Figure 5.1: Small Centrifuge Test Series on 30-mm thick Specimens with 20 mm of Ponded Water (modified from Plaisted 2009)

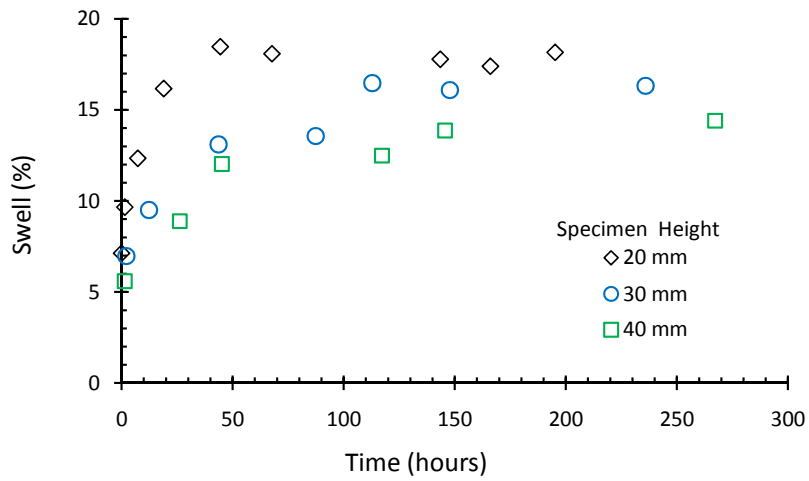


Figure 5.2: Small Centrifuge Test with Variable Specimen Heights at 200 G with 20 mm of Ponded Water (modified from Plaisted 2009)

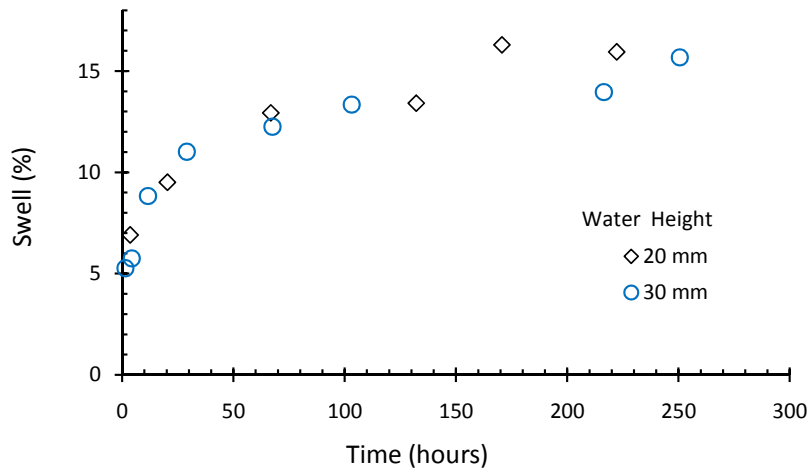


Figure 5.3: Small Centrifuge Test Series with Variable Water Height (WH) on a 20-mm thick Test Specimen at 300g (modified from Plaisted 2009)

5.2 Preliminary Tests in the Large Centrifuge

Preliminary tests were performed in the centrifuge permeameter which involved stopping the centrifuge so that the height of the specimen could be determined using the vertical dial

stand. In later tests, a linear position sensor was added to the testing setup so that the height of the soil specimen could be monitored continually during testing without the need for stopping the centrifuge. During preliminary testing, the mass of water in the outflow chamber was also weighed in order to determine the outflow rate from the soil specimen. In later tests, a pressure transducer was added to the outflow chamber so that the volume of outflow and thus the rate of outflow from the specimen could be monitored throughout the duration of test without the need for stopping the centrifuge.

Preliminary testing was conducted on a 30-mm thick specimen of clay with 20 mm of overlying water at 200 G to replicate a test series that had been conducted in the small centrifuge. The results from this test series are shown in Figure 5.4. The flux rate calculated from the measurement of the volume of water in the outflow chamber is presented in Figure 5.5. Based on the trends in swell and flux rate with time, the soil specimen reached its equilibrium swell and steady state flow after about 3-4 days. As with the results from the small centrifuge test series the scatter in the swell is considerable due to the approach of stopping the centrifuge to take measurements. However, comparison of the swelling from the small centrifuge tests and the centrifuge permeameter tests show that the swelling measured in the centrifuge permeameter exceed the swelling that were measured in the small centrifuge tests for the same testing conditions. Specifically, while a swell of 16% was measured in the small centrifuge for a test performed at 200 G on a 30-mm thick specimen of clay with 20 mm of overlying water, a swell of 20% was measured in the centrifuge permeameter. Despite this discrepancy in the preliminary tests, the reliability of measurements of vertical swell performed after the addition of a linear position sensor to the testing setup is demonstrated using the final testing protocol (Section 5.3). Accordingly, this difference may be of no great consequence to future test series, but for the sake of comparison may be attributed to the erroneous testing procedure of needing to bring the centrifuge to a halt in order to measure specimen height.

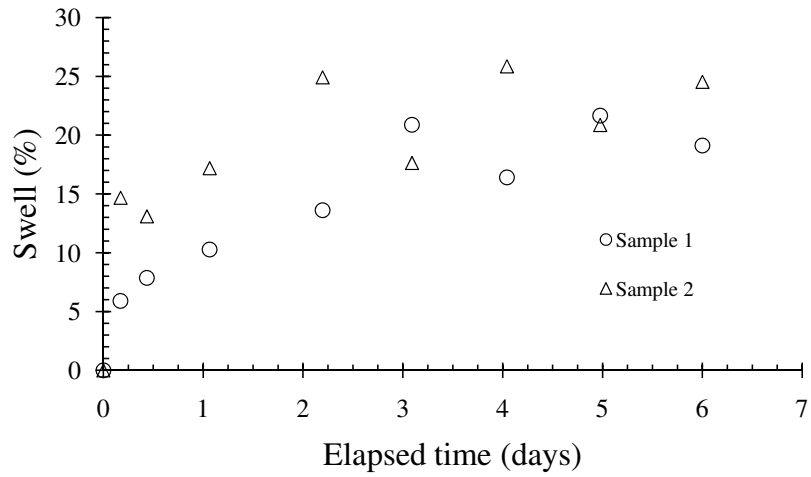


Figure 5.4: Series (o): Manual Swell Measurement for 30-mm thick Specimens with 20 mm of Pondered Water at 200 G

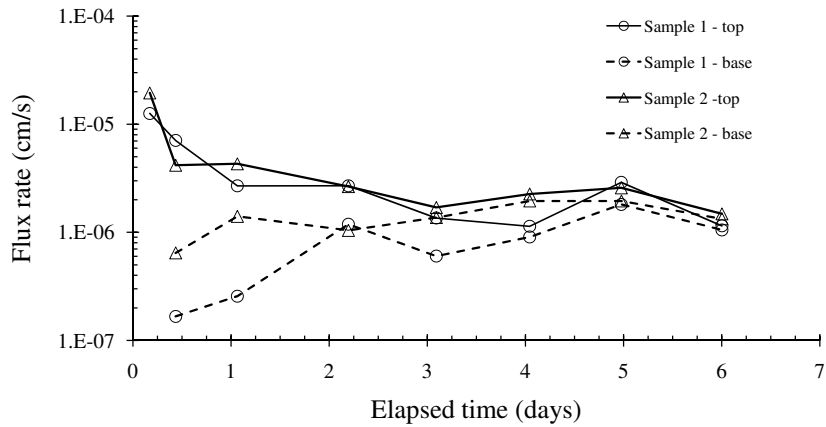
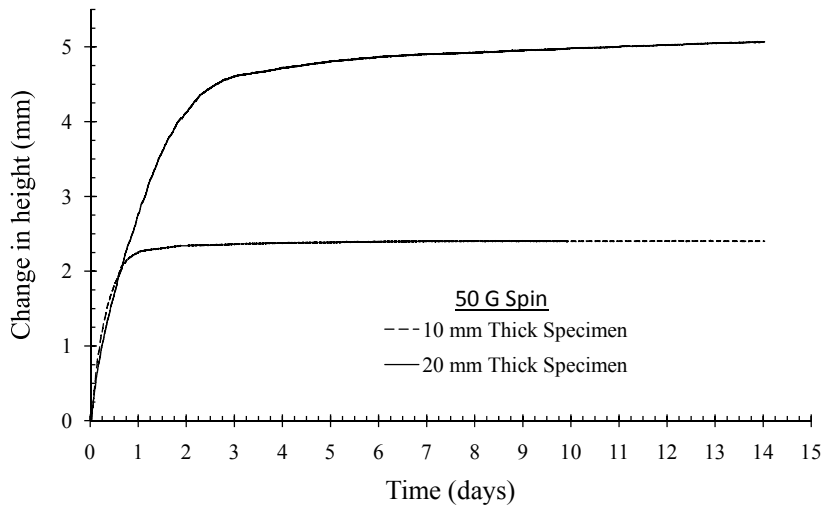


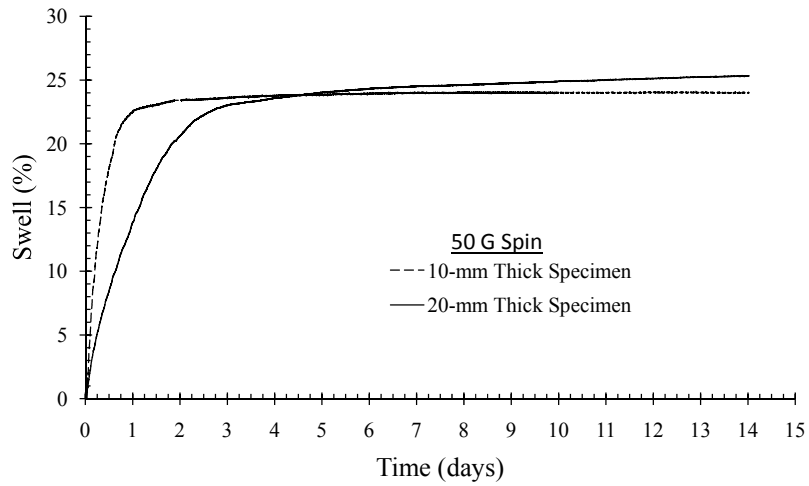
Figure 5.5: Series (o): Discrete Outflow Measurements for 30-mm thick Specimens with 20 mm of Pondered Water at 200 G

After adding a linear position sensor to the testing setup a test series was performed at 50 G on 1 and 20-mm thick test specimens with 30 mm of pondered water for a period of 14 days. For this test series, pondered water was added at the beginning of testing as in the small centrifuge. In later tests, water was added and maintained in flight (Section 3.2.11). Accordingly, as the pondered water moved through the soil specimen during the test,

the height of the ponded water did not stay constant with respect to the base of the soil specimen. The change in height of these soil specimens over the course of testing is shown in Figure 5.6(a). The swell of the soil specimens is shown in Figure 5.6(b). The rate of displacement of the 10-mm thick soil specimen can be seen to have decreased significantly after two days. For the 20-mm thick soil specimen, however, the rate of displacement does not decrease significantly until after a period of three days and does not decrease to the same degree as the 10-mm thick soil specimen. The continued swelling of the soil specimens at lower rates can be attributed to the decreasing water height with testing time.



(A)



(B)

Figure 5.6: Series (o): (a) Displacement and (b) Swell for Centrifuge Tests Performed at 50 G on 20-mm and 10-mm thick Test Specimens with 30 mm of Pondered Water

5.3 Series (i): Centrifuge Tests with Constant Water Height and Surcharge Mass

After finalizing the instrumentation for the testing setup, a testing plan was set forth for evaluating the effects of rotational velocity, soil height, and equilibrium time on the swell and moisture movement in a compacted specimen. The testing plan is summarized in table 5.1. Tests were conducted for durations of 24, 48, and 72h hours at G-levels of 25, 50, and 100 G. During each test, a 10-mm and a 20-mm thick specimen were flown. During testing, the height of the soil specimen was measured in flight. After testing, the soil specimen was dissected into slices and the water content profile along the length of the specimen was determined. A total of nine tests were conducted for this portion of testing. The nine tests conducted as part of Series (i) required a total of 18 days to complete.

Table 5.1: Testing Plan for Series (i) on 10-mm and 20-mm thick Specimens

Duration (hours)	G-level		
	25	50	100
24	#1	#2	#3
48	#4	#5	#6
72	#7	#8	#9

#X: Test Number

Since a constant surcharge mass and a constant water height were used atop the soil specimen, the water pressure and total stress applied over the profile only varied with the G-level. The water pressure and total stress applied over the profile increased with G-level as shown in Figure 5.7. In this test series, the height of water above the specimen at the

start of testing was 20 mm for each test. Accordingly, the 20 mm of water provided twice the water pressure at 50 G as at 25 G and so on. The total stress is the sum of the water pressure and the surcharge pressure provided by the surcharge mass. For these tests, the total stress was varied between approximately 250 and 750 psf.

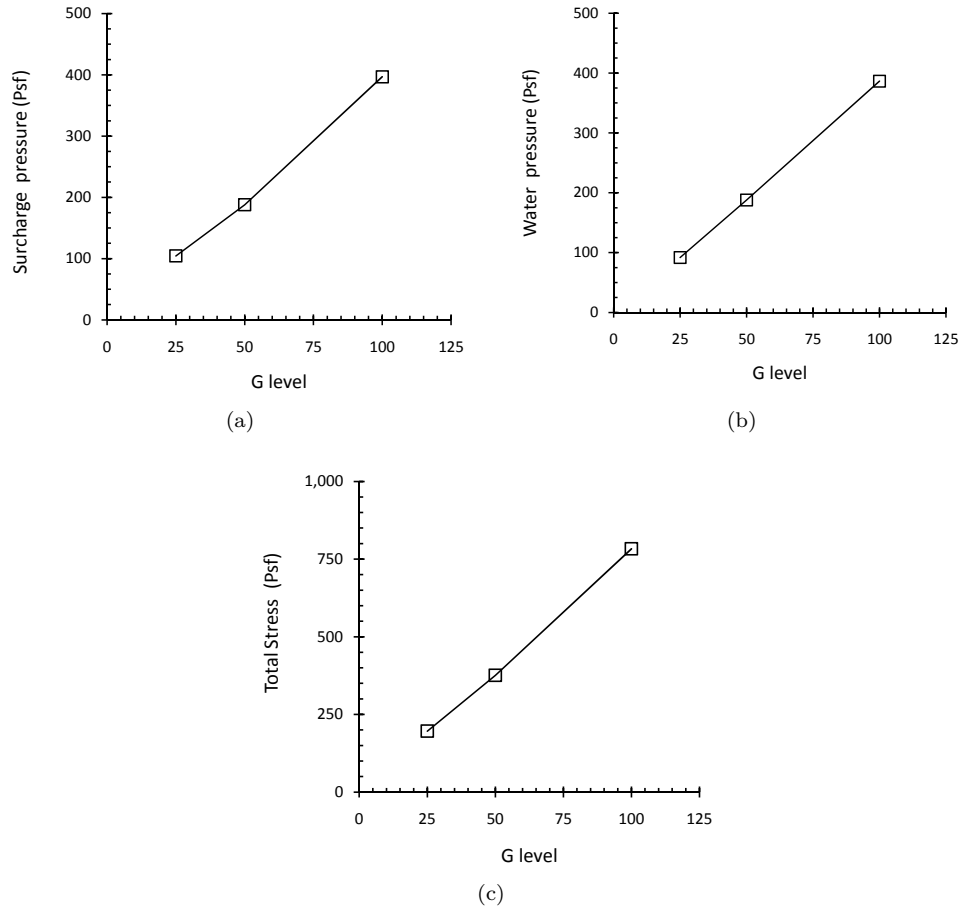


Figure 5.7: Variability of Surcharge Pressure, Water Pressure, and Total Stress Applied Over the Profile with G-level in Series (i)

5.4 Series (ii): Centrifuge Tests with Constant Total Stress

In order to evaluate the effect of surcharge pressure, a second test series, Series (ii), was conducted. In Series (ii), the surcharge mass and water height were modified for each test so as to maintain a constant water pressure and total stress. This is dissimilar to Series (i), where a constant mass and a constant water height were used atop the soil specimen (Section 5.3) and subsequently the water pressure and total stress applied over the soil profile varied with the G-level.

A comparison of the water pressure and total stress with G-level in Series (i) and Series (ii), in which these values are held constant with G-level, is shown in Figure 5.8. In Series (ii), the water pressure was maintained at 400 psf, the highest water pressure tested at in Series (ii). While the height of water of 20 mm above the top of the specimen was used in Series (i), the height of water in Series (ii) was as follows: 20 mm at 100 G; 40 mm at 50 G; and 80 mm at 100 G. Likewise, the mass of the surcharge was doubled for 50 G and quadrupled for 25 G in relation to the mass used in Series (i) and for the tests performed at 100 G in Series (ii).

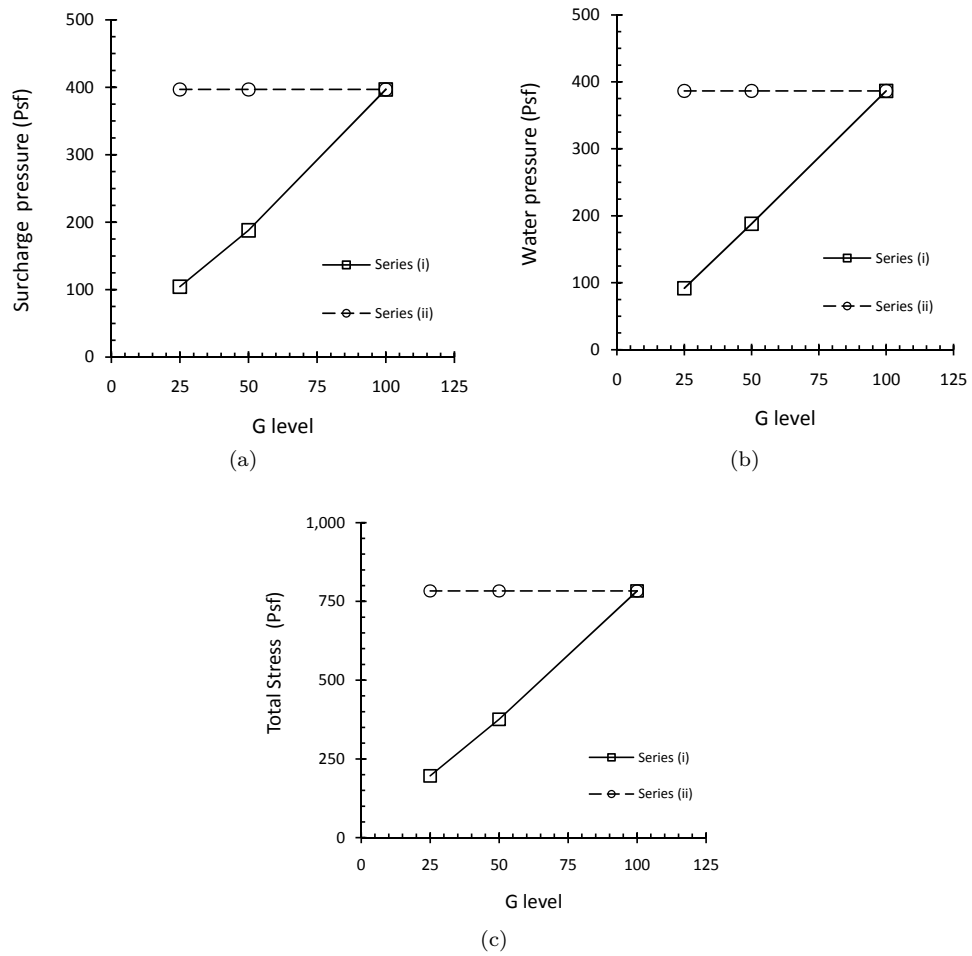


Figure 5.8: Trials for Constant Surcharge Pressure, Water Pressure, and Total Stress Applied Over the Profile with G-level in Ongoing Series (ii) in Comparison to Those in Series (i)

Chapter 6

Experimental Testing Results

In this section, the results of Series (i) and Series (ii) testing are presented. Additionally, the results from long-term, 14 day, swell tests conducted in the centrifuge are also presented. For each of the test presented in this section, the swelling of the soil specimen over the course of testing is presented. Additionally, the measured swelling and void ratio of each of the soil specimens are compared in terms of total stress. Detailed analysis of these tests series including the rate of swelling, secondary swelling, measured wetting front advancement, effective stress analysis, and the modeling of the advancement of a wetting front within the specimen are presented in Chapter 7.

6.1 Series (i): Centrifuge Tests with Constant Surcharge Mass and Water Height

In Series (i), the surcharge mass and the height of water were maintained constant as described in Section 5.3. Accordingly, the water pressure and the surcharge pressure applied over the specimens vary for each of the tests of the series. In this test series, both water and surcharge pressures increase proportionally to the G-level. These tests provided a good indication of the results that were to be expected from further centrifuge testing. Specifically,

these tests showed that the 20-mm thick specimens did not reach a steady height within the 72 hour testing period.

The vertical displacements of the specimens during the test for Series (i) are shown with respect to time in Figure 6.1. Both tests on 10-mm and 20-mm thick specimens are shown in this figure. The displacements of the 10-mm thick specimens are represented by solid lines whereas the displacements of the 20-mm thick specimens are represented by dashed lines. As expected, the observed displacement decreased with increasing G level for both the 10-mm and 20-mm thick specimens.

When the tests were stopped at the end of the 72 hour testing period, the displacements of all of the 20-mm thick specimen exceeded those of the 10-mm thick specimen at the same G-level. The proportion of the displacements of the 20-mm thick to the displacements to the 10-mm thick specimens as a function of the G-level is shown in Figure 6.2. The ratio of displacements between the 20-mm and 10-mm thick specimens appeared to be relatively insensitive to the G-level. The 20-mm thick specimens displaced, on average, 1.6 times as much as the 10-mm thick specimens.

The swell of the soil specimens during centrifuge testing were calculated based on the heights that the soil settled to in the centrifuge, H_2 , at the start of testing. The swell of the soil specimens are shown with respect to time in Figure 6.3. At the end of the test, the swell of the 20-mm thick specimens exceeded the swell of the 10-mm thick specimens at the same G-level.

While the swell of the 10-mm thick soil specimens appear to have leveled off to a final swelled height at the end of the test, the 20-mm thick specimens have not. This issue is further addressed in Section 7.1.2, where the swell rate of centrifuge specimens are evaluated. Since, however, the swelling of the 10-mm thick specimens appears to have leveled off at the end of the test, a state of equilibrium appears to have been reached. Accordingly, the swell observed at the end of testing can be compared to the total stress over the surface of the specimen at the end of testing.

The swell at the end of the test are plotted versus total stress in Figure 6.4. The

void ratio of the specimens at the end of the test are plotted versus total stress in Figure 6.5. From these figures, it is evident that as in free swell testing, the degree of swelling, and subsequently the final void ratio, decreased with increasing total stress on the soil specimen. A comparison between the degree of swelling and final void ratio at different total stresses for free-swell and centrifuge tests will be presented in Section 7.5.

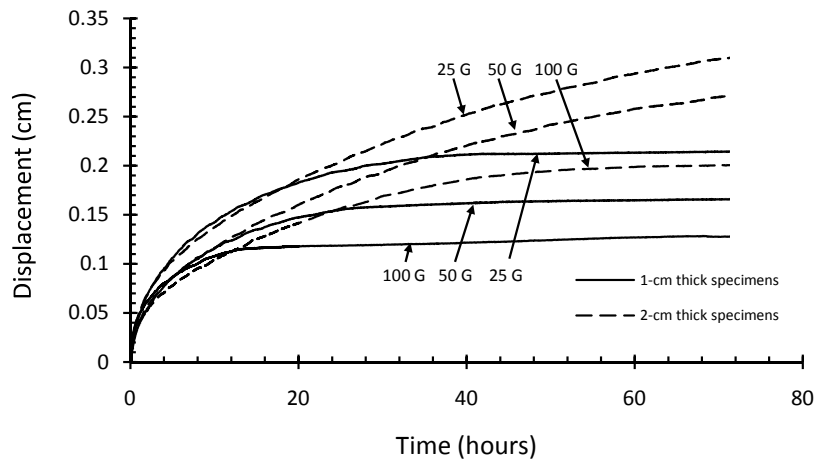


Figure 6.1: Measured Displacements for the 72 Hour Tests

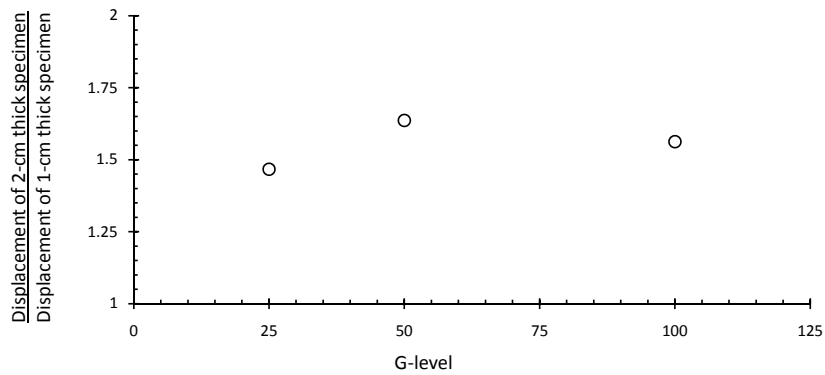


Figure 6.2: Ratio of the Displacement of 20-mm thick to 10-mm thick Specimens after 72 Hours of Testing

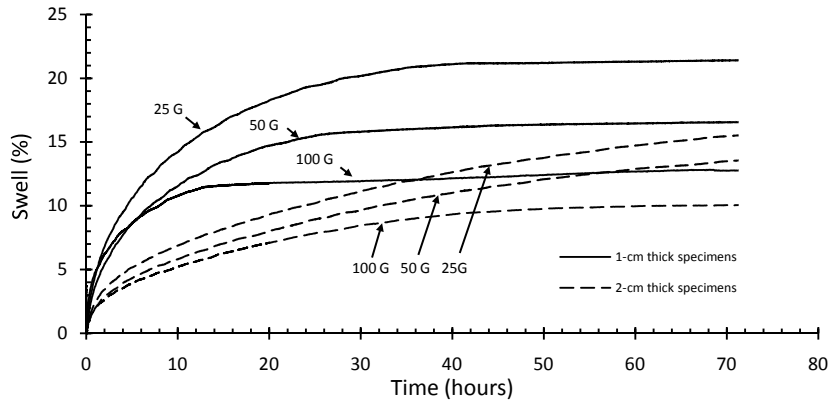


Figure 6.3: Swell Versus Time for the 72 Hour Tests

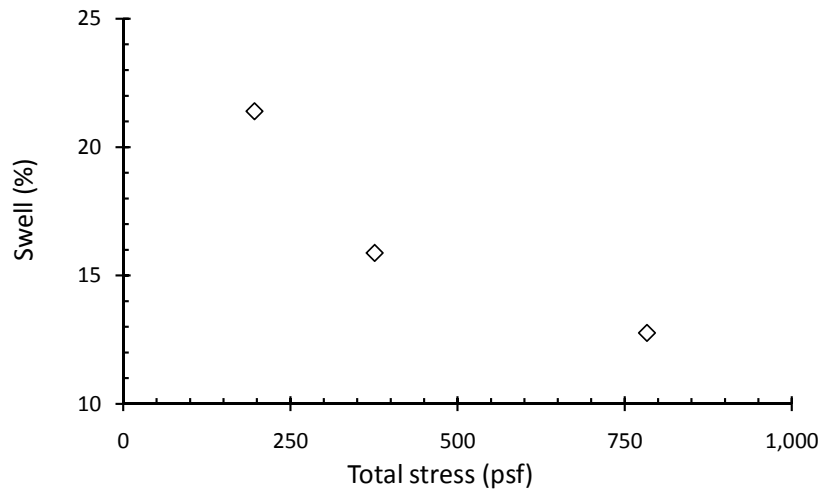


Figure 6.4: Final Vertical Swell Versus G-level for 72 Hour Tests on 10-mm thick Specimens

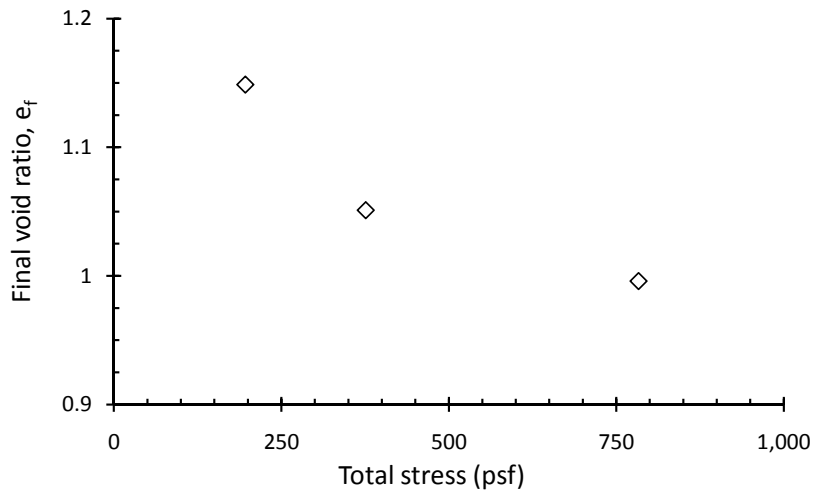


Figure 6.5: Final Void Ratio Versus G-level for 72 Hour Tests on 10-mm thick Specimens

6.2 Series (ii): Centrifuge Tests with Constant Water Pressure and Total Stress

In Series (i), the water and surcharge pressures increased with G-level since the water height and surcharge mass were held constant. As a result, the relative effects of G-level, water pressure, and surcharge could not be determined. In order to determine the relative effects of these components, a second test series, Series (ii), was developed. In this test series, the effect of varying total stress at different G-levels was evaluated by comparing the swelling of specimens under specific values of total stress that were held constant for various G-levels. The tests conducted on specimens tested at G-levels of 25, 50, and 100 with a water pressure applied over the specimens of 400 psf (20 KPa) are summarized in Table 6.1. The mass of the surcharge was modified to result in surcharge pressures of 100, 200, 400, 800, and 1,200 psf were used in testing. Given the applied water pressure of 400 psf, this resulted in total stresses of 500, 600, 800, 1,200, and 1,600 psf. Without the addition of any surcharge mass, the surcharge pressure from the top plate alone is 100 psf at 25 G. Accordingly, tests with

a surcharge pressure of 100 psf could not be conducted at 50 and 100 G. Likewise, a test with a surcharge pressure of 200 psf could not be conducted at 100 psf.

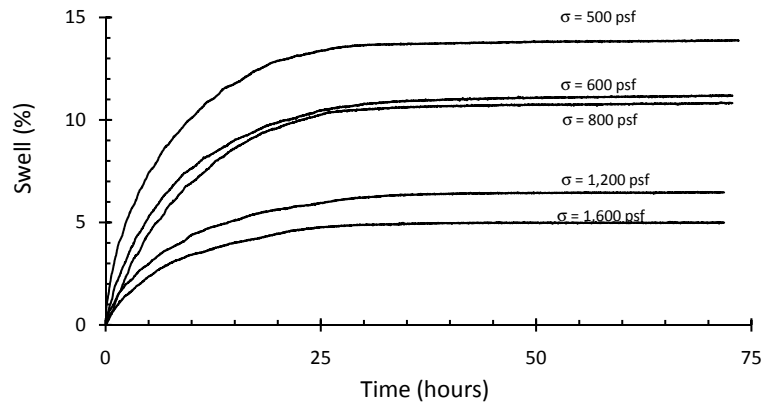
Table 6.1: Total Stress at which 10-mm thick Specimens were Tested at 25, 50, and 100 G with a Water Pressure Applied Over the Specimens of 400 psf (20 KPa)

G	Total Stress, σ (psf)				
	500	600	800	1,200	1,600
25	x	x	x	x	x
50	o	x	x	x	x
100	o	o	x	x	x

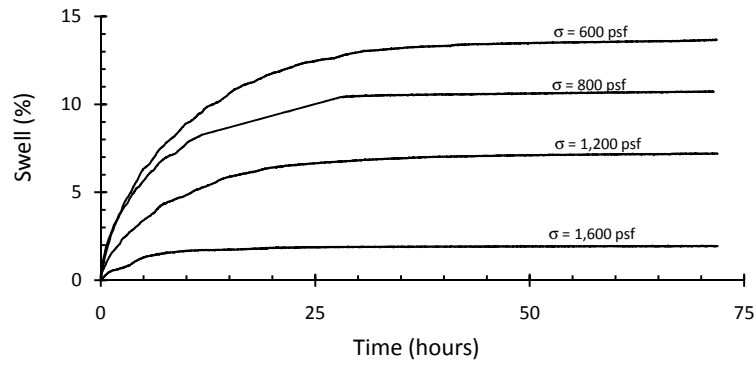
x = tested

o = not possible with current setup

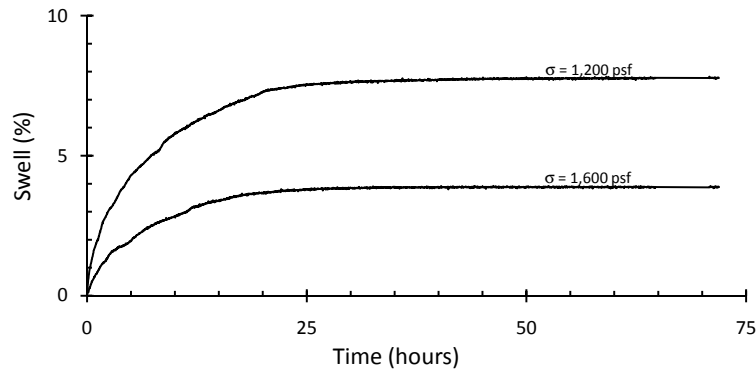
The swell of the soil specimens over the course of testing are plotted in Figure 6.6. Based on these plots of swell versus time, it appears that the rate of swelling greatly reduces between one and two days of testing for tests performed at 25, 50, and 100 G. Furthermore, the rate of swelling appears to decrease more rapidly at higher values of total stress which are associated with lower measured swell. Additional evaluation of the rate of swell measured during these tests are discussed in Section 7.1.2.



(a) 25 G



(b) 50 G



(c) 100 G

Figure 6.6: Swelling Versus Time for Specimens Tested for 72 Hours at 25, 50, and 100 G with a Water Pressure of 400 psf (20 KPa) Applied Over the Specimens

The final void ratio and final swell of these test specimens are presented in Figures 6.7 and 6.8. Good agreement is found between the swell measured in tests conducted at 25, 50, and 100 G regardless of the increase in body forces acting on the soil particles. The final void ratio and final swell observed in 10-mm thick specimen tested in Series (i) are also presented in these Figures 6.7 and 6.8. The results of the tests from Series (i) were found to be in good agreement with the trends between void ratio, swell, and total stress found in Series (ii).

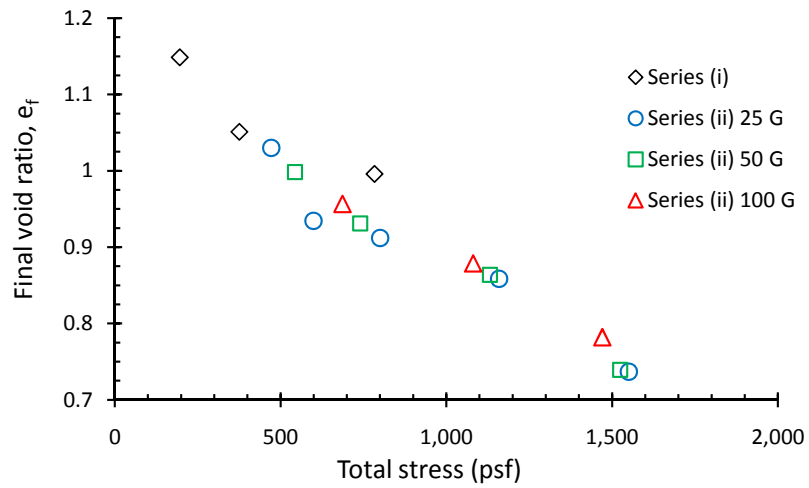


Figure 6.7: Void ratio Versus Total Stress for 10-mm thick Specimens with a Water Pressure of 400 psf (19 KPa) Applied Over the Specimens

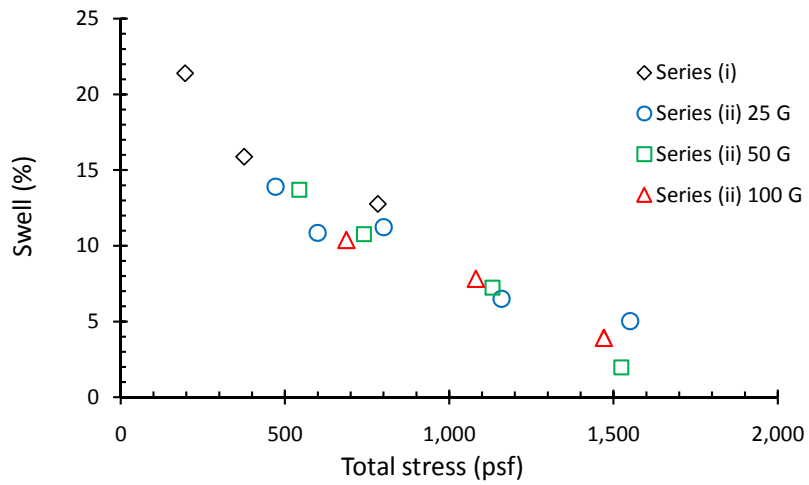


Figure 6.8: Swelling Versus Total Stress for 10-mm thick Specimens with a Water Pressure of 400 psf (19 KPa) Applied Over the Specimens

The effect of varying the water pressure applied over the specimen was evaluated by varying the height of ponded water at 50 G with the same confining mass. The swell obtained using 10-mm and 20-mm thick specimens tested at an surcharge pressure of 19 KPa (400 Psf) and at a G-levels of 50 are plotted in Figure 6.9. Based on these results, the swell of the specimen was observed to decrease with an increase in the water pressure for the 10-mm thick specimens. As for the 20-mm thick specimens, the effect of water height on swelling appears to be minimal for the 72-hour testing duration. Series (ii) was designed around keeping the applied water pressure constant. In order to draw any firm conclusions concerning the effect of water height on swelling, further investigation is needed and is suggested in Section 8.2.

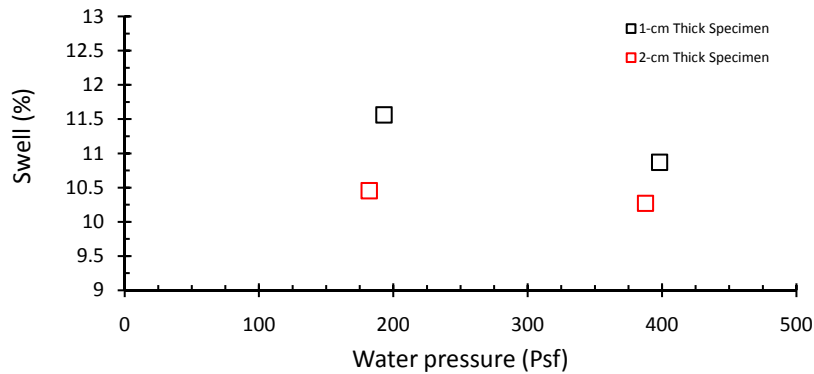


Figure 6.9: Swelling Versus the Water Pressure Applied Over the Specimen with a Constant Surcharge Mass

6.3 Long-Term Swell Tests in the Centrifuge

Centrifuge tests lasting for a period of 14 days were conducted in order to investigate the long-term swelling behavior of 10-mm and 20-mm thick soil specimens. Tests were conducted at G-levels of 50 and 100 with a water pressure of 400 psf and an surcharge pressure of 400 psf. The results of these tests are presented in Figure 6.10. As previously observed in Series (i), the 10-mm thick specimens swelled more than the 20-mm thick specimens. Furthermore, the specimens tested at 50 G were observed to swell more than the test specimens tested at 100 G for the same water and surcharge pressures.

The swell of these soil specimens obtained after 72 hours of testing is compared to the swell after 14 days of testing in Table 6.2. For the 10-mm thick specimens, over 80% of the swell measured at a period of 14 days had occurred after 72 hours for tests conducted under both 50 and 100 G. For the 20-mm thick specimens, approximately, 70% of the swell measured at a period of 14 days had occurred after 72 hours. For the 10-mm thick specimens tested in free-swell, between 84% and 96% of the swell measured at a period of 14 days had occurred after 72 hours (Table 4.1). These tests are, however, difficult to compare since the effective stress within the centrifuge has yet to be discussed. It is, however, interesting to notice that a similar proportion of the swell measured at a period of 14 days has occurred

after 72 hours for both free-swell and centrifuge testing. The magnitude of swelling for free-swell and centrifuge tests is compared in 7.5. The swelling rates of these test specimens are evaluated in Section 7.2 where the swelling rates are compared to those observed in free-swell testing.

In order to evaluate the effects of the specimen height on swelling versus time, the swelling of the specimen can be normalized by the swelling of the specimen at the end of the 14 day testing period (Figure 6.11). When the swelling of the specimen is normalized by the final swell of the soil specimen, it becomes evident that the 10-mm and 20-mm thick specimens follow similar trends as one another regardless of the G level. The effects of specimen height on the time dependent process of swelling can also be evaluated by normalizing the time by the square of the height of drainage (Figure 6.12). When the time is normalized by the square of the height of drainage, it becomes evident that the process of swelling appears to be a function of the G level where the specimens flown at a higher G level undergo less swelling due to increased body forces. Taking these two evaluations one step further, the swelling of the soil specimen can be normalized by the swelling of the specimen at the end of the 14 day testing period and the time can be normalized by the square of the height of drainage (Figure 6.13). By performing both of these normalizations, it is revealed that the ultimate swell is controlled by the G level but that the process of swelling versus time appears to be largely independent of the G level and is dependent on the height of the soil specimen (i.e. the height of drainage for centrifuge specimens).

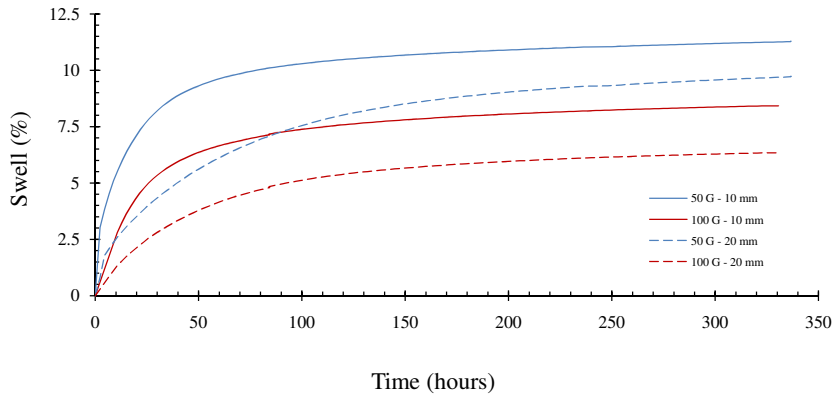


Figure 6.10: Swelling Versus Time for Specimens Tested for 14 Days at 50 and 100 G with a Surcharge Pressure of 400 psf (20 KPa) and a Water Pressure of 400 psf (20 KPa) Applied Over the Specimens

Table 6.2: Swell after 72 hours / Swell after 14 Days

	10-mm thick Specimen	20-mm thick Specimen
50 G	0.88	0.69
100 G	0.82	0.71

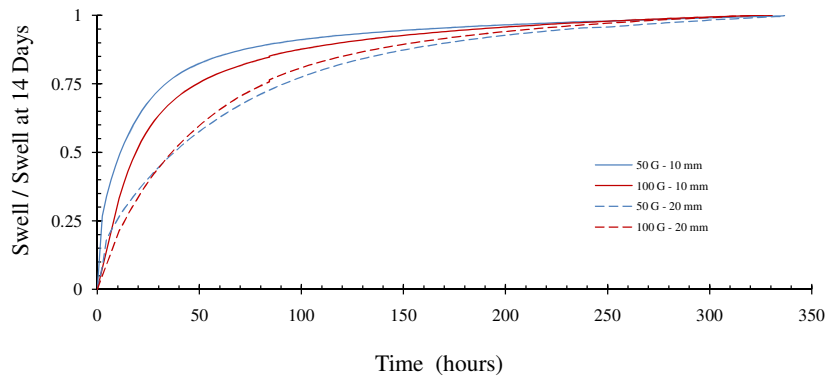


Figure 6.11: Proportion of 72 Hour Swelling Versus Time for Specimens Tested for 14 Days at 50 and 100 G with a Surcharge Pressure of 400 psf (20 KPa) and a Water Pressure of 400 psf (20 KPa) Applied Over the Specimens

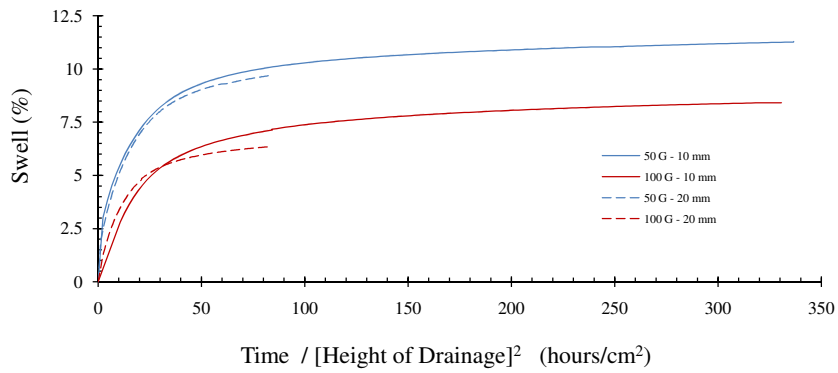


Figure 6.12: Swelling Versus Time Divided by the Square of the Height of Drainage for Specimens Tested for 14 Days at 50 and 100 G with a Surcharge Pressure of 400 psf (20 KPa) and a Water Pressure of 400 psf (20 KPa) Applied Over the Specimens

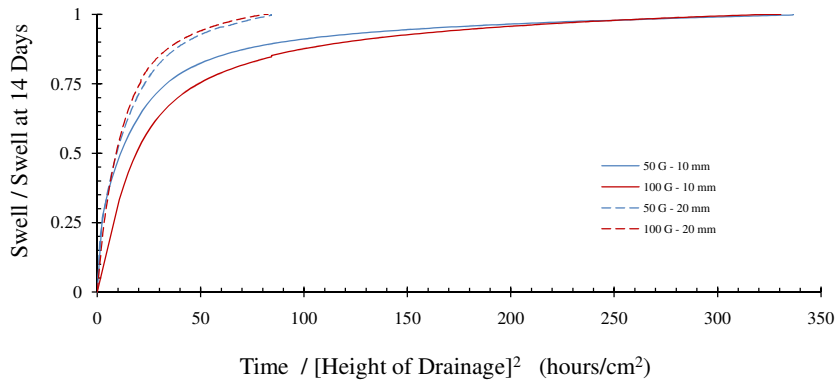


Figure 6.13: Proportion of 72 Hour Swelling Versus Time Divided by the Square of the Height of Drainage for Specimens Tested for 14 Days at 50 and 100 G with a Surcharge Pressure of 400 psf (20 KPa) and a Water Pressure of 400 psf (20 KPa) Applied Over the Specimens

Chapter 7

Analysis of Test Results

The results of centrifuge, free swell testing, and 1-G infiltration tests are analyzed in this section. The analysis include an evaluation of the swelling rates during testing, total swelling, outflow rates and hydraulic conductivity values measured during centrifuge testing. In addition, an interpretation is made of incremental swell and swelling correlations. Finally, a numerical simulation of the wetting front advancement during testing is conducted.

7.1 Primary and Secondary Swelling

In the previous section, the displacement rates of free-swell and centrifuge tests that were conducted for 14 days were compared. In this section, the swelling rates of free-swell, centrifuge, and 1-G infiltration tests are compared. In order to provide a means of comparing the large number of tests, a differentiation was made between primary and secondary swelling. The slopes of primary and secondary swelling as well as the time of secondary swelling were determined for each test. The means by which primary and secondary swelling were differentiated were described in Section [4.1.1](#).

7.1.1 Free-Swell Tests

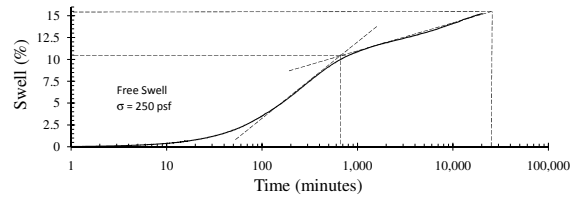
For the free-swell tests, primary and secondary swelling for tests conducted with total stresses of 250 psf, 500 psf, 1,000 psf, 2,000 psf, and 4,000 psf are shown in Figure 7.1. For the free-swell tests, the slope of the primary swelling decreases with increasing total stress (Figure 7.2 a). Since a higher total stress on a specimen at the beginning of testing compresses the specimen more, it leads to a decrease in the pore volume within the soil specimen. This compressed pore space likely leads to a decrease in the hydraulic conductivity of the specimen and a higher degree of saturation. This increased saturation likely leads to a reduction of capillary forces within the specimen. With a reduction in hydraulic conductivity and capillary forces, the rate of flow of water and thus the rate of swell of the specimen are reduced. The decrease in the rate of primary swelling with increasing total stress can potentially be explained by this phenomena.

The slope of secondary swelling decreases with increasing total stress and revealed a linear relationship for loads exceeding 1,000 psf (Figure 7.2 b). It is possible that primary swelling is driven by capillarity and that secondary swelling is driven by a long-term process of hydrating clay particles. If the negative pore water pressures have been largely revealed after primary swelling, then the total stress on the specimen should be equal to the effective stress on the specimen. The specimens under higher effective stress are expected to have lower hydraulic conductivities. If the clay is in fact undergoing a long-term hydration process than lower hydraulic conductivities would restrict the flow of water and thus decrease the rate of secondary swelling.

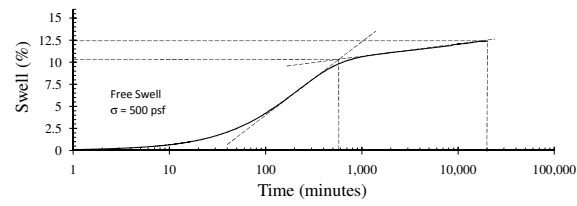
The proportion of secondary swelling to total swell was also observed to decrease with total stress (Figure 7.2 c). The proportion of secondary swelling to total swelling was, however, found to reach a steady value of approximately 12.5% for loads of exceeding 1,000 psf. A potential explanation for the decrease in the proportion of secondary swelling with total stress is a higher final void ratio for the tests conducted under lower total stresses. Accordingly, test which will undergo greater expansion will experience a greater change in void ratio from the initial condition and thus require more time.

The time of secondary swelling was found to decrease with total stress (Figure 7.2 d). The explanation of a decrease in the initial capillary forces due to the compression of soil samples under higher total stresses is also applicable for this phenomena. Since higher capillary forces are expected to be present in soil specimens at lower total stresses, moisture movement into the specimens is accelerated. When capillarity is no longer drawing water into the soil specimen the clay is undergoing a long term hydration process.

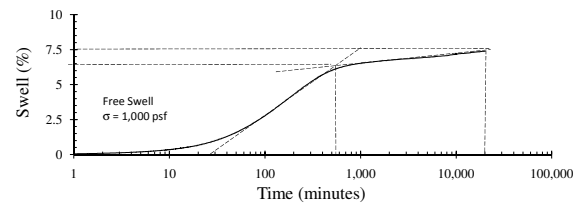
The slope of secondary swelling from these free-swell tests are compared with the values of saturated hydraulic conductivity measured in flexible-wall permeameter tests in Figure 7.3. This comparison is possible since free-swell and flexible-wall permeameter tests were conducted at stresses of 1,000 psf, 2,000 psf, and 4,000 psf. Furthermore, unlike in centrifuge and 1-G infiltration testing, the stress effective stress in free-swell test specimens should be essentially uniform. Accordingly, the value of the saturated hydraulic conductivity of the soil should not vary significantly across free-swell specimens. Since the log of the slope of secondary swelling was found to be linear with the log of the hydraulic conductivity, it is thought that the rate of secondary swelling may be controlled by the saturated hydraulic conductivity of the soil.



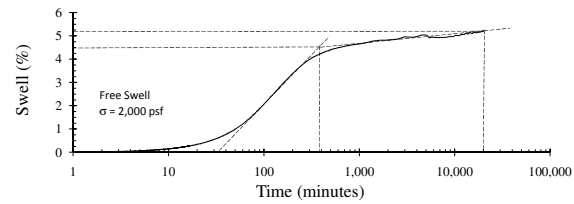
(a)



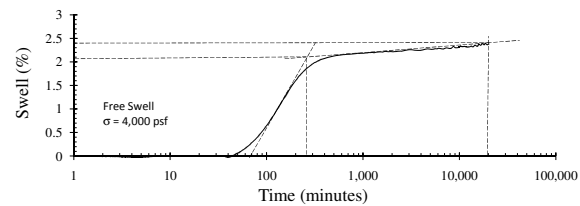
(b)



(c)

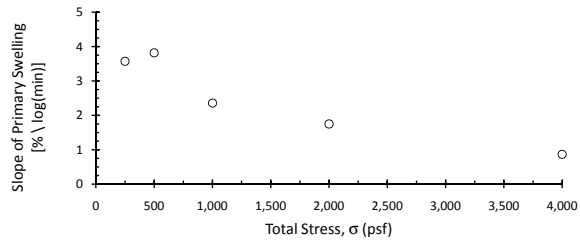


(d)

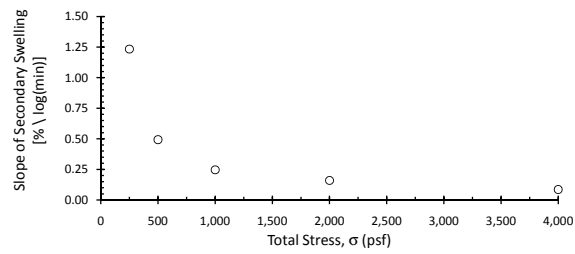


(e)

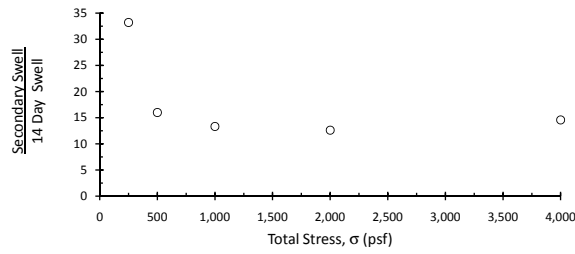
Figure 7.1: Primary and Secondary Swelling in Free Swell Tests: (a) 250 psf; (b) 500 psf; (c) 1,000 psf; (d) 2,000 psf; and (e) 4,000 psf



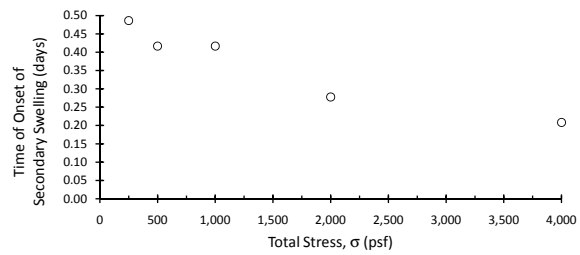
(a)



(b)



(c)



(d)

Figure 7.2: Primary and Secondary Swelling for Free-Swell Tests: (a) Slope of Primary Swelling; (b) Slope of Secondary Swelling; (c) Proportion of Secondary Swell; and (d) Time of the Onset of Secondary Swelling

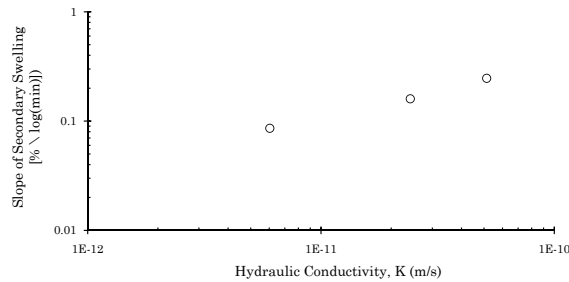


Figure 7.3: Comparison of the Slope of Secondary Swelling from Free Swell Tests to the Values of Saturated Hydraulic Conductivity Measured in Flexible-Wall Permeameter Tests

7.1.2 Centrifuge Tests

For centrifuge tests conducted at 25, 50, and 100 G, primary and secondary swelling are shown in Figures 7.4, 7.5, and 7.6. For these centrifuge tests, the slope of primary swelling decreased linearly with increasing total stress (Figure 7.7a). As hypothesized for the results of the free-swell tests, the decrease in the slope of primary swelling with increasing total stress is likely due to a reduction in the void space which leads to a reduction in the hydraulic conductivity and a decrease in the capillary forces which drive the flow of water into the soil specimen. The centrifuge tests conducted at 25, 50, and 100 G present very similar relationships between the slope of primary swelling and total stress. Based on these findings, it appears that the increased gravimetric potential had no significant effect on the rate of primary swelling.

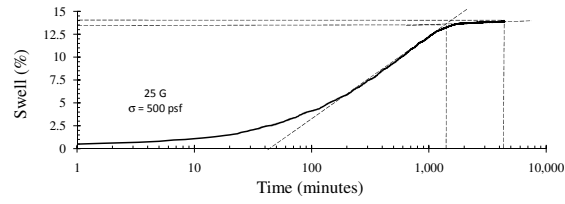
Aside from the increase in gravitational potential provided by the centrifuge, a significant difference between free-swell testing and centrifuge testing is that centrifuge testing involves an infiltration. Since the effects of gravitational potential on the rate of primary swelling appear to be minimal, one might expect that water flow due to capillary forces will be the dominate mechanism causing water to flow into the soil specimens. Furthermore, since the free-swell tests are exposed to water at the top and bottom faces of the specimen it might be expected that the rate of infiltration and thus the rate of primary swelling may be

twice as great for free-swell testing than for centrifuge testing. Regardless of this rationale, the rate of primary swelling was found to be similar for the free-swell and centrifuge tests.

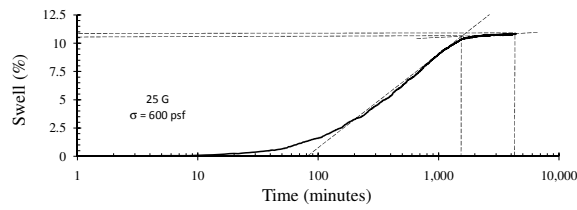
Just as with free-swell tests, the slope of secondary swelling for the centrifuge tests decreased with total stress (Figure 7.7b). The slope of secondary swelling for the centrifuge tests was, however, different for each G level. The slope of secondary swelling for the 25 G tests was less than that for tests conducted at 50 and 100 G over the range in loads tested. The slope of secondary swelling was, however, similar for all three acceleration levels at a total stress of approximately 1,600 psf. It might be presumed that the higher G level is providing a faster flow rate of water through the specimen and thus a means of flushing air and providing water for clay particles that are hydrating.

The proportion of secondary swelling to total swelling was found to be independent of the level of total stress with a constant value of approximately 3% for the centrifuge tests conducted at 25 G (Figure 7.7c). The proportion of secondary swelling to total swelling for the tests conducted at 50 and 100 G was found to be greater than for tests conducted at 25 G. As with the rate of secondary swell, it is possible that the higher G levels provided a faster flow rate of water through the specimen and thus aided in flushing air and providing water for clay particles that are hydrating.

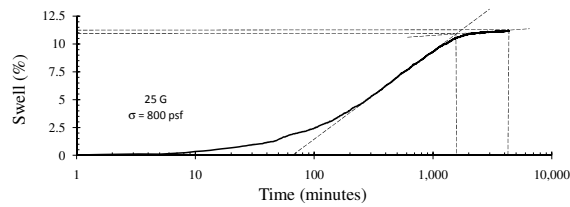
The time of the onset of secondary swelling was less than one and a half days for all of the centrifuge tests conducted in this study (Figure 7.7d). The time of the onset of secondary swelling was found to decrease with total stress for tests conducted at 50 and 100 G. Unlike the trends observed in from the results of free-swell testing and centrifuge testing at 50 and 100 G, as discussed in the previous section, the time of the onset of secondary swelling was found to increase with increasing total stress for the tests conducted at 25 G. The time of onset of secondary swelling was observed to be two to three times as large as the time of onset of secondary swelling observed in the free-swell tests.



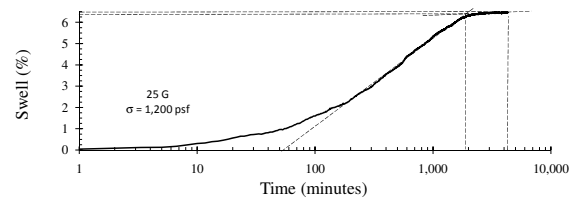
(a)



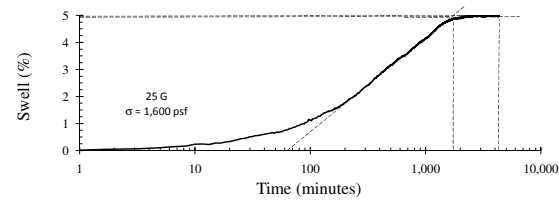
(b)



(c)

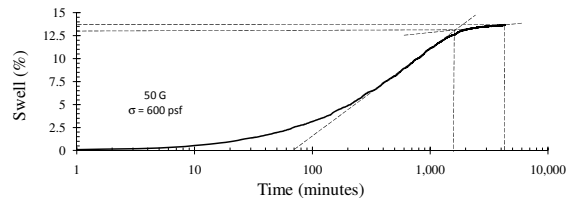


(d)

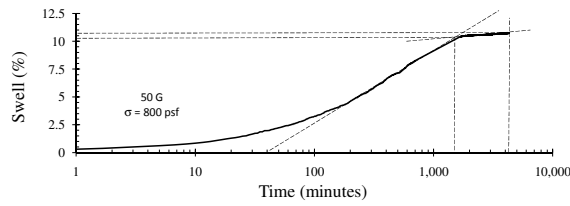


(e)

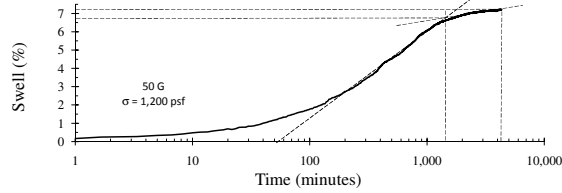
Figure 7.4: Primary and Secondary Swelling in 25 G Centrifuge Tests: (a) 500 psf; (b) 600 psf; (c) 800 psf; (d) 1,200 psf; and (e) 1,600 psf



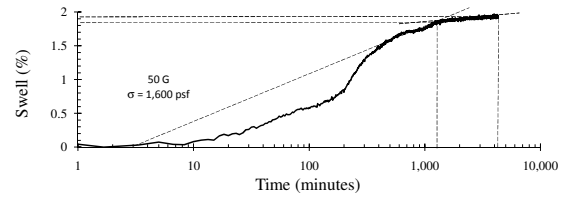
(a)



(b)

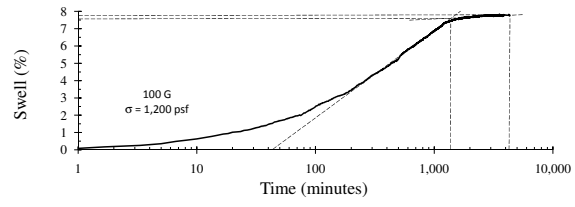


(c)

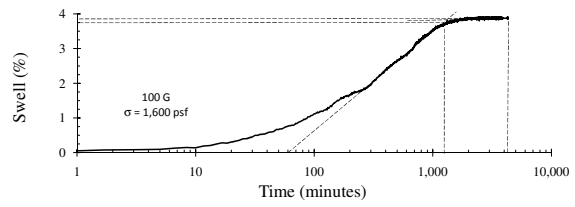


(d)

Figure 7.5: Primary and Secondary Swelling in 50 G Centrifuge Tests: (a) 600 psf; (b) 800 psf; (c) 1,200 psf; and (d) 1,600 psf

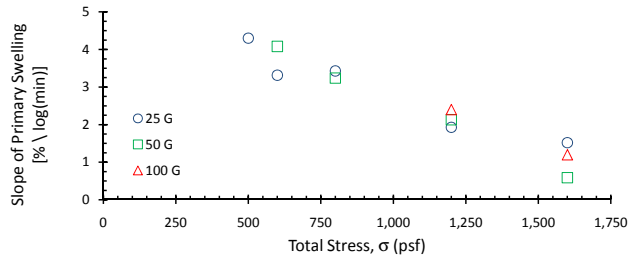


(a)

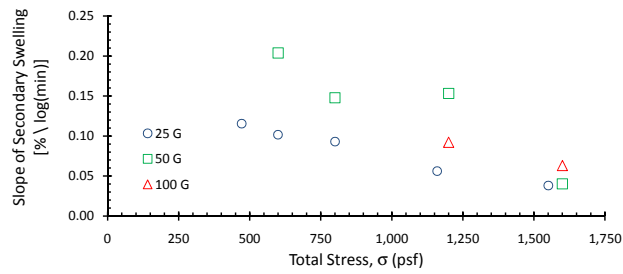


(b)

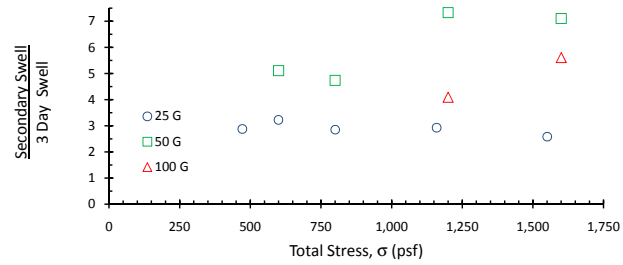
Figure 7.6: Primary and Secondary Swelling in 100 G Centrifuge Tests: (a) 1,200 psf and (b) 1,600 psf



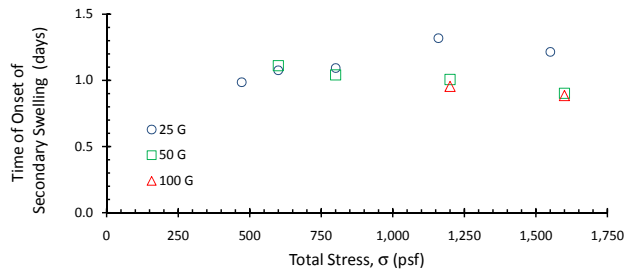
(a)



(b)



(c)



(d)

Figure 7.7: Primary and Secondary Swelling for Centrifuge Tests: (a) Slope of Primary Swelling; (b) Slope of Secondary Swelling; (c) Proportion of Secondary Swell; and (d) Time of the Onset of Secondary Swelling

7.1.3 1-G Infiltration

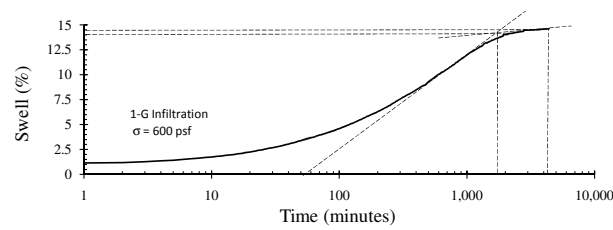
Primary and secondary swelling for the 1-G infiltration tests conducted at total stresses of 600 psf, 800 psf, and 1,200 psf are shown in Figure 7.8. For the 1-G infiltration tests, the slope of primary swelling was found to decrease linearly with total stress (Figure 7.9 a). The rate of primary swell was found to be similar to the rates of swelling observed in free-swell and centrifuge testing. Again, it is believed that higher values of total stress lead to a smaller volume of voids and thus a lower hydraulic conductivity and lower capillary forces allowing and drawing water flow into the specimens. Accordingly, the rate of the flow of water into the specimen and thus the slope of primary swelling were expected to decrease with total stress.

The rate of secondary swelling was found to increase linearly with total stress (Figure 7.9 b). This finding is contrary to the observations for free-swell and centrifuge testing, where the secondary swelling rate was found to decrease with total stress. For free-swell and centrifuge testing, it was hypothesized that the rate of secondary swelling decreases with total stress as the hydraulic conductivity of the specimen decreases with increasing effective stress. As clay particles in the specimen are potentially undergoing a long-term hydration process in the soil specimen, the hydraulic conductivity of the specimen will control the flow of water into the specimen. Since, however, more test data is available for free-swell and centrifuge tests, it is recommended that additional 1-G infiltration testing is of interest for future investigations (Section 8.2).

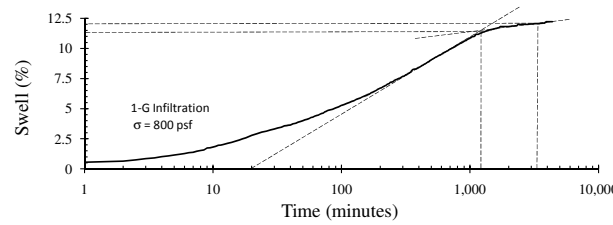
The proportion of secondary swelling to total swelling was found to increase with total stress (Figure 7.9 c). For the 1-G infiltration test performed at a total stress of 1,200 psf, the proportion of secondary to total swelling was found to be four to five times greater than for free-swell and centrifuge testing under similar total stresses. Again, it is recommended that additional 1-G infiltration tests are performed to investigate this phenomena.

The time of the onset of secondary swelling was found to decrease with total stress

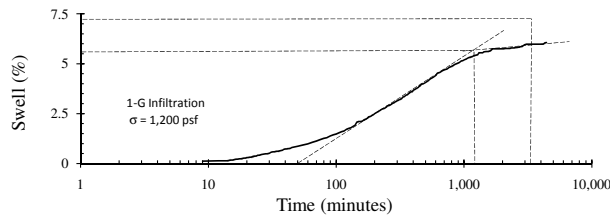
and was less than one day for all of the samples tested (Figure 7.9 d). The time of onset of secondary swelling was found to be less than for centrifuge testing but greater than for free-swell tests. Since the 1-G infiltration tests involve infiltration as in the centrifuge test, involve an elevated water pressure at the top of the specimen, but are conducted at 1-G, they are a hybrid between the two tests. This may explain why the time of onset of secondary swelling falls between values observed in centrifuge and free-swell testing.



(a)

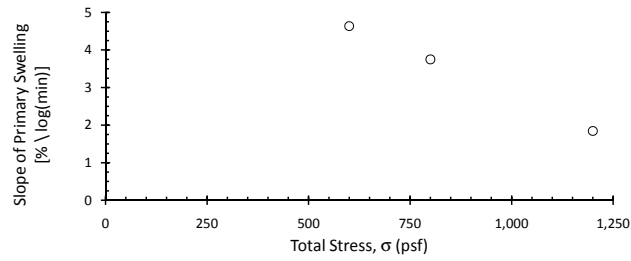


(b)

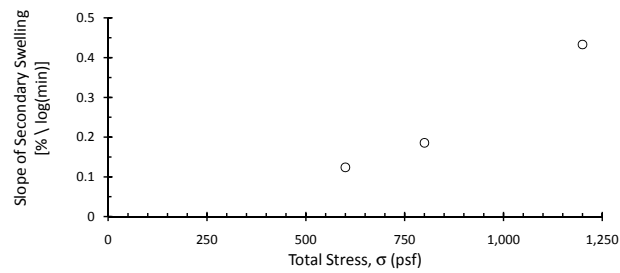


(c)

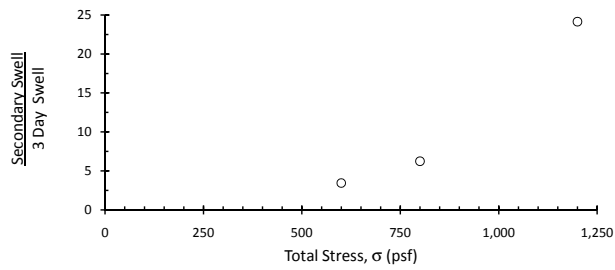
Figure 7.8: Primary and Secondary Swelling in 1-G Infiltration Tests: (a) 600 psf; (b) 800 psf; and 1,200 psf



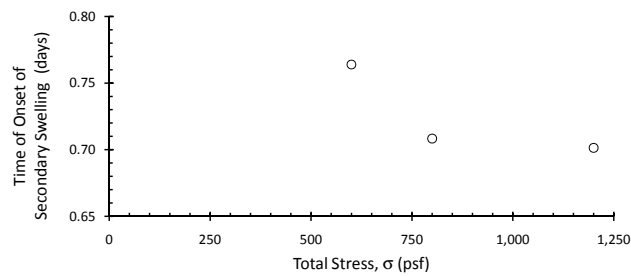
(a)



(b)



(c)



(d)

Figure 7.9: Primary and Secondary Swelling for 1-G Infiltration Tests: (a) Slope of Primary Swelling; (b) Slope of Secondary Swelling; (c) Proportion of Secondary Swell; and (d) Time of the Onset of Secondary Swelling

7.1.4 14 Day Centrifuge Tests

The slope of primary and secondary swelling in 14 day centrifuge tests on 10-mm and 20-mm thick specimens at 50 and 100 G are examined in this section. The slope of secondary swelling was significantly easier to determine for the 14 day tests than for the 72 hour centrifuge and 1-G infiltration tests as data was gathered for another log-cycle in time. Primary and secondary swelling for the 10-mm and 20-mm thick specimens are shown in Figure 7.10 and 7.11.

The slope of primary swelling was found to decrease with G-level (Figure 7.12 a). The slope of primary swelling for the 10-mm thick specimens were greater than the slope of primary swelling for the 20-mm thick specimens at 50 and 100 G. A trend was, however, not found for the slope of secondary swelling (Figure 7.12 b). The slope of secondary swelling increased with the G-level for the 10-mm thick specimens but decreased for the 20-mm thick specimens. Furthermore, the slope of secondary swelling for the 20-mm thick specimen tested at 50 G exceeded that of the 10-mm thick specimen tested at 50 G, while the opposite was true for the tests conducted at 100 G (Figure 7.12 c). A trend was, however, found between the time of the onset of secondary swelling and G-level for the 10-mm and 20-mm thick specimens (Figure 7.12 d).

The time of the onset of secondary swelling was found to decrease with G-level. Furthermore, the time of the onset of secondary swelling for the 20-mm thick specimens was found to exceed the time of the onset of secondary swelling for the 10-mm thick specimens. The ratio of the time of the onset of secondary swelling for the 20-mm thick specimen to the 10-mm thick specimen was 2.7 for the 50 G test and 4.0 for the 100 G test.

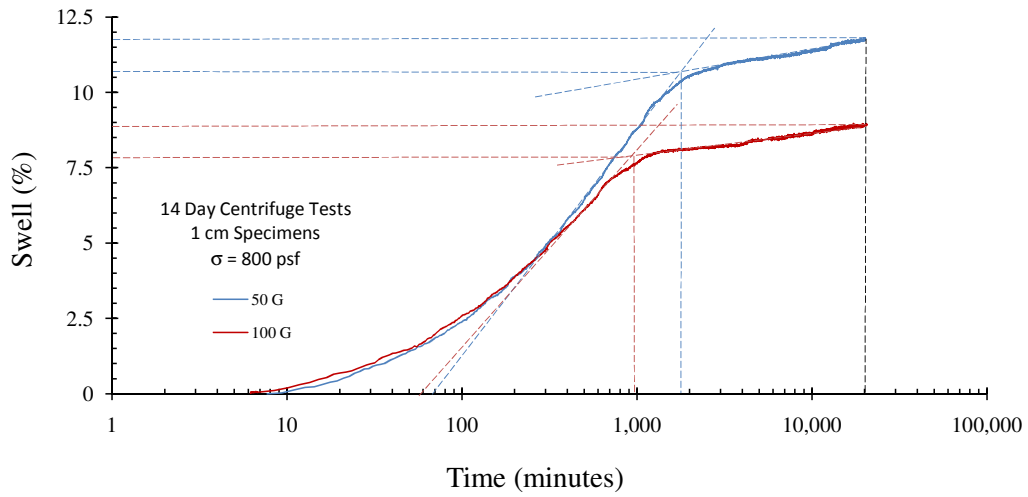


Figure 7.10: Primary and Secondary Swelling for 14 Day Centrifuge Tests on 10-mm thick Soil Samples

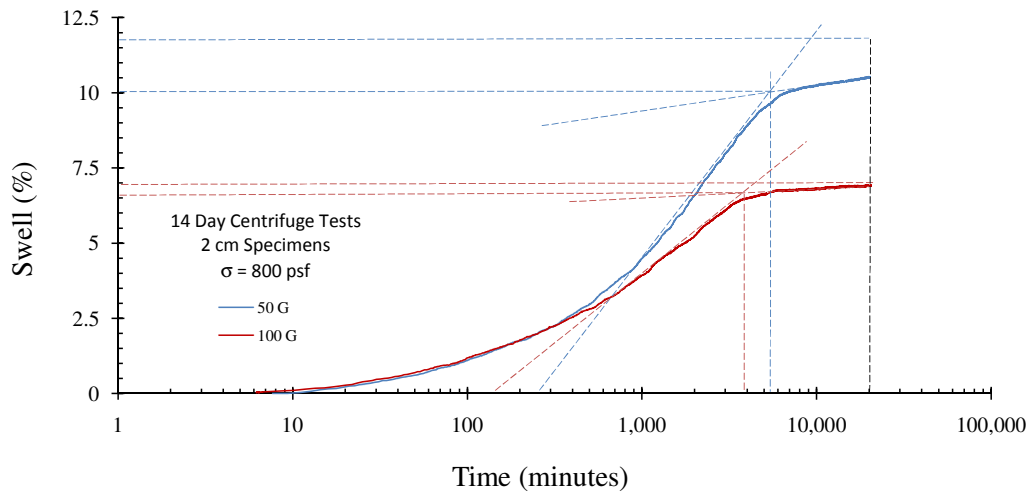
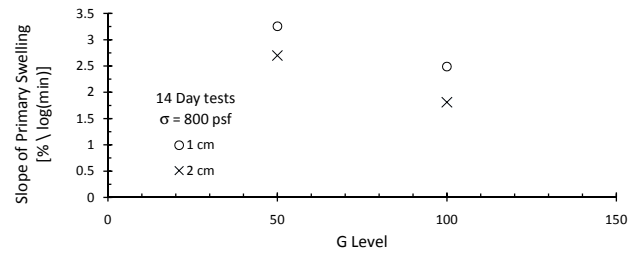
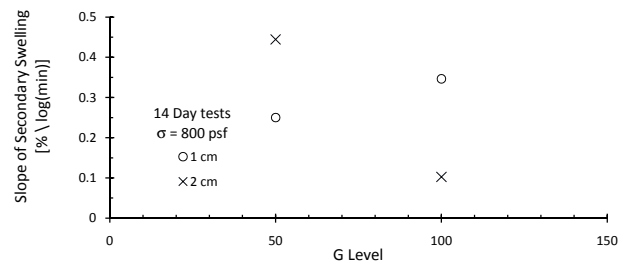


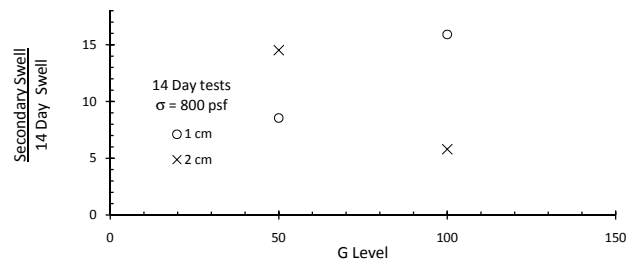
Figure 7.11: Primary and Secondary Swelling for 14 Day Centrifuge Tests on 20-mm thick Soil Samples



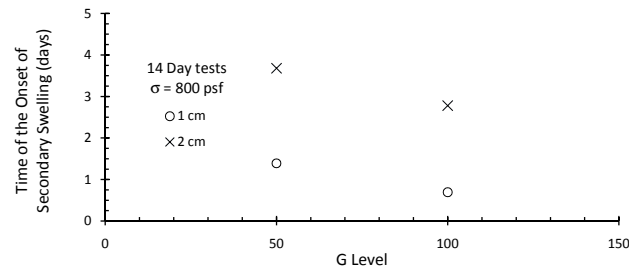
(a)



(b)



(c)



(d)

Figure 7.12: Primary and Secondary Swelling for 14 Day Centrifuge Tests: (a) Slope of Primary Swelling; (b) Slope of Secondary Swelling; (c) Proportion of Secondary Swell; and (d) Time of the Onset of Secondary Swelling

7.1.5 Comparison of Primary and Secondary Swelling Observed from Free-Swell, Centrifuge, and 1-G Infiltration Tests

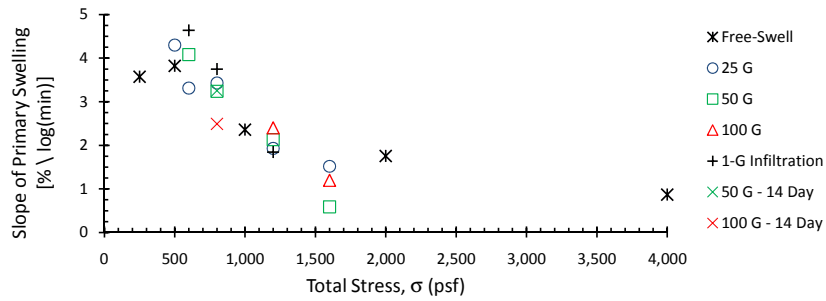
In order to understand the rate of primary and secondary swelling in the free-swell, centrifuge, and 1-G infiltration tests, the slope of primary and secondary swelling, the proportion of secondary to total swelling, and the time of secondary swelling for each test are compared in this section. The slope of primary swelling, slope of secondary swelling, proportion of secondary swelling, and the time of the onset of secondary swelling will first be compared in terms of total stress and then in terms of the final measured value of swell.

The slope of primary swelling was found to generally decrease with total stress for all three test procedures (Figure 7.13 a). Furthermore, the relationship between the slope of primary swell and total stress was found to be similar for all three test procedures. One possibility for the observed decrease in the rate of primary swelling is a reduction of the voids of the specimen and thus decreases the hydraulic conductivity of the specimen leading to a slower rate of primary swelling. Furthermore, this reduction in the void space leads to an increase in the saturation of this specimen. In turn, the increase in saturation caused by a higher total stress leads to a reduction in the capillary forces (i.e. initial suction) in the soil and thus decreases the flow rate of water into the soil.

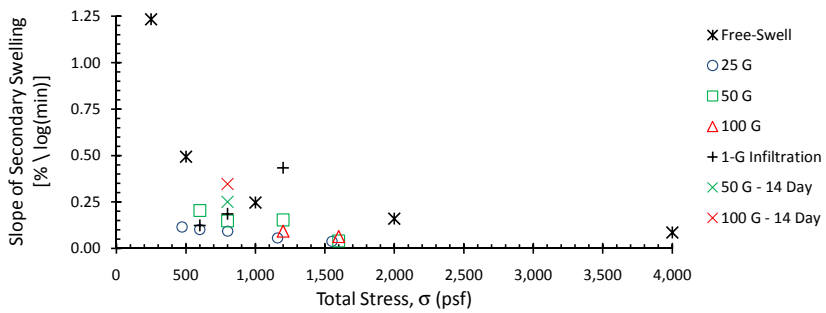
The slope of secondary swelling was found to be higher for free-swell testing than for centrifuge testing (Figure 7.13 b). While the slope of secondary swelling was found to decrease with increasing total stress for free-swell and centrifuge tests, it was found to increase for 1-G infiltration tests. The slope of secondary swelling at the highest total stress used for 1-G infiltration testing was found to exceed the slope of secondary swelling for free-swell and centrifuge tests subjected to similar loads. The proportion of secondary to total swell was found to be less than 11% for free-swell and centrifuge tests conducted at loads greater than 500 psf.

The time to the onset of secondary swelling was found to be greatest for centrifuge

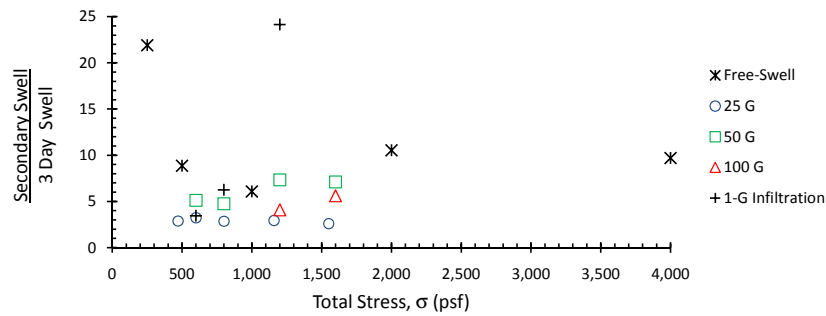
tests and least for free-swell tests (Figure 7.13 d). The time of the onset of secondary swelling was found to be less than one and a half days for all three of the test procedures. The time of the onset of secondary swelling was found to decrease with total stress for all of the tests with the exception of the centrifuge tests conducted at 25 G where it was found to increase with total stress. When the time of onset of secondary swelling is subsequently compared to the observed swelling this will be discussed further.



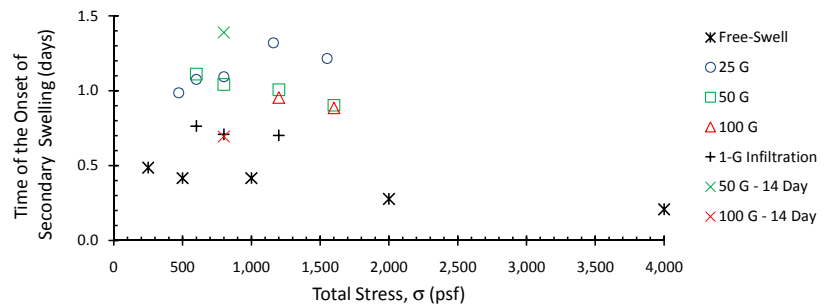
(a)



(b)



(c)



(d)

Figure 7.13: Primary and Secondary Swelling for All Tests: (a) Slope of Primary Swelling; (b) Slope of Secondary Swelling; (c) Proportion of Secondary Swell; and Time of Secondary Swell

In order to determine if a relationship exists between the slope of primary swelling and the slope of secondary swelling, these two parameters were plotted against one another in Figure 7.14 for each of the test methods. The slope of secondary swelling was found to increase with the slope of primary swelling for the free-swell and centrifuge tests. In the case of the 1-g analog tests, the slope of secondary swelling was found to decrease with the slope of primary swelling. Furthermore, the slope of secondary swelling for free-swell tests were found to be greater than the slope of secondary swelling for centrifuge tests for similar rates of primary swelling. A larger slope of primary swelling is thought to be the result of high capillary forces and high hydraulic conductivity. A high slope for primary swelling may be related to a high slope for secondary swelling since the hydraulic conductivity of the specimen is greater and thus any long-term hydration process would have more ready access to water.

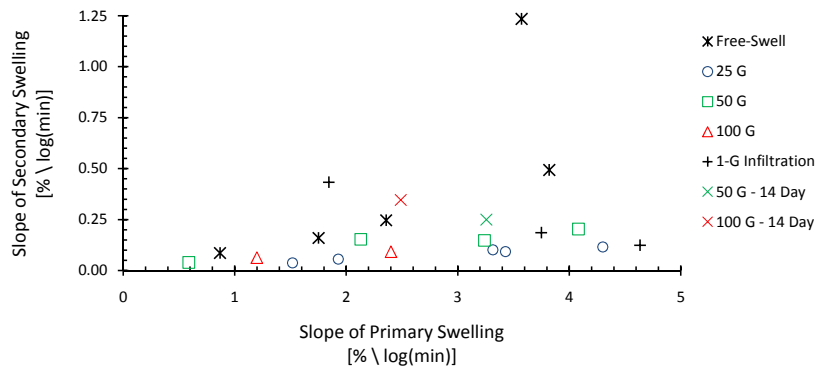


Figure 7.14: Slope of Secondary Swelling Versus the Slope of Primary Swelling for All Tests

The initial evaluations of primary and secondary swelling in free-swell, 1-G infiltration, and centrifuge test are presented in terms of the total stress. Another possibility is to evaluate primary and secondary swelling for each of these test in terms of the observed

swelling. Since the observed swelling is associated with the effective stress, it is possible to learn something of the relationship between effective stress and primary and secondary swelling. For each of these different testing procedures, the effective stress state within the specimens is discussed in detail in Section 7.6.

The slope of primary swelling was found to increase with swell (Figure 7.15 a). With the exception of the free-swell test that reached a swell of 15%, all of the tests follow a similar trend between the slope of primary swelling and swell. It was previously proposed that the rate of primary swelling decreases with increasing total stress due to a decrease in the void ratio leading to a decrease in the hydraulic conductivity and a decrease in the initial suction in the soil. Since, however, the rate of primary swelling was found to be directly proportional to swell, it appears that the moisture front likely moved through the different soil specimens at similar rates and that the slope of primary swell is greater for specimens that undergo greater swelling.

The slope of secondary swelling differed greatly in the three different test methods when compared in terms of swell (Figure 7.15 b). While the slope of secondary swell was found to increase with swell for the free-swell and centrifuge tests, it was found to decrease with swell for the 1-g analog tests. Furthermore, the slope of secondary swelling for the free-swell specimen that swelled to 15% was significantly larger than for all of the other test specimens. It is possible that the cause of the observed smaller slope of secondary swelling for swell values greater than 10% for centrifuge and 1-G infiltration tests than for free-swell tests are the result from the fact that the centrifuge and 1-G infiltration tests involve the progression of a uni-directional wetting front and a gradient in total head across the specimen. With a uni-directional wetting front and a gradient in total head across the specimen air can be driven from the specimen and clay particles can be given ready access to water for hydration. In the case of free-swell tests, the bi-direction wetting front driven by capillary forces results in the potential for trapping air at the center of the specimen. Furthermore, since there is not a uniform gradient in total head across the entire specimen, hydrating clay particles are not given ready access to water.

The proportion of secondary swell was found to be less than 11% for all of the tests except the 1-g analog tests that swelled to 7% and the free-swell tests that swelled to 15% (Figure 7.15 c). The proportion of secondary swelling observed in free-swell testing was found to generally be greater than that observed for free-swell testing. The time of the onset of secondary swelling was found to increase with swell for all of the tests except the centrifuge tests conducted at 25 G (Figure 7.15 d).

The time of onset of secondary swelling was found to be greater for centrifuge testing and least for free-swell testing. The time of the onset of secondary swelling was likely greater for centrifuge and 1-G infiltration tests because the height of drainage was twice as large as that of the height of drainage in the free-swell tests. As demonstrated in the subsequent section, the process of swelling appears to be diffusive and thus the time to swelling should be proportional to the square of the height of drainage. When the time of secondary swelling is scaled by the square of the height of drainage, the scaled time of swelling for free-swell testing was found to be similar to but greater than the scaled times for centrifuge and 1-G infiltration testing (Figure 7.16). It is possible that the smaller scaled time of secondary swelling for centrifuge and 1-G infiltration result from the increased water pressure at the top boundary of the soil specimens.

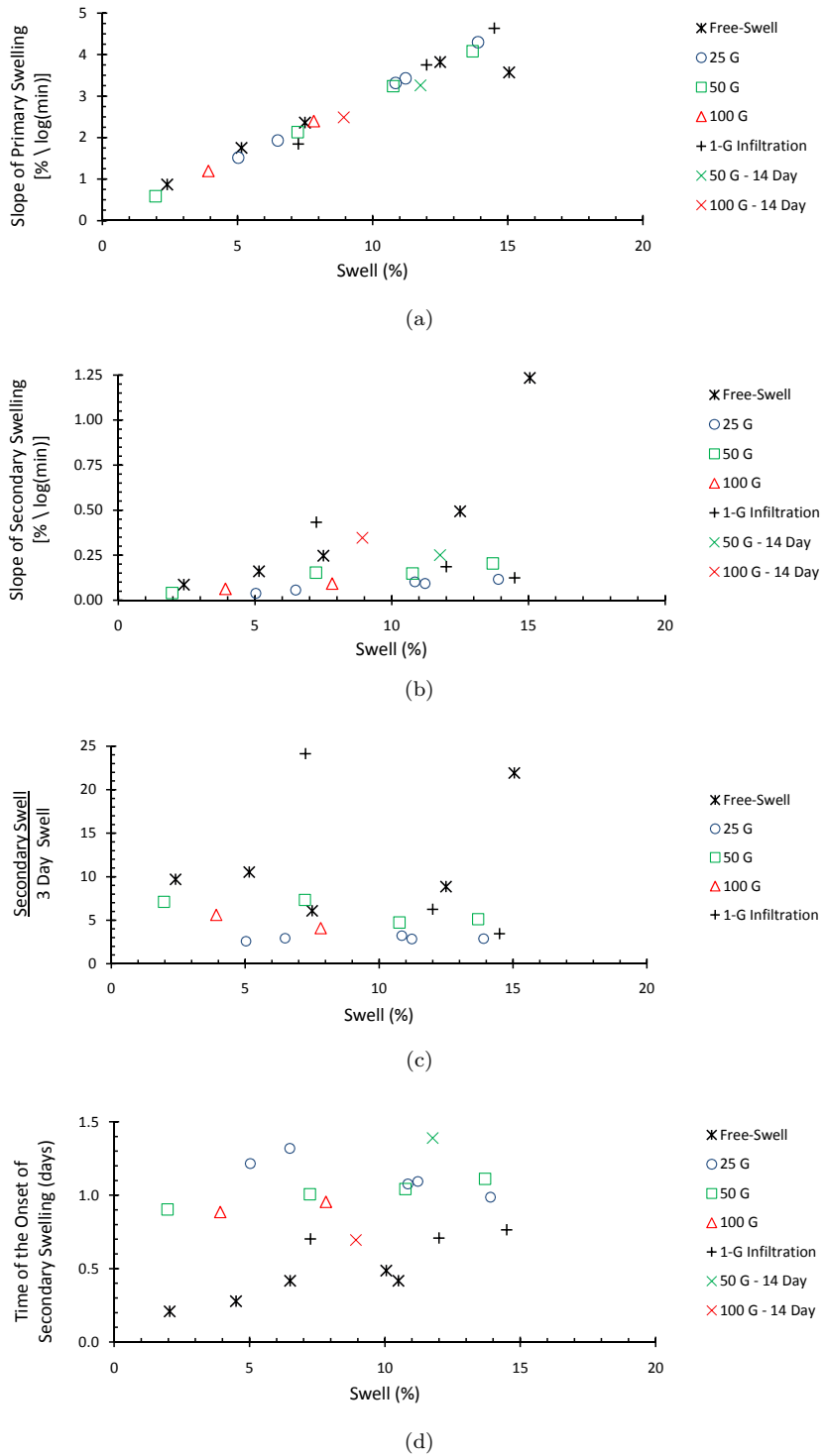


Figure 7.15: Primary and Secondary Swelling for All Tests: (a) Slope of Primary Swelling; (b) Slope of Secondary Swelling; (c) Proportion of Secondary Swell; and (d) Time of the Onset of Secondary Swelling

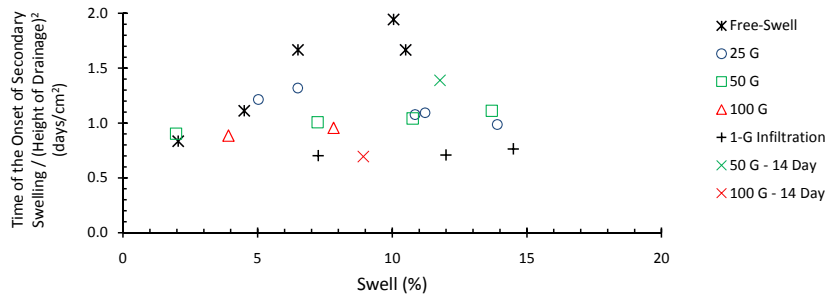


Figure 7.16: Time of Secondary Swelling Scaled by the Square of the Height of Drainage

7.1.6 Square-Root of Time Analysis

The rate of primary and secondary swelling were first evaluated in terms of the slope of the swelling versus the logarithm of time. The rate of primary and secondary swelling can also be evaluated with respect to the square-root of time. If the rates are considered in terms of the square-root of time and the process of swelling is a diffusive process than the first portion of the swelling curve should plot linearly with the square-root of time.

Swelling is plotted versus the square-root of time for free-swell tests, centrifuge tests, 1-G infiltration tests, and 14-day centrifuge tests in Figures 7.17 through 7.20. For each of the testing method, the first portion of the swelling curve plots linearly with the square-root of time. This indicates that the process of flow and subsequently swelling in each of the experiments is initially a diffusive process.

The slope of primary swelling is presented in terms of total stress and swell in Figures 7.21 (a) and (b). In log-time space, the slope of primary swelling showed a similar trend for free-swell, centrifuge, and 1-G infiltration tests. In square-root of time space, the slope of primary swelling shows a strong linear trend for centrifuge and 1-G infiltration testing, but the slope of primary swelling for free-swell appears unrelated. It is unclear why the

square-root of time slope of primary swelling appears unrelated to total stress of swell for the free-swell tests.

The slope of secondary swelling is plotted versus total stress and well in Figures 7.22 (a) and (b). The slope of secondary swelling follows similar trends for free-swell, centrifuge, and 1-G infiltration tests.

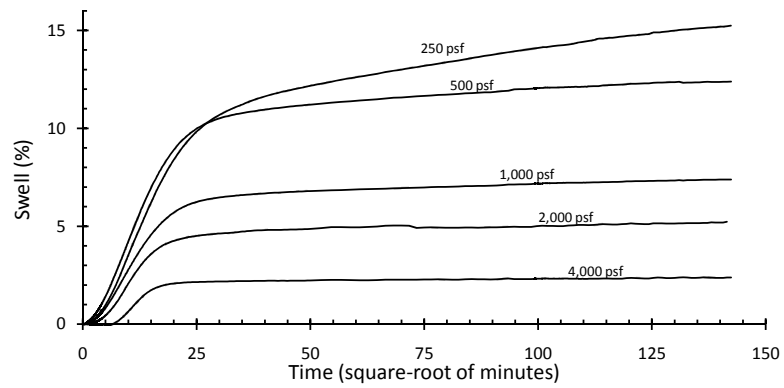
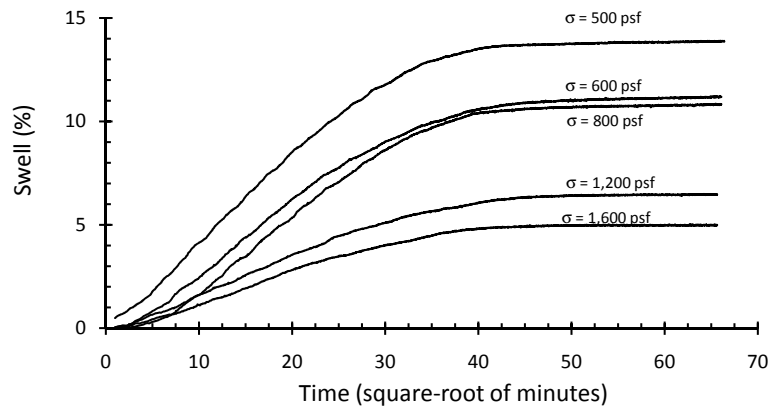
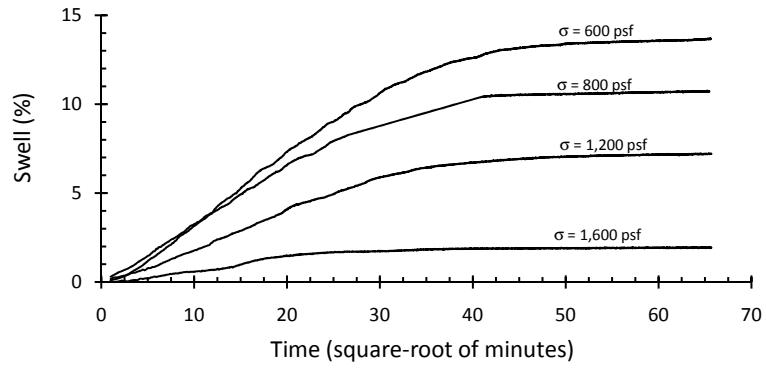


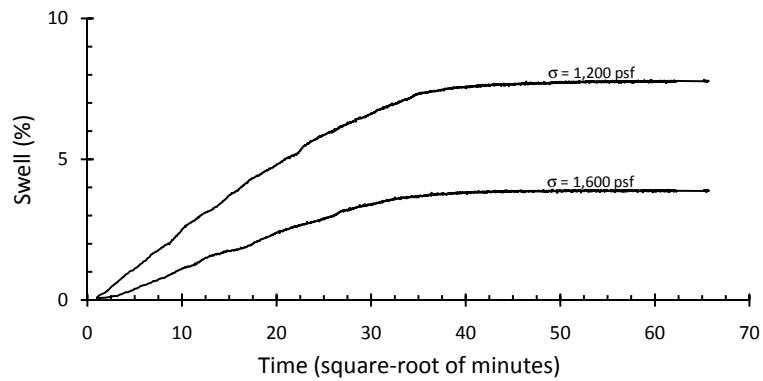
Figure 7.17: Swell versus the Square-root of Time for Free-Swell Tests



(a) 25 G



(b) 50 G



(c) 100 G

Figure 7.18: Swell versus the Square-root of Time for Centrifuge Tests: (a) 25 G; (b) 50 G; and (c) 100 G

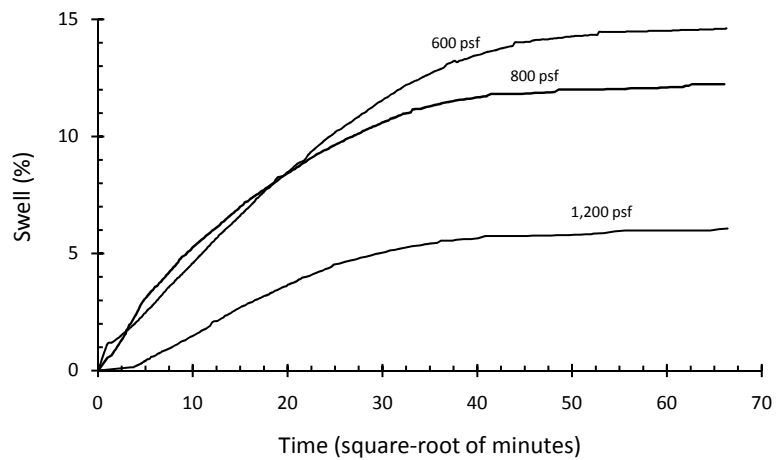


Figure 7.19: Swell versus the Square-root of Time for 1-G Infiltration Tests

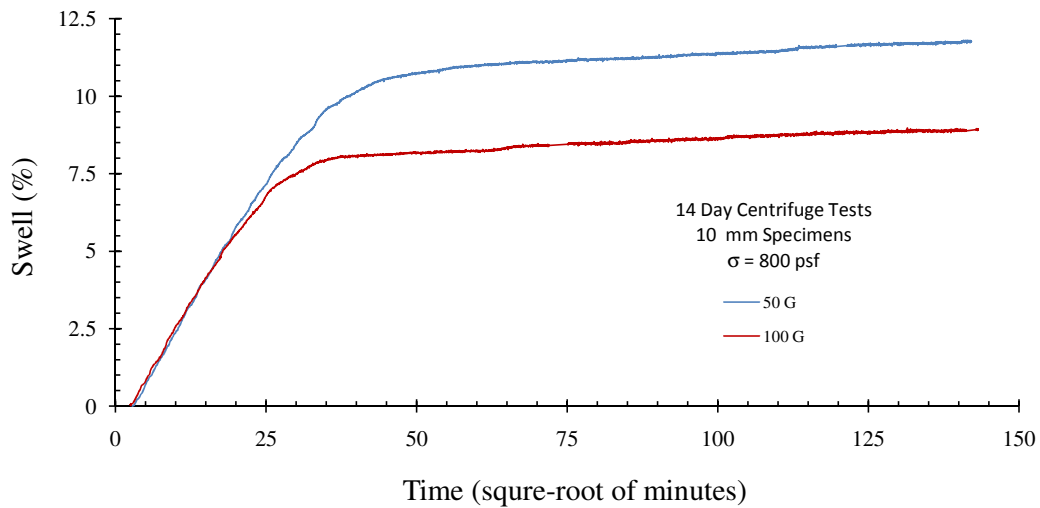
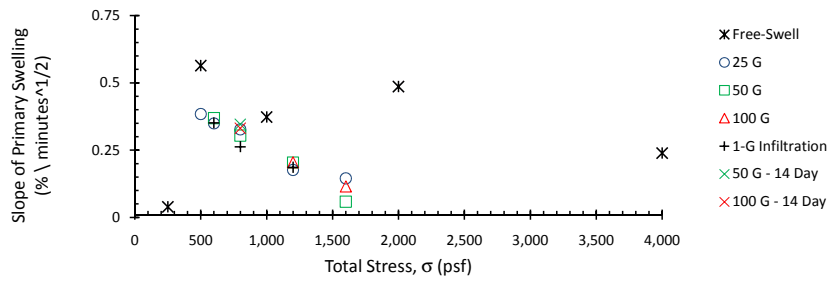
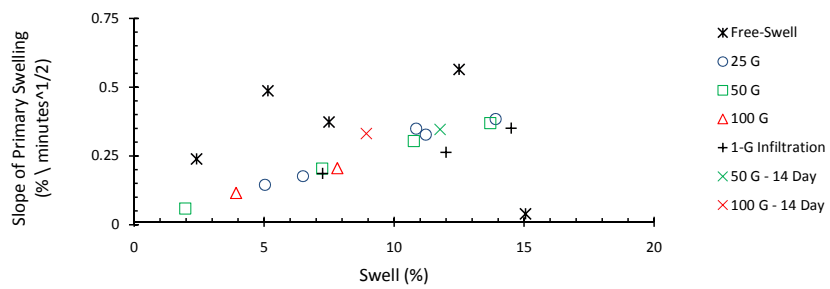


Figure 7.20: Swell versus the Square-root of Time for 14 Day Centrifuge Tests



(a)



(b)

Figure 7.21: The Slope of Primary Swelling in Root-Time Space in Terms of: (a) Total Stress and (b) Swell

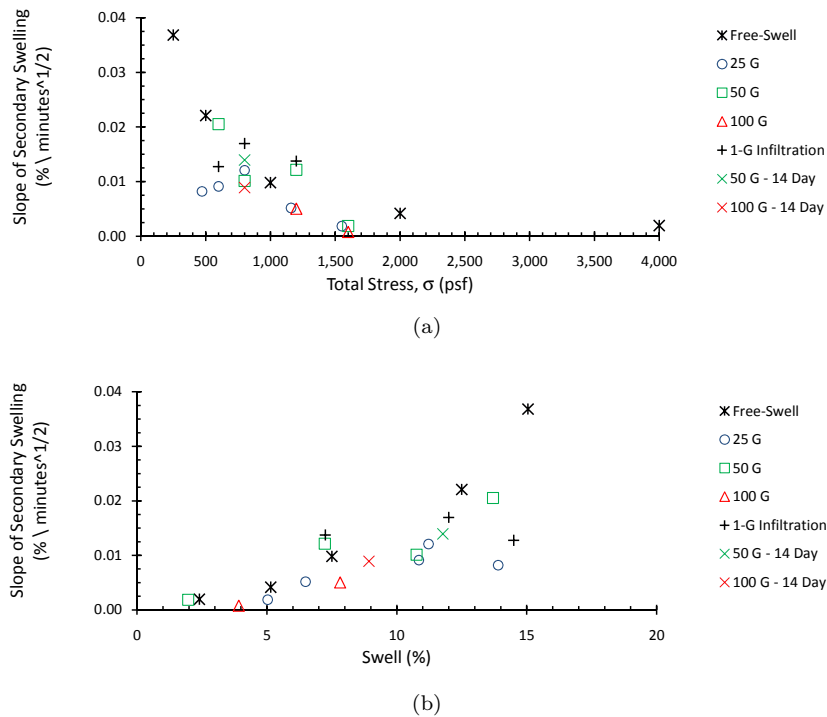


Figure 7.22: The Slope of Secondary Swelling in Root-Time Space in Terms of: (a) Total Stress and (b) Swell

7.2 Secondary Swelling - Displacement Rates for Long-Term, 14 Day, Tests

As discussed in Sections 6.3 and 4.1, 14 day swelling tests were conducted in the centrifuge and with free swell test specimens. The measured values of swell for the centrifuge and free swell tests, with similar ultimate swell, are compared in Figures 7.23 and 7.24. For these tests, the free swell tests appear to level off earlier than the centrifuge tests conducted at 50 and 100 G. In order to better evaluate this trend, the displacement rate over the course of testing was calculated for these tests and is presented in Figure 7.25. The displacement rates for centrifuge and free-swell test specimens undergoing like final strains were found to be similar. Accordingly, it appears that the mechanism controlling secondary swelling of the

soil is independent of the boundary conditions and is instead intrinsic to the soil specimen. This further supports the idea that the long-term process of swelling is driven by a process of clay hydration in which water is potentially being drawn to the soil particles by osmotic suction as the clay particles are naturally negatively charged and attract the hydrogen atom in the water molecules.

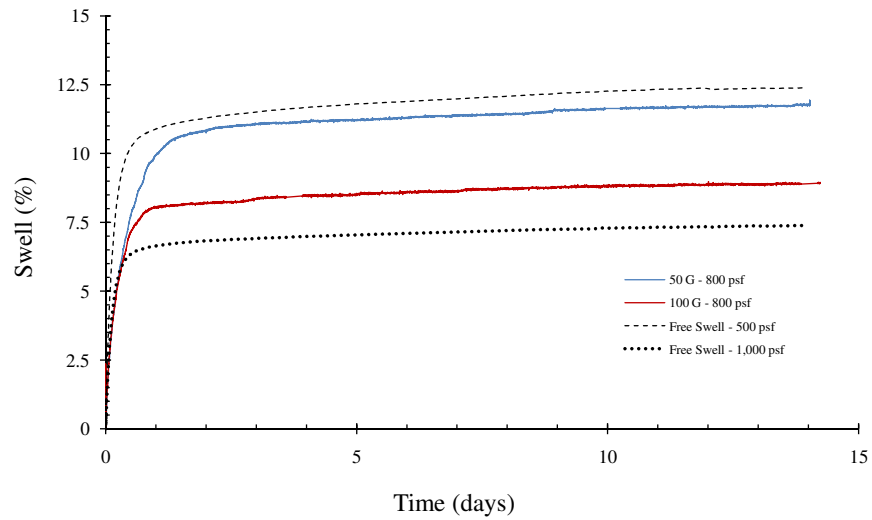


Figure 7.23: Swell Versus Time for Specimens Tested for 14 Days in Centrifuge and Free Swell Tests

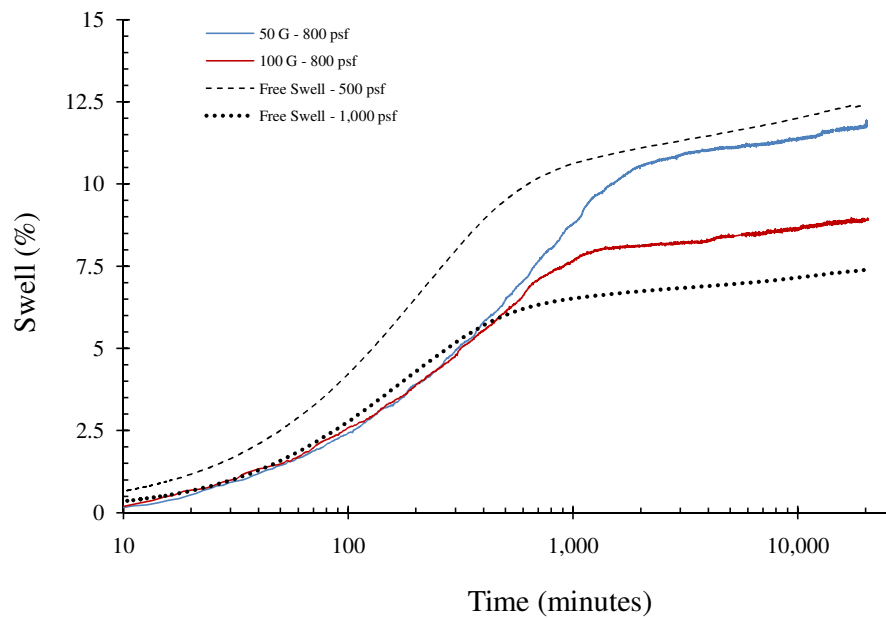


Figure 7.24: Semi-log Plot of Swell Versus Time for Specimens Tested for 14 Days in Centrifuge and Free Swell Tests

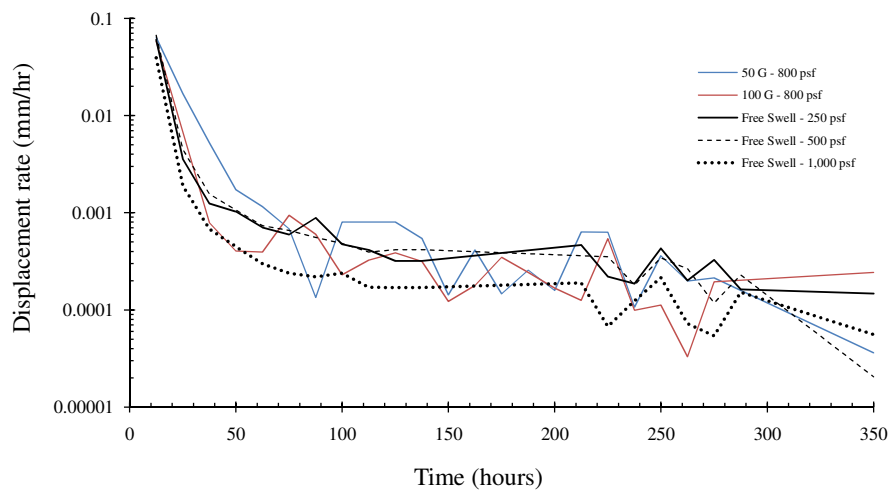


Figure 7.25: Displacement Rate Versus Time for Specimens Tested for 14 Days in Centrifuge and Free Swell Tests

7.3 Wetting Front Advancement During Centrifugation

After test completion, each specimen was removed from the centrifuge and weighed, excess ponded water was poured off, specimens were weighed again, and then they were extruded from the cylinder. As each specimen was extruded, it was cut into slices of approximately 3.33 mm in thickness. Consequently, for a 10-mm thick specimen, three specimens were obtained. For the 20-mm thick specimen, six specimens were attained. The height of each slice was measured and then the slices were placed into the oven and dried. The water content and dry unit weight of each slice was then determined.

In this section, water content profiles are presented for centrifuge test conducted for durations of 24, 48, and 72 hours. It should be emphasized that the water content profiles measured for the tests of various durations were obtained from different test specimens as the specimens are destructively sampled for water content at the end of each test. For the purposes of discussion, however, the water profile is expressed as “progressing” through the specimen.

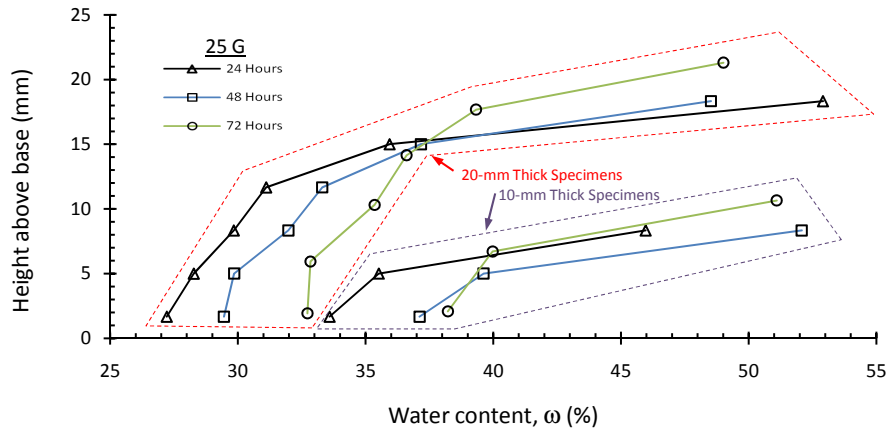
The water content profiles measured after 24, 48, and 72 hours for testing performed at 25, 50, and 100 G on 10-mm and 20-mm thick specimens are presented by G-level in Figure 7.26. To clarify, 10-mm thick and 20-mm thick specimens are both shown in each of these figures. At each G-level, the water content profile moves through the specimen with respect to time. For the 20-mm thick specimens this water content profile generally changes more significantly than for the 10-mm thick specimens. The change in the water content profile also appears to shift more at higher elevations within the soil specimens than towards the base.

The water content profiles are plotted in terms of time for Series (i) in Figure 7.27. At each testing time, lower water contents are generally obtained for increasing G-levels. It is, however, curious that the shape of the water content profiles at 24, 48, and 72 hours after the start of testing are so similar at each G-level. At 24, 48, and 72 hours of testing, water contents within the 25 G specimens were generally less than the water contents within the 50 G specimens, which were less than the water contents in the 100 G specimens at similar

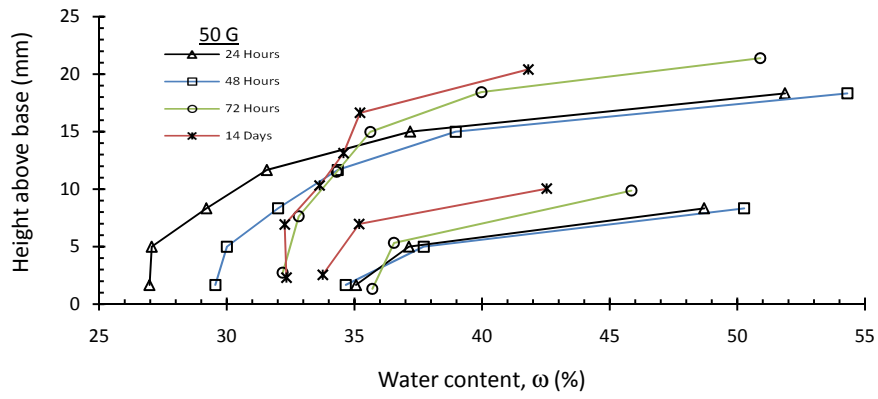
elevations.

In order to compare the water content profiles in the 10-mm and 20-mm thick test specimens, the water contents in the specimens are plotted versus depth in the soil profile presented in Figure 7.28. From these plots, it is evident that the water content profile in the a 10-mm thick specimen is very similar to the water content profile of the upper 10-mm of a 20-mm thick specimen. The total stress profiles in the 10-mm thick specimens and the upper 10 mm of the 20-mm thick specimen are virtually identical as the same surcharge pressure was used for each specimen and the total unit weight of the soil for each specimen is thought to be very similar. The water pressure imposed at the top of each profile was the same, but the 20-mm thick test specimen has a smaller hydraulic gradient imposed across it than the 10-mm specimen. Accordingly, the water pressure would be less in the top 10 mm of the 20-mm thick specimen than in the 10-mm thick specimen. As such, the effective stress would be less in the 10-mm thick specimen and thus the swelling and consequently the water content would be greater. The pore pressure profile within the specimen is explored in detail in Section 7.6.

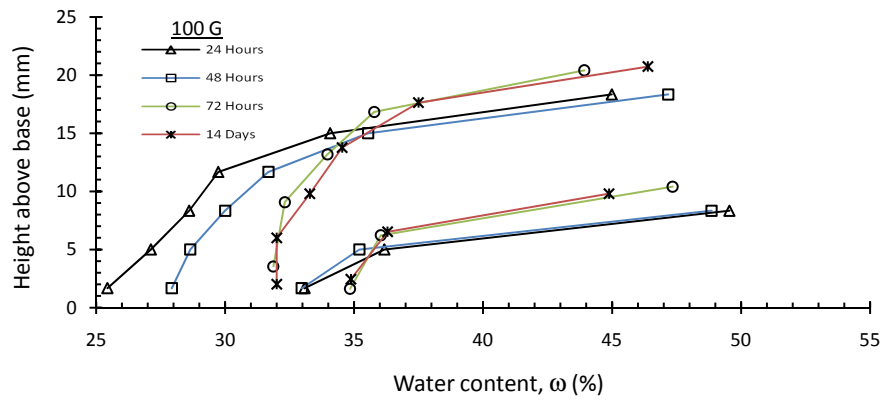
In order to investigate the long-term moisture changes in a centrifuge tests, a 10-mm thick soil specimen was flown at 50 and 100 G for a period of 14 days. The water content profiles for these specimens are plotted in Figure 7.29. The water contents were found to increase from 24 hours to 480 hours while the samples remain saturated indicating that long-term swelling is still occurring in the centrifuge specimens. This indicates that the clay particles are undergoing a long-term hydration process.



(a)

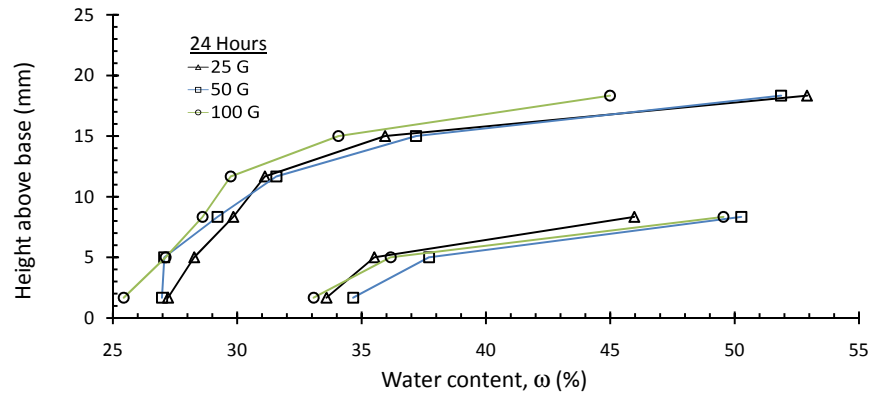


(b)

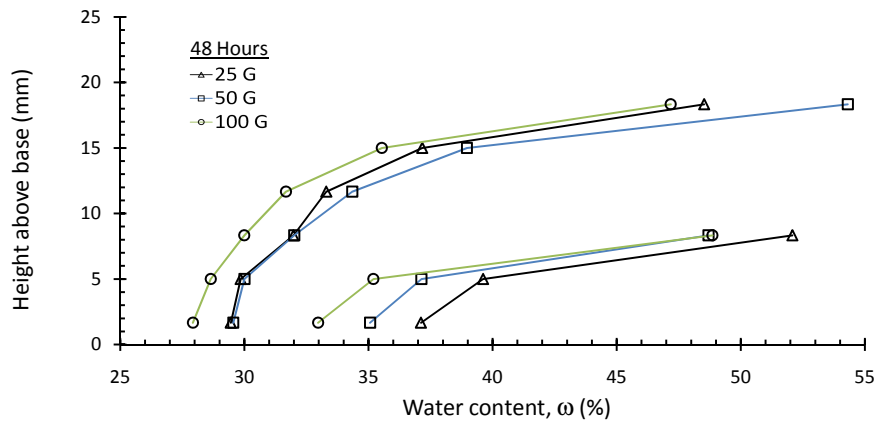


(c)

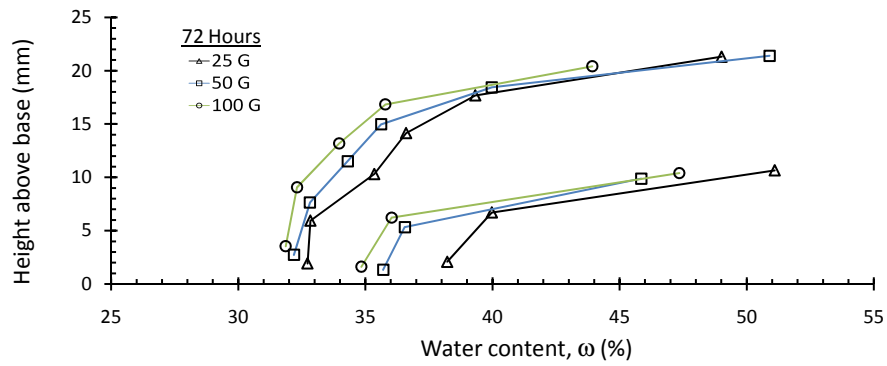
Figure 7.26: Water Content Profiles by G-level



(a)

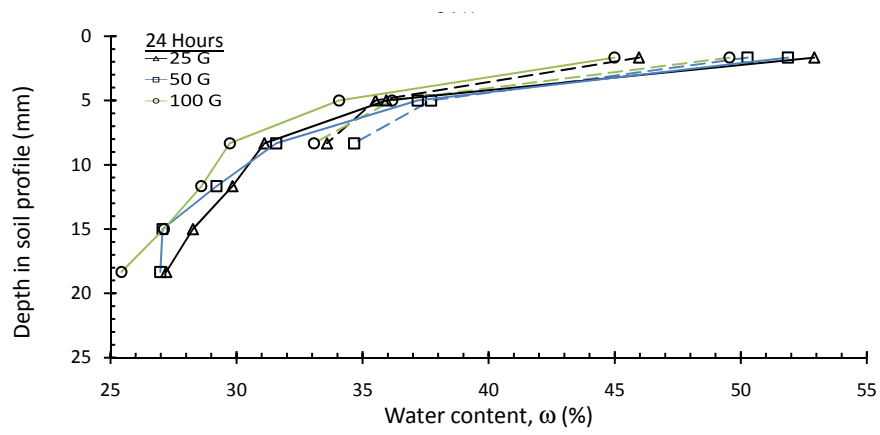


(b)

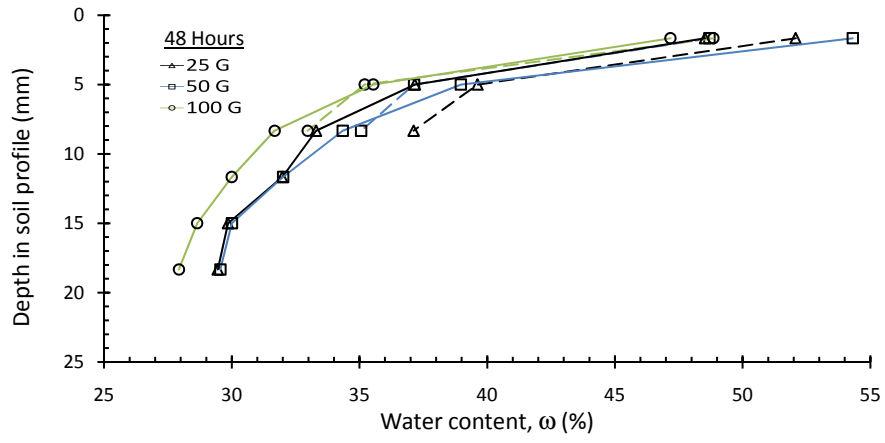


(c)

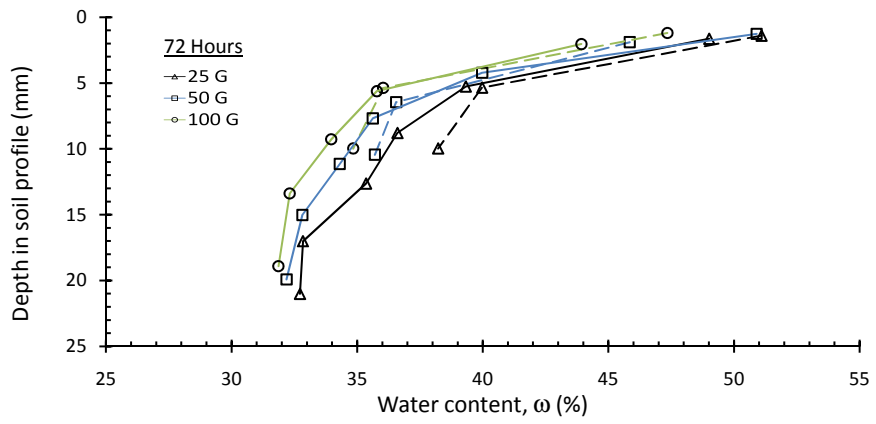
Figure 7.27: Water Content Profiles by Time



(a)



(b)



(c)

Figure 7.28: Water Content Profiles by Time with Respect to Depth
162

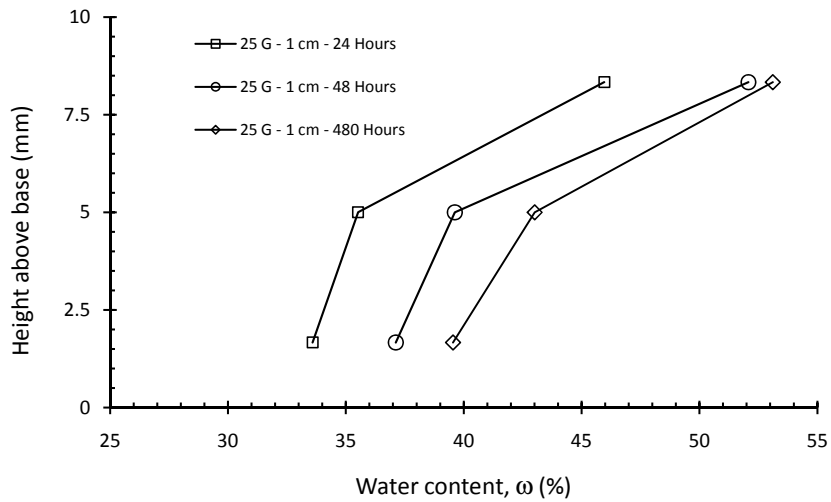


Figure 7.29: Water Content Profiles for Long-term Tests

7.4 Outflow Rates and Hydraulic Conductivity from Centrifuge Testing

The cumulative outflow measured from the centrifuge tests conducted on 10-mm and 20-mm thick specimens at 50 and 100 G are presented in Figure 7.30. Outflow from the 10-mm thick specimens for tests at 50 and 100 G was first measured after 40 hours of testing. For the 20-mm thick specimen tested at 100 G, outflow was first measured after 100 hours of testing. For the 20-mm thick specimen tested at 50 G, outflow was first measured after 160 hours of testing. Accordingly, it took at least twice as long for outflow to occur from the 20-mm thick specimens tested at 50 and 100 G than for the 10-mm thick specimen.

Given the cumulative outflow from each of the test specimens, the outflow rate was determined and the hydraulic conductivity value for each specimen was calculated after outflow was observed assuming the specimen was saturated. Assuming that the specimens reached saturation, the approximate values for the hydraulic gradients through each specimen are presented in Table 7.1. While the water pressure applied over the specimen was

approximately constant for each of the long-term centrifuge tests, the total head applied over each specimen for each test was a function of the different elevations heads for different specimen thicknesses and different G-levels.

Values of hydraulic conductivity were calculated for each specimen as soon as out-flow occurred and are plotted in Figure 7.31. Before reaching an approximately constant value, calculated values of hydraulic conductivity are observed to increase with time as the specimen is presumably reaching a higher degree of saturation. The measured value of hydraulic conductivity, approximately $2 \cdot 10^{-11}$ m/s from centrifuge testing is in good agreement with the range of hydraulic conductivities, $5 \cdot 10^{-12}$ m/s to $5 \cdot 10^{-11}$ m/s, which was measured as part of the soil characterization phase of this study (Section 3.1.6).

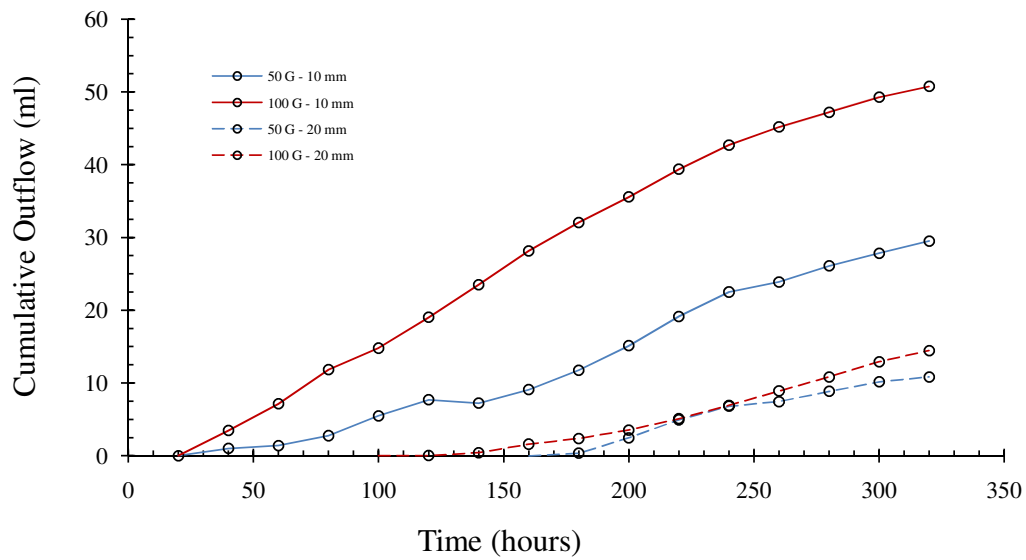


Figure 7.30: Cumulative Outflow Versus Time for 10-mm and 20-mm thick Specimens Tested for 14 Days in Centrifuge

Table 7.1: Hydraulic Gradient for 14 Day Centrifuge Tests

	50 G	50 G	100 G	100 G
Thickness of Soil Sample (mm)	10	20	10	20
Height of Water Above Soil (mm)	40	40	20	20
Pressure Head (mm of H_2O)	2,000	2,000	2,000	2,000
Elevation Head (mm)	500	1,000	1,000	2,000
Total Head (mm)	2,500	3,000	3,000	4,000
Hydraulic Gradient, i	250	150	300	200

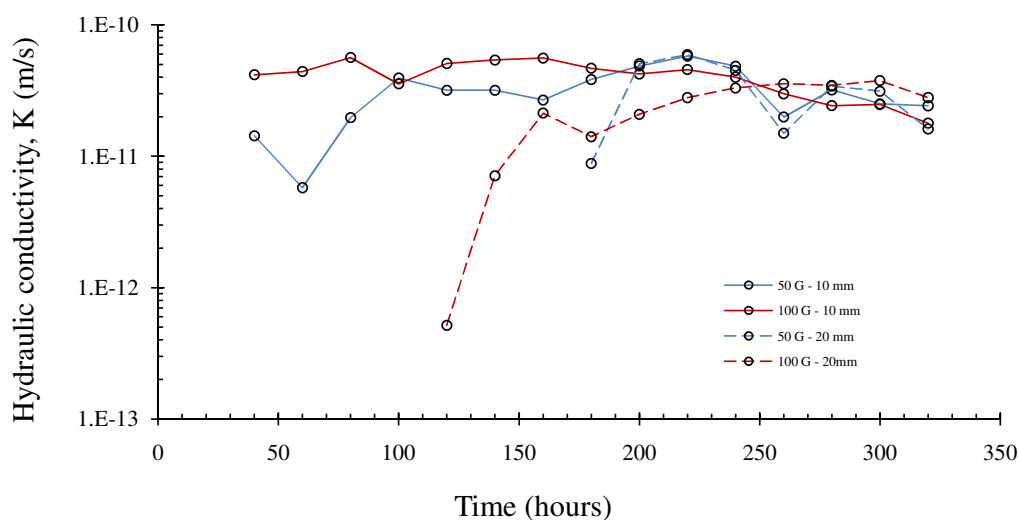


Figure 7.31: Hydraulic Conductivity Versus Time for 10-mm and 20-mm thick Specimens Tested for 14 Days in Centrifuge

7.5 Total Stress Comparison of Free Swell and 1-G Infiltration Results with Centrifuge Testing

The results of the tests series with a constant water pressure of 400 psf applied over the specimen which were run at 25, 50, and 100 G are also plotted with the results from free swell testing in Figures 7.32 and 7.33. In these figures, the final void ratio and swell measured for the centrifuge, free-swell, and 1-G infiltration tests are plotted versus the total stress applied over the profile. For free swell testing the effective stress at the end of testing assumed to

be the total stress since the pore water pressures within the specimen at the end of testing are assumed to be zero. For centrifuge tests the total stress is the sum of the water pressure and the surcharge pressure. The state of effective stress within the centrifuge test specimens is dependent on the pore water pressures within the soil specimen which are evaluated in Section 7.6. Interestingly, strong agreement is found between the centrifuge, free-swell, and 1-G infiltration tests for total stress values of less than 1,000 psf. At higher values of total stress, the results of free-swell testing show high void ratios or swelling than for centrifuge testing. Free swell tests were not conducted at higher values of total stress so they can not be compared. When, incremental swelling, pore water pressures, and effective stress are considered in the centrifuge test specimens (Section 7.6), good agreement is shown between free-swell and free swell tests.

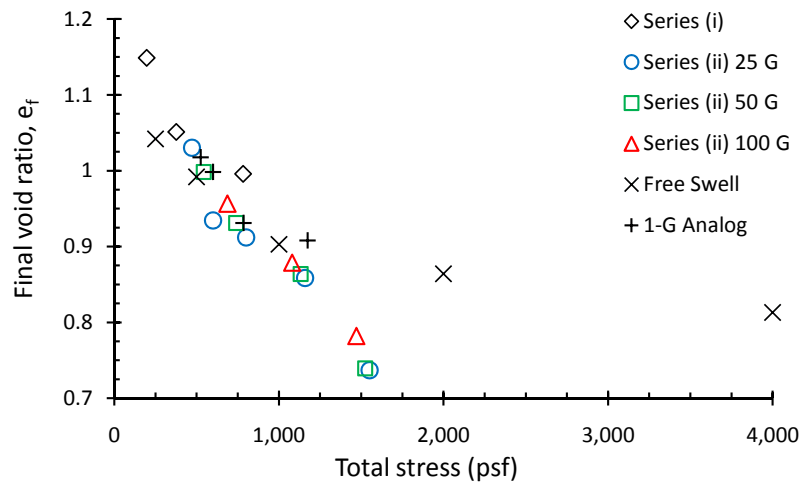


Figure 7.32: Final Void Ratio Versus Total Stress for Centrifuge Tests, Free Swell Tests and 1-G Infiltration Tests on 10-mm thick soil specimens with a Water pressure of 400 psf (19 KPa)

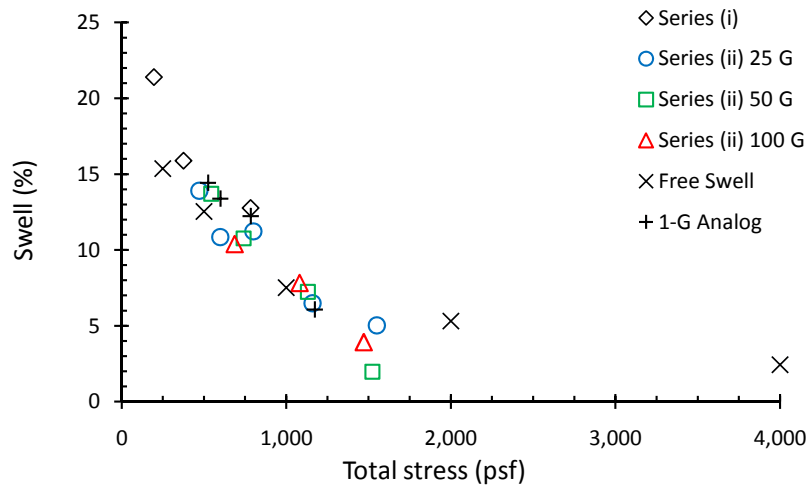


Figure 7.33: Swell Versus Total Stress for Centrifuge Tests, Free Swell Tests and 1-G Infiltration Tests on 10-mm thick soil specimens with a Water pressure of 400 psf (19 KPa)

7.6 Effective Stress Comparison of Free Swell and 1-G Infiltration Results with Centrifuge Testing

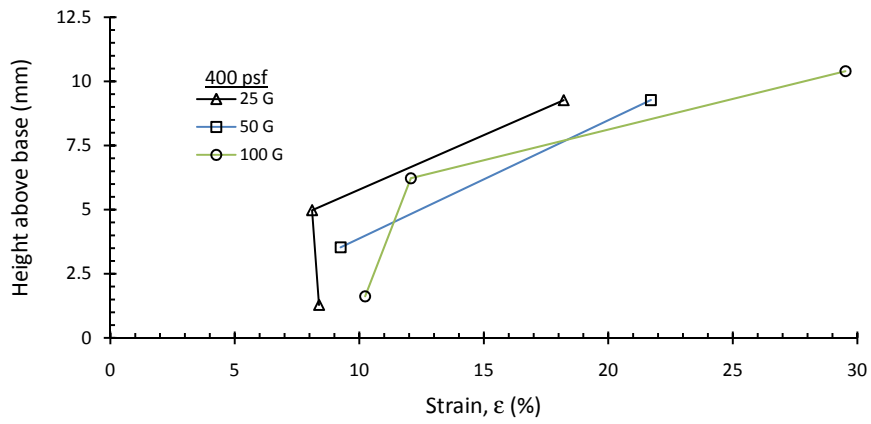
In Section 6.2, the effect of total stress and G-level on the swelling of specimens was evaluated. In this section, the effect of total stress and G-level on the incremental values of swell, measured by destroying the specimens at the end of testing, is evaluated. The relationship between effective stress and swelling for soil specimens tested in the centrifuge is also evaluated.

7.6.1 Incremental Swell Profiles in Centrifuge Specimens

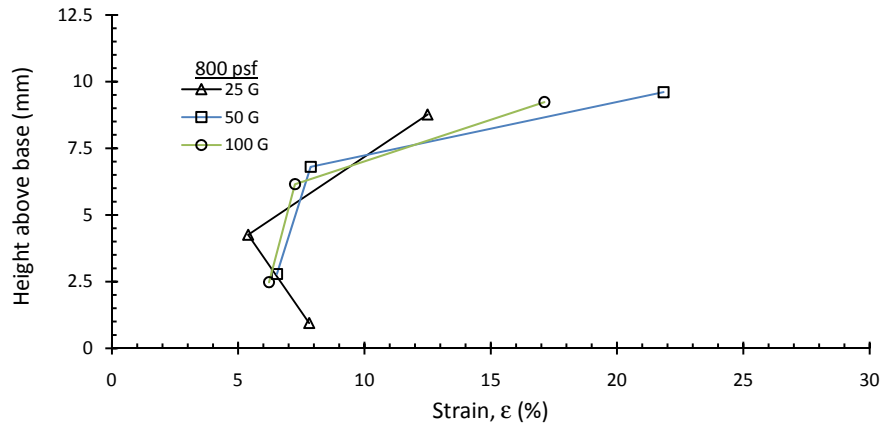
At the end of each test, the thickness of each soil slice was measured after the specimens were cut into slices in order to sample the water content profiles. The saturation profiles were then calculated based on the measured heights, the gravimetric moisture content, the dry unit weight, and the specific gravity of the Eagle Ford clay (Section 3.1.4). The resulting saturation profiles resulted in values of saturation ranging from 0.95 to 1.05. This indicated

an error in the height measurement system. The degree of saturation did, however, not appear to vary with height in any specific pattern. Accordingly, the saturation throughout the 10-mm and 20-mm thick profiles can be assumed to be 100% within a 5% error, for the 10-mm thick specimens after 72 hours of testing. Assuming the specimen to be 100% saturated, the dry density of each soil slice was calculated. From the dry density, the incremental swell for each slice was calculated assuming an initially uniform dry density profile. In actuality the initial dry density profile is likely not uniform due to initial settlements prior to the placement of water above the test specimen. The incremental swell profiles determined by assuming a saturation of 100% are shown in Figure 7.34. The dry density in the soil specimens was found to generally increase with increasing G-level for the samples.

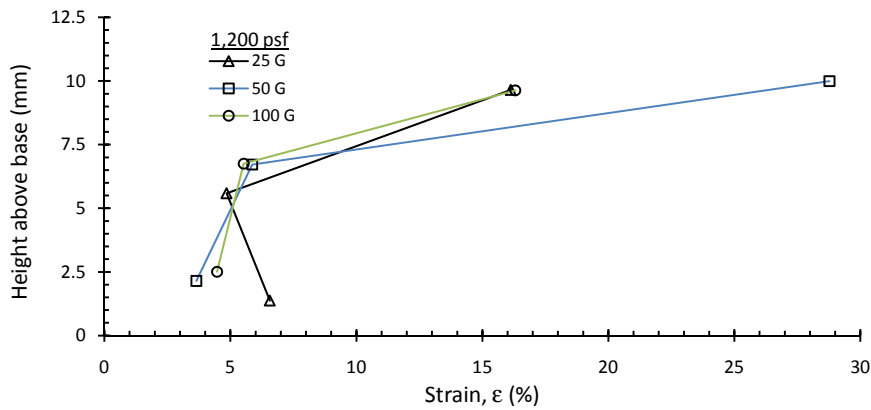
Figure 7.34: Incremental Swell Profiles for Specimens Tested at 25, 50, and 100 G with a Water Pressure of 400 psf (20 KPa) Applied Over the Specimens



(a)



(b)



(c)

Figure 7.35: Incremental Swell Profiles for Specimens Tested at 400, 800, and 1,200 psf with a Water Pressure of 400 psf (20 KPa) applied over the Specimens

7.6.2 The Interpretation of Incremental Swell Profiles in Centrifuge Specimens

The incremental values of swell can be used to generate a relationship between swell and effective stress if the total stress and pore water pressure are known throughout the profile. Since it was not possible to instrument a 10-mm thick soil specimen in order to measure the pore water pressure profile, an approximation of the swell versus effective stress can be obtained by assuming a constant hydraulic conductivity across the soil specimen and assume that the loss in pore water pressure across the soil specimen is linear, reaching a value of zero at the base of the specimen. The total stress profile in turn can be determined based on the surcharge pressure, water pressure, and the measured variation the total unit weight across the specimen from the slices that are taken at the end of testing.

The incremental swell profile based on incremental measurements of water content for a centrifuge test conducted for 72 hours at 50 G is shown in Figure 7.36. Total stress profiles for these same tests are also shown along with water pressure profiles are shown assuming a linear loss in water pressure across the specimen. The assumption of a linear loss in water pressure across the specimen is discussed later in this section. From the total stress and water pressure profiles, the effective stress profile can be calculated assuming that the specimen is saturated. Given the effective stress and incremental swell profiles, swell can be related to incremental swelling.

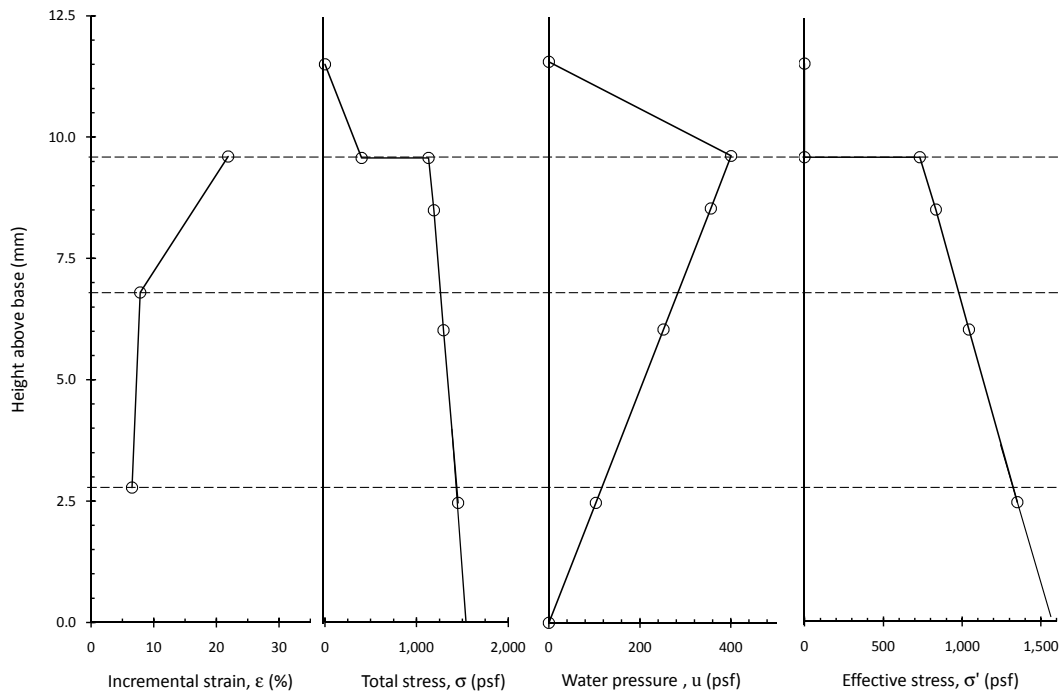


Figure 7.36: Incremental Swell Analysis Steps for specimens flown for 72 hours at 50 G with a water pressure of 400 psf and surcharge pressure of 800 psf

The relationship between incremental swelling and effective stress that results from this analysis is shown in Figure 7.37 along with the relationship measured during free swell testing. For the analysis, data from the upper 1/3 slice of the specimen was not incorporated as excessive swelling occurred in this region at the end of testing and the measured gravimetric water contents were inconsistent with gravimetric water contents measured from the lower 2/3 of the specimen. While slicing the soil specimen, it was often observed that this upper layer retained water that was ponded and excess swelling occurs in this layer when the specimen was extruded from the test cylinder. The relationships determined from free-swell testing and consolidation testing were found to be quite similar. The centrifuge tests at 25, 50, and 100 G also appear to lead to similar trends. Assuming a linear loss in pore pressure with height, the swell within the centrifuge specimens was found to exceed that of free-swell testing for a given value of effective stress.

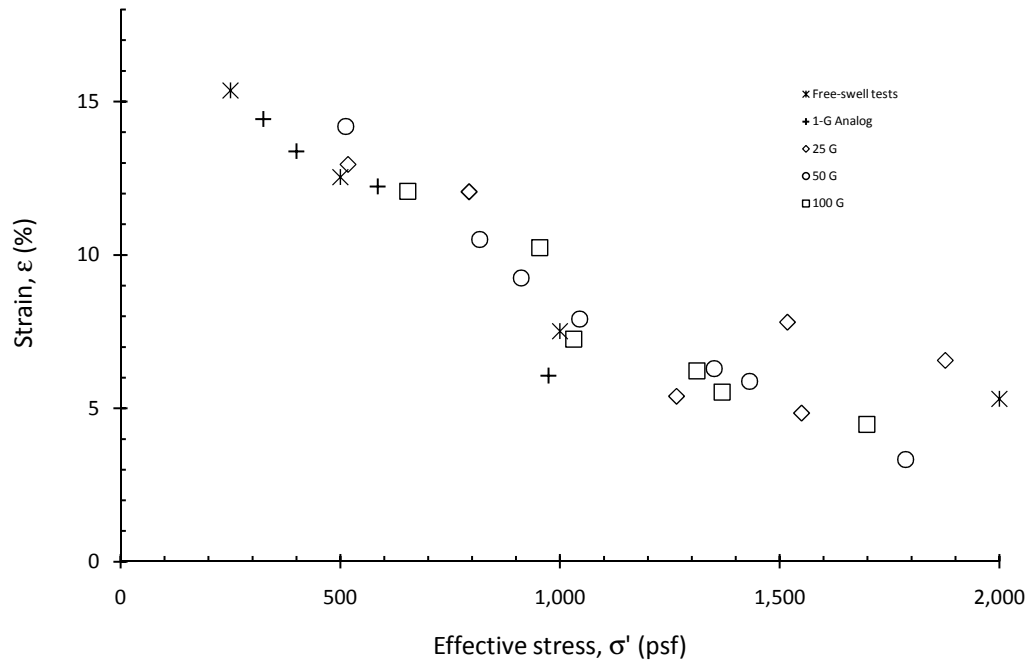


Figure 7.37: The Relationship between Swell and Effective Stress as Measured in the Centrifuge Permeameter (10-mm thick Specimens Tested at 25, 50, and 100 G with a Water Pressure of 400 psf (20 KPa) Applied Over the Specimens)

The assumption that the loss in total head and thus the loss in water pressure across the specimen is linear may be incorrect. Two other reasonable assumptions are that of a constant water pressure profile or a partially draining boundary. Profiles for a linear loss in pore water pressure across the specimen, a constant water pressure across the specimen, and a partially draining boundary are plotted in Figure 7.38. A partially draining boundary would lead to a pore water pressure that increases in proportion to the G-level with depth in the specimen. This is why the water pressure at the base of a specimen tested at 100 G with a partially draining boundary exceeds that of specimens tested at 25 and 50 G.

Incremental swelling values are plotted versus incremental swell for all G-levels assuming the different pore water pressure profiles in Figure 7.39. Also plotted in this figure are the results from free-swell and 1-G infiltration testing. Based on these results, it appears that the pore water pressure profiles that assume a linear loss or a constant value are in

the best agreement with the results of free-swell testing. The relationship between swell and effective stress determined assuming a partially draining boundary condition is in best agreement with the results of 1-G infiltration testing. There are, however, two reasons why it is unlikely that flow is restricted at the bottom boundary. The first reason is that the bottom boundary in the centrifuge setup consists of filter paper and a plastic plate with drilled holes. When the specimen is disassembled at the end of testing there was not any evidence of a filter cake, intrusion of the soil into the filter, or clogging of the drilled holes in the plastic plate. The second reason is that the hydraulic conductivity measured during centrifuge testing matches that from index property testing. Accordingly, it appears that flow is not restricted. As a result, it is likely that a linear loss in water pressure is the most reasonable assumption. Since the objective of the test is to relate swell with effective stress and assuming a linear loss in pore water pressure yields the greatest swelling, assuming a linear loss in pore water pressure is the most conservative of the considered pore water pressure distributions.

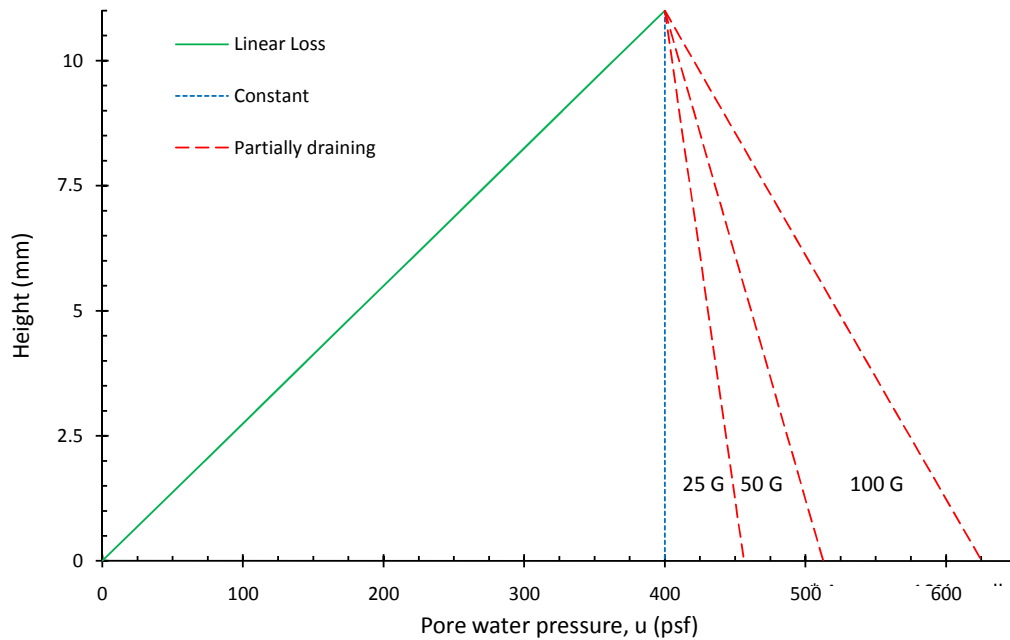


Figure 7.38: Various Pore Water Pressure Assumptions

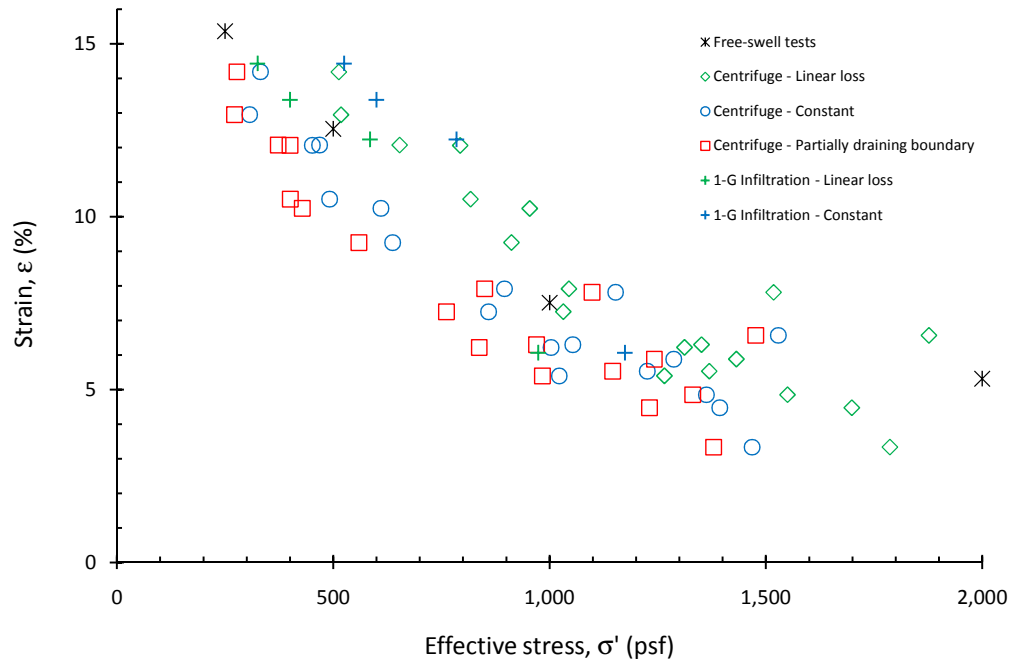


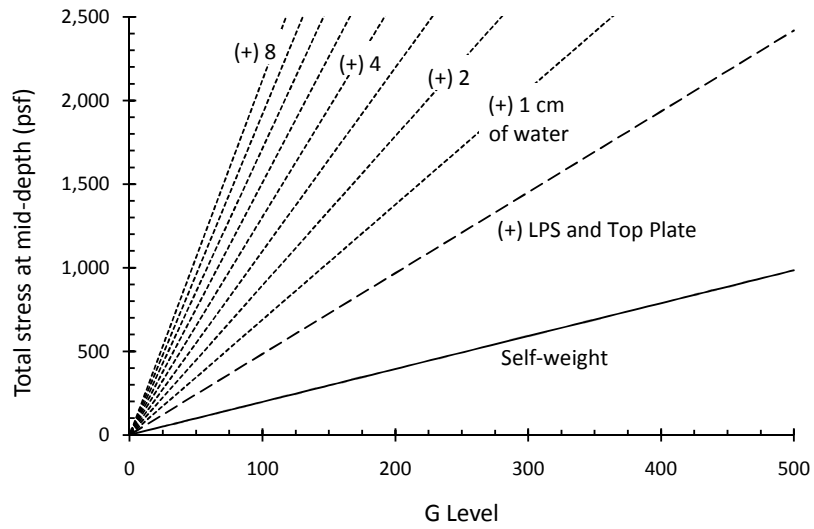
Figure 7.39: The Relationship Between Swell and Effective Stress as Measured in the Centrifuge Given Various Assumptions as to the Pore Water Pressure Distribution in the Soil Specimen

7.6.3 The Effective Stress at Mid-Depth in a Centrifuge Specimen Given a Linear Loss in Pore Water Pressure

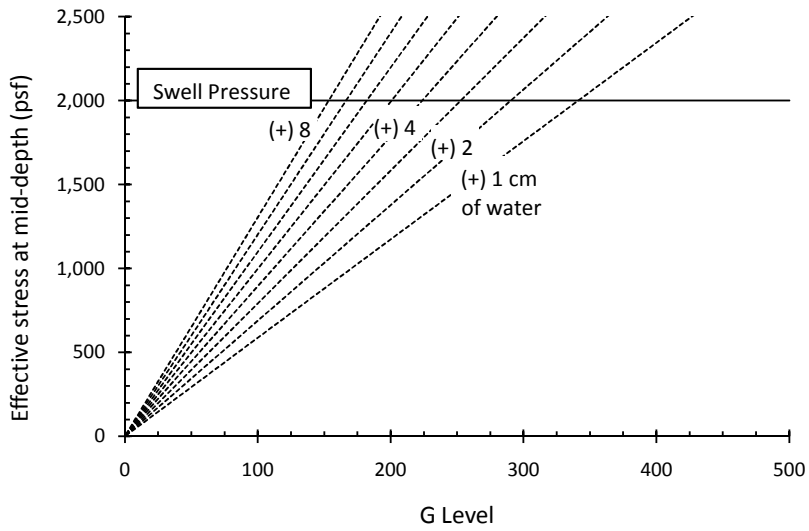
The stress profile in a soil specimen can be predicted considering a total stress on the soil surface, G-level, a height of water, and total unit weight of the soil. The variation of the total stress on the soil surface with G level was discussed in detail in Section 3.2.12.

Following on this topic, and given the discussion of incremental stress-swell relationships in the previous section, the total stress and effective stress profiles can be approximated for soil specimens for testing. For a 10-mm thick soil specimen and given a linear loss in pore water pressure with depth the relationships between total and effective stress at mid-depth, height of ponded water, and G-level was calculated and is shown in Figure 7.40. The same relationship for a 20-mm thick soil specimen is shown in Figure 7.41. These relationships

can be used when selecting the range in G-level and the height of ponded water for testing. Furthermore, the amount of added surcharge mass will directly contribute to an increase in total and effective stress, given that the sidewalls of the centrifuge permeameter are properly greased, and can thus be used to increase the total and effective stress throughout the profile for a given G-level and water height.

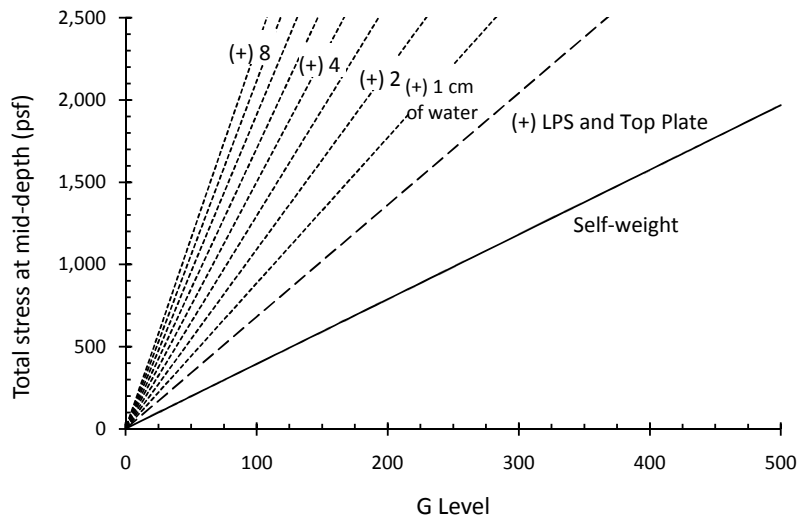


(a)

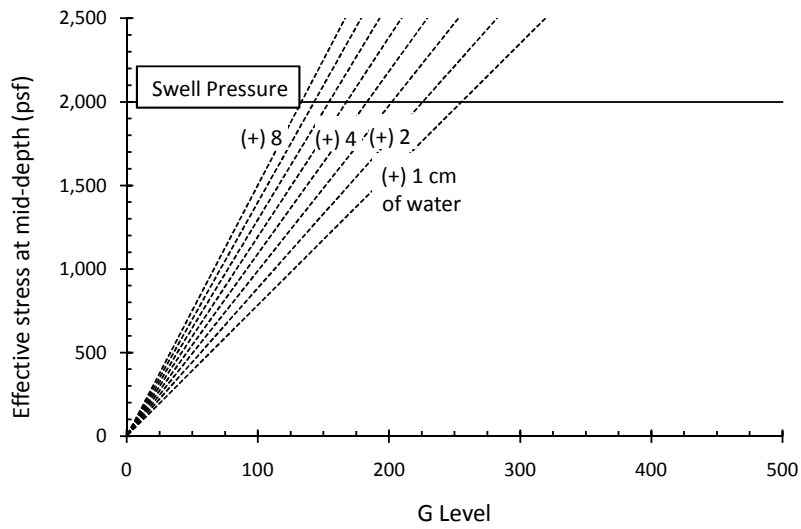


(b)

Figure 7.40: (a) Total Stress and (b) Effective Stress at Mid-depth for a 10-mm thick Soil Sample Given a Linear Loss in Pore Water Pressure with Depth



(a)



(b)

Figure 7.41: (a) Total Stress and (b) Effective Stress at Mid-depth for a 20-mm thick Soil Sample Given a Linear Loss in Pore Water Pressure with Depth

7.7 Comparison of Laboratory Testing Results with Predictions from Empirical Correlations

Given the measured relationship between swell and effective stress, it is interesting to compare the results of laboratory testing to correlations reported in the literature and presented in Section 2.2.2. A list of the index properties used in evaluating the correlations is presented in Table 7.2. The values of swell calculated from the correlations are presented in Table 7.3. It should be noted that predictions are not listed for McDowell (1956), Cover and Lytton (2001), and Rao et al. (2004). McDowell's correlations were not used because it is not applicable to laboratory testing results. Cover and Lytton (2001) and Rao et al. (2004) were not used because the properties required for the correlation can not readily be measured and are not typical index properties (e.g. matric suction compression index and free swell index). From the six relationships that were evaluated, the values of predicted swells ranged from 15 to 29% with a mean value of 24%. In accordance with the relationship between swell and effective stress as determined from free swell testing, centrifuge testing, and 1-G infiltration testing a swell of 24% relates to an effective stress less than 250 psf. The minimum value of 15%, as predicted from West (1980), correlates to an effective stress of approximately 250 psf. Since these are very generalized correlations and since they do not account for the effective stress in the soil, they were not expected to agree with laboratory testing results. It is, however, interesting to see that the resulting value of swell from these correlations generally exceeds swell measured during testing.

Table 7.2: Index Property Testing Used in Evaluating the Correlations in the order in which they are used in the Correlations

Property	Value
Plasticity index, PI	49
Liquid limit, LL	88
Shrinkage limit, SL	18
Clay content, c	89 %
Initial water content, ω_o	24 %
Dry unit weight, γ_d (pcf)	97.5
Void ratio, e	2.7
Effective stress, σ'	Variable
Overburden pressure, q (kPa)	NA
Matric suction compression index, γ_h^*	NA
Initial and final water potentials, h_i and h_f	NA
Mean principal compression index, γ_σ^*	NA
Initial and final normal stress, σ_i and σ_f	NA
Free swell index, FSI	NA

Table 7.3: Correlations from the Literature for Determining Swelling Potential, S (percent swell)

Source	Correlation	% Swell
McDowell (1956)	Chart Solution	Figure 7.42
Seed, Woodward, and Lundgren (1962)	$S = 2.16 \cdot 10^{-3} \cdot PI^{2.44}$	29
Ranganathan and Satyanarayan (1965)	$S = 4.13 \cdot 10^{-4} \cdot (LL - SL)^{2.67}$	35
Nayak and Christensen (1971)	$S = 2.29 \cdot 10^{-2} * PI^{1.45} \cdot \left(\frac{c}{\omega_o}\right) + 6.38$	30
Vijayvergiya and Ghazzalay (1973)	$\log(S) = \frac{1}{19.5} (\gamma_d + 0.65 \cdot LL - 130.5)$	18
Chen (1975)	$S = 0.2558 \cdot e^{0.08381 \cdot PI}$	16
Weston (1980)	$S = 1.95 \cdot 10^{-4} \cdot LL^{4.17} \cdot \omega_o^{-2.33}$ $S = 4.11 \cdot 10^{-4} \cdot LL^{4.17} \cdot \sigma'^{-0.386} \cdot \omega_o^{-2.33}$	15 See Figure 7.42
Covar and Lytton (2001)	$S = -\gamma_h \cdot \log_{10} \left(\frac{h_f}{h_i}\right)$ $-\gamma_\sigma \cdot \log_{10} \left(\frac{\sigma_f}{\sigma_i}\right)$	NA
Rao et al. (2004)	$S = 4.24 \cdot \gamma_d - 0.47 \cdot \omega_o - 0.14 \cdot q$ $+0.06 \cdot FSI - 55$	NA

The correlation presented by McDowell (1956) is a chart solution. The solution as presented follows the procedure outlined in Section 2.1.2. The dry and wet conditions were

calculated as follows:

$$\text{Dry Condition} = 0.2 \cdot (LL) + 9 = 0.2 \cdot (88) + 9 = 27 \quad (7.1)$$

$$\text{Wet Condition} = 0.47 \cdot (LL) + 2 = 0.47 \cdot (88) + 2 = 43 \quad (7.2)$$

It should, however, be noted that the calculated “Dry Condition” for this soil is less than the 18% measured shrinkage limit of the soil. Since the placement condition of the soil for the experiments was 24%, then the placement conditions relate to “dry conditions” or “optimum conditions” as denoted by McDowell (1956). Accordingly, given a plasticity index of 49, and reading from Figure 2.5, the percent volumetric change is 8%. The percent free swell is then calculated as follows:

$$\text{Percent Free Swell} = (\text{Percent Volumetric Change}) \cdot 1.07 + 2.6 = 11.16 \quad (7.3)$$

Adjusting for the percent passing the # 40 sieve, the PVR was calculated as 7%. Given the relationship between volumetric swell and stress presented by McDowell for the family curves, Figure 2.6, The volumetric swell can be calculated at a series of stress levels. Assuming a pore water pressure of zero and thus the effective stress being equal to the total stress for the purpose of this analysis, the swell predictions can be compared to the relationship measured in this study via free-swell tests, 1-G infiltration tests, and Centrifuge Tests (Figure 7.42).

Given the various correlations that were reported in the literature, the correlation presented by Weston (1980) yields values of predicted swell which are closest to the values of swelling measured during testing (Figure 7.42). For values of effective stress greater than 1,000 psf Weston’s relationship is very accurate. For values of effective stress less than 1,000 psf, Weston’s relationship under-predicts swelling by approximately 5%. The other

relationship which accounts for a range of effective stress is that presented by McDowell (1956). McDowell's relationship under-predicts swell by a factor of approximately three. In addition to relationships which account for a range of effective stress, several relationships were presented that predicts swelling for a nominal load. Of these relationships, the predicted swelling using Vijayvergiya and Ghazzalay (1973) along with the prediction using Chen (1975) best matched the results of laboratory testing.

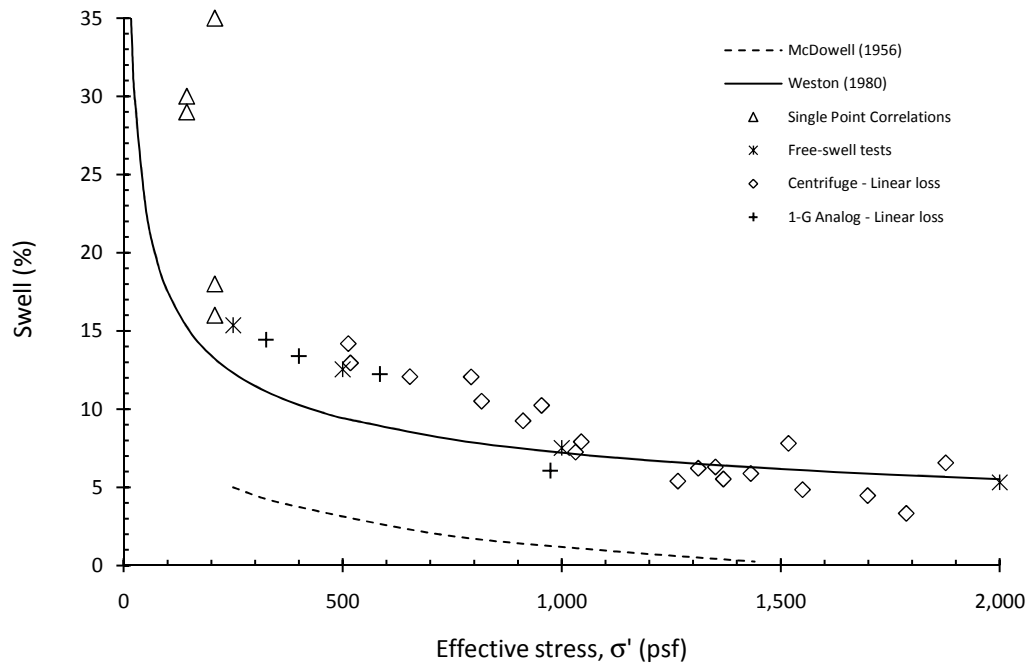


Figure 7.42: The Relationship Between Swell and Effective Stress as Measured in the Centrifuge Given Various Assumptions as to the Pore Water Pressure Distribution in the Soil Specimen

7.8 Modeling Wetting Front Advancement in the Centrifuge

In order to determine the relative effects of suction and gravity in driving the flow of water into an expansive clay, numerical modeling of the flow of water through the unsaturated

clay was performed. Numerical modeling was performed using the finite difference method which was utilized to solve Richard's Equation for infiltration under conditions of free-swell, centrifuge, and 1-G infiltration testing.

Since limited information is available in the literature as to the relationship between suction, volumetric water content, volume change, and hydraulic conductivity, the effects of volume change on these other properties was not independently considered. Furthermore, while the relationship between suction and volumetric water content for expansive clays is present in the literature, little has been reported on the relationship between those two variables and the hydraulic conductivity. Accordingly, the hydraulic conductivity of the soil for this modeling was predicting using an empirical relationship.

7.8.1 Finite Difference Model

The finite-different approach to describing the water flow through an unsaturated soil is based on Gilbert (2004), but accounts for varying gravitational acceleration. For this evaluation, Darcy's law is assumed valid and Richard's equation describing transient flow in a non-expansive soils is utilized. It is recognized that assuming a non-expansive soil is limiting when the soil being evaluated is an expansive clay. It is, however, important to note that the relationship between swelling, matric suction, and total stress is not part of this investigation and thus modeling of this order of detail is beyond the scope of this study. Furthermore, this analysis is intended to provide relative comparisons of flow under free-swell, centrifuge, and 1-G infiltration testing.

Richard's equation describing the transient flow flow of water through unsaturated soil and under different acceleration fields is as follows:

$$\frac{\delta\theta}{\delta t} = \frac{\delta}{\delta z} \left[K(\psi) \left(\frac{\delta\psi}{\delta z} + G \right) \right] \quad (7.4)$$

where θ is the volumetric water content, z is the elevation, $K(\psi)$ is the hydraulic conductivity of a soil at a given matric suction, ψ is the matric suction, and G is the

G-level. For this approach, the soil is divided up into a series of nodes each having a height of δ_z , and time is divided up into a series of time steps, each δ_t long. Considering the i^{th} node at the k^{th} time step, the flow rate downward into node i from node $i - 1$, $Q_{in,k}$ is:

$$Q_{in,k} = \left[\frac{(z_{i-1} - z_i) + (\psi_{i-1,k} - \psi_{i,k})}{\delta z} \right] K(\psi_{i-1,k-1}) A \quad (7.5)$$

Likewise, the flow rate downward from node i during time step k , $Q_{out,k}$ is:

$$Q_{out,k} = \left[\frac{(z_i - z_{i+1}) + (\psi_{i,k} - \psi_{i+1,k})}{\delta z} \right] K(\psi_{i,k-1}) A \quad (7.6)$$

The change in the volume of water for node i between time steps $k - 1$ and k is:

$$\Delta_{volume,k} = [\theta(\psi_{i,k}) - \theta(\psi_{i,k-1})] A \delta z \quad (7.7)$$

where $\theta(\psi_{i,k})$ is the volumetric water content as a function of the pressure head. For conservation of mass, Equations 7.5, 7.6, and 7.7 can be combined:

$$(Q_{in,k} - Q_{out,k}) \delta t = \Delta_{volume,k} \quad (7.8)$$

$$\left\{ \left[\frac{(z_{i-1} - z_i) + (\psi_{i-1,k} - \psi_{i,k})}{\delta z} \right] K(\psi_{i-1,k-1}) - \left[\frac{(z_i - z_{i+1}) + (\psi_{i,k} - \psi_{i+1,k})}{\delta z} \right] K(\psi_{i,k-1}) \right\} A \delta t = [\theta(\psi_{i,k}) - \theta(\psi_{i,k-1})] A \delta z \quad (7.9)$$

The change in gravitational potential per unit height is the G-level, thus:

$$\left[G + \frac{(\psi_{i-1,k} - \psi_{i,k})}{\delta z} \right] K(\psi_{i-1,k-1}) - \left[G + \frac{(\psi_{i,k} - \psi_{i+1,k})}{\delta z} \right] K(\psi_{i,k-1}) = [\theta(\psi_{i,k}) - \theta(\psi_{i,k-1})] (\delta z / \delta t) \quad (7.10)$$

$$= \left[\frac{K(\psi_{i-1,k-1})}{\delta z} (\psi_{i-1,k} - \psi_{i,k}) \right] - \left[\frac{K(\psi_{i,k-1})}{\delta z} (\psi_{i,k} - \psi_{i+1,k}) \right] = [\theta(\psi_{i,k}) - \theta(\psi_{i,k-1})] (\delta z / \delta t) + G \cdot [K(\psi_{i,k-1}) - K(\psi_{i-1,k-1})] \quad (7.11)$$

$$\begin{aligned} & \left[\frac{K(\psi_{i-1,k-1})}{\delta z} \right] \psi_{i-1,k} - \left[\frac{K(\psi_{i-1,k-1})}{\delta z} + \frac{K(\psi_{i,k-1})}{\delta z} \right] \psi_{i,k} + \left[\frac{K(\psi_{i,k-1})}{\delta z} \right] \psi_{i+1,k} \\ & = [\theta(\psi_{i,k}) - \theta(\psi_{i,k-1})] (\delta z / \delta t) + G \cdot [K(\psi_{i,k-1}) - K(\psi_{i-1,k-1})] \end{aligned} \quad (7.12)$$

Which can be expressed in matrix form as follows:

$$[A_k] \left\{ \vec{\psi}_k \right\} = \left\{ \vec{b}_k \right\} \quad (7.13)$$

where $[A_k]$ is an $n \times n$ matrix with the following coefficients in row j :

$$a_{i,i-1} = \left[\frac{K(\psi_{i-1,k-1})}{\delta z} \right] \quad (7.14)$$

$$a_{i,i} = - \left[\frac{K(\psi_{i-1,k-1})}{\delta z} + \frac{K(\psi_{i,k-1})}{\delta z} \right] \quad (7.15)$$

$$a_{i,i+1} = \left[\frac{K(\psi_{i,k-1})}{\delta z} \right] \quad (7.16)$$

with all other coefficients being equal to zero. $\left\{ \vec{\psi}_k \right\}$ is an $n \times 1$ vector with $\psi_{i,k}$ in row i , and $\left\{ \vec{b}_k \right\}$ is an $n \times 1$ vector with the following in row i :

$$[\theta(\psi_{i,k}) - \theta(\psi_{i,k-1})] (\delta z / \delta t) + G \cdot [K(\psi_{i,k-1}) - K(\psi_{i-1,k-1})] \quad (7.17)$$

Boundary conditions are established by setting values for $\psi_{1,k}$ and $\psi_{n,k}$ for all times, k . Initial conditions are set by setting values for $\psi_{i,1}$ for all i . As in the simulations conducted in this section, a constant pressure boundary conditions were used. Constant head boundary conditions are established by setting $A_{1,1}$ and $A_{n,n}$ equal to one. Thus, the boundary conditions are set by the values of $\psi_{1,0}$ and $\psi_{n,0}$.

Given the boundary conditions and the initial conditions, Equation 7.13 must be solved iteratively as the both sides of Equation 7.13 are functions of ψ . To help with

convergence during this iterative procedure, the following linear approximation can be made between soil moisture and matric suction:

$$\theta(\psi_{i,k}) - \theta(\psi_{i,k-1}) = \frac{\delta\theta}{\delta\psi} (\psi_{i,k} - \psi_{i,k-1}) \quad (7.18)$$

This linear approximation can be incorporated into Equation 7.13 by modifying Equation 7.19 as follows:

$$a_{i,i} = - \left[\frac{K(\psi_{i-1,k-1})}{\delta z} + \frac{K(\psi_{i,k-1})}{\delta z} + \frac{(\delta\theta/\delta\psi) \delta z}{\delta t} \right] \quad (7.19)$$

and by setting the terms of $\{\vec{b}_k\}$ as:

$$b_{i,k} = - \left(\frac{\delta\theta}{\delta\psi} \right) \psi_{i,k-1} \left(\frac{\delta z}{\delta t} \right) + K(\psi_{i,k-1}) - K(\psi_{i-1,k-1}) \quad (7.20)$$

7.8.2 Hydraulic Parameters

The relationships between hydraulic conductivity, suction, and saturation was established in order to model the infiltration of water into an expansive clays in a free swell test, an infiltration test, and a centrifuge infiltration test. With an expansive clay, the surcharge pressure would also be an important factor. This, however, complicates the assessment as independent relationships between hydraulic conductivity, suction, and saturation exist for different seating loads as a result of volumetric changes that occur in these soils. Accordingly, a series of simulations were performed using generic relationships between suction and saturation for a remolded expansive clay (i.e. the Soil Water Retention Curve) from the literature (Chao et al. 2008). Furthermore, the relationship between hydraulic conductivity and saturation was established by fitting the van Genuchten (1980) model to the SWRC and then using the saturated hydraulic conductivity of Eagle Ford clay along with the Mualem (1978) derivation for approximate the relationship between the hydraulic conductivity and saturation. The relationships used in this simulation are shown in Figure 7.43.

The exact relationship used for the simulation, and the exact results of the simulation will not be stressed as they are not specifically for this soil. The results of simulating the different conditions for free swell testing, infiltration testing, and centrifuge infiltration testing will, however, be compared to determine the effects of an increased gravitational potential on infiltration into an expansive clay.

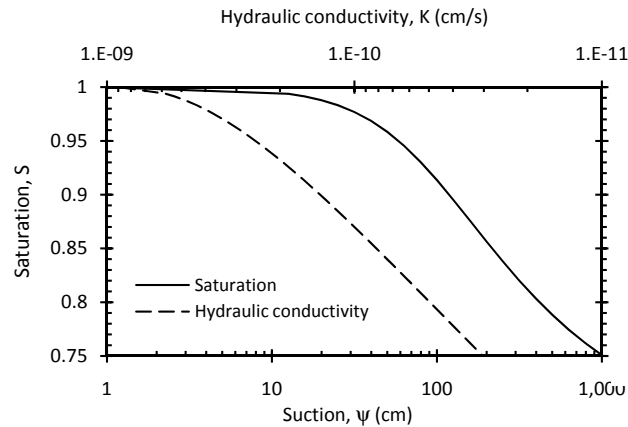


Figure 7.43: Generic Saturation and Hydraulic Conductivity Functions for an Expansive Clay

In free swell testing, a specimen is loaded, allowed to settle, and then is inundated with water to start the swelling process (For a full explanation of the experimental procedure and the results of Free Swell testing on Eagle Ford clay, see Section 4.1). Accordingly, the total head applied over the specimen and the total head at the base of the specimen are equal at the start of testing. Furthermore, the soil starts out having an initial matric suction (Assumed to be 2.16 m of suction at 85% saturation for these simulations), and flow is driven into the top and bottom of the soil specimen from a difference in pore water pressure. This gradient in water pressure is accompanied by a unit gradient in gravitational potential which encourages flow from the top of the soil specimen and discourages flow from the base. This gradient in gravitational gradient is important to consider as it is the factor that differentiates the testing conditions under free swell and centrifuge testing.

7.8.3 Modeled Wetting Front Advancement

The results from modeling moisture movement into a free swell specimen are shown in Figure 7.44. A clear wetting front can be seen to move from the top and bottom of the specimen towards the middle of the specimen. Furthermore, the effects of gravity are evident in that the moisture fronts originating from the top and bottom of the soil specimen converge around 4 mm in elevation, as supposed to the middle of the soil specimen at 5 mm elevation. In accordance with the simulation, a total time period of 13 days is required for the entire specimen to be fully saturated.

In centrifuge infiltration testing and in 1 G analog testing, a water head of 2 m is applied to the top of the specimen. In the 1 G analog test, flow of water into the specimen is driven by a unit gravitational grading and a gradient in pore water pressure. In the centrifuge test, the flow of water into the specimen is driven by an increased gravitational gradient and the same gradient in pore water pressure. The results of modeling infiltration into the 1 G analog testing setup and the centrifuge testing setup are shown in Figures 7.45 and 7.46. In the 1 G analog test, 64 hours were required for the specimen profile to become saturated. In the centrifuge test, 88% of the time required in 1 G analog testing, or 56 hours, was required for the specimen profiles to become saturated.

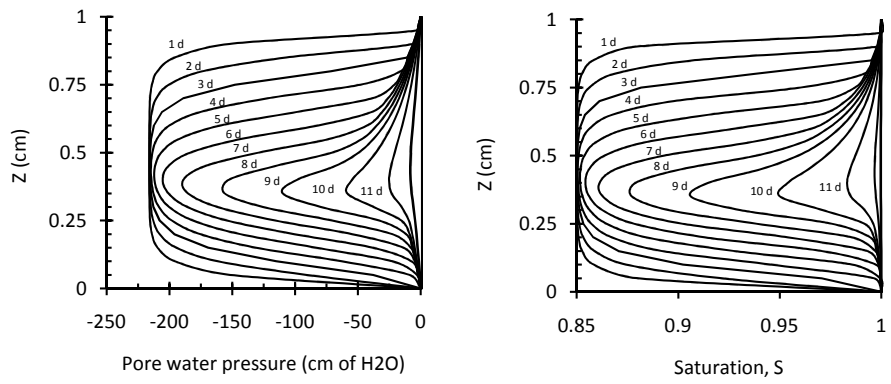


Figure 7.44: Moisture Front Progression during Free Swell

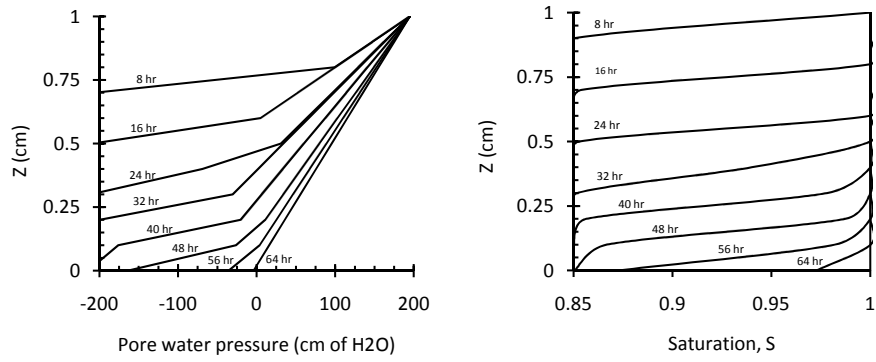
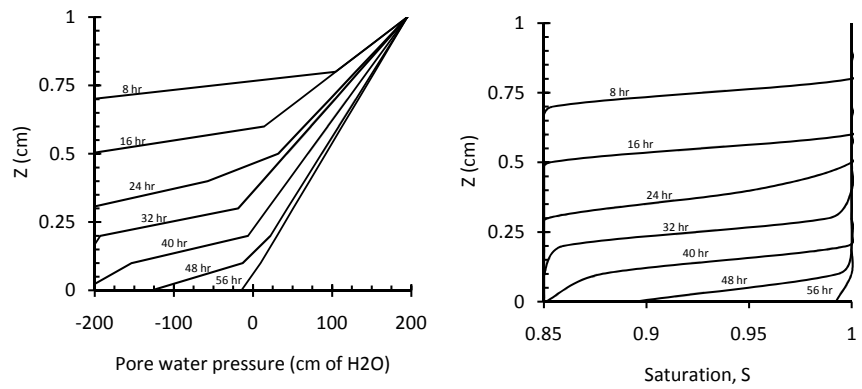
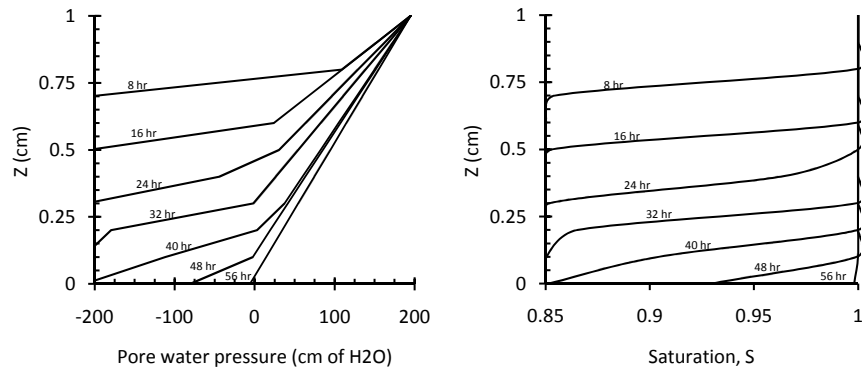


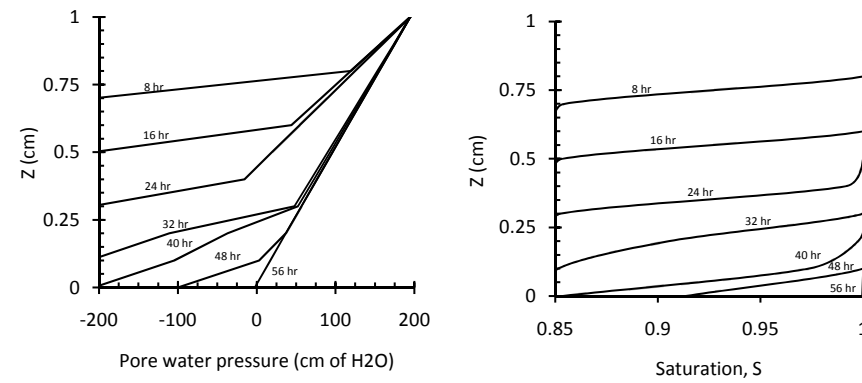
Figure 7.45: Moisture Front Progression During Infiltration



(A) 25 G



(B) 50 G



(C) 100 G

Figure 7.46: Moisture Front Progression During Infiltration in an Accelerated Gravity Field: (a) 25 G; (b) 50 G; and (c) 100 G

Chapter 8

Conclusions and Recommendations

8.1 Conclusions

The primary objectives of this study were: (1) to develop a laboratory testing procedure in which a centrifuge permeameter is used to evaluate the swell potential of expansive clay; (2) to relate the results of centrifuge tests with traditional swell tests; and (3) to provide insight into the long-term mechanisms of swelling under conditions of infiltration and submersion. Through a series of exploratory centrifuge testing on expansive clay with ponded water, a procedure was developed for evaluating the swell potential of an expansive clay using a centrifuge permeameter. Considering a linear loss of pore water pressure across centrifuge specimens, the results of centrifuge testing were related to the result of free-swell testing and a methodology for establishing the relationship between effective stress and swelling was established. Different components of the investigation are listed with their specific conclusions as follows:

A preliminary evaluation of the results of centrifuge testing revealed that:

- The amount of swelling observed in a specimen decreases with increasing G-level.
- The amount of swelling decreases with an increase in the height of water on the top of a centrifuge specimen.
- The amount of compression measured when a compacted specimen is spun up in the centrifuge increases with G-level.
- The amount of expansion measured at the end of testing, measured from the time that the braking system is activated on the centrifuge to the time the centrifuge comes to a stop, increases with G-level.
- The time required to reach a steady swell height increases with the height of the soil sample.
- The time dependent process of swelling is proportional to the square of the height of drainage.
- The time dependent process of swelling appears to be independent of the G level.

A preliminary comparison of the results of free-swell, centrifuge, and 1-G infiltration testing revealed that:

- The relationship between swell and total stress were found to be similar for centrifuge, free-swell, and 1-G infiltration testing for total stresses less than 1,000 psf.
- For total stresses greater than 1,000 psf, the final void ratio measured from free-swell testing exceeds that measured from centrifuge testing.

A comparison of displacement rates for free-swell and centrifuge tests on Eagle Ford clay that were conducted for 14 days revealed that:

- The displacement rates for centrifuge and free-swell test specimens undergoing like final strains were found to be similar.

- Displacement rates in free-swell tests decreased more rapidly than in centrifuge tests over the first 50 hours of testing.
- Displacement rates for centrifuge tests were comparable to the displacement rates for centrifuge tests after 175 hours of testing.

A comparison of primary and secondary swelling rates for free-swell, centrifuge, and 1-G infiltration tests revealed:

- The rate of primary swelling decreased with total stress and increased in a highly linear relationship with the total swell of the specimens.
- The rate of primary swelling was found to be directly proportional to the amount of swelling and independent of the G-level.
- The rate of secondary swelling decreased with total stress. Since the specimens were found to be essentially saturated after primary swelling, it is thought that the reduction in the saturated hydraulic conductivity with total stress leads to lower rates of secondary swell for specimens tested under higher total stresses.
- The proportion of secondary swelling was higher in free-swell tests than in centrifuge tests.
- The time of the onset of secondary swelling was highest for centrifuge tests and lowest for free-swell tests. All centrifuge tests specimens reached secondary swell within 36 hours of the start of testing. All free-swell specimens reached secondary swell within 12 hours of the start of testing.

Analysis of the outflow rates observed during the 14 day centrifuge tests revealed:

- The saturated hydraulic conductivity of the soil was measured within the same order of magnitude as in flexible wall permeameter tests.

- The saturated hydraulic conductivity of the soil was measured within one week of testing in the centrifuge while traditional testing in flexible wall permeameter tests required approximately a month and a half of testing time.

Water content profile measurements taken at 24, 48, 72, and 480 hours of testing from 10-mm and 20-mm thick centrifuge specimens flown at 25, 50, and 100 G revealed that:

- A wetting front progresses through the specimen during the swelling process.
- Between 24, 48, and 72 hours the water content profile within 20-mm thick specimens changed more significantly than for 10-mm thick specimens.
- The progression of the water content profile within the 10-mm thick specimens was very similar to the progression of the water content profile within the upper 10 mm of the 20-mm thick samples.
- The shapes of the water content profiles were found to be very similar for tests conducted at 25, 50, and 100 G.
- At 24, 48, and 72 hours of testing, water contents within the 25 G specimens were generally less than the water contents within the 50 G specimens, which were less than the water contents in the 100 G specimens at similar elevations.
- The water content profile of a 25 G test was found to increase from 48 hours to 480 hours indicating long-term swelling occurring in the centrifuge. The saturation of the specimen was, however found to be approximately 100% after 48 hours of testing indicating that this long-term process was not driven by matric suction and may instead be driven by osmotic suction.

Interpretation of incremental swell profiles in centrifuge specimens led to the following conclusions:

- Assuming a linear loss in pore water pressure across a 10-mm thick soil specimen after 72 hours of testing leads to the most reasonable relationship between swelling and effective stress.

- The value of swell measured for the upper one-third of a 10-mm thick soil specimen is prone to errors due to excessive swelling at the soil surface and is likely erroneous.
- The measured values of swell and the calculated values of effective stress for the lower two-thirds of a 10-mm thick soil specimen are to be used for determining the relationship between swell and effective stress.
- The relationships between swell and effective stress were found to be similar for centrifuge, free-swell, and 1-G infiltration testing.
- The empirical relationship for swelling prediction presented by Weston (1980) was found to yield values of predicted swell that are the closest to the values of swelling measured during testing.

Modeling of the infiltration process in the centrifuge, free swell, and 1-G infiltration tests revealed:

- A time period of 10 days was theoretically required to exceed a saturation of 95% in free-swell tests, while a period of less than three days was required to exceed a saturation of 95% for 1-g analog and centrifuge tests.
- In comparing the 1-G infiltration tests to those for centrifuge tests, the centrifugal acceleration was found to accelerate the advancement of the wetting front. This acceleration was, however, found to reduce the time required to reach a saturation of exceeding 95% by a period of approximately 10 hours.
- The initial flow of water through the soil specimens compacted at optimum water content appears to be driven principally by a gradient in suction head rather than a gradient in gravitational head.

8.2 Recommendations for Future Investigations

Several investigations which would build upon the findings of this study include:

- Performing free-swell, centrifuge, and 1-g analog tests on test specimens compacted wet and dry of optimum at different densities in order to evaluate the effects of placement conditions on swelling.
- Perform additional testing to evaluate the effect of water pressure on swelling.
- Perform centrifuge tests on expansive soil using the peristaltic or syringe pump to subject the soil specimen to a steady state flow rate that imposes a hydraulic conductivity less than the saturated value to study swelling under unsaturated conditions.
- Perform centrifuge tests in which the base of the specimen is subjected to a controlled suction or a positive water pressure.
- Perform centrifuge tests in which the volume of water added to maintain a constant head above the specimen is measured. Given that the volume of added water is measured, the outflow from the soil specimen is measured, and the swelling of the soil specimen is measured, a mass balance can be performed in order to determine the average saturation of the specimen throughout the duration of the centrifuge test.
- Add the capability of siphoning off water at the end of centrifuge swell testing in order to minimize swelling of the upper portion of the soil specimen that may occur between the termination of testing and the time at which the centrifuge comes to a full stop.
- Perform additional 1-G infiltration tests where the effects of water pressure and overburden pressure are both evaluated.
- Conduct 1-G infiltration tests where water is infiltrated from the base of the specimen in order to take advantage of the buoyancy of trapped air so that the specimen might become saturated more quickly.
- Measure the soil water retention curve and hydraulic conductivity function for the Eagle Ford Clay under a range of surcharge pressures and use the measured hydraulic characteristics to model infiltration under free-swell, centrifuge, and 1-g analog testing.

- Conduct incremental load consolidation tests starting at a pressure equal to the swell pressure in order to determine the relationship between void ratio and effective stress for swelling and consolidation alike.

Appendix A

Swell Testing with Basic Centrifuge Equipment

If swell testing were to be widely used in industry to quantify the swell potential of expansive soils, then such testing would have to be able to be carried out using equipment that could readily be afforded. In the centrifuge testing setup as describe in this setup one of the largest costs is the in-flight solid-state data acquisition system. If the data acquisition system is removed from the centrifuge testing setup, and the centrifuge is downsized, as in the testing setup describe in Plaisted (2008), then it is feasible that such equipment and testing methods could be widely adopted. If, however, in-flight monitoring were not to be conducted, then the change in void ratio and thus the swell of the specimen could only be determined from measurements taken at the beginning and end of testing. Since, in this testing program, the height of the soil specimens is monitored throughout the testing process and the heights were measured before and after testing, the accuracy of testing without an in-flight data acquisition system can be accessed.

During testing, several measurements of the height of the soil specimen are taken in order to determine the volumetric changes which the soil specimen is undergoing during

testing (Section 3.2.13). The compacted height of the soil specimen, H_1 , is measured with a vertical dial gauge (VDG). The specimen is then placed in the centrifuge and the height of the specimen is measured with a linear position sensor (LPS). The specimen is then flown in the centrifuge and settles to H_2 . Following this, water is ponded above the soil specimen and the specimen is flown in the centrifuge for a period of time (e.g. 72 hours for much of the testing in this study). After this period of time, the height of the soil specimen is taken, H_3 , and the centrifuge is stopped at which time the soil expands to H_4 . The soil specimen is then removed from the centrifuge and the height of the soil specimen, H_5 , is measured again with the VDG.

The two main variables of interest in terms of the volumetric swell that the specimen undergoes during testing are the final void ratio and the swell. The final void ratio being the void ratio of the specimen at the end of testing when it has neared equilibrium with the boundary conditions imposed on the final void ratio and the swell being the linear swell of the specimen at this instance. In the case that in-flight measurements of the height of the soil specimen are taken, H_3 can be used to determine the final void ratio of the soil and H_2 and H_3 can be used to determine the swell. In the case that in-flight measurements are not available, the final void ratio can be best approximated from H_4 and the swell can be best approximated from H_3 and H_4 . Accordingly, in the case where in-flight measurements are not available, the compression and expansion of the soil at the beginning and end of testing are not accounted for. As a result, there is an error in the final void ratio and swell as determined only using the vertical dial gauge.

In order to compare the measurements of final void ratio and swell determined using only the vertical dial gauge and those determined with the linear position sensor, the results from test series II (Section 6.2) are plotted in Figure A.1. In terms of void ratio, the lack of in-flight height measurements leads to measuring too great of a void ratio. In terms of swell, the lack of in-flight height measurements mostly leads to measuring more swell. In order to quantify error in the measured values of the final void ratio and swell that occurs due to the lack of in-flight height measurements, the ratio of values of final void ratio determined

using VDG measurements to values of final void ratio using LPS are plotted versus the total stress for the test and according to G-level in Figure A.2. Likewise, the ratio of the swell determined from VDG and LPS readings is plotted in Figure A.3.

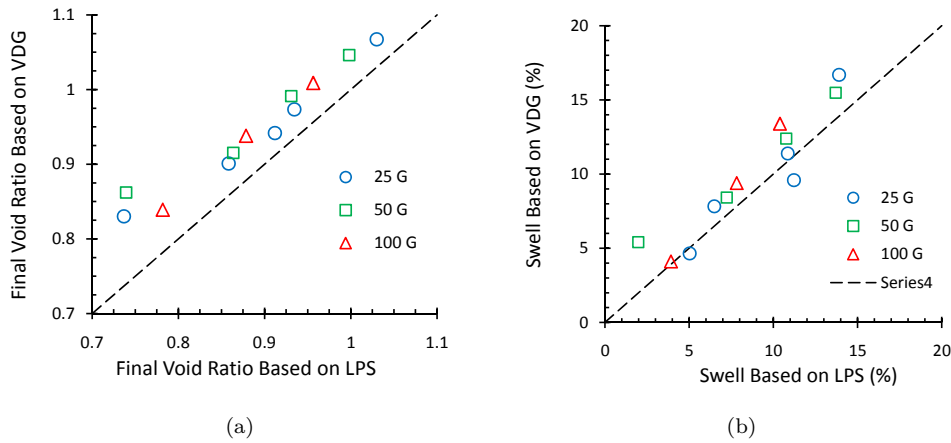


Figure A.1: (a) Final Void Ratio and (b) Swell for Measurements Taken with a Vertical Dial Gauge (VDG) and in-flight Linear Position Sensor (LPS)

The final void ratio determined from VDG measurements were on average 6% greater than the values using LPS measurements. The error in the final void ratio was found to generally increase with G-level and total stress. This error, was, however, expected to generally increase with G-level and total stress as the amount of swelling occurring in a specimen generally decreases with increasing G-level and total stress. The value of swelling determined from VDG measurements was found to be on average 10% greater than the value of swelling determined from LPS measurements. Accordingly, since the measurements from the VDG alone do not accurately represent the final void ratio and swelling of the soil, it appears that in-flight measurements of the height of the soil specimen are necessary for accurate testing. It is, however, very possible that additional testing may provide additional insight that would allow VDG measurements to be used for determining the final void ratio and swell. Based on the measurements presented from Test Series II neither the accuracy or the precision of the values determined from VDG measurements warrant testing without

an in-flight data acquisition system.

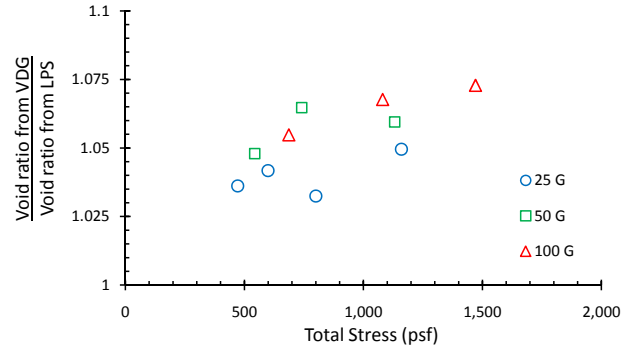


Figure A.2: Ratio of Final Void Ratio Determined from Vertical Dial Gauge (VDG) Measurements to the Final Void Ratio Determined from in-flight Linear Position Sensor (LPS) Measurements

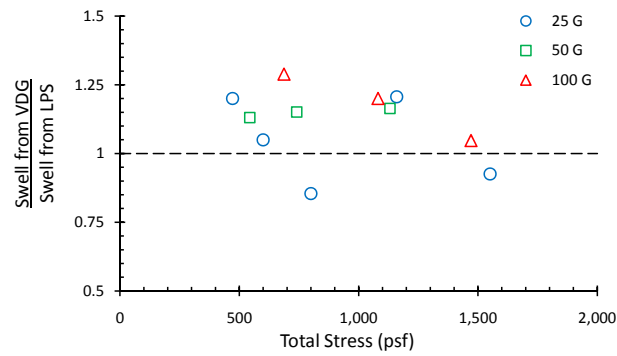


Figure A.3: Ratio of Swell Determined from Vertical Dial Gauge (VDG) Measurements to the Final Void Ratio Determined from in-flight Linear Position Sensor (LPS) Measurements

Bibliography

- J. Aguetant. *The Fully-Softened Shear Strength of High Plasticity Clays*. PhD thesis, The University of Texas at Austin, August 2006.
- A. I. Al-Mhaidib. Swelling behavior of expansive shales from the middle region of Saudi Arabia. *Geotechnical and Geological Engineering*, 16:291–307, 1999.
- A. Al-Rawas. The factors controlling the expansive nature of the soils and rocks of northern Oman. *Engineering Geology*, 53:327–350, 1999.
- M. Al-Shamrani. Influenced of lateral restraint on the swelling behavior of expansive soils. *Journal of The Southeast Asian Geotechnical Society*, pages 101–111, 2004.
- G. Al-Sulaimani and S. Abduljawad. Determination of swell potential of al-qatif clay. *Geotechnical Testing Journal*, 16.4:469–484, 1993.
- J. Allen. Forced ventilated swell-shrink test for potential vertical expansive soil movement. Master's thesis, The University of Texas at Austin, 2004.
- I. Ashayeri and S. Yasrebi. Free-swell and swelling pressure of unsaturated compacted clays; experiments and neural networks modeling. *Geotechnical and Geological Engineering*, 27.1: 137–153, 2009.
- ASTM. D698 standard test method for laboratory compaction characteristics of soil using standard effort., a.

ASTM. D854 standard test method for specific gravity of soil solids by water pycnometer., b.

ASTM. D2216 standard test method for laboratory determination of water (moisture) content of soil and rock by mass., c.

ASTM. D2435 standard test method for one-dimensional consolidation properties of soils., d.

ASTM. D2488 standard test method for description and identification of soils (visual-manual procedure)., e.

ASTM. D4318 standard test method for liquid limit, plastic limit, and plasticity index of soils., f.

ASTM. D4546 standard test methods for one-dimensional swell or collapse of cohesive soils., g.

ASTM. D6527 standard test method for determining unsaturated and saturated hydraulic conductivity in porous media by steady-state centrifugation., h.

ASTM. D422-63 standard test method for particle-size analysis of soils, i.

ASTM. D 4943 standard test method for shrinkage factors of soils by the wax method, j.

M. F. Attom, M. M. Abu-Zreig, and M. T. Obaidat. Changes in clay swelling and shear strength properties with different sample preparation techniques. *Geotechnical Testing Journal*, 24.2:157–163, 2001.

A. Basma. Prediction of expansion degree for natural compacted clays. *Geotechnical Testing Journal*, 16.4:542–549, 1993.

A. Basma, A. Al-Homoud, and E. Al-Tabari. Effects of the method of drying on the engineering behavior of clays. *Applied Clay Science*, 9.3:153–164, 1994.

- A. Basma, A. Al-Hamoud, and A. Husein. Laboratory assessment of swelling pressure of expansive soils. *Applied Clay Science*, 9:355–368, 1995.
- A. A. Basma, A. S. Al-Homoudb, A. I. H. Malkawib, and M. A. Al-Bashabsheh. Swelling-shrinkage behavior of natural expansive clays. *Applied Clay Science*, 11:211–227, 1996.
- J. Bear. *Dynamics of Fluids in Porous Media*. Elsevier, New York, 1943.
- L. S. Bennethum, M. Murad, and J. Cushman. Modified darcy's law, terzaghi's effective stress principle and fick's law for swelling clay soils. *Computers and Geotechnics*, 20:245–266, 1997.
- M. E. Bilir, D. Sari, and Y. V. Muftuoglu. A computer-controlled triaxial test apparatus for measuring swelling characteristics of reconstituted clay-bearing rock. *Geotechnical Testing Journal*, 31:279–284, 2008.
- A. Bishop and G. Aitchison. *Discussion in: Pore Pressure and Suction in Soils*. Butterworths, London, 1961.
- G. Blight. The time-rate of structures on expansive clays. In *Moisture Equilibria and Moisture Changes in Soils Beneath Covered Areas*, pages 89–92, 1965.
- G. Blight and J. De Wet. The acceleration of heave by flooding. In *Moisture Equilibria and Moisture Changes in Soils Beneath Covered Areas*, pages 89–92, 1965.
- Broadbent. *Operating Manual for GT450/1.4 Centrifugal Permeameter/Geotechnical Drum*. Thomas Broadbent and Sons Limited, 1 edition, 2006.
- Bucher and Muller-Vonmoos. Bentonite as a containment barrier for the disposal of highly radioactive wastes. *Applied Clay Science*, 4:179–192, 1989.
- D. Cameron, P. Walsh, and S. Fityus. The shrink swell test. *Geotechnical Testing Journal*, 28.1:1–10, 2005.

- N.-J. O. D. Chao, K.C. and J. Cumbers. Soil water retention curves for remolded expansive soils. In *Proceedings of the 1st European Conference on Unsaturated Soils*, Durham, UK, July 2008.
- F. Chen. *Foundations on Swelling Soils*. Elsevier, Amsterdam, 1975.
- F. H. Chen. The use of piers to prevent the uplifting of lightly loaded structures founded on expansive soils. *Engineering Effects of Moisture Changes in Soils; Concluding Proceedings of the International Research and Engineering Conference on Expansive Clay Soils*, 2:152–171, 1965.
- A. Covar and R. Lytton. Estimating soil swelling behavior using soil classification properties. *Expansive Clay Soils and Vegetative Influences on Shallow Foundations, ASCE Geotechnical Publications*, 115:44–63, 2001.
- O. Cuisinier and F. Masrouri. Testing the hydromechanical behavior of a compacted swelling soil. *Geotechnical Testing Journal*, 27:1–9, 2004.
- V. Dakshanamurthy. Stress-controlled study of swelling characteristics of compacted expansive clays. *Geotechnical Testing Journal*, 2.1:57–60, 1979.
- A. Dhowian. Simplified heave prediction model for expansive shale. *Geotechnical Testing Journal*, 13.4:323–333, 1990.
- Y. Du, S. Li, and S. Hayashi. Swelling-shrinkage properties and soil improvement of compacted expansive soil, ning-liang highway, china. *Engineering Geology*, 53:321–358, 1999.
- Z. A. Erguler. A simple test and predictive models for assessing swell potential of ankara (turkey) clay. *Engineering Geology*, 67:331–352, 2003.
- M. J. Farrow. In-depth characterization of the eagle ford shale. In *Spring Civil Engineering Papers*, 1997.

- V. Ferber, J.-C. Auriol, Y.-J. Cui, and J.-P. Magnan. On the swelling potential of compacted high plasticity clays. *Engineering Geology*, 104:200–210, 2009.
- S. Gizienski and L. Lee. Comparison of laboratory swell tests to small scale field tests. *Engineering Effects of Moisture Changes in Soils; Concluding Proceedings of the International Research and Engineering Conference on Expansive Clay Soils*, 2:108–119, 1965.
- R. W. H. Seed and R. Lundgren. Prediction of swelling potential for compacted clays. *Journal of the Soil Mechanics and Foundation Engineering Division*, 88:53–87, 1962.
- R. Hasenpatt, W. Degen, and G. Kahr. Flow and diffusion in clays. *Applied Clay Science*, 4:179–192, 1989.
- J. Haynes and R. Mason. Subgrade soil treatment at the apparel mart, dallas, texas. *Engineering Effects of Moisture Changes in Soils; Concluding Proceedings of the International Research and Engineering Conference on Expansive Clay Soils*, 2:172–182, 1965.
- S.-C. Hsu and P. P. Nelson. Characterization of eagle ford shale. *Engineering Geology*, 67:169–183, 2002.
- D. Jones and W. Holtz. Expansive sils - the hidden disaster. *Civil Engineering*, 43.8:49–51, 1973.
- R. K., R. S., and G. S. Swelling behavior of a desiccated clay. *Geotechnical Testing Journal*, 23.2:193–198, 2000.
- R. Katti. *Behavior of Saturated Expansive Soil and Control Methods*. Balkema, Netherlands, 2002.
- J. Kirby, A. Bernardi, A. Ringrose-Voase, R. Young, and H. Rose. Field swelling, shrinking, and water content change in a heavy clay soil. *Australian Journal of Soil Research*, 41.5:963–978, 2003.
- J. Kuhn. Effect of cracking on the hydraulic properties of unsaturated highly plastic clays. Master's thesis, The University of Texas, 2005.

- J. Lee and P. Fox. Efficiency of seepage consolidation for preparation of clay substrate for centrifuge testing. *Geotechnical Testing Journal*, 28.6:1–9, 2005.
- N. Lu and W. Likos. *Unsaturated Soil Mechanics*. Wiley, New York, 2005.
- R. Lytton, C. Aubeny, and R. Bulut. Design procedure for pavements on expansive soils: Volume 1. Technical Report 0-4518-1 (V1), Texas Transportation Institute, 2005a.
- R. Lytton, C. Aubeny, and R. Bulut. Design procedure for pavements on expansive soils: Volume 3. Technical Report 0-4518-1 (V3), Texas Transportation Institute, 2005b.
- R. Lytton, C. Aubeny, and R. Bulut. Re-evaluation of potential vertical rise design procedures 0-4518-s. Technical Report 0-4518-S, Texas Transportation Institute, 2005c.
- R. Lytton, C. Aubeny, and R. Bulut. Design procedure for pavements on expansive soils: Volume 2. Technical Report 0-4518-1 (V2), Texas Transportation Institute, 2006.
- F. T. Madsena and M. Muller-Vonmoos. The swelling behaviour of clays. *Applied Clay Science*, 4:143–156, 1989.
- J. McCartney and J. Zornberg. The centrifuge permeameter for unsaturated soils (cpus). In *Proceedings of the International Symposium on Advanced Experimental Unsaturated Soil Mechanics*, pages 299–304, Trento, Italy, June 2005. A.A. Balkema.
- C. McDowell. Interrelationship of loads, volume change, and layer thickness of soils to the behavior of engineering structures. In *Highway Research Board, Proc. 35th Annual Meeting*, number 426, pages 754–772, Washington, D.C., 1956.
- C. McDowell. Remedial procedures used in the reduction of detrimental effects of swelling soils. *Engineering Effects of Moisture Changes in Soils; Concluding Proceedings of the International Research and Engineering Conference on Expansive Clay Soils*, 2:239–254, 1965.
- R. Mitchell. Centrifuge techniques for testing clay linear samples. *Canadian Geotechnical Journal*, 31:577–583, 1994.

- Y. Mualem. Hydraulic conductivity of unsaturated porous media: Generalized macroscopic approach. *Water Resources Research*, 91, No. 2:325–334, 1978.
- H. B. Nagaraj, M. M. Munnas, and A. Sridharan. Critical evaluation of determining swelling pressure by swell-load method and constant volume method. *Geotechnical Testing Journal*, 32.4:1–10, 2009.
- N. Nayak and R. Christensen. Swelling characteristics of compacted expansive soils. *Clays and Clay Minerals*, 4:251–261, 1974.
- R. Olson. *State of the Art: Consolidation Testing*. Number STP 892. ASTM, 1986.
- R. Olson. Course notes on incremental vertical-flow consolidation test. *Consolidation and Settlement of Soft Soils*, 2007.
- V. Osipov, N. Bik, and N. Runjantseva. Cyclic swelling of clays. *Applied Clay Science*, 2.7:363–374, 1987.
- J. Pellissier. The toluene and wax-freezing method of determining volumetric free swell. *Geotechnical Testing Journal*, 14.3:309–314, 1991.
- M. Popescu. Engineering problems associated with expansive clays from romania. *Engineering Geology*, 14:43–53, 1979.
- A. Puppala and L. Hoyos. Realistic design guidelines for low classification roads in high pi clays. Texas Department of Transportation Project Number 0-5430, 2009.
- V. Ranganatham and B. Satyanarayana. Interaction of primary factors on swell and swell pressure. *Journal of India National Society of Soil Mechanics and Foundation Engineering*, 8:23–41, 1969.
- A. Rao, B. Phanikumar, and R. Sharma. Prediction of swelling characteristics of remoulded and compacted expansive soils using free swell index. *Quarterly Journal of Engineering Geology and Hydrogeology*, 37.3:217–226, 2004.

- R. Robinson, T. Tan, and F. Lee. A comparative study of suction-induced seepage consolidation versus centrifuge consolidation. *Journal of Geotechnical Testing*, 26.1:1–10, 2003.
- R. Robinson, G. Dasari, and T. Tan. Three-dimensional swelling of clay lumps. *Geotechnique*, 54:29–39, 2004.
- C. Robison. Hydrocarbon source rock variability within the austin chalk and eagle ford shale (upper cretaceous), east texas, u.s.a. *International Journal of Coal Geology*, 34:287–305, 1997.
- W. R. Seed, H.B. and R. Lundgren. Prediction of swelling potential for compacted clays. *Journal of the Soil Mechanics and Foundations Division, ASCE*, 88:53–87, 1962.
- T. Sikh. Swell potential versus overburden pressure. *Geotechnical Testing Journal*, 16.3:393–396, 1993.
- D. Singh and A. Gupta. Modeling hydraulic conductivity in a small centrifuge. *Canadian Geotechnical Journal*, 37:1150–1155, 2000.
- M. V. Smalley. Electrical theory of clay swelling. *Langmuir*, 10:2884–2891, 1994.
- A. Sridharan and K. Prakash. Free swell ratio and clay mineralogy of fine-grained soils. *Geotechnical Testing Journal*, 27.2:1–6, 2004.
- A. Sridharan, S. Rao, and N. Murthy. A rapid method to identify clay type in soils by the free-swell technique. *Geotechnical Testing Journal*, 9.4:198–203, 1986.
- K. Subba Rao and S. Tripathy. Effect of aging on swelling and swell-shrink behavior of a compacted expansive soil. *Geotechnical Testing Journal*, 26.1:1–11, 2003.
- D. Taylor. Research on the consolidatin of clays. Technical Report Serial No. 82, The Department of Civil and Sanitary Engineering, 1942.
- R. Taylor, editor. *Geotechnical Centrifuge Technology*. Spon Press, 1994.
- K. Terzaghi. *Theoretical Soil Mechanics*. John Wiley and Sons, New York, 1943.

- Tripathy. Water content-void ratio swell-shrink paths of compacted expansive soils. *Canadian Geotechnical Journal*, 39:938–959, 2002.
- M. Tuller and D. Or. Hydraulic functions for swelling soils: Pore scale considerations. *Journal of Hydrology*, 272:50–71, 2003.
- TxDOT. Tex-124-e - determining potential vertical rise, 1999. URL <http://manuals.dot.state.tx.us/dynaweb/>.
- M. van genuchten. A closed-form equation for predicting the hydraulic conductivity of unsaturated soils.". *Soil Science Society of America*, 44:892–898, 1980.
- V. Vijayavergiya and O. Ghazzaly. Prediction of swelling potential for natural clays. *Proceedings of the Third International Conference on Expansive Soils, Haifa*, 1:227–236, 1973.
- E. Weisberg and S. Frydman. Study of flow in compacted columns of swelling clay. *Transportation Research Record*, No. 1277, Modern Geotechnical Methods: Instrumentation and Vibratory Hammers:8–17, 1990.
- D. Weston. Expansive road treatment for southern africa. *Proceedings of the Fourth International Conference on Expansive Soils, Denver*, 1:339–360, 1980.
- C. Xiquan and L. Zhongwei. Calculation of movement of building foundation on expansive soil. In *Proceedings of the Fifth International Expansive Soils Conference, Adelaide*, pages 175–178, 1984.
- D. Znidarcic, H.-Y. Ko, and O. Cinicioglu. A new centrifugal testing method: Decending gravity test. *Geotechnical Testing Journal*, 29.5:1–10, 2006.
- J. Zornberg and J. Kuhn. Field suction and effect of cracking in highly plastic clay. Technical Report 0-5202, Center for Transportation Research, 2007.

Vita

Jeffrey Albin Kuhn was born in Baltimore, Maryland on April 11, 1981, the son of Dr. Albin Owings and Susan Arold Kuhn. He has two sibilings, an older sister Laura Arold Kuhn and a younger sister Julie Elizabeth Kuhn. After graduating from Centennial High School in Ellicott City, Maryland, he started his undergraduate studies in Civil Engineering at The University of Maryland. He recieved his Bachelor of Science degree and a citation in Environmental Studies from The University of Maryland in May, 2003. Jeff headed west to Austin and entered graduate school at The University of Texas to study geotechnical engineering in August, 2003. After recieving his Masters of Science in Engineering he continued his studies at The University of Texas in pursuit of a Doctorate. He found and married the love of his life Lou in August of 2008. Lou and Jeff welcomed their daughter, Ella Elizabeth, to their family on March 15 of 2010. Ella was welcomed into the world by a loving family including six aunts and one uncle.

Permanent Address: 10032 Inkpen Place
Baltimore, MD 21042

This dissertation was typeset by the author.